AFOSR-TR-

SUPERCONDUCTING ELECTRONIC FILM STRUCTURES

I. R. Gavaler and J. Talvacchio
Superconductor Materials and Electronics

Final Report for the Period
January 1, 1988 to December 31, 1990

AFOSR Contract No. F49620-88-C-0039
Research Sponsored by the
Air Force Office of Scientific Research
Air Force Systems Command
United States Air Force

February 14, 1991

Approved for public release, distribution unlimited.

Westinghouse STC
1310 Beulah Road
Pittsburgh, Pennsylvania 15235

(2)

SUPERCONDUCTING ELECTRONIC FILM STRUCTURES

J. R. Gavaler and J. Talvacchio
Superconductor Materials and Electronics

Final Report for the Period
January 1, 1988 to December 31, 1990

AFOSR Contract No. F49620-88-C-0039
Research Sponsored by the
Air Force Office of Scientific Research
Air Force Systems Command
United States Air Force

February 14, 1991

Approved for public release, distribution unlimited.

Westinghouse STC
1310 Beulah Road
Pittsburgh, Pennsylvania 15235

DISCLAIMER NOTICE

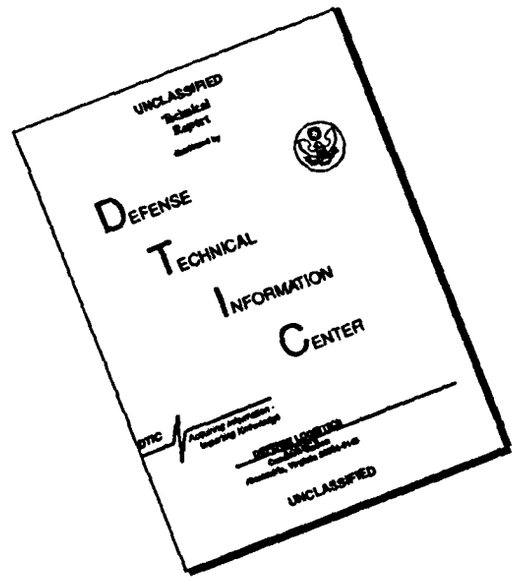

THIS DOCUMENT IS BEST QUALITY AVAILABLE. THE COPY FURNISHED TO DTIC CONTAINED A SIGNIFICANT NUMBER OF PAGES WHICH DO NOT REPRODUCE LEGIBLY.

Unclassified
SECURITY CLASSIFICATION OF THIS PAGE

REPORT DOCUMENTATION PAGE

Form Approved
OMB No. 0704-0188

1a. REPORT SECURITY CLASSIFICATION Unclassified	1b. RESTRICTIVE MARKINGS
2a. SECURITY CLASSIFICATION AUTHORITY Unclassified	3. DISTRIBUTION/AVAILABILITY OF REPORT Approved for public release; distribution unlimited.
2b. DECLASSIFICATION/DOWNGRADING SCHEDULE N/A	
4. PERFORMING ORGANIZATION REPORT NUMBER(S) 91-9SL2-SUPER-R1	5. MONITORING ORGANIZATION REPORT NUMBER(S)
6a. NAME OF PERFORMING ORGANIZATION Westinghouse Science and Technology Center 6b. OFFICE SYMBOL (If applicable)	7a. NAME OF MONITORING ORGANIZATION Same as 8a
6c. ADDRESS (City, State, and ZIP Code) 1310 Beulah Road Pittsburgh, Pennsylvania 15235	7b. ADDRESS (City, State, and ZIP Code) Same as 8c 22
8a. NAME OF FUNDING/SPONSORING ORGANIZATION Air Force Office of Scientific Research 8b. OFFICE SYMBOL (If applicable)	9. PROCUREMENT INSTRUMENT IDENTIFICATION NUMBER F49620-88-C-0039
8c. ADDRESS (City, State, and ZIP Code) Bldg 410 Bolling AFB, DC 20332	10. SOURCE OF FUNDING NUMBERS PROGRAM ELEMENT NO. 61102F; PROJECT NO. 2306; TASK NO. C1; WORK UNIT ACCESSION NO.

11. TITLE (Include Security Classification)
SUPERCONDUCTING ELECTRONIC FILM STRUCTURES

12. PERSONAL AUTHOR(S)
Gavaler, J. R. and Talvacchio, J.

13a. TYPE OF REPORT	13b. TIME COVERED	14. DATE OF REPORT (Year, Month, Day)	15. PAGE COUNT
Final	FROM 1-1-88 TO 12-31-90	1991 Feb 14	212

16. SUPPLEMENTARY NOTATION

17. COSATI CODES			18. SUBJECT TERMS (Continue on reverse if necessary and identify by block number)
FIELD	GROUP	SUB-GROUP	superconductors, yttrium, barium, copper, oxides, high, critical, temperature, thin films, tunneling, barriers, thallium, sputtering.

19. ABSTRACT (Continue on reverse if necessary and identify by block number)

The overall objective of this program was to obtain both an understanding and control of superconducting and normal-state properties of layered, mostly epitaxial film structures incorporating high-critical-temperature oxide superconductors. Fulfillment of this objective has been a major step forward in the development of a technology base for superconducting electronics capable of operating above the temperature of 50K, particularly for passive devices. The technology is based primarily on single-crystal YBCO films deposited by single-target sputtering. Based on a wide variety of characterization techniques, including tunneling and rf surface resistance, they are equal or superior to films made by any other method. Microwave devices fabricated with such films (in other programs at Westinghouse) showed markedly improved performance compared to conventional devices. The capability of sputtering YBCO films on large areas and on both sides of substrates was developed. State-of-the-art TBCCO and LSCO films were also prepared and evaluated. Procedures were developed for control of film orientation

20. DISTRIBUTION/AVAILABILITY OF ABSTRACT	21. ABSTRACT SECURITY CLASSIFICATION
☑ UNCLASSIFIED/UNLIMITED ☐ SAME AS RPT ☐ DTIC USERS	UNCLASSIFIED
22a. NAME OF RESPONSIBLE INDIVIDUAL Weinstock	22b. TELEPHONE (Include Area Code) 202-767-4932
	22c. OFFICE SYMBOL NE

DD Form 1473, JUN 86 *Previous editions are obsolete.*

SECURITY CLASSIFICATION OF THIS PAGE
Unclassified

Particular attention was given to film surfaces and interfaces with substrates, epitaxial buffer layers, and tunnel barriers. Specific results of the program are detailed in published papers appended to this report. In addition to work performed solely at Westinghouse, collaborations with other research groups provided results of a broader scientific interest than otherwise would have been possible within the scope of this program.

1. FINAL REPORT, SUPERCONDUCTING ELECTRONIC FILM STRUCTURES

January 1, 1988 to December 31, 1990

AFOSR Contract No. F49620-88-C-0039

J. R. Gavaler and J. Talvacchio

2. ABSTRACT

The overall objective of this program was to obtain both an understanding and control of superconducting and normal-state properties of layered, mostly epitaxial film structures incorporating high-critical-temperature oxide superconductors. Fulfillment of this objective has been a major step forward in the development of a technology base for superconducting electronics capable of operating above the temperature of 50K, particularly for passive devices. The technology is based primarily on single-crystal YBCO films deposited by single-target sputtering. Based on a wide variety of characterization techniques, including tunneling and rf surface resistance, they are equal or superior to films made by any other method. Microwave devices fabricated with such films (in other programs at Westinghouse) showed markedly improved performance compared to conventional devices. The capability of sputtering YBCO films on large areas and on both sides of substrates was developed. State-of-the-art TBCCO and LSCO films were also prepared and evaluated. Procedures were developed for control of film orientation. Particular attention was given to film surfaces and interfaces with substrates, epitaxial buffer layers, and tunnel barriers. Specific results of the program are detailed in published papers appended to this report. In addition to work performed solely at Westinghouse, collaborations with other research groups provided results of a broader scientific interest than otherwise would have been possible within the scope of this program.

3. OBJECTIVES

The objectives of the Westinghouse-AFOSR program are:

1. Investigate methods of high-T_c oxide film growth.
2. Search for optimal tunneling barriers, encapsulation, and metallic contact materials compatible with high-T_c oxide superconductors.
3. Grow epitaxial high-T_c oxide films and coherent, layered film structures incorporating tunneling barriers.
4. Study tunneling into high-T_c oxide films and other pertinent electronic properties of films.
5. Develop and evaluate new fabrication and device concepts exploiting the unique properties of high-T_c oxide superconductors.
6. Investigate the integration of semiconductor and high-T_c superconducting films by characterizing their interfaces.

4. ACCOMPLISHMENTS

4.1 PREAMBLE

The research reported here was done under a Westinghouse-AFOSR Program which began in January 1988 and ended December 31, 1990. The specific objectives of this program are listed in Section 3 of this report. These objectives are identical to the Tasks of the Work Statement. The first five of these tasks were operative during the entire three years. The sixth task was added for just the second half of the first year of the program.

The overall objective was to fabricate and characterize layered film structures incorporating high-critical-temperature oxide superconductors in a manner permitting electronic device applications. Components fabricated from these film structures will form a base for the technology of superconducting electronics capable of operating at or above 50K. A summary of the research performed during the three years of the program is given in this report. A more detailed description is contained in scientific publications generated under the auspices of the program. These are included as an appendix to this report.

4.2 HIGH OXIDE FILM GROWTH

There are three materials systems which include superconducting compounds that have critical temperatures sufficiently greater than 50K to allow the fabrication of superconducting devices capable of operating at or above this temperature. The prototypal compounds from each of these systems are $YBa_2Cu_3O_7$ (YBCO), $Tl_2Ca_2Ba_2Cu_3O_{10}$ (TBCCO), and $Bi_2Sr_2Ca_2Cu_3O_{10}$ (BSCCO). Of these three compounds, it was decided not to investigate the growth of BSCCO films because of the reported severe difficulty in obtaining single phase 2223 films, the phase which has a T_c of 110K. For TBCCO it is equally difficult to obtain the pure 125K 2223 phase; however the competing

1223 and 2212 phases both have T_c's greater than 110K. This system thus could not be ignored for potential applications at temperatures >>50K and part of the work under this task was directed toward the preparation of films of this compound. However, most of the work on film growth for this program was concentrated on YBCO. This compound, both in bulk and thin film form, had been better characterized than any of the other oxide superconductors. Its combination of properties indicated that it was the best candidate for potential high-temperature applications.

In addition to YBCO and TBCCO, growth experiments were performed on a third oxide superconductor, namely, $La_{2-x}Sr_xCuO_4$ (LSCO). Although LSCO has a relatively low critical temperature of about 40K and thus could not be used to fulfill the overall objective of this program, these studies were done to gain insights in various problems areas including tunneling, multilayer epitaxy, and surface smoothness. In the next three sections the work done on YBCO, TBCCO, and LSCO film growth is summarized.

4.2.1 YBCO Films

During the past three years a variety of thin film growth methods for the preparation of YBCO films were investigated under this as well as other complementary research programs here at Westinghouse. These techniques include sputtering, evaporation, chemical vapor deposition, and laser ablation. Films with excellent superconducting properties were produced by each of these methods. However, taking all factors into consideration including structural and chemical homogeneity, surface smoothness, and relatively low formation temperature, the properties of films made by sputtering were deemed to be superior. Therefore most of the research effort on YBCO film growth for this program was directed toward optimizing this deposition technique.

The initial YBCO films prepared by sputtering were made by first depositing an amorphous film and then ex-situ annealing at 850°C to crystallize the superconducting compound. These films were found to have a-axis epitaxy and T_c's above 80K. However they were also found to have degraded surface layers, primarily due to diffusion of Ba toward the surface during annealing. A

fast-ramp in-situ annealing process was developed to alleviate this problem. Using this process, films were prepared which were shown to be superconducting up to their surfaces. Tunnel junctions made with these films as base electrodes exhibited a superconducting gap structure. However, as will be discussed in more detail in Section 4.5 of this report, the quality of these junctions was very poor. When efforts to improve junction quality failed, emphasis was directed toward developing a lower temperature sputtering technique to determine whether improved junctions could be achieved by further improving the surface quality of the YBCO films.

An extensive study of single target sputtering of YBCO at ≤700°C substrate temperatures was instituted. The critical parameters in this process were identified and then optimized to allow the reproducible deposition of films with T_c's >90K and J_c's >>10^6 Amps/cm^2, at 77K. In addition to determining their critical temperatures and currents the films were characterized as follows: Structural properties were studied by x-ray diffraction, rocking curve widths, scanning electron microscopy, and transmission electron microscopy. The properties measured at rf frequencies were ac susceptibility and rf surface resistance with shielding currents flowing on either the free-surface side of the films or on the substrate side. The chemical composition and homogeneity were determined by electron microprobe or energy-dispersive spectroscopy (EDS) with Auger spectroscopy depth profiles used to check composition uniformity in the direction of film growth. Surface composition and structure were examined by x-ray and ultraviolet photoelectron spectroscopy, and by reflection high-energy and low-energy electron diffraction, respectively. Additional characterization made as part of collaborative research with groups outside Westinghouse involved the measurement of optical reflection and absorption, magnetic penetration depth, complex conductivity, Hall effect, thermoelectric properties, quasiparticle lifetime, flux flow, x-ray absorption, and anisotropy of magnetization and critical current. Based on these data the YBCO films made for this program were determined to be equal or superior to those made elsewhere regardless of technique used.

Data were also gathered which contributed toward the understanding of the film growth process. Experimental results were obtained which indicated that the >90K YBCO orthorhombic structure is sufficiently unstable that even a relatively mild particle bombardment of the substrate surface during film growth can prevent its formation. Under such conditions, a closely related structure is formed which has inferior superconducting properties. From analyses by x-ray diffraction and by EDS, this material is indistinguishable from the highest-T_c YBCO phase. It was also found that to form YBCO films which have optimum properties, a stronger oxidizing agent than molecular oxygen must be present. Otherwise, films which are compositionally and structurally similar to the >90K YBCO phase are formed. These also have inferior superconducting properties. It was found that water vapor is a sufficiently strong oxidizing agent to fulfill this requirement.

A surprising result from this study was the finding that films need not have overall 1:2:3 stoichiometry in order to have optimum superconducting properties. In such cases, the excess elements are present as second phase particles. The properties of off-stoichiometric films were found to be degraded only when the volume fraction of second phase particles became significant. Although the presence of minor amounts of second-phase particles on the surface of films was demonstrated to have no deleterious effect on either their superconducting properties or their application in single-layer devices, such particles present a serious problem in multilayer devices such as trilayer Josephson junctions. Although essentially particle-free YBCO films can and have been deposited, conditions under which this can be done in a controlled and reproducible manner have not yet been established. Further work in this area is therefore very important.

Finally, it is worth noting that the methods and understanding of YBCO thin film growth developed under this program currently serve as the materials base for more than fifteen projects in HTS electronics at Westinghouse.

4.2.2 TBCCO Films

TBCCO films were prepared by co-sputtering from Tl, Ba-Ca, and Cu targets. Because of the high vapor pressure of Tl at the temperatures required to crystallize the superconducting phases, films deposited at such temperatures were invariably Tl deficient and non-superconducting. To obtain superconducting films it was necessary to post-anneal the as-deposited films in a closed container under a pressure of thallium. Using this technique optimum T_c's of 117K (R = 0) and 113K (inductive) were achieved. Qualitative agreement with the best results elsewhere were also observed in the areas of epitaxial growth, phase homogeneity, rf surface resistance, smoothness, and surface composition. Single-phase films were obtained with the formal Tl:Ba:Ca:Cu ratio equal to 2212 and 1223. However, with the exception of critical temperature, TBCCO films were found to inferior to YBCO for the study of fundamental scientific issues and utility in a wide range of applications. A significant improvement in TBCCO films is not expected unless an in-situ growth technique is developed.

4.2.3 LSCO Films

Using techniques developed for YBCO growth, the very first set of LSCO films deposited were found to be superconducting. Ultimately, T_c's of 31K were obtained which exceeded by 2K the highest previously reported value for LSCO films. Critical current densities and rf surface resistances were also better than for LSCO produced anywhere else. The optimum growth temperature was found to be approximately 50°C lower than that required for YBCO. In common with YBCO, the best films grew epitaxially with a c-axis orientation on $SrTiO_3$, $LaAlO_3$, and $NdGaO_3$ substrates. In contrast to YBCO, excellent quality c-axis films could be grown directly on sapphire at relatively low temperatures.

4.3 OPTIMUM BARRIERS, ENCAPSULATION, AND METALLIC CONTACTS

The goals of this task were primarily technological. For high-T_c films to be used as the basis of a new technology, it must be necessary to 1) be able to make good electrical contact to them, 2) ensure that their properties do not degrade over time, and 3) provide flexibility to device designers by growing them on large-area substrates with a variety of dielectric properties.

Based on its availability in large wafers, as well as its mechanical and thermal properties, sapphire is the best substrate candidate either for high-Q or high-frequency applications (> X band) where a relatively low dielectric loss tangent or dielectric constant is required. However, the growth of YBCO directly on sapphire is impeded by the large lattice mismatch and the fact that Al contamination severely degrades the properties of YBCO.

To improve the quality of YBCO films on sapphire, the use of two epitaxial buffer layers was investigated. The study of MgO(100) buffer layers on α-Al_2O_3 ($1\bar{1}02$) was initiated under this program. Additional development at Westinghouse continued under DARPA sponsorship. The successful growth of $La_{2-x}Sr_xCuO_4$ (LSCO) on sapphire (described in Section 4.2.3) suggested the use of this perovskite-related structure as another possible buffer layer for YBCO. The YBCO films grown on LSCO-buffered sapphire were found to have T_c's >90K and self-field J_c's $>10^6$ A/cm^2 at 77K. Two compositions of LSCO were used; an insulator with $x = 0$ and a $T_c = 30$K superconductor with $x \simeq 0.2$. Patent applications were filed for both the epitaxial MgO and LSCO buffer layers. Films of YBCO grown on either type of buffer layer had rf properties superior to Cu at frequencies lower than S band. In common with YBCO and the best high-dielectric-constant substrates, LSCO has a perovskite-related structure and a close lattice match to YBCO. For these reasons, it should ultimately be a better buffer layer material than MgO although its performance in this project was similar to epitaxial MgO buffer layers.

The issue of whether HTS films must be encapsulated to prevent degradation was addressed by remeasuring the transport properties of ultrathin

films made over a period of one year. It was found that contact resistance to the surface of high-quality YBCO films increased after only a few hours of exposure to the atmosphere. Films up to 10 nm thick degraded throughout their thickness over a period of weeks. However, measurements of thicker films indicated that the degraded 10 nm passivated the surface and protected films from further atmospheric degradation. Encapsulation thus does not appear to be an important requirement for the long-term application of high-quality films.

Gold contacts to high-T_c superconductors were annealed in oxygen at 600°C to obtain contact resistances $<10^{-10}$ Ω-cm^2 in a joint Westinghouse/AFOSR program in 1987. AFOSR and Westinghouse have been granted a broad patent for this technique. It has been used successfully throughout this program and at most laboratories in the world for both routine measurements and prototype device production. There does not appear to be a need for further investigation of this issue.

4.4 EPITAXIAL FILMS AND LAYERED STRUCTURES

The emphasis of this program on epitaxial growth reflects a belief that epitaxial films will be required for virtually all HTS applications in both cryogenic electronics and basic scientific studies. An x-ray diffractometer has been used on a routine basis to establish the growth orientation of all films. All of the high-T_c films grown, YBCO, TBCCO, and LSCO, were grown with a c-axis orientation on the (100) faces of all the important single-crystal substrate materials. X-ray rocking curves widths were found to correlate with the extent of mismatch between the lattice constant of YBCO and the substrate. A minimum rocking curve width was obtained for each film when the lattice constant of the substrate most closely matched that of film.

The relative orientation of superconductor and substrate in the plane of the films were measured by Weisenburg x-ray camera, LEED, RHEED, or electron diffraction. All of the film/substrate combinations which produced a c-axis orientation also produced epitaxial films which were aligned with major axes in the substrate. For YBCO, the substrates used for c-axis growth were (001) faces of $LaAlO_3$, $NdGaO_3$, $SrTiO_3$, MgO, yttria-stabilized ZrO_2 (YSZ),

and $(1\bar{1}02)$ sapphire. Low substrate temperatures (~600°C) for either the superconductor or a $PrBa_2Cu_3O_7$ (PrBCO) buffer layer were used to grow predominantly a-axis YBCO films. Epitaxial films were also grown on the (110) face of $SrTiO_3$ and MgO.

Transmission electron microscopy was used to characterize a small selection of YBCO films. It was found that a typical film grown on $LaAlO_3$ was not only epitaxial, but had a single crystal matrix. Within the matrix were some a-axis grains (~3%) and CuO particles. The films were untwinned over the ~1 mm^2 area examined by TEM.

Often, when second-phase particles were present in the films, they also grew epitaxially. In Y-rich YBCO, $Y_2Cu_2O_5$ precipitates found in TEM were aligned with the substrate. In the case of LSCO films grown on sapphire, approximately 3% of the film grew epitaxially with a (211) growth orientation in a matrix of 97% c-axis oriented material. The epitaxial relationship between MgO(001) substrates and YBCO(001) films was particularly interesting due to the large lattice mismatch. From LEED and RHEED patterns, it was shown that a small fraction of c-axis YBCO grains were misaligned by 45° in the plane of the film.

Based on the unique tools available to this program, it was possible to demonstrate (from in-situ LEED and RHEED patterns) that all epitaxial LSCO and YBCO films maintained their perovskite-related structure to within a monolayer of the surface whether they had a c-axis or a-axis orientation. The a-axis YBCO films exhibited a "3x1 surface reconstruction" due to the 3:1 ratio of c-axis to a-axis lattice constants. The c-axis YBCO films exhibited a new manifestation of the anisotropy within the a-b plane – a 2x1 surface reconstruction when the surface was fully oxygenated.

To determine whether YBCO film surfaces were metallic, an ultraviolet photoelectron spectroscopy (UPS) study was performed as a function of film temperature. Film surfaces exposed to the vacuum environment at room temperature were insulating. However, film surfaces cooled to 50K in oxygen and then exposed to vacuum were metallic with a non-zero density of electronic states similar to that observed in UPS spectra obtained in other laboratories on

cold, cleaved single crystals of YBCO. The indication was that the oxygen diffused out from the surface at a diffusion rate which could be slowed by cooling.

Layering of epitaxial HTS films with deposited insulators and normal conductors is necessary for sandwich-type S-I-S and S-N-S Josephson junctions, compact transmission and delay lines, crossovers and interconnects in integrated circuits, and pickup coils in sensor applications. Epitaxial multilayers were fabricated with YBCO(001) superconductors and $SrTiO_3$(001), LSCO(001), $PrBa_2Cu_3O_7$(001) (PrBCO), and $LaAlO_3$(001). (The PrBCO multilayers were developed under SDIO sponsorship). Deposited $LaAlO_3$(001) layers are the most promising for thick dielectrics due to their low loss tangent. Deposited $La_{2-x}Sr_xCuO_4$(001) layers with $x = 0.3$ are the most promising for Josephson junctions since their relatively high conductivity permits the greatest barrier thickness.

4.5 ELECTRONIC PROPERTIES AND TUNNELING INTO HTS FILMS

The initial attempts to demonstrate tunneling into a high-T_c oxide superconductor employed an S-I-S configuration which had YBCO as the base electrode and a conventional superconductor (Nb) as the counter electrode. The YBCO base electrodes had a-axis orientation and were grown by sputtering amorphous films and then post annealing these films as described in Section 4.2.1 of this report. MgO was used as the barrier layer. Some of the junctions had pinhole-free barriers and exhibited tunneling. An MgO barrier thickness of approximately 4.5 nm was found to be optimal. The junctions, however, showed no Josephson critical current and had a large excess conductance below the energy gap. Nevertheless, gap values could be accurately extracted from derivative curves (dV/dI vs. V). From these data an energy gap, $\Delta(0)$, of 19.5 mV was obtained for YBCO ($2\Delta/kT \simeq 5.5$). Attempts to improve junction quality by investigating other barrier materials and using gold proximity layers were unsuccessful.

An important result was obtained from trilayers with thinner barrier layers. Superconducting shorts between electrodes were observed. Although

disappointing with respect to the primary goal of producing practical tunnel junction, this result was important in that it provided non-ambiguous evidence that the YBCO films were superconducting up to their surfaces. It also dismissed some theoretical speculation prevalent at that time which suggested that it might be impossible to maintain a supercurrent between a high-T_c oxide and a classical superconductor.

Interestingly, reports of YBCO based junctions from other laboratories throughout the world described junction performance very similar to those detailed here. In every case, dI/dV measurements showed a gap-like feature which indicated a low-temperature energy gap of approximately 20 mV for YBCO. Also, in every case a high density of sub-gap states in the YBCO was observed. In fact, the similarity of these results has led to some speculation that these sub-gap states are intrinsic to YBCO and other high-T_c oxide superconductors. It is our opinion, however, that such speculation is premature and that the poor junction performance obtained thus far is more probably a material problem associated with the difficulty of preparing non-degraded YBCO material to within a coherence length of a film surface. This belief has led to our discontinuing the post-annealing method for preparing YBCO films to be used in junctions and the development of the in-situ technique described in Section 4.2.1. This was done under the rationale that lower temperature growth should be able to produce films with better surface quality. To date, however, junctions made with in-situ sputtered films show no improvement and the fabrication of high quality YBCO based tunnel junctions remains one of the major unsolved problems in the area of high-T_c superconductivity.

The most important electronic property of high-T_c superconductors for a large class of analog signal processing applications is the rf surface resistance, R_s. It is related to tunneling measurements and the electronic structure of superconductors in that a low density of electronic states below the superconducting gap energy leads to a low R_s. Early in the program, R_s was measured by inserting a YBCO film in a Nb or Cu resonating cavity or by replacing a cavity endplate with YBCO. The sensitivity of these techniques was adequate when losses in the YBCO were greater than in Cu at 77K and

greater than in Nb at 4.2K. However, the crystalline as-deposited films grown in the latter half of the program had R_s values too low to be measured by these techniques. Two new techniques were adopted which were based on all-high-T_c resonators. Design parameters of both types of resonators were adjusted to maximize sensitivity to low-R_s films.

The R_s measurements showed that the best YBCO films made here by off-axis sputtering had the lowest R_s reported at 77K, 200 $\mu\Omega$. Since R decreases as a film is cooled below T_c, R_s at 77K is minimized mainly by maximizing T_c. The slightly higher T_c values obtained under this program relative to other laboratories is tentatively attributed to the use of water vapor in the sputtering gas. At 4.2K, films prepared here and elsewhere have a residual surface resistance comparable to that of Nb at 4.2K which is much greater than expected from a straightforward application of BCS theory. Nevertheless, R_s of YBCO films is sufficiently low that microwave devices demonstrated by other programs at Westinghouse – bandpass filters, delay lines, STALOs, and antenna matching networks – showed markedly improved performance over conventional devices and were limited in their performance by factors other than the measured R_s.

Films were sent to a number of other laboratories (see Section 7) to aid in calibrating and understanding surface resistance data.

4.6 NEW FABRICATION AND DEVICE CONCEPTS

Two new fabrication capabilities were demonstrated in 1990 with the deposition of in-situ-grown YBCO films on 2-inch diameter substrates and on both sides of substrates. Both $LaAlO_3$(100) and LSCO-buffered sapphire single-crystal substrates were used for growth of 2-inch diameter films. They were the only practical substrates for HTS growth that are available in such sizes ($NdGaO_3$ is now available, as well).

Further investigation of YBCO films on 2-inch wafers is presently being continued under two device-development programs. For one program, sponsored by DARPA, two 2-inch diameter YBCO films are being tested as the endplates in a cylindrical dielectric resonator. The Q and phase noise of the

dielectric resonator will determine whether it can replace state-of-the-art stabilized local oscillators (STALOs). The second program requires a large film area to make a 15 ns delay line (measured to be 14.6 ns) from a microstrip transmission line. Films on 2-inch diameter substrates will also be required for a pending DARPA program to make an integrated channelized receiver. Several other programs now require films on 1-inch diameter wafers.

Film growth of high quality YBCO on both sides of a single substrate was achieved by changing the technique for mounting substrates from one requiring bonding of the substrate for good thermal conduction to one in which the substrate was heated solely by radiation. Two-sided deposition is presently being used by device development programs at Westinghouse to fabricate microstrip structures. Previously, microstrip lines were assembled by stacking a patterned YBCO film on one substrate on top of a YBCO ground plane on a second substrate, or using a gold ground plane deposited on the back of the patterned YBCO film. The problems solved by two-sided deposition were, respectively, air gaps between the two substrates and high losses in the gold ground plane.

The high quality of YBCO films grown on 2-inch diameter substrates was established by measurements of T_c, J_c, and R_s. The maximum critical temperatures and currents of pieces cut from the large wafer were similar to that achieved on smaller substrates. The T_c varied by only $\pm$1K and the J_c by $\pm$20% at 77K. A pair of 1/2 x 1/4 inch chips cut from a 2-inch $LaAlO_3$/YBCO wafer had R = 200 $\mu\Omega$ at 77K and 10 GHz. The uniformity and reproducibility of substrate temperature was found to be the most important parameter in determining film uniformity. The temperature of the substrate holder was measured by a unique optical pyrometer which measures the emissivity of a surface with reflected IR laser light at the same time as it measures light intensity.

Preliminary experimental work was performed to investigate the properties of flux-flow transistors (FFT) being developed at the University of Wisconsin and Sandia Laboratory. From the perspective of a device physicist, the crucial issue in the fabrication of FFTs is whether weak links exhibiting

Josephson behavior are necessary in the FFT constrictions. Westinghouse YBCO films were patterned into 3 μm wide bridges using wet chemical etching in a dc SQUID configuration. No signs of weak links were observed as indicated by either a reduction of the critical current density compared with a wide stripe, or modulation of the critical current in a magnetic field. Films of this quality represent one extreme case from which FFTs can be patterned. The other extreme can be satisfied by ultrathin YBCO films that are more likely to show granular behavior. Films of both extremes were used in previous studies of FFTs: Nb at Wisconsin and granular TBCCO at Sandia. The YBCO films fabricated as part of this program were patterned into FFT structures at the University of Wisconsin.

New devices are possible if high-T_c superconductors can be deposited on ferroelectric or piezoelectric substrates. Survey experiments found that LSCO buffer layers permitted YBCO superconducting films to be grown on Si and GdGa garnet (GGG), but not on YAG or $LiNbO_3$. Epitaxial bismuth titanate films were grown on YBCO.

4.7 SUPERCONDUCTOR/SEMICONDUCTOR INTERFACE CHARACTERIZATION

A new method for fabricating contacts between superconducting stripline interconnects and semiconductor devices was conceived for which a patent disclosure was filed. Epitaxial films of cubic ZrO_2 (YSZ) were studied as a buffer layer for YBCO growth on silicon. The growth temperatures required for YBCO films were too high to consider growth on GaAs. This task was funded for just the second half of 1988. Although the growth temperature of YBCO films was reduced to a minimum of approximately 600°C in the latter half of the project, it is still too high for integration of a high-T_c superconductor and GaAs on a single wafer.

4.8 OTHER ACCOMPLISHMENTS

In support of the work described above, a file of preprints and reprints on high-T_c superconductivity has been maintained. The list of papers was

entered into a computer and keywords were assigned to the papers to aid in retrieval. Special issues of the Journal of Superconductivity were published in 1989 and 1990 with the lists of papers and an extensive index. A 1990 update is scheduled for publication in early 1991. The entire bibliographic database and the attendant search software that was in use at Westinghouse for the last three years was made available in computerized form to the entire technical community through *High-T_c Update* in August 1990.

5. PUBLICATIONS

1. "Effects of Irradiation Damage on the Normal-State and Superconducting Properties of NbN Thin Films," J. Y. Juang, D. A. Rudman, J. Talvacchio, and R. B. van Dover, Phys. Rev. B 38(4) (1988).

2. "Near-Surface Atomic Segregation in YBCO Thin Films," J. R. Gavaler and A. I. Braginski, Physica C 153-155, 1435 (1988).

3. "Material Constraints on Electronic Applications of Oxide Superconductors," A. I. Braginski, Physica C 153-155, 1598 (1988).

4. "Crystal Lattice Measurements in Superconducting Materials," F. W. Lytle, E. C. Marques, R. B. Greegor, H. G. Ahlstrom, E. M. Larson, D. E. Peterson, and A. J. Panson, SPIE Proc. Vol. 879 Sensing, Discrimination, and Signal Processing and Superconducting Materials and Instrumentation, ed. by R. Nichols and J. A. Ionson (SPIE, Bellingham, Washington, 1988) pp. 142-149.

5. "Fabrication of High-T_c Superconducting $YBa_2Cu_3O_7$ Films," J. R. Gavaler, A. I. Braginski, J. Talvacchio, M. A. Janocko, M. G. Forrester, and J. Greggi, in MRS Vol. EA-14: High-Temperature Superconductors II, ed. by D. W. Capone II, W. H. Butler, B. Batlogg, and C. W. Chu (Mater. Res. Soc., Pittsburgh, 1988) pp. 193-196.

6. "In-Situ Fabrication, Processing, and Characterization of Superconducting Oxide Films," A. I. Braginski, J. Talvacchio, J. R. Gavaler, M. G. Forrester, and M. A. Janocko, in SPIE Proceedings Vol. 948, High-T_c Superconductivity: Thin Films and Devices, ed. by R. B. van Dover and C. C. Chi (SPIE, Bellingham, Washington, 1988) pp. 89-98.

7. "Critical Currents of 85K Bi-Sr-Ca-Cu-O," G. R. Wagner, J. Talvacchio, and A. J. Panson, Mater. Lett. 6, 390 (1988).

8. "Prospects for Thin-Film Electronic Devices of High-T_c Superconductors," A. I. Braginski, M. G. Forrester, J. Talvacchio, and G. R. Wagner, Proc. 5th International Workshop on Future Electron Devices (Miyagi-Zao, Japan, 1988) pp. 171-179.

9. "Electrical Contact to Superconductors," J. Talvacchio, in Electrical Contracts – 1988, ed. by C. A. Haque and P. Theisen (IEEE, New York, 1988) pp. 109-120.

10. "Superconducting Stripline Resonator Performance," B. R. McAvoy, G. R. Wagner, J. D. Adam, and J. Talvacchio, IEEE Trans. Magn. 25(2), 1104 (1989).

11. "Comparison of $YBa_2Cu_3O_7$ Films Grown by Solid-State and Vapor-Phase Epitaxy," J. Talvacchio, J. R. Gavaler, J. Greggi, M. G. Forrester, and A. I. Braginski, IEEE Trans. Magn. 25(2), 2538 (1989).

12. "Optimization of YBCO Surfaces for Tunnel Junctions," J. R. Gavaler, A. I. Braginski, M. G. Forrester, J. Talvacchio, and J. Greggi, IEEE Trans. Magn. 25(2), 803 (1989).

13. "Electrical Contact to Superconductors," J. Talvacchio, IEEE Trans. CHMT, 12(1), 21 (1989).

14.* "Bibliography of High-T_c Superconductivity," J. Talvacchio, J. Superconductivity 2(1), 1-210 (1989).

15. "'MBE' of Superconducting Materials," A. I. Braginski and J. Talvacchio, to appear in Modern Superconducting Devices, ed. by S. T. Ruggiero and D. A. Rudman (Academic Press, New York, 1989).

16. "Preparation and Characterization of Superconducting Surfaces in High-T_c Superconductors," G. R. Wagner, R. M. Silver, J. Talvacchio, J. R. Gavaler, and A. J. Panson, Proc. 2nd Workshop on HTS Electron Devices, Shikabe, Japan (1989) pp. 335-340.

17. "Physical Characterization of HTS Films, A. I. Braginski, "Proc. 2nd Workshop on HTS Electron Devices, Shikabe, Japan (1989), pp. 313-316.

18. "Properties of YBCO-Based Tunnel Junctions," J. R. Gavaler, M. G. Forrester, and J. Talvacchio, Physica C 162-164, 1051 (1989).

19.* "High-T_c Superconductivity in 1989," J. Talvacchio, J. Superconductivity, 3(1), 1-155 (1990).

20. "Optimization of T_c and J_c in Sputtered YBCO Films," J. R. Gavaler, and J. Talvacchio, Physica B 165-166, 1513 (1990).

21. "High-T_c Film Development for Electronic Applications," J. Talvacchio, and G. R. Wagner, in Superconductivity Applications for Infrared and Microwave Devices, SPIE Proc. Vol. 1292 (1990).

22. "Anomalous Hall Effect in Superconductors near their Critical Temperatures," S. J. Hagen, C. J. Lobb, R. L. Greene, M. G. Forrester, and J. H. Kang, Phys. Rev. B, 41 11630 (1990).

*Not included due to its large number of pages.

23. "YBCO and LSCO Films Grown by Off-Axis Sputtering," J. Talvacchio, M. G. Forrester, J. R. Gavaler, and T. T. Braggins, in Science and Technology of Thin Film Superconductors II, edited by R. McConnell and S. A. Wolf (Plenum, New York, 1990).

24. "Flux Flow Nernst Effect in Epitaxial YBCO Films," S. J. Hagen, C. J. Lobb, R. L. Greene, M. G. Forrester, and J. Talvacchio, Phys. Rev. B 42(10), 6777 (1990).

25. "Fabrication and Characterization of YBCO-based S-N-S-type Josephson Junctions," M. G. Forrester, J. Talvacchio, J. R. Gavaler, to be published in IEEE Trans. Magn. 27(2) (1991).

26. "Large-Area YBCO Films for Microwave Applications," J. Talvacchio, M. G. Forrester, J. R. Gavaler, and T. T. Braggins, to be published in IEEE Trans. Magn. 27(2) (1991).

27. "Critical Parameters in Single Target Sputtering of YBCO," J. R. Gavaler, J. Talvacchio, T. T. Braggins, and J. Greggi, to be submitted to J. Appl. Phys. (1991).

6. PERSONNEL

J. R. Gavaler
J. Talvacchio
A. I. Braginski*

} Principal Co-Investigators

T. T. Braggins
M. G. Forrester
M. A. Janocko
A. J. Panson
G. R. Wagner

*Until June 1, 1989.

7. COUPLING ACTIVITIES*

1. "Near-Surface Atomic Segregation in YBCO Thin Films," J. R. Gavaler and A. I. Braginski, Contributed presentation at High-T_c Superconductors and Materials and Mechanisms of Superconductivity, Interlaken, February 1988.

2. "Material Constraints on Electronic Applications of Oxide Superconductors," A. I. Braginski, Invited presentation at High-T_c Superconductors and Materials and Mechanisms of Superconductivity, Interlaken, February 1988.

3. "In-Situ Fabrication, Processing, and Characterization of Superconducting Oxide Films," J. Talvacchio, A. I. Braginski, J. R. Gavaler, M. A. Janocko, and M. G. Forrester, Invited presentation to SPIE Meeting, Newport Beach, March 1988.

4. "Near-Surface Composition and Properties of YBCO Films," J. R. Gavaler, M. A. Janocko, J. Talvacchio, M. G. Forrester, and A. I. Braginski, Contributed presentation at the March Meeting of the American Physical Society, New Orleans, March 1988.

5. "Microstructural Investigation of Epitaxial YBCO Films," J. Greggi, J. Talvacchio, J. R. Gavaler, and A. I. Braginski, Contributed presentation at the March Meeting of the American Physical Society, New Orleans, March 1988.

6. "$SrTiO_3$ Substrate Preparation and Nucleation of $YBa_2Cu_3O_7$ Thin Films," J. Talvacchio, Contributed presentation at the March Meeting of the American Physical Society, New Orleans, March 1988.

7. "Critical Currents of 85K Bi-Sr-Ca-Cu-O," A. J. Panson, G. R. Wagner, and J. Talvacchio, Contributed presentation at the March Meeting of the American Physical Society, New Orleans, March 1988.

8. "Fabrication of High-T_c Superconducting $YBa_2Cu_3O_7$ Films," J. R. Gavaler, A. I. Braginski, J. Talvacchio, M. A. Janocko, M. G. Forrester, and J. Greggi, Invited presentation to the Materials Research Society Spring Meeting, Reno, April 1988.

*Speaker's name is underlined.

9. "Epitaxial Growth and In-Situ Analysis of Thin Films for Superconductive Electronics," J. Talvacchio, Seminar at IBM T. J. Watson Research Center, Yorktown Heights, May 1988.

10. "Prospects for Thin-Film Electronic Devices of High-T_c Superconductors," A. I. Braginski, M. G. Forrester, J. Talvacchio, and G. R. Wagner, Invited presentation to the 5th International Workshop on Future Electron Devices, Miyagi-Zao, Japan, June 1988.

11. "Mechanisms of J_c Limitation in High-T_c Oxide Superconductors," A. I. Braginski, Invited panel presentation to the 5th International Workshop on Future Electron Devices, Miyagi-Zao, Japan, June 1988.

12. "Progress Toward Electronic Applications of High-T_c Superconductors," A. I. Braginski, Invited presentation to the Materials Research Society International Meeting on Advanced Materials, Tokyo, June 1988.

13. "Electronic Applications of High-T_c Superconductors," A. I. Braginski, Seminars at Hitachi CRL, Sumitomo, Matsushita, Fujitsu-Atsugi, and NTT Ibaraki Laboratories, June 1988.

14. "Comparison of $YBa_2Cu_3O_7$ Films Grown by Solid-State and Vapor-Phase Epitaxy," J. Talvacchio, J. R. Gavaler, J. Greggi, and A. I. Braginski, Contributed presentation to the Applied Superconductivity Conference, San Francisco, August 1988.

15. "Evaluating Superconductor Resonator Materials," B. R. McAvoy, G. R. Wagner, J. D. Adam, J. Talvacchio, and M. M. Driscoll, Contributed presentation to the Applied Superconductivity Conference, San Francisco, August 1988.

16. "Optimization of YBCO Surfaces for Tunnel Junctions," J. R. Gavaler, A. I. Braginski, M. G. Forrester, and J. Talvacchio, Contributed presentation to the Applied Superconductivity Conference, San Francisco, August 1988.

17. "Materials for High-Temperature Superconducting Electronics," J. Talvacchio, Physics Department Colloquium at the University of Akron, September 1988.

18. "Electrical Contact to Superconductors," J. Talvacchio, Invited presentation to the Applied Superconductivity Conference, San Francisco, August 1988.

19. "Properties of Surfaces and Interfaces of High-T_c Superconductor Films for Electronic Applications," J. Talvacchio, Invited presentation to the Electrochemical Society Meeting, Symposium on High-Temperature Superconductor Technologies, Chicago, October 1988.

20. "Properties of Surfaces and Interfaces of High-T_c Superconductor Films for Electronic Applications," J. Talvacchio, Invited presentation to the International Superconductor Applications Convention, San Francisco, January 1989.

21. "Properties of Surfaces and Interfaces of High-T_c Superconductor Films for Electronic Applications," J. Talvacchio, Seminar at Superconductor Technologies Inc., Santa Barbara, January 1989.

22. "Fabrication and Electrical Properties of YBCO Tunnel Junctions," J. R. Gavaler, M. G. Forrester, and J. Talvacchio, Contributed presentation to the American Physical Society March Meeting, Bull. Am. Phys. Soc. 34(3), 422 (1989).

23. "Relationship between the Microstructure of High-T_c Superconductors and Electronic Applications," J. Talvacchio, Invited presentation to the Scanning Electron Microscopy Conference, Salt Lake City, May 1989.

24. "Physical Characterization of HTS Films," A. I. Braginski, Invited presentation to the Second International Conference on Future Electron Devices, Shikabe, Japan, June 1989.

25. "Preparation and Characterization of Superconducting Surfaces in High-T_c Superconductors," G. R. Wagner, R. M. Silver, J. Talvacchio, and J. R. Gavaler, Contributed presentation to the Second International Conference on Future Electron Devices, Shikabe, Japan, June 1989.

26. "Properties of YBCO-Based Tunnel Junctions," J. R. Gavaler, M. G. Forrester, and J. Talvacchio, Contributed presentation to the Conference on Materials and Mechanisms of Superconductivity and High-T_c Superconductivity, Stanford, July 1989.

27. "Preparation of Surfaces of High-T_c Films for Superconducting Electronics," J. Talvacchio, R. M. Silver, M. G. Forrester, B. R. McAvoy, and J. R. Gavaler, Invited presentation at the New York Institute of Superconductivity Annual Conference on Superconductivity and Applications, Buffalo, September 1989.

28. "Processing of High-T_c Thin Films in Japan," J. Talvacchio and A. C. Anderson, Invited presentation to the Superconductive Electronics Workshop, Cambridge, Maryland, October 1989.

29. "HTS Film Development for Passive Microwave Components and Multilayer Devices," J. Talvacchio, J. R. Gavaler, M. G. Forrester, R. M. Silver, B. R. McAvoy, G. R. Wagner, S. A. Talisa, and T. T. Braggins, Contributed poster presentation to the Superconductive Electronics Workshop, Cambridge, Maryland, October 1989.

30. "Growth and Properties of Epitaxial High-T_c Superconductor Films," J. Talvacchio, Invited presentation at the American Association of Crystal Growers Conference, Atlantic City, October 1989.

31. "Surface Properties of High-T_c Superconductor Films," J. Talvacchio, M. G. Forrester, R. M. Silver, J. R. Gavaler, B. R. McAvoy, G. R. Wagner, and T. T. Braggins, Invited presentation at the SPIE Symposium on Superconducting Thin Films, Santa Clara, October 1989.

32. "Microstructure of High-T_c Superconducting Films for Electronic Applications," J. Talvacchio, University of Minnesota Physics Department Colloquium, Minneapolis, November 1989.

33. "Properties of HTS Films for Microwave and Multilayer Electronic Devices," J. Talvacchio, University of Alberta Physics Department Colloquium, Edmonton, Alberta, December 1989.

34. "Photoelectron and Electron Diffraction Studies of High-T_c Superconductor Surfaces," J. Talvacchio, Invited presentation to the "Pittsburgh" Conference on Applied Spectroscopy and Analytical Chemistry, New York City, March 1990.

35. "Surface Resistance of High-T_c Superconducting Films," J. Talvacchio, G. R. Wagner, S. H. Talisa, B. R. McAvoy, J. R. Gavaler, M. G. Forrester, and T. T. Braggins, Invited presentation to the Topical Conference on rf Properties of High-T_c Superconductors, Williamsburg, March 1990.

36. "Fabrication and Characterization of YBCO-based S-N-S Josephson Junctions," M. G. Forrester, J. Talvacchio, J. H. Kang, and J. R. Gavaler, Contributed presentation to the March Meeting of the American Physical Society, Anaheim, March 1990.

37. "Properties of HTS Films for Microwave and Multilayer Electronic Devices," J. Talvacchio, University of Rochester Electrical Engineering Department Colloquium, Rochester, April 1990.

38. "YBCO Films for Passive Microwave and Active Multilayer Devices," J. Talvacchio, J. R. Gavaler, T. T. Braggins, M. G. Forrester, M. A. Janocko, S. H. Talisa, B. R. McAvoy, and G. R. Wagner, Invited presentation to the SERI Superconducting Thin Film Conference, Colorado Springs, April 1990.

39. "Surface and Interface Properties of HTS Films," J. Talvacchio, Invited presentation to the AVS Symposium on High-T_c Superconductivity, Cleveland, May 1990.

40. "Optimization of T_c and J_c in Sputtered YBCO Films," J. R. Gavaler and J. Talvacchio, Contributed presentation to 19th International Conference on Low Temperature Physics (LT 19), Brighton, England, August 1990.

41. "Large-Area YBCO Films for Microwave Applications," J. Talvacchio, M. G. Forrester, J. R. Gavaler, and T. T. Braggins, Contributed presentation to the Applied Superconductivity Conference, Aspen, September 1990.

42. "Defect Structures in YBCO Thin Films and Multilayers," J. R. Gavaler, J. Talvacchio, M. G. Forrester, T. T. Braggins, and J. Greggi, Contributed presentation to the Applied Superconductivity Conference, Aspen, September 1990.

43. "Fabrication and Characterization of YBCO-based S-N-S-type Josephson Junctions," M. G. Forrester, J. Talvacchio, J. R. Gavaler, Contributed presentation to the Applied Superconductivity Conference, Aspen, September 1990.

44. "Epitaxial YBCO Films on Sapphire for Microwave Applications," T. T. Braggins, J. Talvacchio, J. R. Gavaler, R.W. Weinert, G. R. Wagner, and M. G. Forrester, Contributed presentation to the Applied Superconductivity Conference, Aspen, September 1990.

OUTSIDE COLLABORATIONS

Institution/Collaborator	Effort / Special Requirements
NASA Lewis Research Center Dr. K. B. Bhasin	Microwave transmission; complex impedance - ultrathin films
University of Illinois Prof. P. Coleman	Fabry-Perot interferometer measurements of R_s - large area films (>1 in. dia)
MIT Lincoln Laboratory Dr. A. C. Anderson	Stripline resonators - relatively large area films
China Lake Naval Weapons Dr. R. Dinger	Ring resonators; R_s measurements, antennas - relatively large areas
AT&T Bell Laboratories Dr. J. Kwo	Structure, anisotropic properties of LSCO - single-crystal LSCO films
Argonne National Laboratory Dr. D. J. Miller	TEM studies of epitaxial heterostructures - YBCO and LSCO epitaxial multilayers
University of Texas Prof. A. L. de Lozanne	Buffer layers for growth on sapphire - epitaxial insulator films
University of Oregon Prof. J. M. Valles, Jr.	*Tunneling* studies - oriented films, surfaces
University of Florida Prof. D. Tanner	Infrared reflection and absorption - single crystal LSCO films
Case Western Reserve University Prof. D. E. Farrell	Anisotropic magnetic properties - single crystal LSCO films
University of Wisconsin Prof. J. E. Nordman	Evaluation of vortex-flow transistors - epitaxial YBCO films

OUTSIDE COLLABORATIONS
(continued)

Institution/Collaborator	Effort / Special Requirements
SUNY Stony Brook Prof. F. Jona	Model surface structure using LEED IV curves - in-situ LEED data on epitaxial films
Harvard University Prof. M. Tinkham	R_s measurements as a probe of proximity effect – epitaxial S-N bilayers
Hewlett-Packard R. C. Taber	Surface resistance measurements
Yale University Prof. D. E. Prober	Degradation and restoration of film surfaces - in-situ film studies
University of Wuppertal N. Klein	Surface resistance measurements
Argonne National Laboratory Dr. D. H. Kim	Vortex dynamics in superconductors - epitaxial YBCO and NbN patterned films
Northeastern University Prof. S. Sridhar	Correlation of λ, R_s with morphology
Los Alamos National Laboratory Dr. D. W. Cooke	R_s measurements - relatively large areas
University of Maryland Prof. C. J. Lobb	Hall effect measurements; vortex dynamics - epitaxial S-I-S trilayers
Stanford University Dr. S. M. Anlage	Measurements of λ, quasiparticle lifetimes - ultrathin films

8. PATENTS

1. J. Talvacchio, "Epitaxial Buffer Layers for Growth of Oxide Superconductors on Sapphire," Disclosure No. RDS-88-046, filed October 1988.

2. J. Talvacchio, "Method for Making High-Current, Ohmic Contact between Semiconductors and Oxide Superconductors," Disclosure No. RDS-88-057, to be filed.

3. J. Talvacchio and R. M. Silver, "Method for Preparation and Preservation of Surfaces of High-T_c Superconductor Films," Disclosure No. RDS-89-046, filed June 1989.

4. M. G. Forrester and J. Talvacchio, "Lanthanum Copper Oxide Buffer Layers for Growth of High-T_c Superconductor Films," Disclosure No. RDS 90-065, filed February 1991.

5. J. R. Gavaler and T. T. Braggins, "The Sputtering of YBCO Films in Water Vapor," Disclosure No. 90-074, filed February 1991.

APPENDIX

Effects of ion irradiation on the normal state and superconducting properties of NbN thin films

J. Y. Juang and D. A. Rudman
Department of Materials Science and Engineering, Massachusetts Institute of Technology, Cambridge, Massachusetts 02139

J. Talvacchio
Westinghouse Research and Development Center, Pittsburgh, Pennsylvania 15235

R. B. van Dover
AT&T Bell Laboratories, Murray Hill, New Jersey 07974

(Received 31 December 1987)

The effects of ion-beam-induced damage on the normal state and superconducting properties of NbN were investigated in both single crystal and polycrystalline thin films. Three sets of films were damaged by 200-keV Ar^+ ions with dosages up to 5×10^{16} ions/cm^2. The superconducting critical temperature (T_c) of the single crystal films decreased by 20% at the highest ion dosage. Changes in the resistivity, T_c, and critical field (and its slope at T_c) suggest that T_c is suppressed by a reduction of the electron density of states at the Fermi energy due to the vacancies created by ion irradiation. The effects of ion damage are much less pronounced for the polycrystalline films. *In situ* grain growth was observed during the ambient temperature irradiation processes, which confirms the role of grain boundaries as a sink for ion-induced defects, hence minimizing the effects of irradiation in polycrystalline films.

I. INTRODUCTION

The effects of lattice disorder on the superconducting properties of high critical temperature (T_c) superconductors, especially the $A15$ materials,[1] have received extensive attention for a number of years, not only because it is important in evaluating the potential performance of the materials in practical applications, but also for the insight it gives into understanding the fundamental mechanisms governing superconductivity. This has become even more crucial with regard to the newly discovered high-T_c oxide superconductors, typified by $YBa_2Cu_3O_7$, in which the destruction of superconductivity has been observed under irradiation by oxygen and arsenic ions.[2] The ordering of oxygen vacancies[3,4] in these materials has been found to play an important role in obtaining high T_c, since it determines the spacing and configuration of Cu—O—Cu—O strings. The irradiation may perturb the ordering of oxygen vacancies, and hence destroy the superconductivity.

Stoichiometric NbN is a metastable ceramic compound at ambient temperatures, with ordered nitrogen vacancies and residual impurities believed to be responsible for stabilizing the superconducting $B1$ phase.[5] However, NbN has been found to be very resistive to irradiation damage. For example, fast neutron doses over 10^{22} n/cm^2 produced only a 6% reduction in T_c.[6] As compared to other materials, the deposited damage energy per atom needed to change the properties of the material is about 2 to 3 orders of magnitude higher in NbN than in the new oxide superconductors, and about 1 order of magnitude higher than in $A15$ materials. It was believed[6] that the highly defective nature of NbN is responsible for the immunity of NbN to irradiation-induced damage, since it was believed that neither the electron density of states nor the degree of lattice disorder can be changed by introducing further disorder.

Recently, Jung[7] questioned whether the fast neutron damage levels used by Dew-Hughes and Jones were large enough to reach the saturation level for T_c degradation. Jung used 600 keV Ar^{2+} irradiation with doses up to 2×10^{17} ions/cm^2 to damage sputtered NbN films. The T_c of the films decreased from 15.5 to 7.5 K with damage, a much larger decrease than was found in the neutron damage study. The reduction of T_c was attributed to an increased number of vacancies in both the Nb and N sublattices, which, Jung inferred, in turn changed the electron density of states at the Fermi surface, and hence affected the T_c of the material. Since, traditionally, one expects no dependence of T_c on nonmagnetic disorder, a fact often referred to as Anderson's theorem,[8] Jung's conclusion seems plausible. However, T_c can also be influenced by localization effects, and by changes in the electron-phonon and electron-electron coupling, all of which can be a function of disorder in a material. Considering the highly defective nature of NbN and the contradiction between the reported results, a more systematic study on this subject is in order.

Unlike the effects on T_c, lattice disorder can have a very profound effect on the superconducting behavior in a magnetic field, since even in the Bardeen-Cooper-Schrieffer[9] (BCS) theory the critical field is determined by an electronic density correlation function at finite wave numbers, which is very sensitive to scattering. This is the basis of the Werthamer-Helfand-Hohenberg[10] (WHH) theory, which constitutes the standard dirty limit superconductivity theory. As has been found in most NbN films, the upper critical field (H_{c2}) deviates from the ex-

pected behavior of a dirty type-II superconductor in several aspects. First, the expected linear relation between the measured resistivity and the critical field slope at T_c, $(dH_{c2}/dT)_{T_c}$, is not observed in most NbN films.[11] Second, the temperature dependence of the upper critical field falls below the prediction of the nonparamagnetically limited WHH theory at low temperatures.[11,12] Finally, H_{c2} of most NbN films is anisotropic to some extent.[11-13] This is unexpected for cubic-structured dirty superconductors such as NbN. We have previously shown that the detailed microstructure of the films, and the associated grain boundary resistance, play an important role in each of these features, and particularly in the critical field anisotropy.[14]

In this study we will use both low resistivity single crystal and polycrystalline films to systematically investigate the effects of ion irradiation damage on NbN. By comparing results on films with and without significant grain boundary effects, the role of lattice disorder on T_c and critical field can be rigorously compared.

II. EXPERIMENTAL PROCEDURES

The success of growing NbN films epitaxially[15] on MgO and Al_2O_3 substrates provides us with an excellent opportunity to measure the fundamental properties of a "clean" NbN sample; one not dominated by grain boundary effects. A set of single crystal thin films 75 nm thick was made by one of the authors (J.T.) using a UHV sputtering deposition chamber attached to a molecular-beam epitaxy (MBE) analytical chamber. The samples were deposited onto (0001)-oriented Al_2O_3 substrates held at 700 °C, and grew epitaxially as single crystal (111)-oriented NbN as determined by low-energy electron diffraction (LEED). The resistivities of these samples range from 60 to 65 $\mu\Omega$ cm, with superconducting transitions around 17.0 K and transition widths (defined as 5–95 %) less than 0.1 K. Thus, they represent a set of identical clean NbN films.

It must be emphasized here that one of the major problems in previous studies of sputtered NbN films is the variability of film properties made in different deposition systems, or even from run to run in the same system. Both the microstructure and the composition can vary with only subtle changes in deposition conditions. As we have pointed out previously[14] for the angular dependence of $H_{c2}(T)$, these differences can affect the properties drastically. For example, different film microstructures produce very different angular dependence of $H_{c2}(T)$. It is therefore very important to begin any comparative study of NbN with samples that are well characterized and indistinguishable in their properties.

In order to reveal the role of grain boundaries on the superconducting properties, two sets of polycrystalline films were prepared by one of the authors (R.B.vD.) using reactive dc magnetron sputtering of Nb in an argon-nitrogen atmosphere onto SiO_2 substrates held at ambient temperatures (< 90 °C). Each set of samples was made in the same deposition run, with thicknesses of 44 and 135 nm. Films prepared by this technique were previously reported[16] to have fine (~ 5 nm) randomly oriented grains. These films have lower T_c than the single crystal films, with slightly larger transition widths, < 0.2 K. To further quantify the microstructure of these films, additional transmission electron microscopy (TEM) investigations have been conducted both before and after irradiation as part of this study.

Disorder was introduced into these films by bombarding the samples with 200-keV Ar^+ ions at ambient temperatures with doses ranging from 2×10^{14} to 5×10^{16} ion/cm^2. The ion energy was chosen to ensure that the projected range of the ions was greater than the film thickness, minimizing the implantation of argon in the films. Auger microprobe depth profile analysis showed no detectable argon in any region of any of these films. Note, however, that the limit of detection for argon in the presence of niobium is only about 1%. With these doses, the deposited damage energy per atom (E_a) ranges from about 10 to 10^4 eV/atom.[17] These energies are much larger than the characteristic energy (E_{a0}) needed to reduce T_c for many other superconducting nitrides.[18]

For each level of ion damage, T_c, residual resistivity (ρ_0), and critical field [$H_{c2}(T)$] were measured for each sample. T_c (defined as the midpoint of the transition) was measured resistively using a standard four-point configuration. ρ_0 was taken as the resistivity measured at temperatures just above T_c. The critical field was measured at the Francis Bitter National Magnetic Laboratory using a temperature controlled cryostat. The temperature was determined with a calibrated carbon glass resistor at zero field and controlled in the field by a capacitance thermometer. The magnetic field was applied perpendicular to the film surface for all measurements. This field orientation is the correct one to connect the upper critical field (and the critical field slope) to the measured in-plane resistivity. This observation is important in polycrystalline NbN films, where the resistivity is typically anisotropic due to the film microstructure. Surprisingly, most of the previous work on NbN fails to recognize this correspondence, and measures the parallel critical field.[19]

Only the polycrystalline samples were investigated by TEM. The samples were prepared by diluted HF acid etching. The film surface was protected by acid-resistant tape, and then immersed into diluted HF acid. The acid dissolved the SiO_2 substrate, leaving the NbN film. The flaked fragments were examined in a JEOL 200CX TEM to investigate any microstructure changes that might have occurred in the films during the irradiation processes.

III. RESULTS AND DISCUSSION

Systematically modifying the superconducting properties of the sample by introducing damage with ion irradiation proved to be a usable approach for this material. The transition widths for these samples showed nearly no change in zero field after irradiation. In an applied field, the transitions are about 1 T wide for all samples, and no broadening of the transition with increasing field was found even after irradiation damage, indicating the extreme uniformity of the samples. As a typical example,

Fig. 1 shows resistive transitions with increasing applied field for a single crystal sample damaged with a dosage of 2×10^{14} Ar^+/cm^2. The sharpness of these transitions allows unambiguous determination of both T_c and H_{c2}. In the following subsections we present our results on the effects of ion damage on transport and magnetic properties of NbN.

A. T_c, residual resistivity, and ion damage

The T_c degradation and residual resistivity changes induced by the ion damage are very different for the single crystal and polycrystalline samples. Figure 2 shows the resistivity changes as a function of ion fluence for all three sets of samples. For the single crystals, the resistivity increases as the dosage increases, then saturates at a value of about 150 $\mu\Omega$ cm. Note that the sample damaged with the largest dose (5×10^{16} ion/cm^2) has a resistivity of 450 $\mu\Omega$ cm and showed two transitions, indicating that the sample has been changed drastically and may not represent a single phase material any longer. The transitions of this particular sample are 11.1 and 9.2 K, respectively. It is suspected that after this high dosage irradiation, some part of the sample may have decomposed into pure Nb. In fact, it has been shown elsewhere[7] that for NbN under Ar^{2+} irradiation the lattice constant initially expanded, then contracted with increasing ion fluences, an indication of nitrogen loss during irradiation. Thus, we shall leave this particular sample out in the rest of the discussion.

It is also interesting to note that the saturation value of the residual resistivity is 150 $\mu\Omega$ cm instead of the 250 $\mu\Omega$ cm calculated by Hake[20] assuming a minimum mean-free path of half of the lattice constant. As Hake's calculation included several poorly known parameters, this difference is not surprising. However, we note that this value is about the same as the saturation resistivities found in many materials, including $A15$ superconductors[21] and other nitrides.[18] This may represent the fact that the dominating scattering mechanism in transport phenomena in this class of materials is the same, since all these materials have similar lattice constant and electronic structures.

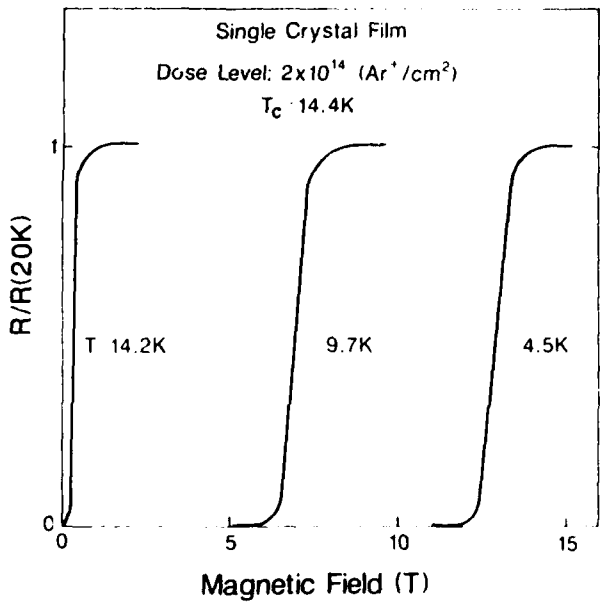

FIG. 1. Typical resistive transitions for a damaged single crystal film, demonstrating that the transition is not broadened in a magnetic field.

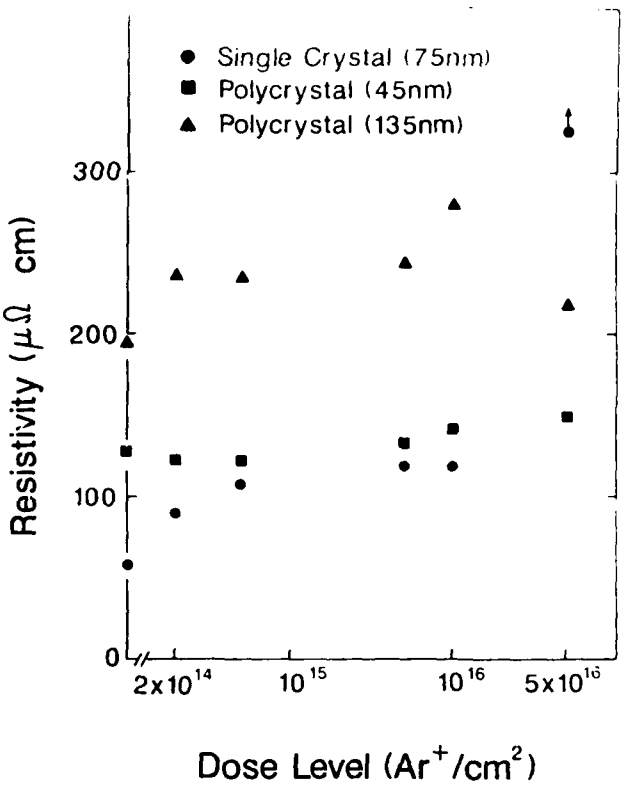

FIG. 2. Resistivity as a function of ion implantation dose level for all three sets of samples. At the highest dose level the single crystal sample showed abnormally high resistivity and multiple transitions (450 $\mu\Omega$ cm).

In contrast, the resistivities of the polycrystalline samples show only minor variations with ion fluences. It is believed that these variations are due more to modifications of the microstructure and grain boundaries of the samples as a consequence of defect migration during the irradiation than to changes in the NbN itself. It has been suggested[22] that defect migration can occur at ambient temperature under irradiation for $A15$ materials. More recently, it has also been found that grain growth can be greatly enhanced over the thermally activated processes in several thin film systems (Ge, Si, and Au) by ion beam bombardment.[23] Considering the very fine grain structure of our polycrystalline films, it is likely that some kind of defect recovery, or even grain growth, occurred during the irradiation.

To quantify this speculation, we have examined the grain structure of these films by TEM. Figures 3(a)–3(c) show typical results observed for samples after different levels of irradiation. Figure 3(a) shows the microstructure of the starting undamaged film. A dense, randomly oriented, fine-grain-size structure is confirmed. Figures 3(b) and 3(c) show, clearly, that *in situ* grain growth does

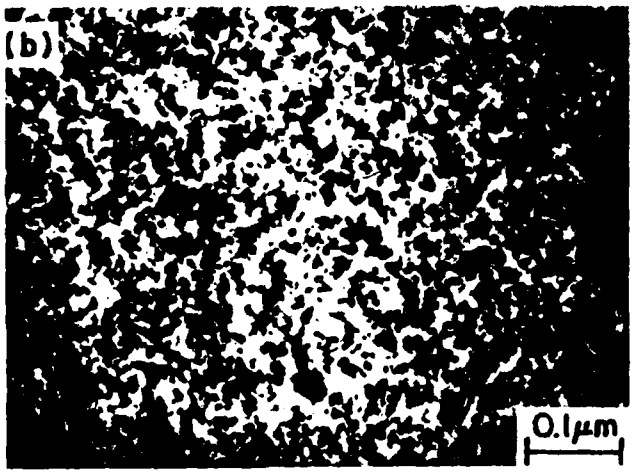

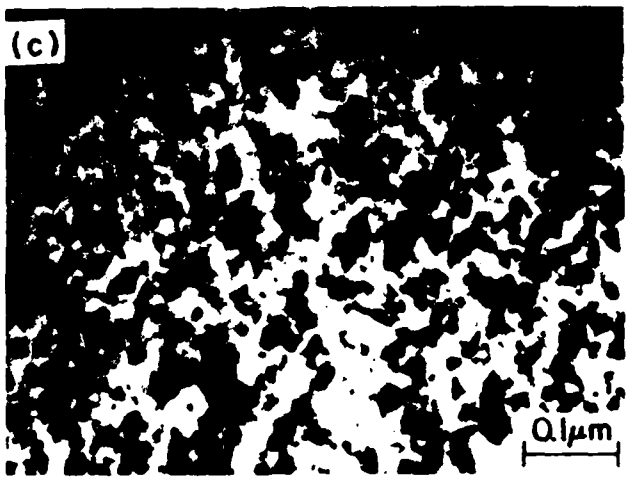

FIG. 3. Bright field TEM micrographs of the 45 nm thick polycrystalline samples showing the changes induced during irradiation. Part (a) is as deposited, (b) is after an ion dose of 5×10^{15} Ar^+/cm^2, and (c) is after 5×10^{16} Ar^+/cm^2. Notice both grain growth and defect density *reduction* occurs with increasing ion fluence. Similar results were found in the 135 nm thick films.

occur in NbN during the ion irradiation process even at ambient temperatures. Notice that the micrographs illustrate not only the increase in grain size but also the reduction in defect density within the grains as ion dose is increased. Therefore, it is reasonable to assume that any disorder introduced into the NbN by the ion fluence can "anneal" at room temperature due to the presence of grain boundaries, which can act as sinks for defects. It is difficult, however, to quantitatively correlate the detailed variations in resistivities seen in Fig. 2 with this microscopic analysis, since it involves changes in both grains and grain boundaries. The latter, in particular, are known to play an important role in determining the properties of the material, as we shall discuss later.

Figure 4 shows the T_c as a function of ion fluence. For the single crystal samples, T_c initially drops rapidly, then saturates at around 13 K, corresponding to a degradation of 20%. For the polycrystalline samples, we find that T_c, similar to resistivity, stays almost unchanged. These decreases are less than that found by Jung;[7] in his result T_c dropped by over 50% even though his samples were polycrystalline. On the other hand, it is certainly more noticeable than the result reported by Dew-Hughes and Jones,[6] in which T_c decreased by only 6% under neutron irradiation. Comparisons between these different results are difficult, since different sample microstructures and irradiating species were involved. The important question to be asked is what particular mechanism is responsible for the degradation of T_c?

We now focus on the degradation of T_c in the single crystal samples, since the results are not complicated by grain boundary effects. It is well established that the existence of both metal and nonmetal vacancies can cause

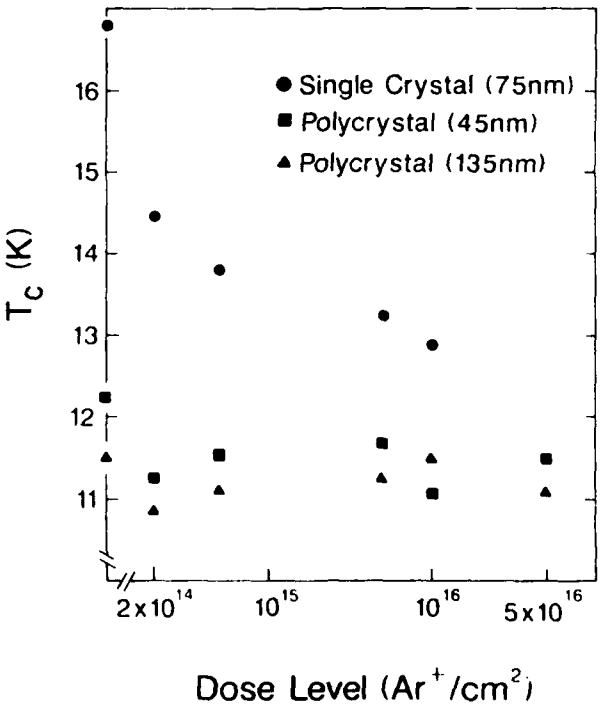

FIG. 4. Critical temperature as a function of ion dose for all three sets of samples.

T_c degradation in NbN. However, the exact mechanism by which these vacancies change the T_c is not clear. Whether the changes are only in the electron density of states at the Fermi surface, brought about by changes in the crystal chemistry, or whether other mechanisms such as localization or changes in the electron-phonon coupling are operating through these defects, remains to be clarified. Since the saturation resistivity, in this case 150 $\mu\Omega$ cm, is far below the Mott resistivity for a metal-insulator transition,

$$\rho_M = (3\pi^2\hbar/e^2k_F) \approx 1-1.5 \text{ m}\Omega\text{ cm} ,$$

it is unlikely that an Anderson localization mechanism is operating in these systems. Instead, the resistivities of these films are in the regime of weak localization. As has been pointed out by Fukuyama *et al.*,[24] the main effects of weak localization in suppressing T_c are the following: Changes in the one-particle density of states, increases in the effective Coulomb interaction of the electrons, and depairing due to the retardation effect of the interaction.

Although the discrepancies between the three-dimensional weak localization theories[24,25] are still substantial, we can make a rough estimation of the effects of localization on T_c in NbN. For this approximation we assume that the only effect of weak localization is to change the density of states in the NbN. Using a free-electron model we estimate that $k_F l \sim 5$ for NbN with a resistivity of 150 $\mu\Omega$ cm. Following the treatment of Al'tshuler and Aronov,[26] the resulting change in the density of states with this $k_F l$ value is only 1%. To estimate the corresponding effect on T_c, we use McMillan's original formula[27] for T_c in a strong-coupled superconductor

$$\frac{1.45T_c}{\Theta_D} = \exp\left\{\frac{-1.04[1+N(0)V_{\text{ph}}]}{N(0)\{V_{\text{ph}}-U_c[1+0.62N(0)V_{\text{ph}}]\}}\right\} , \quad (1)$$

which provides an explicit (although empirical) dependence on the density of states $N(0)$. Starting with parameters that produce the measured T_c in the undamaged sample,[28] we find that a 1% reduction in the electron density of states produces only a 2% reduction in T_c. While the assumption that all other parameters are unchanged by the damage requires further justification, the large difference between the observed 20% reduction in T_c and the preceding estimate leads us to believe localization effects are not the predominant factor in the depression of T_c.

Recently, Marksteiner *et al.*[29] used the Korringa-Kohn-Rostoker coherent-potential approximation (KKR-CPA) to calculate the electronic structure of substoichiometric NbN_x. They have shown that the introduction of nitrogen vacancies lowers the Fermi energy and reduces the density of states at the Fermi level. The trend is in good qualitative agreement with the experimental results found by Storms *et al.*,[30] which showed that vacancies in either sublattice of NbN appear to reduce the transition temperature by an amount which is inversely proportional to the intrinsic transition temperature of the material. Since the defects produced by ion bombardment in our experiment are presumably Frenkel pairs (vacancy-interstitial pairs), it seems that the degradation of T_c in NbN with ion fluence can be explained by a "classical" reduction of the density of states at the Fermi energy.

To further support this argument, recall the "universal" plot between T_c and residual resistivity in many high-T_c $A15$ compounds that shows a well-defined linear relation between these two parameters. This implies a universal degradation of T_c with disorder in these materials, and is believed to be strong evidence for the importance of the density of states in determining T_c.[1,21] Figure 5 shows the plot of T_c versus residual resistivity for the NbN samples in this study. For $\rho_0 < 150$ $\mu\Omega$ cm, T_c is linear in ρ_0, while for $\rho_0 > 150$ $\mu\Omega$ cm, T_c is almost independent of ρ_0. This supports the proposed density of states mechanism as the controlling factor for the degradation of T_c in NbN, and at the same time reinforces the identification of 150 $\mu\Omega$ cm as the maximum resistivity obtainable in NbN. An extrapolation of the linear part of this figure to zero resistivity predicts a T_c for 21 K for the cleanest NbN. This is the same value anticipated by Dew-Hughes and Jones,[6] where they use the T_c versus nitrogen vacancy concentration plot to deduce the T_c for vacancy-free NbN as 21 K.

As we have mentioned above, the saturation value of the resistivity (ρ_{sat}) is almost the same for a number of refractory-metal-based superconducting materials and may represent a common limiting mechanism for the transport properties of this class of materials. For NbN thin films, resistivities greater than 150 $\mu\Omega$ cm can be obtained in polycrystalline samples, and are attributed to large grain boundary resistances and not to an intrinsic property of the NbN itself. We have tried including in Fig. 5 the data for many as-deposited polycrystalline

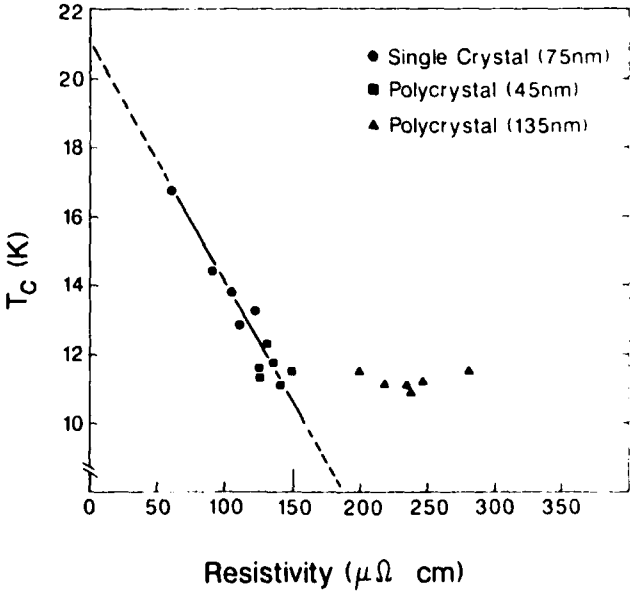

FIG. 5. Critical temperature vs resistivity for all samples in this study. The linear decrease in T_c with increasing disorder up to 150 $\mu\Omega$ cm is similar to that found in other superconductors.

NbN films. The results scatter badly for samples with resistivities greater than 150 $\mu\Omega$ cm, indicating that the wide range of compositions and grain boundary configurations resulting from the different deposition conditions affect the measured film resistivity in a manner only poorly related to the film T_c. This emphasizes the importance of the systematic manner in which disorder was introduced in our samples.

To summarize this subsection, we find that both T_c and residual resistivity vary monotonically with ion fluence for single crystal films, and are relatively unaffected for polycrystalline films. We interpret these results as follows: The disorder induced by ion damage, presumably mainly metal and nonmetal Frenkel defects (interstitial-vacancy pairs), is the controlling factor in reducing T_c in NbN as a consequence of a reduction in the electron density of states at the Fermi energy. Both T_c and resistivity saturate after high levels of damage; T_c around 13 K and ρ_0 around 150 $\mu\Omega$ cm. The saturation value of ρ_0 is striking; it is about the same value found in many other superconductors under various damage processes, and may represent the maximum intrinsic resistivity for this class of materials.

For polycrystalline samples, the effects of ion damage are minimized due to the presence of grain boundaries. Dynamical annealing occurs during the process of damage, as confirmed by the ion-bombardment-induced grain growth in the samples. This *in situ* grain growth during the irradiation process, to our knowledge the first such observation for a refractory material like NbN, makes it difficult to predict the effects of the irradiation on superconducting properties. Studies are currently in progress to examine the effects of ion damage on the critical current in these samples.

B. Critical field slopes and resistivity

From the critical field slopes near T_c, several important superconducting and normal state parameters can be estimated. The Ginzburg-Landau-Abrikosov-Gor'Kov (GLAG) relation[31] for dirty superconductors, in Oe K^{-1},

$$-(dH_{c2}/dT)_{T_c} = 4.48\times 10^4 \gamma \rho_0 , \qquad (2)$$

which predicts a linear dependence of dH_{c2}/dT on ρ_0 provided γ is constant. Here, γ is the coefficient of electronic specific heat in erg/cm^{3}K^2, and for fields applied perpendicular to the film ρ_0 is the measured in-plane resistivity in $\mu\Omega$ cm. We emphasize here that both the intrinsic resistivity of the NbN and the grain boundary resistivity contribute to the critical field. We have previously found[11] that, for perpendicular fields, the critical field slopes tend to saturate for high-resistivity polycrystalline samples. Although the saturation value is badly scattered (see data from previous studies in Fig. 7), it is much larger than one would calculate from Eq. (2) (2.15 T/K) using a maximum resistivity for the NbN alone of 150 $\mu\Omega$ cm and the bulk specific heat coefficient[32] (3.2×10^3 ergs/cm^{3}K^2). Similarly, it has become evident from our study of the angular dependence of $H_{c2}(T)$ that the critical field anisotropy commonly found in NbN films has its origin in the anisotropic resistivity of the grain boundaries.[14,19] For high-resistivity films it is obvious that the grain boundary resistivity contributes, significantly, to the determination of the critical field.

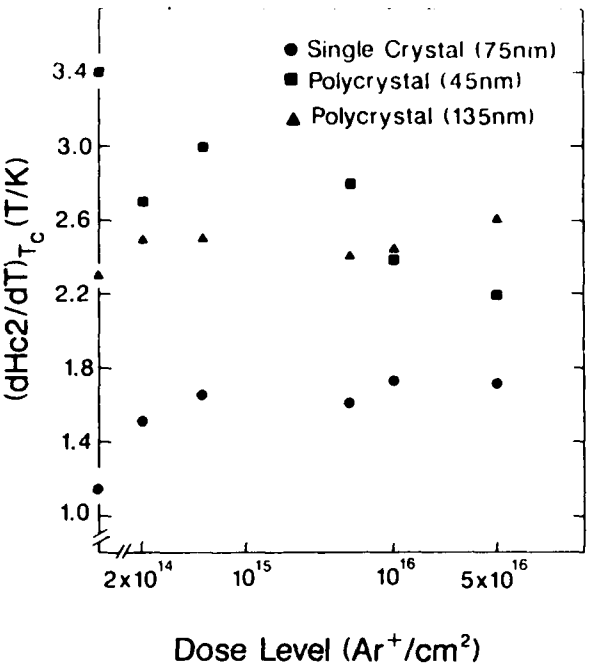

FIG. 6. Slope of the upper critical field near T_c as a function of ion dose level.

Figure 6 shows the results of $(dH_{c2}/dT)_{T_c}$ as a function of ion fluence for the samples used in this study. For the single crystal samples the slope saturates at a value of 1.8 T/K, near the ideal saturation value predicted above and about the same value found in bulk NbN.[28,33] As shown in Fig. 7, the plot of $(dH_{c2}/dT)_{T_c}$ versus residual

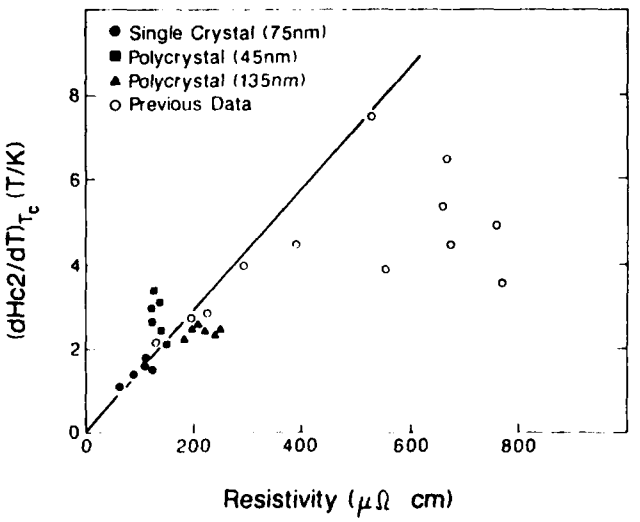

FIG. 7. Slope of the upper critical field plotted vs resistivity for all samples in this study and for several previous undamaged samples made with varying resistivities. The straight line is from Eq. (2) using the bulk value of γ (no adjustable parameters).

resistivity, all the data points for the single crystal films fall near the straight line obtained from Eq. (2) using a constant γ. (See the following discussion for implications of this result.) For the polycrystalline films, the slopes show some variations with the ion fluence (Fig. 6). Again, these variations are believed to be due mostly to changes in the grain boundary resistance through changes in the grain boundary composition and grain size during the irradiation processes, and not to intrinsic changes in the NbN itself.

It is interesting to note that, for the thinner polycrystalline films (44 nm), the critical field slope is initially much higher than for the thicker films (135 nm), although its resistivity is much smaller. These are the only films we have measured with critical field slopes that lie above the predicted line. As these films were damaged (and *in situ* grain growth occurred), the critical field slope decreased, eventually falling below the predicted line. In contrast, in the thicker films the slope first increased slightly with damage, and then saturated near 2 T/K. The detailed explanation for these two different behaviors in presumably similar films in not clear at present.

In comparing the results for the single crystal films to the preceding subsection on critical temperature, an apparent inconsistency exists. We reached the conclusion in Sec. III A that T_c degradation for single crystal NbN is due to a decrease in the electron density of states at the Fermi energy through the increasing disorder introduced by ion damage. Therefore, in principle, the slope of the critical field should deviate from the linear relation with resistivity predicted by Eq. (2) since a decrease in the density of states should be reflected in a proportional decrease in γ. However, using McMillan's formula for T_c [Eq. (1)], only a 20% reduction in the density of states is needed to account for the observed reduction in T_c. This small change in γ will produce only a slight shift from linearity in the resistivity range of interest, and thus would not effect the general observations made earlier. While it may be simply fortuitous, we note that the saturation value for dH_{c2}/dT found for the single crystal samples (1.8 T/K) is, in fact, approximately 20% smaller than the value calculated from Eq. (2) using the bulk value for γ.

IV. CONCLUSIONS

In this study we have found disorder, as introduced by ion irradiation, does affect the normal state and superconducting properties of single crystal NbN. The observed 20% reduction of T_c can be accounted for by a corresponding reduction in the electron density of states, most likely due to changes in crystal chemistry rather than localization effects. The damage-induced increase in resistivity is reflected in a nearly linear increase in the slope of the critical field. For polycrystalline NbN films the presence of grain boundaries plays an important role in determining both the normal state and superconducting properties. During ion irradiation the grain boundaries act as a sink for the induced disorder, making the films relatively insensitive to damage. This process is reflected in the unusual *in situ* grain growth observed in these films during implantation.

ACKNOWLEDGMENTS

The authors wish to thank Professor T. P. Orlando and Professor J. M. Graybeal for stimulating discussions during this work. Help from Dr. D. K. Christen of Oak Ridge National Laboratory in calculating the deposited damage energy is also greatly appreciated. Work at Westinghouse was supported in part by the U.S. Air Force Office of Scientific Research under Contract No. F49620-85-C-0043.

[1]See, for example, several papers in *Superconductivity in d- and f-Band Metals*, edited by H. Suhl and M. B. Maple (Academic, New York, 1980).

[2]G. J. Clark, A. D. Marwick, R. H. Koch, and R. B. Laibowitz, Appl. Phys. Lett. **51**, 139 (1987).

[3]G. Van Tendeloo, H. W. Zandbergen, and S. Amelinckx, Solid State Commun. **63**, 389 (1987).

[4]A. Ourmazd, J. A. Rentschler, J. C. H. Spence, M. O'Keeffe, R. J. Graham, D. W. Johnson, Jr., and W. W. Rhodes, Nature **327**, 308 (1987).

[5]G. Oya and Y. Onodera, J. Appl. Phys. **45**, 1389 (1974).

[6]D. Dew-Hughes and R. Jones, Appl. Phys. Lett. **36**, 856 (1980).

[7]V. Jung, in *Proceedings of the 17th International Conference on Low Temperature Physics, LT-17*, edited by U. Eckern, A. Schmid, W. Weber, and H. Wuhl (North-Holland, Amsterdam, 1984), p. 109.

[8]P. W. Anderson, J. Phys. Chem. Solids **11**, 26 (1959).

[9]J. Bardeen, L. N. Cooper, and J. R. Schrieffer, Phys. Rev. **108**, 1175 (1957).

[10]E. Helfand and N. R. Werthamer, Phys. Rev. Lett. **13**, 686 (1964); Phys. Rev. **147**, 288 (1966); N. R. Werthamer, E. Helfand, and P. C. Hohenberg, *ibid.* **147**, 295 (1966).

[11]J. Y. Juang, D. A. Rudman, R. B. van Dover, W. R. Sinclair, and D. D. Bacon, *Advances in Cryogenic Engineering* (Plenum, New York, 1986), Vol. 32, p. 651.

[12]M. Ashkin and J. R. Gavaler, J. Appl. Phys. **49**, 2449 (1978).

[13]M. Ashkin, J. R. Gavaler, J. Greggi, and M. Decroux, J. Appl. Phys. **55**, 1044 (1984).

[14]D. A. Rudman, J. Y. Juang, R. B. van Dover, S. Nakahara, D. W. Capone II, and J. Talvacchio, IEEE Trans. Magn. **MAG-23**, 831 (1987).

[15]J. Talvacchio and A. I. Braginski, IEEE Trans. Magn. **MAG-23**, 859 (1987).

[16]D. D. Bacon, A. T. English, S. Nakahara, F. G. Peters, H. Schreiber, W. R. Sinclair, and R. B. van Dover, J. Appl. Phys. **54**, 6509 (1983).

[17]E_a was calculated using the code developed by I. Manning and G. P. Murller [Comput. Phys. Commun. 7, 85 (1974)]. We thank Dr. D. K. Christen of Oak Ridge National Laboratory for helping us in determining E_a.

[18]D. K. Christen, J. T. Ellis, S. T. Sekula, J. R. Thompson, J. D Lewis, W. R. Anderson, and S. J. Pennycook, IEEE Trans. Magn. **MAG-23**, 1014 (1987).
[19]J. Y. Juang, D. A. Rudman, J. A. X. Alexander, and T. P. Orlando (unpublished).
[20]R. R. Hake, Appl. Phys. Lett. **10**, 189 (1967).
[21]R. C. Dynes, J. M. Poate, L. R. Testardi, A. R. Storm, and R. H. Hammond, IEEE Trans. Magn. **MAG-13**, 640 (1977); See also Ref. 1.
[22]B. S. Brown, R. C. Birtcher, R. T. Kampwirth, and T. H. Blewitt, J. Nucl. Mater. **72**, 76 (1978).
[23]H. A. Atwater, C. V. Thompson, and H. I. Smith, Mater. Res. Soc. Sym. Proc. **74**, 499 (1987).
[24]H. Fukuyama, H. Ebisawa, and S. Maekawa, J. Phys. Soc. Jpn. **53**, 1919 (1984).
[25]D. Belitz, Phys. Rev. B **35**, 1651 (1987).
[26]B. L. Al'tshuler and A. G. Aronov, Zh. Eksp. Teor. Fiz. **77**, 2028 (1979) [Sov. Phys.-JETP **50**, 968 (1979)].
[27]W. L. McMillan, Phys. Rev. **167**, 331 (1968). The specific prefactor chosen is unimportant, since we are only concerned with changes in T_c due to changes in $N(0)$.
[28]T. H. Geballe, B. T. Matthias, J. P. Remeika, A. M. Clogston, V. B. Compton, J. P. Maita, and H. J. Williams, Physics **2**, 293 (1966).
[29]P. Marksteiner, P. Weinberger, A. Neckel, R. Zeller, and P. H. Dederichs, Phys. Rev. B **33**, 6709 (1986).
[30]E. K. Storms, A. L. Giorgi, and E. G. Szklarz, J. Phys. Chem. Solids **36**, 689 (1975).
[31]T. P. Orlando, E. J. McNiff, Jr., S. Foner, and M. R. Beasley, Phys. Rev. B **19**, 4545 (1979).
[32]C. Geibel, H. Rietschel, A. Junod, M. Pelizzone, and J. Muller, J. Phys. F **15**, 405 (1986); see also Ref. 12.
[33]M. P. Mathur, D. W. Deis, and J. R. Gavaler, J. Appl. Phys. **43**, 3158 (1972).

Physica C 153-155 (1988) 1435-1436
North-Holland, Amsterdam

NEAR-SURFACE ATOMIC SEGREGATION IN YBCO THIN FILMS*

J. R. GAVALER and A. I. BRAGINSKI

Westinghouse R&D Center, Pittsburgh, PA 15235

In amorphous YBCO films annealed in O_2 at 475 to 550°C prior to crystalline compound formation, atomic segregation of Ba to the film surface is observed. The thickness of the segregated layer decreases with increasing oxygen pressure during film deposition. Fast heating to the compound-formation temperature minimizes segregation.

1. INTRODUCTION

It is widely known that the free surfaces of $Y_1Ba_2Cu_3O_7$ (YBCO) specimens which have been fabricated to date in bulk or thin film form are not superconducting. This is the cause of high contact resistances and the lack of success in tunneling between thin films. The formation of a semiconducting or insulating surface layer has been generally attributed to reactions with H_2O and CO_2 in the ambient air.

The purpose of our study was to determine the cause(s) of the free surface degradation in thin films. We used, to a large extent, in-situ film fabrication and surface analysis, by X-ray photoelectron spectroscopy (XPS), to eliminate effects of uncontrolled reactions with the ambient air.

2. FILM FABRICATION AND CHARACTERIZATION

The YBCO films were either co-evaporated or co-sputtered. Co-evaporation from metallic e-beam gun sources on $SrTiO_3$ (100) and sapphire substrates, typically in the absence of oxygen and at ambient temperature, produced polycrystalline deposits. Reactive-co-sputtering (1) was carried out from metallic targets onto substrates held at T_s = 440°C in the presence of oxygen partial pressures between 1.3×10^{-4} to 3.9×10^{-2} Pa. This process produced either polycrystalline or epitaxial films, depending upon the substrate used and its surface preparation. Standard substrates were (100) or (110) $SrTiO_3$, and sapphire. Typical co-evaporated and fully crystallized film thicknesses were 0.6 to 1 μm while co-sputtered films were 0.3 to 0.5 μm. Both deposition processes were carried out in a four-chamber ultra-high-vacuum (UHV) deposition and analysis system. (2) The oxidation of films at atmospheric pressure of dry O_2 was performed at 475 to 550°C, prior to the reaction anneal. This first oxidation step was carried out in three variants: 1) entirely in-situ, for 20 min, 2) entirely ex-situ, for 4 hours, and 3) in situ followed by ex-situ "1+2". The reaction to form YBCO at 800 to 850°C and the subsequent oxygen intercalation during cooling, both at 1 atmosphere O_2 pressure, were also carried out either ex-situ or in-situ. Superconducting properties of polycrystalline sputtered films which were ex-situ reacted have been reported earlier. (1) Properties of films co-evaporated from metallic sources and ex-situ reacted were similar. Best epitaxial specimens exhibited similar resistive transitions but higher critical current densities.

Bulk film compositions were determined by energy-dispersive X-ray spectroscopy (EDS), the electron microprobe and by a dc plasma spectrometer. Compositional depth profiles were obtained ex-situ by uncalibrated Auger electron spectroscopy (AES) normalized to the bulk composition obtained by other methods. The near-surface film compositions were determined by in-situ X-ray photoelectron spectroscopy (XPS) with Al-radiation. The approach adopted in this study was to observe changes in the near-surface composition occurring after various in-situ fabrication steps and to correlate both, compositional depth profiles and surface compositions of completely reacted specimens with preparative conditions. Most of the results reported below were obtained for co-sputtered films.

3. RESULTS AND DISCUSSION

In-situ XPS spectra of film surfaces obtained after co-sputtering at 440°C in $p(O_2)$ less than or = 2.6×10^{-4} Pa and prior to in-situ oxidation did not contain any measurable Cu signature although the film composition was close to stoichiometry. In XPS spectra of films as-deposited in $p(O_2)$ greater than or = 4×10^{-4} Pa the relative surface concentrations of metals were nearly stoichiometric. The surface concentration of oxygen corresponded to between 7 and 8.5 oxygen atoms per molecule. Table 1 shows XPS surface compositions of a sample deposited at greater than or = 1×10^{-3} Pa of oxygen. The behavior described was observed in 10 film samples which were analyzed by XPS after deposition at

*Supported in part by AFOSR Contract No. F49620-85-C-0043.

various oxygen pressures. All as-deposited films were X-ray amorphous.

After the in-situ oxidation, the XPS surface composition was always found to have changed. The oxygen content was very high due to surface adsorption and thus no longer relevant. For that reason, data of Table 1 are metallic compositions only. The surface was enriched in Ba while the copper concentration was much reduced and (in other samples) often too low to measure. (3) At this stage the films were still X-ray amorphous.

TABLE 1.
Surface Composition Determined by in-situ XPS after Three Subsequent Fabrication Steps. (Film co-sputtered at $p(O_2)$ greater than or = 1×10^{-3} Pa and annealed in O_2.)

Analyzed After Fabrication Step:	T °C	Y at.%	Ba at.%	Cu at.%
As-deposited	440	17	33	50
In-situ oxidized	500	21	66	13
Ex-situ reacted	850	22	41	37

The reaction annealing, whether in-situ or ex-situ, should have resulted in homogenization of the now crystalline layer. Table 1 indeed indicates that this occurred. In no case has a surface of pre-oxidized sample deteriorated further in this step. The final XPS surface compositions, however, always remained Cu-deficient.

Figure 1 compares two AES depth profiles of sample composition: (A) of a film co-evaporated in the absence of O_2 and annealed entirely ex-situ with (B) that of film co-sputtered at $p(O_2) = 3.4 \times 10^{-4}$ Pa and oxidized per the "1+2" schedule. In the first case the deviation from stoichiometry extends to a depth of, approximately, d = 165 nm, comparable with the penetration depth in YBCO, while in the second the off-stoichiometric layer is about 50 nm thick. Other profile data of films which were oxidized per the "1+2" schedule confirmed that the layer thickness decreased further with increasing $p(O_2)$.

Reduction of the oxidation schedule to in-situ alone "1" has further reduced d. When the film was in-situ reacted at T = 800°C for t = 10 min by radiation surface heating with a steep T(t) ramp, the film surface composition and depth profile showed no evidence of surface segregation. A 50 nm overlayer of gold was in-situ evaporated on the surface of such films kept at room temperature. On top of the gold, 200 nm Nb electrodes were deposited ex-situ, again at room temperature. The resistance between Au/Nb and YBCO was measured at 4.2K. This resistance was less than 4×10^{-10} ohm-cm^2 indicating that the non-superconducting surface layer was largely eliminated.

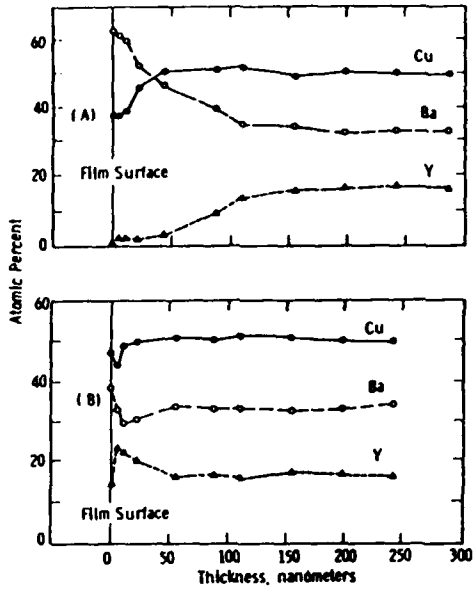

FIGURE 1
AES depth profiles in films deposited at different oxygen pressures: (A) - $p(O_2)$ less than 10^{-7} Pa, (B) - $p(O_2) = 3.4 \times 10^{-4}$ Pa.

4. CONCLUSION

Our results lead to the conclusion that oxidation below the crystallization temperatures causes segregation of Ba toward the surface of amorphous deposits with a resulting depletion in Cu or Y. This leads to the formation of a non-superconducting surface layer on films even those not subject to any reaction with H_2O and CO_2. The segregation is most prominent in films deposited in the absence of oxygen and is expected to disappear if all metallic constituents of the film can be fully oxidized during deposition at a sufficiently high oxygen pressure and temperature to form the desired YBCO crystal structure during film growth. Elimination of pre-oxidation and the use of a steep ramp to the temperature of compound formation minimizes segregation in films deposited at low O_2 pressures and temperatures.

REFERENCES

(1) R.M. Silver, J. Talvacchio, and A.L. de Lozanne, Appl. Phys. Lett. 51, 2149 (1987).
(2) J. Talvacchio, M.A. Janocko, J.R. Gavaler, and A.I. Braginski, in Advances in Cryogenic Engineering-Materials, edited by A.F. Clark and R.P. Reed (Plenum, New York), 1986, pp. 527-541.
(3) N.G. Stoffel, W.A. Bonner, P.A. Morris, and B.J. Wilkens, 1988 MRS Fall Meeting, Symposium S (in print) also observed segregation of Ba to the surface of implanted, amorphous single crystal surfaces.

Physica C 153-155 (1988) 1598-1603
North-Holland, Amsterdam

MATERIAL CONSTRAINTS ON ELECTRONIC APPLICATIONS OF OXIDE SUPERCONDUCTORS*

A. I. BRAGINSKI

Westinghouse R&D Center, Pittsburgh, PA 15235

It is shown that oxide superconductor film surface and interface degradation represents the main obstacle to electronic applications. Surface quality requirements imposed by passive components appear less stringent than those necessary for functional tunnel junctions.

1. INTRODUCTION

Electronic applications of superconductors fall broadly into categories of passive (linear) and active (nonlinear) components and devices. Typical examples are a radio-frequency (rf) transmission line or stripline resonant cavity in the first category and a Josephson junction or a superconducting quantum interferometer (SQUID) in the second. Functional circuits are usually integrated from many such building blocks, thus far attaining the large scale integration (LSI) level of complexity for conventional, low-critical-temperature, T_c, materials. We are less concerned here with single functional elements such as large rf cavities, for example, which fall into the domain of power applications. The physics underlying these applications will be the same as in passive components of integrated circuits.

Almost all electronic applications are based on the use of superconducting thin films and layered film structures which, in addition to superconductors, must incorporate insulating, normal metallic and/or semiconducting films. Superconductors in thin film form are technologically useful when integrated into such structures without degradation of superconducting (bulk) properties at surfaces and interfaces with other materials. Which of the characteristic depth scales for the required film perfection is critical for the device operation, the effective Ginzburg-Landau penetration depth, λ, or the coherence length, ξ, depends upon the type of application, as discussed below. Some interfacial degradation should always be expected as a consequence of deleterious physico-chemical processes occurring during the multiple fabrication steps. Interdiffusion with other layers which results from thermal treatments, interfacial disorder, free surface reactions with processing atmospheres and interfacial strains are simple examples of undesirable effects which impose constraints on a successful application of thin superconducting films.

Ideally, superconductors used in electronic layered film structures should exhibit no significant crystalline and electronic anisotropy, a requirement satisfactorily met by all conventional, low-T_c superconductors. Their thermal expansion coefficients and elastic constants should be compatible with film substrates and other non-superconductors incorporated into a layered structure, a requirement depending on other materials and met, in the past, only to some extent. Furthermore, these superconductors should be refractory, chemically inert and not prone to interdiffusion at elevated temperatures. In these respects NbN has presently the highest score. Longest possible ξ and shortest λ at a given level of T_c and energy gap, Δ, are the major requirements which for type II refractory superconductors are not met well enough. In fact, technological difficulties increase with $\kappa = \lambda_{eff}/\xi$. These requirements, relatively best met by Nb, will be discussed further. Finally, the superconductor should have a critical current density in zero field, J_c, in excess of 10^6 amps/cm^2 at the temperature of utilization, for reasons also discussed below. Conventional superconductors score well in this respect. In-depth reviews of these requirements and problems encountered in conventional superconductors can be found in the literature (1-3).

Advances in material understanding made it possible in the last decade to solve most of the problems resulting from material constraints in niobium-based electronic circuits and, to a lesser extent, in NbN-based components (4). High-T_c oxide superconductors bring an additional set of severe constraints which must be understood and overcome to find design, fabrication and processing approaches leading to successful electronic applications.

2. PROPERTIES OF OXIDE SUPERCONDUCTORS

In the following discussion the $YBa_2Cu_3O_7$ high-T_c cuprate (YBCO) will serve as a generic

* Supported in part by AFOSR Contract No. F49620-88-C-0039.

example of this new class of materials. Other such materials, including the newly discovered Bi-Ca-Sr-Cu-oxide (5,6) exhibit (or can be expected to) a similar behavior, except where noted. Material characteristics and properties which impose main constraints on applications are listed below.

1. The YBCO is a line (point) compound. Any deviation from stoichiometry of metallic components results in the presence of non-superconducting second phase(s). Some of the other cuprates do exhibit narrow ranges of solid solutions with T_c sharply peaking at stoichiometry (7). This offers a potential for processing improvements.

2. The T_c and Δ in YBCO are critically dependent upon the oxygen concentration, x, and drop precipitously to ~60K when x decreases below 6.8 oxygen atoms per molecule. In the range $6 < x < 7$ oxygen is reversibly intercalated into the loose perovskite-type layered crystal structure, down to temperatures as low as 80°C in the case of rf plasma oxidation (8). Reversible intercalation is not occurring to the same extent in lower-T_c $(La,Sr)_2CuO_4$.

3. The orthorhombic crystal structure of YBCO is highly anisotropic and twinned along [110]. The electronic anisotropy is pronounced and manifests itself as anisotropy in normal resistivity, ρ, critical fields H_{c1} and H_{c2}, and J_c. The derived ξ and λ are anisotropic with $\xi_c \ll c$, the cell edge along [001] equal to the separation between the Cu-O chain planes (9,10). In fact, there exists some experimental evidence of weak coupling along [001] (11). It is not known, however, whether it is intrinsic or related to structural or microstructural defects. The YBCO is an extreme type II superconductor, irrespective of crystallographic direction.

4. The in-plane critical current density in single crystal or highly textured films of YBCO with c-axis normal to the plane ("c" orientation) can exceed $J_c = 1 \times 10^6$ amps/cm^2 at 77K (11,12). Polycrystalline aggregates, however, exhibit "granular" behavior with superconducting grains only weakly coupled. In this case the J_c at 77K does not exceed 10^4 amps/cm^2 and falls off exponentially with increasing magnetic field.

5. The YBCO surfaces readily react with water and CO_2 in the ambient atmosphere (13,14). The effect is most pronounced if second phases are present.

6. The YBCO reacts and interdiffuses with practical electronic substrate materials, especially silicon and sapphire, and with the suitable epitaxial substrate, $SrTiO_3$ (15,16). Consequently, film/substrate interfaces are degraded.

7. Atomic segregation occurs on free surfaces of YBCO films deposited at low oxygen pressures and annealed in oxygen (17). Off-stoichiometric surface layers are non-superconducting and resistive.

Table 1 compares relevant superconducting properties of conventional superconductors used in electronics with those of representative oxides. It is seen that κ increases with T_c which suggests that the highest T_c materials will be the most difficult to use in electronics. Evidence of this problem is presented below.

3. PASSIVE COMPONENTS

Superconductors are very attractive for microwave frequency applications because of their extremely low surface losses attributed only to thermally excited quasiparticles. The losses are quantified by the real component, $R_s(f,T)$, of the complex surface impedance. The Mattis-Bardeen theory (18) correctly predicts $R_s(f,T)$ in BCS superconductors once the residual, temperature-independent loss is substracted. Low losses make it possible to construct very high-Q resonant cavities and low-loss transmission lines, at least at frequencies, f, well below the gap frequency and temperatures, T, not exceeding 0.5 T_c. One may assume a rule of thumb that the application of a superconductor is warranted at given f,T if $R_s < 0.1\ R_s(Cu)$.

Analog signal processing devices such as tapped delay lines, chirp filters, convolvers, correlators and phase shifters (19-22) all exploit transmission line properties. High-speed digital data transmission lines, of which computer interconnect is the simplest example, share the same experimental and theoretical base (23). Over most of the microwave frequency range the penetration depth of conventional type II superconductors is shorter than the skin depth. Consequently, losses originate in a surface or interface layer which is penetrated by the rf field and has a thickness of the order of λ. In the stripline configuration, for example, losses in the center conductor originate at both film boundaries: the interface with the substrate and with the dielectric overlayer. To attain low losses, the film properties must approximate those of a bulk superconductor within a depth $d \ll \lambda$ from each boundary.

In the case of high-T_c oxides, which may not be BCS superconductors, one cannot rely on theoretical predictions of $R_s(f,T)$. In fact, experimental data can provide insights into the mechanism of high-T_c superconductivity but only if they represent intrinsic properties of the superconductor. Figure 1 shows $R_s(f)$ data for YBCO measured at T = 4.2K by several groups of authors using cavity or strip line resonators in geometries such that only one surface of a sample (free surface of a film) is exposed to the rf field. Early reports, based on bulk, and apparently inhomogeneous, sintered

TABLE 1
Properties of Representative Superconductors

Material	T_c, K (best value)	$\Delta(0)$, meV	$\xi(0)$, Å	$\lambda(0)$, Å
Conventional, Low-T_c				
Pb	7.2	1.3	900	400
Nb	9.3	1.6	100-300	850
NbN	16-17	3.0	40-70	2000-3000
Nb_3Sn	18	3.4	30	600-900
Oxides, High-T_c				
$La_{1.85}Sr_{0.15}Cu_1O_4$	40	> 7	2.1 (average)	2500-4000 (average)
$Y_1Ba_2Cu_3O_7$	95	>16	4.3(c) 31(a)	1800(c) 270(a)* (Ref. 10)

*Axis normal to plane.

polycrystalline YBCO aggregates indicated very high R_s values (24) about five orders of magnitude above those in Nb (25) which are also plotted for reference. In recently reported random polycrystalline YBCO films having a low $J_c = 7 \times 10^3$ A/cm^2, the R_s was much lower but still about 3 orders of magnitude above that of Nb (26). An epitaxial (textured) polycrystalline film with dominant (70%) "c" texture (c-axis normal to plane) and a high $J_c = 4 \times 10^6$ A/cm^2 exhibited a loss slightly below that of OFHC copper at 100 GHz (27) and higher at 150 GHz. This measurement was relative to Cu and the absolute value of R_s in YBCO was dependent on the R_s data for Cu, not reported. Using R_s(Cu) from literature (28) and the $R_s \propto f^2$ dependence makes it possible to give the bracket estimate of R_s in YBCO which is shown in Fig. 1. The R_s is within less than one order of magnitude above R_s(Nb). Interestingly, a comparable R_s was also observed in bulk single crystal platelets with "c" orientation (29).

The dramatic increase of cavity Q with T decreasing below T_c and the $R_s \propto f^2$ dependence at 4.2 K (26,27) suggest that the losses occur in the superconductor. The wide spread in R_s data, however, makes it clear that the higher values are nonintrinsic and related to granular nature of samples and/or energy gap near the surface reduced due to proximity effect or loss of oxygen. Even the single crystal surface may have been degraded due to surface reactions with the ambient and the presence of embedded Al particles (26). The anisotropic penetration depth $\lambda(0)$ in YBCO is approximately 1800 Å with

*A tentative R_s(Cu) = 42 mΩ at 100 GHz obtained by the authors of (27) would bring R_s(YBCO) down by one order of magnitude.

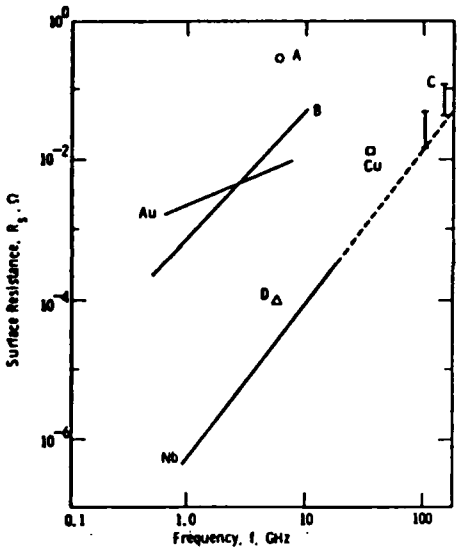

FIGURE 1
Surface resistance vs frequency at 4.2 K: A - Polycrystalline YBCO aggregate (24), B - Polycrystalline YBCO film (26), C - Bracket estimate for epitaxial film with "c" orientation dominant (27), D - Single crystal platelets with "c" orientation. Experimental data for Au and Nb are from (26) and for Cu from (28).

magnetic field in the a-b plane(10) and this determines the depth over which nonintrinsic effects due to near-surface degradation should be minimized.

It is encouraging that the f^2 surface losses at 100 GHz reported for the epitaxial film are already low enough (compared to Cu

losses, where $R_s \propto f^{2/3}$ in the extreme anomalous skin effect regime) to make applications at least marginally attractive at lower frequencies, up to 10-15 GHz, and temperatures up to 40-50K. In practical strip- or micro-strip lines, analog or digital, current densities in the conductor are of the order of 10^6 A/cm^2 so that epitaxial films of "c" orientation will be required in any case. For device practicality, however, two more loss-related problems must be addressed: (1) interdiffusion at the film/substrate interface which may extend to depths exceeding λ and can be expected to degrade this interface, (2) high dielectric losses in presently used epitaxial substrates such as $SrTiO_3$, ZrO_2 or MgO (in decreasing order of $\tan\delta$). Epitaxial diffusion buffer layers on low-loss single-crystalline substrates, especially sapphire, would be a desired solution for which further search is mandatory. Passive electronic components will become a reality when such a solution is found.

4. ACTIVE COMPONENTS

4.1 Tunnel Junctions

The Josephson tunnel junction is the most widely used and critical nonlinear device of today's low-temperature superconducting electronics. The tunneling effect is probing the superconductor to the depth of the order of ξ on each side of the tunnel barrier. A functional thin film tunnel junction made of YBCO must, therefore, have an undegraded electrode material within a depth much less than ξ from each interface with the artificial tunnel barrier. Table 1 shows that this will require compositional and crystalline perfection of the superconductor within the first 20 to 30 Å from barrier interfaces, assuming that the epitaxial electrode films have an "a" orientation (c-axis in-plane). The "c" orientation (c-axis normal to plane) appears totally impractical as it would require superconductor perfection within the first couple of monolayers. The ξ in "a" orientation films is comparable to that of NbN films of which polycrystalline and single-crystal epitaxial tunnel junctions have been fabricated successfully (4,40). Unfortunately, in "a" oriented films, the in-plane high-J_c interconnect lines between devices will be compromised by "difficult" current paths along c-axis. This could make any circuit layout difficult, if not out of the question.

Data already discussed in Section 3 provide a strong evidence that, to date, near-surface YBCO film degradation was occurring to a depth an order of magnitude greater than ξ_a. It is not surprising, therefore, that functional YBCO tunnel junctions have not been reported in the literature. A few groups described attempts to tunnel between films (30) or between a Pb (or Nb) film counterelectrode and bulk, polycrystalline YBCO surface (31-33). The observed current-voltage (I-V) data exhibited only slight deviations from normal tunneling (straight line) characteristics. Perhaps most convincing are the results of Nakayama et al.(30) who have observed Josephson current, hysteresis and Fiske steps in the I-V curve of YBCO/AlO_x/Nb junctions and presented some evidence that tunneling was occurring through the oxidized Al layer which was deposited on a polished bulk YBCO surface. It is unlikely that device-quality junctions with YBCO base-electrode and a low-T_c counterelectrode will be obtained before epitaxial films of "a" orientation can be fabricated with little free surface damage. An all-YBCO junction, capable of operating at, for example, $T_{op} = 0.5\ T_c$, will not be possible until an epitaxial YBCO film (again of "a" orientation) can be grown on a tunnel barrier equivalently free of disorder and interdiffusion at the critical interface. This, indeed, will be a difficult task.

An alternative, purely hypothetical, approach to tunneling between YBCO layers would be to form single crystal films with planar defects such as extra atomic layers parallel to Cu-O planes. These defects could decouple superconducting layers and permit tunneling. For example, there is evidence for additional Cu-O planes in the YBCO crystal structure, possibly forming an ordered defect structure $Y_2Ba_4Cu_8O_{20}$.(34) Other defects of similar nature might be possible and their formation locally controllable, e.g. by ion implantation. Circuits with planar junctions so delineated in "c" oriented films would have the additional advantage of high-J_c interconnect lines at right angles in the film plane. The I-V characteristics reported by Enomoto et al.(11) show evidence of Josephson coupling, Fiske steps and hysteresis for the c-direction of current flow in an "a" oriented single crystal YBCO film. Such effect, not yet confirmed by others, could be either be intrinsic or due to stacking fault defects assuming that its origin is not simply explained by stress-induced microcracks.

4.2 Microbridges

In polycrystalline YBCO, grain boundary regions act as normal (N) links between superconducting (S) grains. The granular behavior of bulk polycrystalline aggregates and random polycrystalline films of YBCO is now well known and intergranular SNS-type Josephson junction (microbridge) characteristics have been observed by many authors. Patterning of narrow bridges in a YBCO film produced an early demonstration of a high-T_{op} dc SQUID (35). Planar devices of this type could be used as magnetometers and sensors of electromagnetic radiation.

The two major material-related problems are: (1) the wide spread of inter-granular junction parameters and 2) the high level of 1/f noise, typical of granular systems and due to trap states in grain boundary regions. In bulk YBCO, large 1/f noise, of a magnitude typical of metal-insulator composites, was observed in the normal state (36). Noise level in bulk rf SQUIDs of YBCO operated at 77K was of the order of 10^4 $\Phi_0/Hz^{1/2}$ (37). In granular YBCO film infrared detectors, the detectivity, D^*, (a signal/noise figure of merit) was 10^6 to 10^7 $cmHz^{1/2}/W$ (38,39), several orders of magnitude below the required value. These device results, while preliminary and possibly attributable to external noise sources, suggest that noise might prove to be the main factor limiting the granular material usefulness.

5. CONTROL OF SURFACES AND INTERFACES

We have shown that degraded YBCO film surfaces and interfaces are presently inhibiting the development of active and passive electronic components. Current processing approaches to overcome this problem are as follows.

1. *Free surface:* In-situ fabrication of epitaxial films, including post-deposition annealing in oxygen, eliminates the exposure to ambient atmosphere prior to the deposition of an overlayer for encapsulation, electrical contact or barrier formation. Fast post-deposition heating of amorphous oxide deposits to the crystallization temperature is intended to minimize atomic segregation on the surface. By this approach we have thus far produced near-zero dc surface resistance contacts to gold, less than 4×10^{-10} ohm.cm^2. The Au overlayer was evaporated at room temperature and not subject to post-annealing. No evidence of surface segregation was found in compositional depth profiles of the YBCO/Au interface, in contrast to profiles of films oxidized in amorphous state over a long time period (17). High-temperature deposition at O_2 partial pressures sufficiently elevated to permit YBCO crystallization during growth should be even more effective in minimizing segregation, even if additional post-annealing is still required. The described approach may be adequate for low-rf-loss passive components and tunneling into YBCO/barrier bilayers using a Pb, Nb or NbN counterelectrode deposited at low temperature. Unfortunately, all-YBCO tunnel junction fabrication will require high-temperature deposition or annealing of the counterelectrode film which is likely to produce interdiffusion with the barrier and result in shorts. However, in the case of epitaxial all-NbN tunnel junctions, processing up to 700°C was possible(40) so that success with YBCO may not be impossible.

2. *Film/ Substrate Interface:* Lowest possible deposition and crystallization temperature helps minimizing the interdiffusion. In $SrTiO_3$/YBCO, for example, our compositional depth profiles show catastrophic interdiffusion once the temperature exceeds 850°C. Buffer layers appear highly desirable and are investigated by many groups. For example, Gurvich and Fiory reported that ZrO_2/Ag, ZrO_2/Nb, MgO/Ag and MgO/Nb worked well as substrate/buffer combinations (16). Some of these may have a potential for YBCO epitaxy. Interdiffusion with ZrO_2 itself is not strong and, in fact, a notable success was recently obtained by Mogro-Campero et al. who deposited high-T_c polycrystalline YBCO on Si/ZrO_2 in spite of a rather violent reaction between YBCO and Si (41). Buffer layers on sapphire and silicon permitting YBCO epitaxy have not been reported.

6. CONCLUSION

Within the constraints imposed by intrinsic oxide superconductor properties, especially the electronic anisotropy and the extreme type II behavior, the prospects for electronic applications will largely depend on the technologist's ability to fabricate layered epitaxial film structures with undegraded, high-quality surfaces and interfaces. The quality requirements imposed by passive components appear less stringent than those necessary for functional tunnel junctions. Usefulness of films of the now emerging new group of Bi-Sr-Ca-Cu superconducting oxides should be evaluated from this point of view. Other problems, including strain effects not discussed here, appear more tractable.

ACKNOWLEDGEMENT

I would like to thank members of the Westinghouse Superconductivity Group and Dr. A. C. Anderson of MIT-Lincoln Laboratory for useful discussions and Mrs. M. B. Cross for careful preparation of this manuscript.

REFERENCES

References listed are only examples drawn from the explosively growing literature of the subject.

(1) M.R. Beasley and C.J. Kircher, in: Superconductor Materials Science, eds. S. Foner and B.B. Schwartz (Plenum Press, N. Y. 1981) pp. 605-684.

(2) S.I. Raider, IEEE Trans. on Magnetics MAG-21 (1985) 110.

(3) A.I. Braginski, J.R. Gavaler, M.A. Janocko and J. Talvacchio, in: SQUID '85 - Superconducting Quantum Interference Devices and their Applications, eds. H.D. Hahlbohm and H. Luebbig (W. de Gruyter, Berlin, 1985) pp. 591-629.

(4) A convincing evidence can be found in Proceedings (Extended Abstracts) of the 1987 International Superconductivity Electronics Conference (ISEC '87), Tokyo, August 1987 (unpublished).
(5) H. Maeda, Y. Tanaka, M. Fukutomi and T. Asano, Jpn. J. Appl. Phys. 27 (1988) No. 2 (in print).
(6) C.W. Chu, J. Bechtold, L. Gao, P.H. Hor, Z.J. Huang, R.L. Meng, Y.Y. Sun, Y.Q. Wang and Y.Y. Xue, Phys. Rev. Lett. 60 (1988) in print.
(7) K. Zhang, B. Dabrowski, C.U. Serge, D.G. Hinks, I.K. Schuller, J.D. Jorgensen and M. Slaski, J. of Physics C, 1988 (in print).
(8) B.G. Bagley, L.H. Greene, J.M. Tarascon and G.W. Hull, Appl. Phys. Lett. 51 (1987) 622.
(9) Y. Iye, T. Tamegai, H. Takeya and H. Takei, in: Superconductivity in Highly Correlated Fermion Systems, eds. M. Tachiki, Y. Muto and S. Maekawa (North-Holland, Amsterdam, 1987) pp. 225-227. This volume is referred to as SHCFS.
(10) W.J. Gallagher, T.K. Worthington, T.R. Dinger, F. Holtberg, D.L. Kaiser and R.L. Sandstrom, in: SHCFS, pp. 228-232.
(11) Y. Enomoto, M. Suzuki, M. Oda and T. Murakami, in: SHCFS, pp. 408-410.
(12) P.M. Mankiewich, J.H. Scofield, W.J. Skocpol, R.E. Howard, A.H. Dayem and E. Good, Appl. Phys. Lett. 51 (1987) 1753.
(13) R.L. Barns and R.A. Laudise, Appl. Phys. Lett. 51 (1987) 1373.
(14) F.G. Karioris and E.R. Vance, Material Lett. 6 (1987) 16.
(15) M. Naito, R.H. Hammond, B. Oh, M.R. Hahn, J.W.P. Hsu, P. Rosenthal, A.F. Marshall, M.R. Beasley, T.H. Geballe and A. Kapitulnik, J. Mater. Res. 2 (1987) 713.
(16) M. Gurvich and A.T. Fiory in: High Temperature Superconductors, eds. M.B. Brodsky, H.L. Tuller, R.C. Dynes and K. Kitazawa (Materials Research Society, Pittsburgh, 1988) p. 297.
(17) J.R. Gavaler and A.I. Braginski, this Conference.
(18) D.C. Mattis and J. Bardeen, Phys. Rev. 111 (1958) 412.
(19) R.S. Withers, A.C. Anderson, J.B. Green and S.A. Reible, IEEE Trans. on Magnetics, MAG-21 (1985) 186.
(20) S.A. Reible, IEEE Trans. on Magnetics MAG-21 (1985) 193.
(21) J.B. Green, L.N. Smith, A.C. Anderson, S.A. Reible and R.S. Withers, IEEE Trans. on Magnetics MAG-23 (1987) 895.
(22) S. Faris, (Hypres) unpublished.
(23) C.C. Chi, W.J. Gallagher, I.N. Duling III, D. Grischkowsky, N.J. Halas, M.B. Ketchen and A.W. Kleinsasser, IEEE Trans. on Magnetics MAG-23 (1987) 1666.
(24) L. Cohen, I.R. Gray, A. Porch and J.R. Waldram, J. Phys. F 17 (1987) L179.
(25) M. Hagen, M. Hein, N. Klein, A. Michalke, G. Mueller, H. Piel, R.W. Roeth, F.M. Mueller, H. Scheinberg and J.L. Smith, J. Magnetism and Mag. Matls. 68 (1987) L1.
(26) M.S. DiIorio, A.C. Anderson, B.-Y.Tsaur, Phys. Rev. B (1988) in print.
(27) J.P. Carini, A.M. Awasthi, W. Beyermann, G. Gruener, T. Hylton, K. Char, M.R. Beasley and A. Kapitulnik, Phys. Rev. B 37 (1988) in print.
(28) J. Benard, N.H. El Minyawi and N.T. Viet, Rev. Phys. Appl. 12 (1978) 483.
(29) D.L. Rubin, K. Green, J. Gruschus, J. Kirchgessner, D. Moffat, H. Padamsee, J. Sear and Q.S. Shu, Phys. Rev. B 37 (1988) in print.
(30) M.G. Blamire, G. Morris, R.E. Somekh and J.E. Evetts, J. Phys. D 20 (1987) 1330; also a presentation at the 1987 MRS Fall Meeting (unpublished).
(31) I. Iguchi, H. Watanabe, Y. Kasai, T. Mochiku, A. Sugishita and E. Yamaka, Jpn. J. Appl. Phys. 26 (1987) L645.
(32) A. Inoue, K. Takeuchi, H. Ito, A. Nakayama, Y. Okabe, M. Kawasaki and H. Koinuma, Jpn. J. Appl. Phys. 26 (1987) L1443.
(33) A. Nakayama, A. Inoue, K. Takeuchi and Y. Okabe, Jpn. J. Appl. Phys. 26 (1987) L2055.
(34) A.F. Marshall, R.W. Barton, K. Char, A. Kapitulnik, B. Oh, R.H. Hammond and S.S. Laderman, Phys. Rev. B 37 (1988) in print.
(35) R.H. Koch, C.P. Umbach, G.J. Clark, P. Chaudhari and R.B. Laibowitz, Appl. Phys. Lett. 51 (1987) 200.
(36) J.A. Testa, Y. Song, X.D. Chen, J. Golben, S.-I. Lee, B.R. Patton and J.R. Gaines, Phys. Rev. Lett. 60 (1988) in print.
(37) J.E. Zimmerman, J.A. Beall, M.W. Cromar and R.H. Ono, Jpn. J. Appl. Phys. 26-3 (1987) 2125.
(38) M. Leung, P.R. Broussard, J.H. Claassen, M. Osofsky, S.A. Wolf and U. Strom, Appl. Phys. Lett. 51 (1987) 2046.
(39) M.G. Forrester and M. Gottlieb (Westinghouse) unpublished data.
(40) J. Talvacchio, J.R. Gavaler and A.I. Braginski, in: Metallic Multilayers and Epitaxy, eds. M. Hong, S.A. Wolf and D.U. Gubser (TMS-AIME, Pittsburgh, 1988) pp. G1-G26.
(41) A. Mogro-Campero, B.D. Hunt, L.G. Turner, M.C. Burrell and W.E. Balz, Appl. Phys. Lett. 52 (1988) in print.

CRYSTAL LATTICE MEASUREMENTS IN SUPERCONDUCTING MATERIALS

F. W. Lytle, E. C. Marques, R. B. Greegor and H. G. Ahlstrom, The Boeing Co., Seattle, WA 98168

E. M. Larson and D. E. Peterson, Los Alamos National Laboratory, Los Alamos, NM 87545

A. J. Panson, Westinghouse Research and Development Center, Pittsburgh, PA 15235

ABSTRACT

The EXAFS technique was used to investigate the structural parameters of the Y and Cu atoms in $YBa_2Cu_3O_7$. An antisite disorder of 0.16±0.05 mole fraction was found between the Y and Cu_2 sites. It was also demonstrated that powder x-ray and neutron diffraction techniques are insensitive to this degree of disorder.

1. INTRODUCTION

We used the extended x-ray absorption fine structure (EXAFS) technique to investigate the near neighbor environment of the Cu and Y atoms in $YBa_2Cu_3O_7$ (YBC). We find a significant amount of antisite disorder between the Cu_2 and Y sites in agreement with our earlier results[1,2]. New data taken at 77K for both the Cu and Y K-edges of excellent quality allowed a more accurate determination of the amount of disorder and the bond distances involved. As discussed below, ordinary diffraction techniques are insensitive to small amounts of antisite disorder in this material; however, other spectroscopies have detected evidence of disorder. Warren et al.[3] used nuclear quadrupole resonance to measure the spin-lattice relaxation rates of ^{63}Cu at the Cu_1 and Cu_2 sites in YBC. They found a large background rate for the Cu_2 site, one explanation of which "include divalent Cu associated with disorder in the Cu_2 planes and antisite defects in which Cu is located on the Y lattice". It will be shown that this is consistent with our results. Collings et al.[4] reported electron spin resonance measurements of $(Y_{.5},Gd_{.5})Ba_2Cu_3O_7$. They observed a Gd signal of Dysonian line shape which indicates that some of the Gd is in a site of distorted coordination, i. e. it is not all in the Y site.

In this paper we report the analyis by multi-shell least squares fitting of Cu and Y K-edge EXAFS data from well characterized YBC. We find consistency between the results for Y and Cu. Y has an extra Y-O short bond and Cu has an extra Cu-O long bond. The bond lengths and relative amounts of each show that 0.16 ± 0.05 mole fraction of the Y is in the Cu_2 site and the Cu_2 atoms are in the Y site.

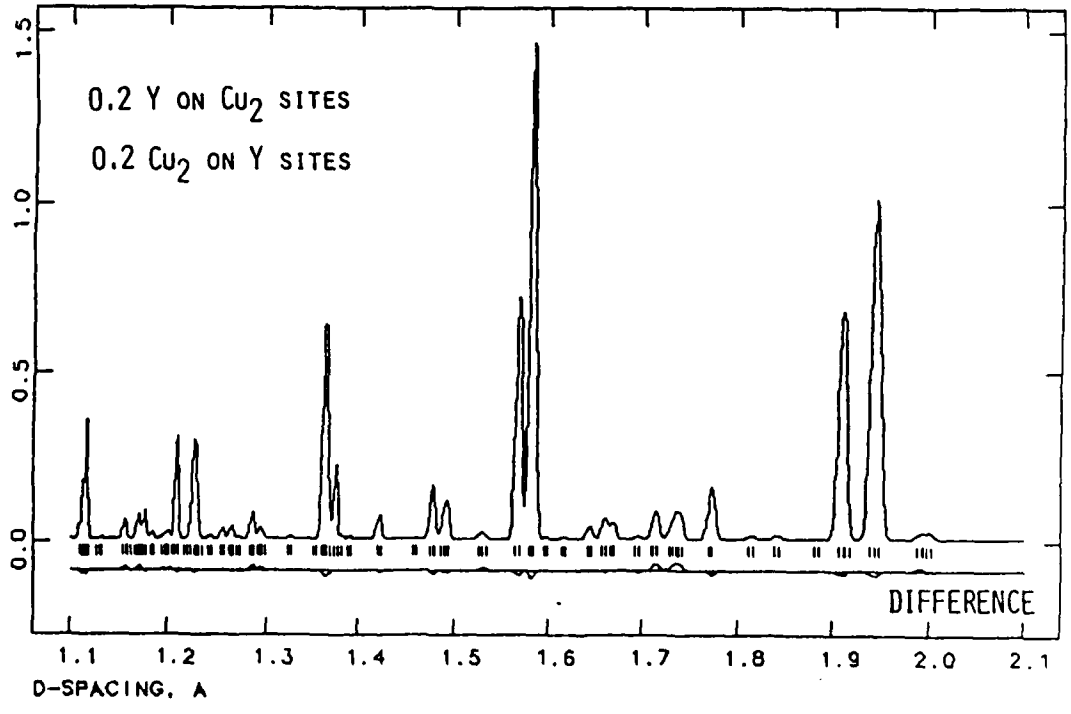

Fig. 1. Comparison of calculated x-ray diffraction patterns for YBC with and without 0.2 mole fraction Cu/Y antisite disorder.

2. COMPARISON OF EXAFS TO DIFFRACTION TECHNIQUES

The x-ray and neutron diffraction techniques commonly used for investigating the structure of materials have limitations in sensitivity when the scattering factors of the different elements are similar. This is the case for neutron diffraction from YBC where the neutron scattering lengths[5] for Cu and Y are 0.76 and 0.79 X 10^{-12} cm, respectively. Obviously, neutron diffraction can't differentiate accurately between Cu and Y. It is not so obvious that x-ray diffraction powder patterns of YBC are also insensitive to significant amounts of antisite disorder. Work in progress has demonstrated this[6] and is illustrated in Fig. 1. The x-ray diffraction pattern has been calculated for the case of Cu K_α radiation using structure parameters obtained from a joint refinement of x-ray and neutron diffraction data[7]. Then a second diffraction pattern has been calculated with 0.2 mole fraction Cu atoms distributed at random on the Y sites and 0.2 mole fraction Y distributed at random on the Cu_2 sites. The difference line shown at the bottom of Fig. 1 indicates how similar the two patterns are to each other. Some other combinations of antisite disorder are compared to the pattern without disorder in Table 1. The small residual errors of these calculations demonstrate that x-ray diffraction powder patterns are insensitive to 0.2-0.3 mole fraction disorder in YBC. Since good Rietveld refinements of diffraction data usually have residuals of approximately 5% the technique would be insensitive. Diffraction experiments could be done with improved sensitivity if the diffraction wavelength is tuned near to the absorption edge of the element of interest, i. e. anomalous dispersion. Some cases may be sufficiently sensitive to detect the effect[6].

X-ray diffraction single crystal data should be more sensitive to disorder. However, there have been difficulties in growing good crystals. Because of differences between crystals, perhaps, the parameters determined from a number of experiments don't agree very well with each other. The crystals also appear to be all twinned down to a scale of ~20 Å. It is not known what effect this will have on refinement of diffraction data, but must add noise and decrease the sensitivity for small structural differences.

Unlike diffraction techniques x-ray absorption spectroscopy has an element specific advantage. The x-ray energy is tuned to an absorption edge of each kind of atom in the material. The structure probe is the quantum interference of the ejected photoelectrons as they scatter from atoms surrounding the absorbing species. The technique is sensitive only to the short range structure around the absorbing atom. In polycrystalline materials directional information can't be obtained. The best that can be done is a radial structure function centered on the absorbing atom and averaged over the different sites of that atom. Specific distances can be used to identify occupancy in various lattice sites. In the following it is demonstrated that both Cu and Y have extra near neighbor distances which can be explained by antisite disorder.

3. EXPERIMENTAL DETAILS AND DATA ANALYSIS

The YBC compounds were well characterized[1,8,9], single phase, with a midpoint in the transition temperature of greater than 90K. They were kept dry under dessicant until prepared for an absorption sample. The sample was ground under acetone and smeared with Duco cement to an effective absorption length of approximately 1. The sample was then mounted in a cryostat, evacuated and cooled to 77K. The normal absorption mode spectra were measured at the Stanford Synchrotron Radiation Laboratory (SSRL) using a double crystal Si(220) monochromator. Multi-passes through the Cu and Y edge regions were measured and averaged in order to obtain data of excellent quality. Comparable data were also obtained for the reference compounds used to extract phase shifts and scattering factors. The ideal refer- compound contains the element of interest in perfectly regular coordination by the back-scattering atom of interest and in a pure form. We were unable to find compounds of either Cu or Y meeting those criteria; therefore, NiO and SrO were chosen for the phase shift and oxygen back scattering envelopes for Cu-O and Y-O, respectively. Both compounds have the NaCl-type structure with regular, octahedral coordination. Also, the structure is loosely packed so that it is possible to cleanly isolate the coordination shells with little leakage from the Fourier components of nearby shells. We have found that the use of adjacent elements in the Periodic Table for the evaluation of the phase shift is accurate. This was proved by using the phase shifts on other compounds of known structure containing Y and Cu

Our data analysis techniques have been described in detail[10,11]. In summary the EXAFS

$$\chi(K) = \sum_j A_j(K) \sin[2KR_j + \phi_j(K)] \tag{1}$$

$$A_j(K) = (N_j/KR_j^2)F_j(K) \exp(-2K^2\sigma_j^2) \tag{2}$$

is Fourier transformed,

$$\Phi_n(R) = (1/2\pi)^{1/2} \int_{K_{min}}^{K_{max}} K^n \chi(K) \exp[i[2KR + \phi_j(K)]]\, dK. \tag{3}$$

to produce a radial structure function centered on the absorbing atom. We proceed by taking the Fourier transform without including the phase shift, $\phi_j(K)$. The total phase,

$$\phi_{total}(K) = 2KR + \phi_j(K) \tag{4}$$

was evaluated from the reference compounds NiO and SrO by back transforming the region of the first structure peak.

$$K^n X_1(K) = (2/\pi)^{1/2} \int_{R_1-\Delta R}^{R_1+\Delta R} \Phi_n(R) \exp[-(2iKR)]\, dR \tag{5}$$

Since the transform is complex with real Re(K) and imaginary Im(k) parts,

$$\phi_{total}(K) = \tan^{-1}[\mathrm{Im}(K)/\mathrm{Re}(K)]. \tag{6}$$

The desired phase shift function results from the simple subtraction,

$$\phi_j(K) = \phi_{total}(K) - 2KR_j. \tag{7}$$

where R_j is accurately known for the reference compounds. The extracted Ni-O and Sr-O phase shifts are shown in Fig. 2. These phase shifts were used to obtain the oxygen phase-corrected transforms of NiO and SrO and then the first peak area was back transformed. The X(K) extrema of these damped, sine waves were used for the back scattering amplitude, F(K), to fit the Cu and Y EXAFS of YBC and are shown in Fig. 3. The difference in thermal disorder at 77K in the two compounds is visible in the damping. SrO is quite similar to Y in YBC and NiO to Cu. This will become apparent in the fitting.

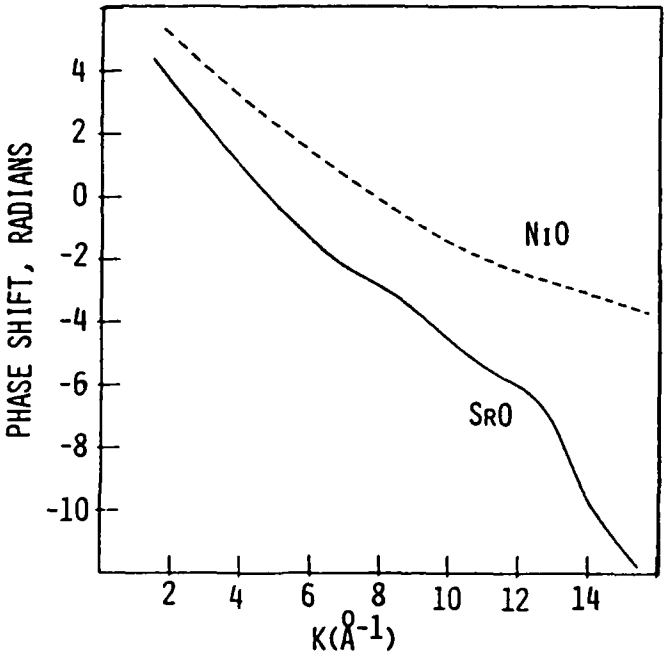

Fig. 2. EXAFS phase shifts extracted from NiO and SrO.

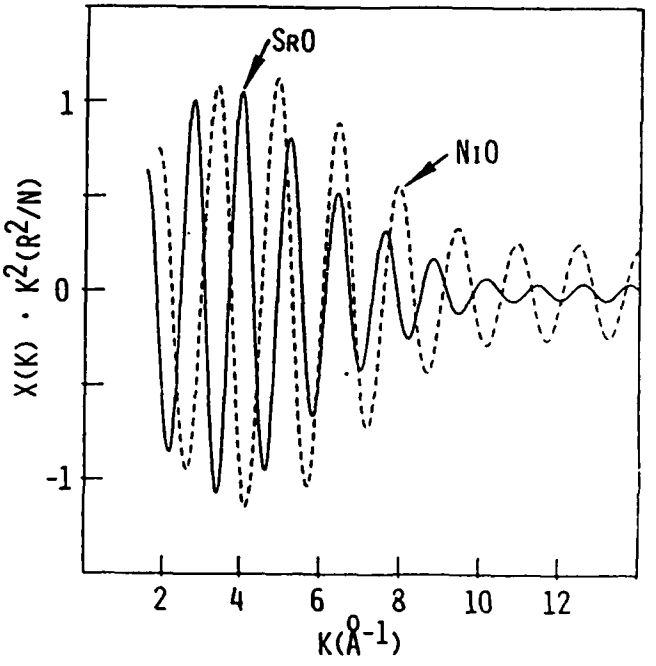

Fig. 3. Oxygen back scattering amplitudes extracted from NiO and SrO. Adjusted for R^2/N.

The phase shifts of Fig. 2 were used to evaluate the oxygen phase corrected transforms of Y and Cu in YBC and are shown in Fig. 4 along with the data, X(K). Over-plotting the Cu and Y transforms shows that they share common distances, approximately. It is not possible to accurately evaluate distances and coordination numbers from transforms because the small structure peaks interfere with the termination ripples which are an unavoidable side effect of the finite Fourier transform. In order to accurately evaluate coordination number and bond distance we use the Fourier transform to filter out the area of the first structure peak(s) and fit the function in K-space to avoid the effect of the termination ripples. These functions were fitted using the parameters of Figs. 2 and 3 with a non-linear, least squares fitting routine[10] capable of varying N, R and $\Delta\sigma^2$ for a number of different bond distances. Table 2 lists the normal Cu-O and Y-O distances as determined from an average of three neutron diffraction determinations[12,13,14] which agree well with each other. These values were averaged appropriate to the resolution of the EXAFS technique as shown in Table 2 and used as first trial for fitting the data. For example, the Y-O fit was begun with N=8, R=2.40 and $\Delta\sigma^2$=0. These parameters were all allowed to vary to obtain the

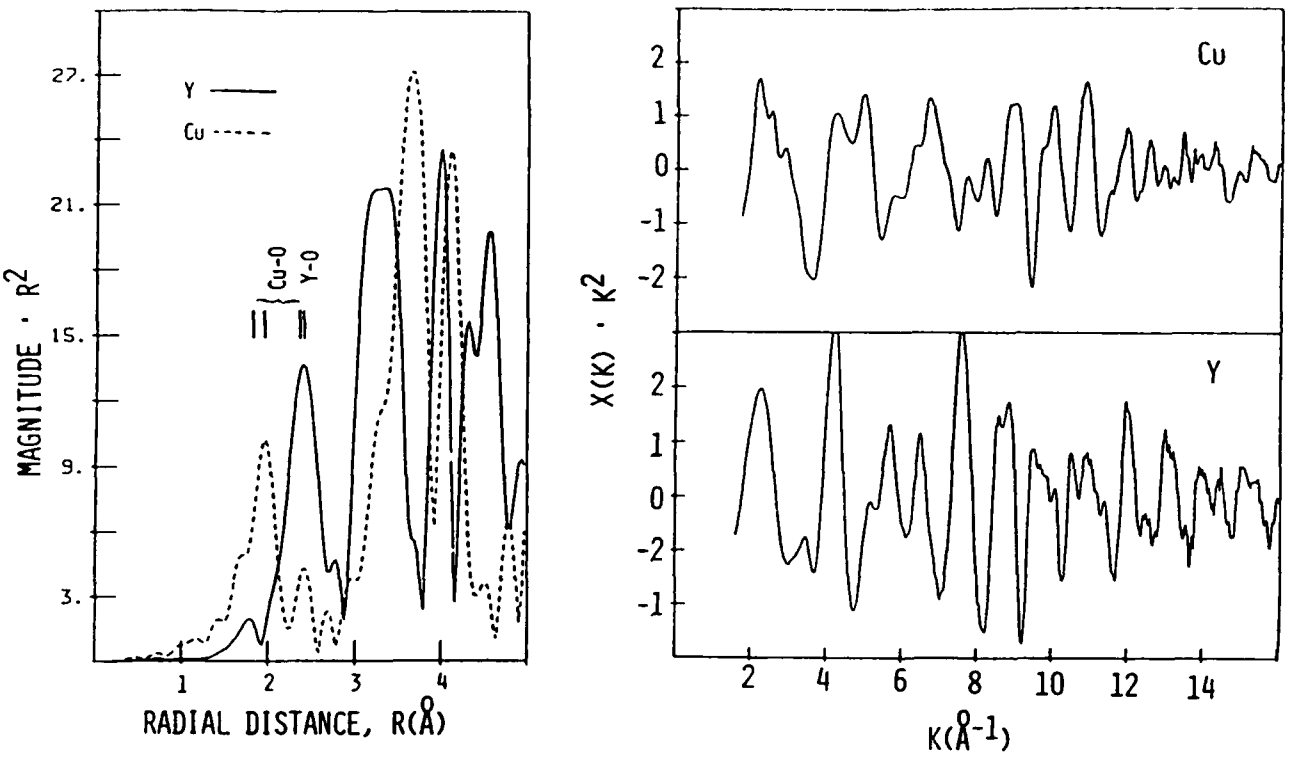

Fig. 4. Right, the measured $X(K)\cdot K^2$ EXAFS functions for the K-edges of Y and Cu in YBC. Left, oxygen phase-corrected transforms, note the common distances for Cu and Y.

best possible fit. The final parameters of the single shell fit are listed in Table 3. Then an additional set of parameters was allowed to vary for another bond distance where N, R, and $\Delta\sigma^2$ could take any value. The only improved fit occurred for a shorter Y-O bond, R=2.1 Å as given in Table 3 and shown in Fig. 5. The $\Delta\sigma^2$ values are relative to SrO at 77K and the negative values indicate slightly stiffer bonds in YBC. This is consistent with the shorter Y-O bond lengths in YBC relative to SrO (2.57Å). For the Cu fit the first trial was begun with the three separate distances and coordination numbers given in Table 2, again varying all parameters to obtain the best three-shell fit as given in Table 3. Then an additional Cu-O distance was allowed to vary all parameters to obtain the final improved fit parameters given in Table 3 and shown in Fig. 6

Table 1. Sensitivity of x-ray diffraction powder patterns to Y/Cu disorder.

Atom distribution	Residual error, R_p
0.3 Cu at random on Y site 0.15 Y on Cu_1, 0.15 Y on Cu_2	0.044
0.3 Cu at random on Y site 0.3 Y on Cu_1	0.036
0.3 Cu at random on Y site 0.3 Y on Cu_2	0.059
0.2 Cu at random on Y site 0.2 Y on Cu_1	0.024
0.2 Cu at random on Y site 0.2 Y on Cu_2	0.039
0.2 Cu at random on Y site 0.1 Y on Cu_1, 0.1 Y on Cu_2	0.029
0.2 Cu at random on Y site 0.15 Y on Cu_1, 0.05 Y on Cu_2	0.027
refined diffraction profile coefficients of last case 3 cycles	0.023

Table 2. Summary of distances determined by neutron diffraction[12, 13, 14].

Bond	Number	Distance, Å	Average	
Cu_1-O_4	2	1.84±0.01	0.67	1.84
Cu_1-O_1	2	1.943±0.002		
Cu_2-O_2	2	1.929±0.001	3.33	1.94
Cu_2-O_3	2	1.961±0.003		
Cu_2-O_4	1	2.31±0.02	0.67	2.31
Y-O_2	4	2.382±0.005	8.0	2.40
Y-O_3	4	2.412±0.01		

Note: The ratio of the number Cu_1/Cu_2 is 1/2.

The distance error covers the differences in the three determinations

Table 3. Summary of fitted structure parameters.

	Number of bonds N	Distance R, Å	Relative disorder $\Delta\sigma^2$, Å^2	Std. dev.
Y, single shell fit	7.5	2.39	-0.0030	0.894
Y, 2 shell fit	0.7±0.3 6.8±1.0	2.1±0.1 2.38±0.02	-0.0028 -0.0034	0.855
Cu, 3 shell fit	0.9 2.3 0.4	1.82 1.94 2.27	0.0066 -0.0002 0.0007	.822
Cu, 4 shell fit	0.9±0.3 2.7±0.5 0.5±0.2 0.9±0.3	1.81±0.05 1.94±0.02 2.25±0.05 2.5 ±0.1	-0.0001 -0.0011 -0.0006 0.012	.601

$$\text{Std. dev.} = \sum_i \frac{(\chi^2_{data} - \chi^2_{calc.})^{\frac{1}{2}}}{\text{No. of data points}}$$

Only a longer Cu-O bond improved the fit to include the "beat" which is visible in the data. The values listed in Table 3 are the average of fits to two different samples. The errors were estimated from the differences in the two samples, by exploring parameter space in detail to prove that a true minimum had been obtained and by determining the relative sensitivity of all the parameters. Plainly, the smaller N components could not be determined as accurately as the major ones. Again, the negative $\Delta\sigma^2$ values show the three expected Cu-O bonds to be slightly stiffer than NiO at 77K; however, the long Cu-O bond of 2.5 Å has significantly more disorder. This is consistent with a large thermal amplitude of Cu in this site, i. e. a soft mode. The longer than expected Cu-O distance, 2.5 vs 2.4 Å, may be the result of errors accumulating in the complicated fit or to an inaccurate phase shift for Cu^{3+}. The Y-O distance of 2.1 Å may indicate that Y is occupying the Cu_2 sites slightly above the normal Cu_2 position. The anisotropic Cu_2-site disorder aligned along the c-axis direction which was found by Williams et al.[7] may be due to this effect. For both Y and Cu the introduction of the antisite bond resulted in significantly better fits to the data as shown in Table 3.

The results of Table 3 may be used to evaluate the mole fraction, x. of each species in each site provided that assumptions can be made about the coordination number of each site. Cu can easily fit into the Y site; however, the larger size of Y relative to Cu and the 2.1 Å bond found in the least squares fit suggests that it is located slightly above the normal Cu_2 site. The coordination would then be four at 2.1 Å plus the apical oxygen at approximately 2.4 Å. Thus, this bond would be included in the other component of the fit to the data. With this assumption, the bond assignments are made in Table 4 in the form of linear equations in x. Note that there are two Cu_2 sites to one Cu_1. The solutions form a consistent set with $x = 0.16 \pm 0.05$ from either the perspective of the Y or Cu atoms. Similar relations may be set up with some fraction of Y in the Cu_1 site; however our results are not consistent with any amount of Y occupying the Cu_1 site. Thus, the degree and type of disorder found is approximately that of the hypothetical diffraction pattern of Fig. 1.

4. DISCUSSION AND CONCLUSIONS

These results are firm evidence for antisite disorder between the Y and Cu_2 sites in YBC. The least squares fits from the perspective of both Y and Cu gave consistent results for both distance and mole fraction. For data of sufficient quality Fourier transforms including phase shift and over a sufficient range of K, 1.8 to 16.0 in Fig. 4, resolved the antisite distances for each atom. It was important not to apply a windowing function (Gaussian or Hanning) in order to cosmetically reduce the termination ripples or the resolution would be lost. We carefully chose zero crossings of X(K) at the beginning and end of the transform. It was also essential to carefully extract the X(K) function from the raw absorption edge using multi-passes of a variable spline or other curve following routine until the residue of this procedure was invisible in the data. Many of the analyses of EXAFS data which have appeared in the literature suffer from these effects.[15] We have digitized EXAFS data published by others and then analyzed it using the techniques discussed herein and verified that antisite disorder was present. It was usually lost by excessive windowing.

Table 4. Evaluation of antisite fraction, x.

Distance, R(Å)	Bond Type				N	x
	Cu_1-O_1	Cu_2-O_2,O_3	Cu_2-O_4	Cu in Y site		
1.94	2(1/3)	+ 4(2/3-x)			= 2.7	0.16
2.25			1(2/3-x)		= 0.5	0.17
2.5				8x	= 0.9	0.11
	Y - O_2,O_3		Y in Cu_2 site			
2.38	8(1-x)	+	1(x)		= 6.8	0.17
2.1			4(x)		= 0.7	0.17

$x_{avg} = 0.16 \pm 0.05$

The relative improvement of the fits when the antisite disorder was introduced for the two elements deserves comment, i. e. 5% for Y and 37% for Cu. This difference in sensitivity is primarily due to the change in coordination as the elements occupy sites with different coordination numbers. The amplitude of X(K) and hence, N determined from the fit, depends upon the coordination number associated with a specific distance. As Cu moves from a site with coordination number = 4 to 8 the EXAFS sensitivity improves by a factor of 2 for the same Cu fraction. Conversely, Y moving from a site with coordination = 8 to 4 decreases by 2.

In an earlier paper[1] we cited examples from the literature where antisite disorder had been detected in Perovskite-like materials. This was observed in materials where the scattering factors of the elements were sufficiently different to detect the effect and in compounds with oxygen atoms missing from a complete Perovskite lattice. The size mismatch of the larger A atom in the B site is apparently accommodated as oxygen vacancies open up the lattice. This appears to be the case in YBC in the neighborhood of the Y and Cu_2 sites. The problem in recognizing the effect has been that the structure results have been determined using data insensitive to the disorder effect.

It remains to be proved whether the observed antisite disorder is related to the superconductivity, but the effect should be considered in any theories sensitive to structure. At this time we know of no one who has presented a consistent, satisfying account of superconductivity in these materials from theories based upon a structure without disorder. Something appears to be missing. The antisite Cu ions occupying Y sites would provide an interconnection between the two Cu_2 planes via a very, loosely bonded Cu ion (perhaps Cu^{3+}), i. e. a soft mode. Our fit to this distance shows a large, apparently thermal, disorder although variable temperature experiments will be necessary to confirm that it is all thermal and not static disorder. Similar antisite disorder exists in the La_2CuO_4-based superconductors[1,2]. Antisite disorder may be essential for high temperature superconductivity.

5. ACKNOWLEDGEMENT

We thank SSRL and the help of the excellent staff. SSRL is funded by DOE and NIH.

6. REFERENCES

1. F. W. Lytle, R. B. Greegor and A. J. Panson, "Discussion of X-ray Absorption Near Edge Structure: Application to Cu in the High Tc Superconductors $La_{1.8}Sr_{0.2}CuO_4$ and $YBa_2Cu_3O_7$", Phys. Rev. B (to be published).
2. F. W. Lytle, R. B. Greegor and A. J. Panson, "Cu Substitution into the La/Y Sites in $La_{1.8}Sr_{0.2}CuO_4$ and $YBa_2Cu_3O_7$: Determination by X-ray Absorption Spectroscopy, in Novel Mechanisms of Superconductivity, p. 1049, S. Wolf and V. Kresin, eds. Plenum, 1987.
3. W. W. Warren, R. E. Walstedt, G. F. Brennert, G. P. Espinosa and J. P. Remeika, Phys. Rev. Lett. 59, 1860 (1987).
4. E. W. Collings, P. J. Melling, S. L. Swartz, R. D. Smith, J. J. Rayment, M. J. Pechan, and M. Pardavi-Horvath, "Magnetic Studies of a 1-2-3 ($Y_{.5}$,$Gd_{.5}$)BaCu Oxide Superconductor" Presented at Int. Cry. Mat. Conf., St. Charles, IL, June 1987. To be published in Advances In Cryogenic Materials, Vol. 34.
5. International Tables for X-ray Crystallography, Vol. 4, p. 270, Kynoch Press, Birmingham, England, 1974.

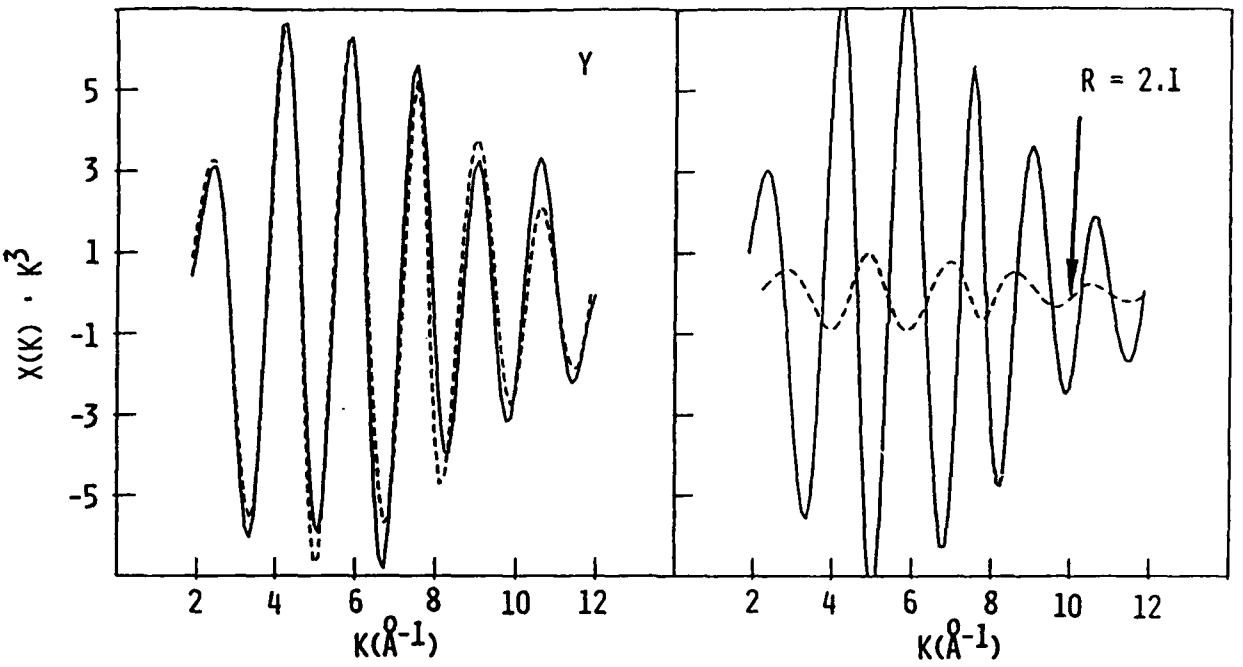

Fig. 5. Left, the dashed line is the fit to the Y data. The individual components of the fit are shown on the right.

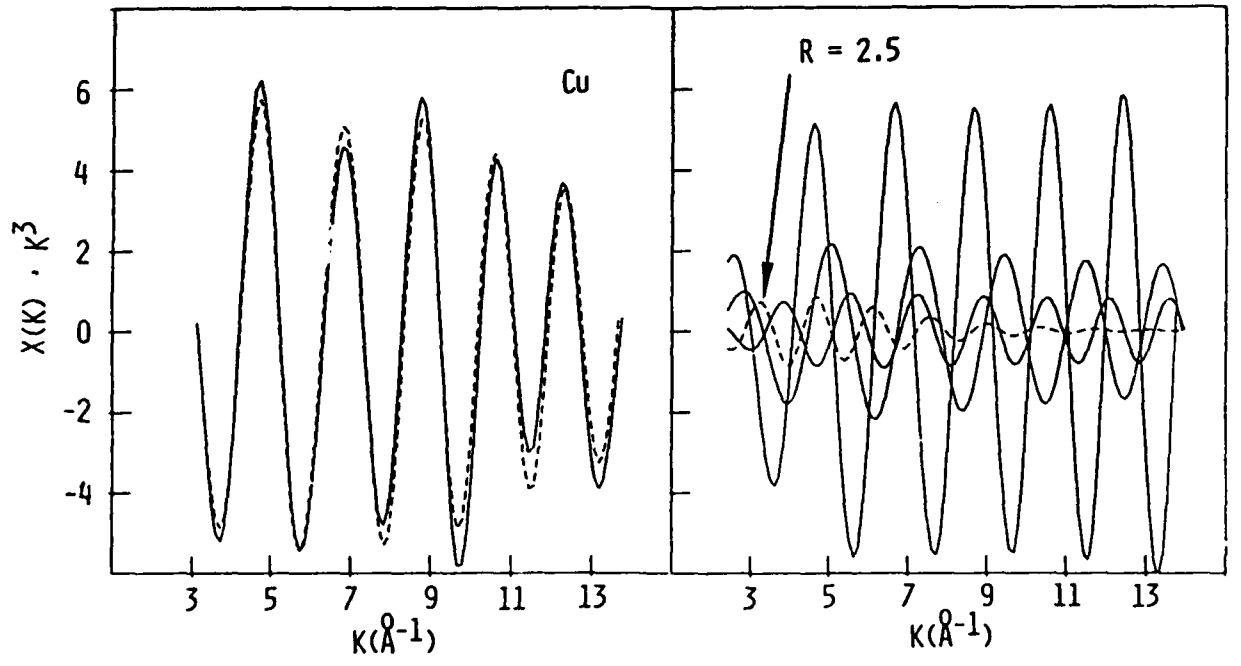

Fig. 6. Left, the dashed line is the fit to the Cu data. The individual components of the fit are shown on the right. They may be identified by their relative amplitudes in Table 3.

6. a) E. M. Larson (work in progress).
b) A. C. Larson and R. B. Von Dreele, "GSAS-Generalized Crystal Structure Analysis System", LA-UR-86-748, Los Alamos National Laboratory.
7. A. Williams, G. H. Kwei, R. B. Von Dreele, I. K. Raistrick and D. L. Bish, "Joint X-ray and Neutron Refinement of the Structure of Superconducting $YBa_2Cu_3O_7$: Precision Structure Anisotropic Thermal Parameters, Strain and Cation Disorder" (preprint).
8. A. J. Panson, A. I. Braginski, J. R. Gavaler, J. K. Hulm, M. A. Janocko, H. C. Pohl, A. M. Stewart, J. Talvacchio and G. R. Wagner, Phys. Rev. B35, 8774 (1987).
9. A. I. Braginski, "Study of Superconducting Oxides at Westinghouse", in Novel Superconductivity, p. 935, eds. S. Wolf and V. Kresin, Plenum Press, 1987.
10. G. H. Via, J. H. Sinfelt and F. W. Lytle, J. Chem. Phys. 71, 690 (1979).
11. F. W. Lytle, R. B. Greegor, E. C. Marques, D. R. Sandstrom, G. H. Via and J. H. Sinfelt, J. Catal. 95, 546 (1985).
12. W. I. F. David, W. T. A. Harrison, J. M. F. Gunn, O. Moze, A. K. Soper, P. Day, J. K. Jorgensen, D. G. Hinks, M. A. Beno, L. Soderholm, D. W. Capone, I. K. Schuller, C. U. Segre, K. Zhang and J. D. Grace, Nature 327, 310 (1987).
13. J. E. Greedan, A. O'Reilly and C. V. Stager, "Oxygen Ordering in the Crtysal Structure of the 93K Superconductor $YBa_2Cu_3O_7$ by Powder Neutron Diffraction", (submitted).
14. M. A. Beno, L. Soderholm, D. W. Capone, D. G. Hinks, J. D. Jorgensen, I. K. Schuller, C. U. Segre, K. Zhang and J. D. Grace, "Structure of the Single Phase High Temperature Superconductor $YBa_2Cu_3O_7$", Appl. Phys. Lett. (to be published).
15. For example: A. Bianconi, A. Castellano, M. De Santis, C. Politis, A. Marcelli, S. Mobilio and A. Savoia, Z. Phys. B67, 307 (1987). H. Oyanagi, H. Ihara, T. Matsushita, M. Tokumoto, M. Hirabayashi, N. Terada, K Senzaki, Y. Kimura and T. Yao, Jap. J. Appl. Phys. 26, L368, (1987). J. B. Boyce, F. Bridges, T. Claeson, T. H. Geballe, C. W. Chu and J. M. Tarascon, Phys. Rev. B35, 7203 (1987).

High Temperature Superconductors II
Vol. EA-14, ed. by D.W. Capone II, W.H. Butler, B. Batlogg, and C.W. Chu
(Matls. Res. Soc., Pittsburgh, 1988)

FABRICATION OF HIGH-T_c SUPERCONDUCTING $YBa_2Cu_3O_7$ FILMS[a]

J. R. GAVALER, A. I. BRAGINSKI, J. TALVACCHIO, M. A. JANOCKO, M. G. FORRESTER AND J. GREGGI
Westinghouse R&D Center, 1310 Beulah Road, Pittsburgh, Pennsylvania 15235

INTRODUCTION

We have investigated the fabrication and properties of high-T_c superconducting films of $YBa_2Cu_3O_7$ (YBCO). The main goal of this investigation is to prepare films which could be used in high operating temperature tunnel junctions. Therefore the focus has been on optimizing the properties of the films with this goal in mind.

EXPERIMENTAL PROCEDURE

Films were deposited by both evaporation and by sputtering in a UHV deposition and analytical facility described previously.[1] Those made by evaporation were deposited onto ambient temperature substrates using three e-beam guns and pure yttrium, barium, and copper metals as the source materials. In some cases, following Mankiewich et al.[2], BaF_2 was used instead of barium as one of sources. The background impurity level during deposition was in the low 10^{-9} Torr region. The sputtered films were also deposited from the pure metals, the barium and yttrium with rf magnetron guns and the copper with a dc magnetron gun. Films were sputtered at substrate temperatures up to 450°C in different argon-oxygen gas mixtures. The total argon-oxygen pressure was kept at 2×10^{-2} Torr. The partial pressure of the oxygen was varied from 3×10^{-6} to 3×10^{-4} Torr. As detailed in a previous publication[3] the sputtering guns in our system are mounted along a 180° arc and point toward the center of the chamber. During deposition the substrate holder, mounted on a manipulator in the center of the chamber, is rotated back and forth to face the three guns sequentially. The deposition rate of the evaporated films was 400 to 500 Å/min. Typically the film thickness was <1 μm. The deposition rate of the sputtered film was ~30 Å/min. and the film thickness 3000 to 4000 Å. The substrates which have been used include sapphire, single crystal ZrO_2, MgO, and $SrTiO_3$. However, most of the depositions discussed in this paper were on single crystal (100) and (110) $SrTiO_3$. Following deposition, all of the films were in-situ or ex-situ annealed at 500°C in one atmosphere of oxygen and then given a second reaction anneal, also in oxygen, at 850°C for times up to one hour. Structural analyses of the films were made by in-situ reflection high energy electron diffraction (RHEED) and by ex-situ X-ray diffraction and transmission electron microscopy (TEM). Chemical analyses were by in-situ X-ray photoelectron spectroscopy (XPS), and ex-situ Auger Electron spectroscopy and energy-dispersive X-ray spectroscopy (EDS). Critical temperatures were measured resistively by the standard four-point van der Pauw method. Current densities were determined both from magnetization data and by measurement of the critical current through a 25 μm wide bridge.

RESULTS AND DISCUSSION

We found that all of our films both as-deposited and after a 500°C oxygen anneal, were amorphous or microcrystalline. After the 850°C anneal, X-ray diffraction data showed that the formation of the YBCO compound had occurred. This result is similar to that documented by many authors who have

a. Supported in part by the Air Force Office of Scientific Research, Contract No. F49620-85-C-0048.

reported that YBCO films can be prepared by a variety of thin film techniques, including evaporation and sputtering. Maximum reported T_c (R=0) values have generally varied between 80 and 90K. In our case, films can be routinely prepared on $SrTiO_3$ substrates by either sputtering or evaporation which are completely superconducting at ~85K. Since in many cases the conditions used to prepare films are nominally similar, the reason(s) for the published differences in maximum T_c's are not entirely clear. One explanation is that the films deviate slightly from ideal "1,2,3" stoichiometry to an extent which depends on the quality of control of the various deposition rates. Another possibility is the films are contaminated to some varying degree. We[4] and others[5] have shown that contaminants such as silicon, aluminum, magnesium, and zirconium from the substrates can depress the T_c's of YBCO films. It has been found by various workers that this type of contamination can be greatly reduced by depositing a buffer layer, such as Pt or Au, between the substrate and the YBCO overlayer.[6] In the case of films deposited on $SrTiO_3$, Auger depth profiling shows that both Sr and Ti from these substrates diffuse into films annealed at 850°C. However these elements apparently caused little degradation in T_c. We have also observed, in a few cases, depressed T_c's from contamination from a molybdenum substrate holder.

We have found that the evaporated films which are deposited without the deliberate addition of oxygen are polycrystalline after final annealing. The initial sputtered films made in our deposition system were also non-epitaxial with no orientation relationship between substrate and film.[3] However later sputtered films grown under nominally the same conditions were clearly epitaxial. The cause of this difference is not known with certainty but it may have been due to a poorer surface quality of our original $SrTiO_3$ substrates. Typically the YBCO structure epitaxially grown on (100) $SrTiO_3$ formed with the a-axis normal and the b- and c-axes parallel to the film surface. In this type of epitaxy, because of the square lattice of the (100) substrate surface, the c-axis of the orthorhombic YBCO overlayer can be expected to grow with equal probability in two possible directions normal to each other. TEM shows that this indeed is what occurs. Figure 1 illustrates a film on (100) $SrTiO_3$ in which there are two types of 'a' direction growth which have the two different 'c' direction orientations. The amount of the two types of growth is equally distributed throughout the film. The parallel lines in this micrograph lying perpendicular to the c-axis are defects on the ab planes.

This type of epitaxy in which the c-axis is parallel to the film surface is desirable for tunneling because the coherence length is longest for the directions normal to the c-axis, i.e. parallel to the CuO planes[7]. However having the c-axis parallel to the film surface limits the critical current density (J_c) of the film for current transported in the film plane. J_c's

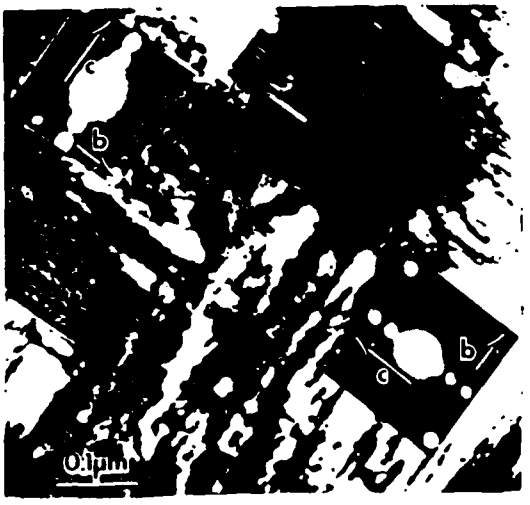

Fig. 1 TEM micrograph of epitaxial YBCO film on $SrTiO_3$ (100). The film exhibits a-axis growth of the 1,2,3 phase in domains with alternating b- and c-axes.

over 10^6 Amp/cm^2 can be obtained in films grown with the c-axis normal to the film surface.[8] Higher annealing temperature (>900°C) appears to favor this 'c' type growth on (100) $SrTiO_3$.[9] Enomoto et al.[10] have reported the growth of single crystal YBCO films on (110) $SrTiO_3$ which grew with the [110] direction normal and the c-axis parallel, to the film surface. Unlike our films grown on a (100) surface, the c-axis in the plane of the film was oriented in only one direction. This apparently was the result of the rectangular lattice on the (110) surface favoring the growth of the c-axis in only one preferred direction, as opposed to the square lattice on the (100) in which the c-axis can grow in either of two orthogonal directions with equal probability. The J_c's of the YBCO on the (110) $SrTiO_3$ were highly anisotropic. The current density, at 4.2K, normal to the c-axis was >> 10^6 Amp/cm^2. With the current parallel to the c-axis, $J_c = 3 \times 10^4$ Amp/cm^2. In our films on (100) $SrTiO_3$ having the "checkerboard" a-axis growth, the J_c's were isotropic with maximum values of 5×10^5 Amp/cm^2 at 4.2K.

Similar to results reported by others, both our epitaxial and polycrystalline films of YBCO have a non-superconducting near-surface layer. This layer is believed to be the cause of the measured high contact resistance and high rf surface resistance. Also our attempts to tunnel between YBCO and a Nb film counterelectrode have resulted, as of this writing, in ohmic I-V curves because of this degraded layer.

It has been widely reported that YBCO reacts with CO_2 and moisture when exposed to room air, causing a degraded surface layer. We have found that films processed entirely in-situ can also have a thick non-superconducting surface layer. Figure 2 shows an Auger depth profile of a film deposited in a partial pressure of oxygen of less than 10^{-9} Torr. The as-deposited metallic film was then annealed in-situ in one atmosphere of O_2 at ~500°C for 20 min. This anneal was found to stabilize the surface sufficiently to make it inert to room air. The film was then ex-situ annealed for one hour at 850°C. As can be noted in Fig. 2, the film contains an approximately 1500 Å non-stoichiometric surface layer. In general, depositions in partial pressures of oxygen of less than 3×10^{-6} Torr produced films in which, after annealing, copper was not even seen by XPS at the surface. Increasing the partial pressure of oxygen during deposition was found to change the near-surface compositions of metal atoms and their depth profiles. In the most oxygen deficient as-deposited films (Fig. 2), annealing caused the strongest

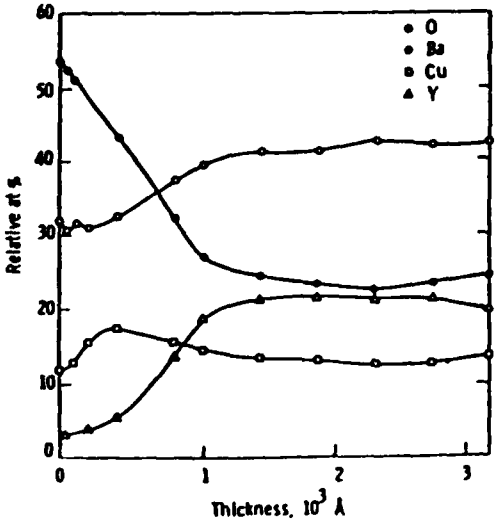

Fig. 2 Uncalibrated AES depth profile data on a YBCO film deposited in less than 10^{-9} Torr O_2. Film surface is at zero thickness.

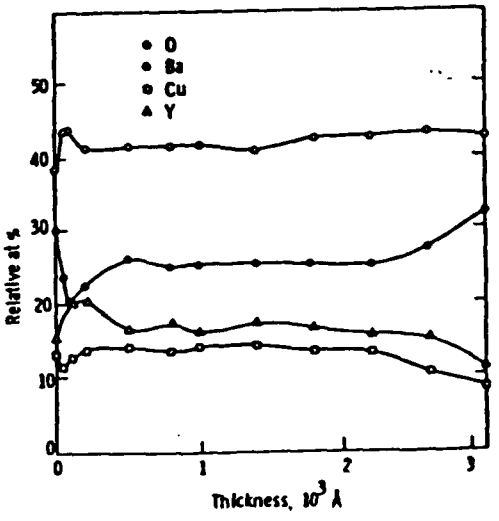

Fig. 3 Uncalibrated AES data on YBCO deposited in ~10^{-5} Torr oxygen. Annealing similar to that of Fig. 2.

atomic segregation of Ba toward the surface with a corresponding depletion of Cu and Y. The least amount of segregation was found in films deposited at the highest oxygen pressure used, i.e. 3×10^{-4} Torr. In this case the thickness of the degraded surface layer was reduced to a few hundred angstroms as shown in Fig. 3.

The above results lead to the conclusion that the oxidation of as-deposited films at temperatures below the YBCO crystallization temperature provides the driving force for the atomic segregation which produces the non-superconducting surface layers. Therefore, to minimize this segregation, it is necessary to deposit the films in as highly oxidized a state as possible. Our results also indicate that the elimination of the low-temperature anneal and the use of high ramp rates to the 850°C reaction temperature should be beneficial. After adopting these procedures, our most recent films show an almost total absence of segregation after annealing. On one of these films a 500 Å gold overlayer was deposited followed by a 2000 Å Nb counterelectrode both at room temperature. The final YBCO/Au/Nb structure was not annealed. The resistance between the Au-Nb and YBCO measured at 4.2K, was less than 4×10^{-10} ohm-cm^2, the sensitivity limit of the measurement, indicating that the non-superconducting surface layer was largely eliminated. We have also found that the non-superconducting surface layer can also be greatly reduced in evaporated films when BaF_2 is used as one of the source materials. In this case the barium apparently is tied up as fluoride and therefore cannot easily diffuse toward the surface during the oxidation-annealing process.

ACKNOWLEDGEMENT

We thank D. Detar (AES Profiling), T. Mullen (EDS), A. M. Stewart (X-ray diffraction), R. T. Blackham (TEM), and Mrs. M. B. Cross (preparation of the manuscript) for their valuable contributions.

REFERENCES

1. J. Talvacchio, M. A. Janocko, J. R. Gavaler, and A. I. Braginski, in Advances in Cryogenic Engineering - Materials, Vol. 32, edited by A. F. Clark and R. P. Reed (Plenum, New York, 1986) pp. 527-541.
2. P. M. Mankiewich, J. H. Scofield, W. J. Skocpol, R. E. Howard, A. H. Dayem, and E. Good, Appl. Phys. Lett. 51, 1751 (1987).
3. R. M. Silver and J. Talvacchio, Appl. Phys. Lett. 51, 2149 (1987).
4. A. I. Braginski, Novel Superconductivity, edited by S. A. Wolf and V. Z. Kresin (Plenum, New York, 1987), pp. 935-949.
5. See for example: M. Gurvitch and A. T. Fiory, High-Temperature Superconductors, ed. by M. B. Brodsky, H. L. Tuller, R. C. Dynes, and K. Kitazawa (Materials Research Society, Pittsburgh, 1988), p. 297.
6. See for example: M. Naito, R. H. Hammond, B. Oh, M. R. Hahn, J. W. P. Hsu, P. Rosenthal, A. F. Marshall, M. R. Beasley, T. H. Geballe, and A. Kapitulnik, J. Mtl. Res. 2, 713 (1987).
7. See for example: T. K. Worthington, Phys. Rev. Lett. 59, 1160 (1987).
8. P. Chaudhari, R. H. Koch, R. B. Laibowitz, T. R. McGuire, and R. J. Gambino, Phys. Rev. Lett. 58, 2684 (1987).
9. J. Kwo, T. C. Hsieh, M. Hong, R. M. Fleming, S. H. Liou, B. A. Davidson, and L. C. Feldman, High-Temperature Superconductors, ed. by M. B. Brodsky, H. L. Tuller, R. C. Dynes, and K. Kitazawa (Materials Research Society, Pittsburgh, 1988), p. 339.
10. Y. Enomoto, T. Murakami, M. Suzuki, and K. Moriwaki, Jpn. J. Appl. Phys. 26, L1248 (1987).

Invited Paper

In-Situ Fabrication, Processing and Characterisation of Superconducting Oxide Films*

A. I. Braginski, J. Talvacchio, J. R. Gavaler, M. G. Forrester and M. A. Janocko

Westinghouse R&D Center, Pittsburgh, PA 15235

ABSTRACT

Surfaces of $Y_1Ba_2Cu_3O_7$ (YBCO) are known to react with H_2O and CO_2 in the ambient atmosphere. The 'in-situ' approach to thin film fabrication and characterization in a closed system makes it possible to investigate the near-surface properties of superconducting YBCO films in the absence of such deleterious reactions. We have fabricated and analyzed superconducting, epitaxial YBCO films entirely or partly in-situ. Oxygen partial pressures during deposition ranged from $< 10^{-9}$ torr to $> 3 \times 10^{-4}$ torr and temperatures from 400 to > 650°C, producing either amorphous or crystalline deposits. We found that annealing of oxygen-deficient amorphous deposits in oxygen caused atomic segregation of Ba and Y to the surface with a corresponding depletion in Cu. This effect made near-surface layers nonsuperconducting even in the absence of H_2O or CO_2. Fast heating to crystallization temperature minimized the segregation. Measurements of dc contact resistance, R_c, and I-V characteristics in cross-strip junctions of YBCO/Au/Nb and YBCO/Au/MgO/Nb indicated near-zero R_c and weak-link I-V characteristics which proved that the in-situ approach permits one to obtain superconducting YBCO film surfaces. In the case of crystalline film deposition at 650°C, the in-situ electron-diffraction of $SrTiO_3$ substrates and 40 to 100 Å thick YBCO films revealed epitaxial crystallization only on clean substrates.

1. INTRODUCTION

The in-situ approach to fabrication, processing and characterisation of superconducting films and layered film device structures is motivated by requirements analogous to those of contemporary semiconductor technology of planar GaAs-based devices. Molecular beam epitaxy (MBE) ultra-high-vacuum (UHV) closed systems with multiple, interconnected chambers evolved to satisfy the need to:

1. Attain cleanliness of an epitaxial substrate or film surface and prevent contamination (e.g. by oxidation or water and organic adsorbate layers) during surface characterisation of the crystalline structure, composition, and contaminants, prior to the subsequent processing step.
2. Sequentially deposit epitaxial layers of similar and dissimilar materials while meeting the first requirement at all fabrication stages.
3. Co-deposit multi-component compounds or alloys from multiple sources while maintaining a precise composition control and uniform coating thickness.
4. Deposit at low growth rates, typically between 0.1 and 10 Å/sec to promote crystalline perfection without incorporating background impurities into the film.
5. Maintain an acceptable throughput in the system.

The main advantages of the in-situ approach are: protection of surfaces from atmosphere, preservation of clean interfaces, and their non-destructive characterisation. The disadvantages are inflexibility due to the need to maintain UHV, and the high level of capital investment, both initially and during any scale-up of technology.

Until this decade, superconducting electronic devices were fabricated exclusively of polycrystalline films deposited in HV, typically 10^{-6} to 10^{-7} torr, so that only the control of film composition could be accomplished, but not epitaxy or control of impurity incorporation. In the early 1980's, attempts to maximise the operating temperature of Josephson tunnel junctions with NbN and A15-structure compound electrodes stimulated some work on epitaxial and single crystal film growth of these conventional, low-critical-temperature, T_c, superconductors (LTS).[1] The recent discovery of high-T_c oxide superconductors (HTS), of which the $Y_1Ba_2Cu_3O_7$ (YBCO) compound, which has a_1T_c = 90-95K, is the generic example used in this paper, will give the in-situ approach more prominence in the technology of superconducting electronics. In fact, this approach now appears necessary for fabrication of multilayered device film structures. The two main reasons are: (1) The pronounced electronic anisotropy of YBCO and other superconducting cuprate crystals, which manifests itself as anisotropy in normal resistivity, ρ, critical fields H_{c1} and H_{c2}, critical current, J_c, and in the two characteristic length scales for superconductivity, the coherence length, ξ, and magnetic field penetration depth, λ.

* Supported in part by AFOSR Contract No. F49620-88-C-0039.

(2) The surface reactivity and instability of YBCO. The anisotropy mandates the use of oriented, epitaxial films while the surface reactivity makes a protective environment necessary.

2. DEVICE CONFIGURATIONS AND CHARACTERISTIC LENGTH SCALES

Almost all electronic applications are based on the use of superconducting thin films and layered film structures which, in addition to superconductors, must incorporate insulating, normal metallic, and/or semiconducting films. Figure 1 shows schematically the cross-section configurations of the two most representative device types: a high-frequency (microwave) transmission strip line, resonator or inductor, generally a linear, passive component; and a tunnel junction (nonlinear, active). In functional electronic circuits, both types are integrated with normal, resistive elements. Large scale integration of such multi-layered circuits has been amply demonstrated in LTS technology.

Superconductors in thin film form are technologically useful when integrated into the structures of Fig. 1, if this is done without degradation of superconducting properties at the surface and interfaces with the other, nonsuperconducting materials. In a superconducting microwave transmission line or resonator, the characteristic depth scale for the required film perfection is set by the magnetic field penetration depth, λ, since λ is smaller than the skin depth.[2] In a tunnel junction, the superconducting coherence length, ξ, sets the scale since the junction characteristics are defined by the superconductor properties within a distance of order ξ from the tunnel barrier. This means that at a distance from an interface much shorter than λ or ξ, respectively, the film must have the properties assumed in device design. However, one should bear in mind that some interfacial degradation of superconducting properties should always be expected as a consequence of deleterious physico-chemical processes occurring during the multiple fabrication steps. Interdiffusion with other layers which results from thermal treatments, interfacial disorder, free surface reactions with processing atmospheres and interfacial strains are examples of degrading effects.

Table 1 compares λ and ξ values, at $T \ll T_c$, in LTS and HTS materials of interest. The HTS data are averages of values in two crystal directions: along the c-axis [001] of the orthorhombic structure (normal to the a-b plane) and in the a-b (100) plane. With increasing T_c, the ξ in cuprates decreases to extremely low values while λ is high and comparable to that in NbN. The immediate implication is that passive components impose much less stringent requirements on oxide film interface perfection than do tunnel junctions. Indeed, tunneling into epitaxial HTS films has not been convincingly demonstrated, and some theoreticians doubt whether gap voltages, which define current-voltage characteristics of a tunnel junction device, even exist for HTS. Table 2 shows ranges of in-plane and normal to plane values of λ, ξ and also maximum J_c in YBCO, based on several recent estimates. Only epitaxial films with a-b planes orthogonal to the film plane (c-axis in film plane) can be considered for tunneling, with ξ roughly comparable to that in Nb_3Sn. With the c-axis normal to the film plane, the required perfection within 2 to 4 Å, or the first couple of monolayers, is clearly unattainable. In contrast, for passive devices, the first measurement of surface resistance on epitaxial films with the c-axis normal to the film plane, indicated that they are preferable not only for the highest possible transport and shielding currents in the film, but also for the lowest surface losses.[3]

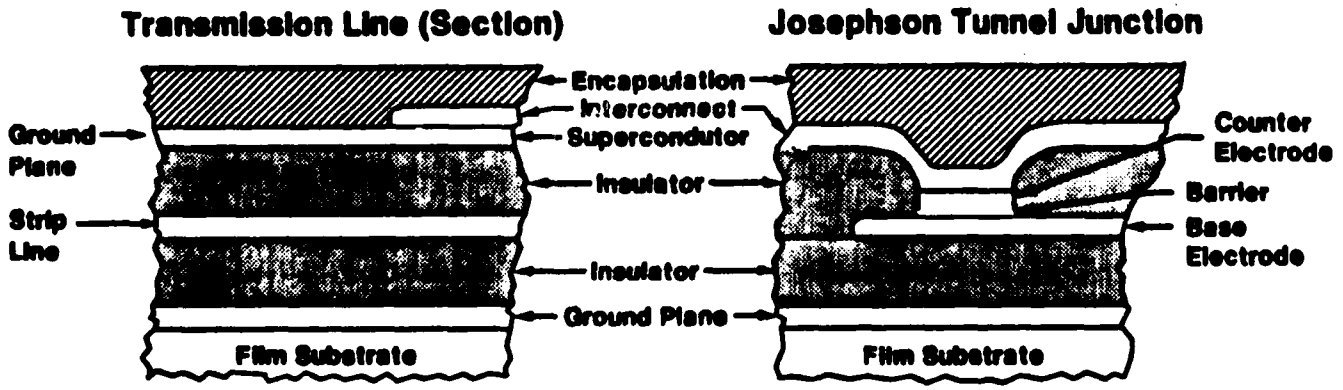

Figure 1. Representative layered film structures of superconducting electronics.

Table 1. Characteristic Lengths of Superconductors, $T << T_c$

Material	Nominal T_c (K)	Coherence Length, ξ (A)	Penetration Depth, λ (A)
Pb	7.2	900	400
Nb	9.2	400	600
NbN	16	40	2000
Nb_3Sn	18	30	800
$BaPb_{0.7}Bi_{0.3}O_3$	13	60	5000
$La_{1.85}Sr_{0.15}CuO_4$	40	<21>	<3500>
$Y_1Ba_2Cu_3O_7$	95	<15>	<150>
Bi-Sr-Ca-Cu-O	85-115	<8>	<700>

Table 2. Anisotropy of λ and ξ in YBCO, $T << T_c$

Parameter	In a-b plane	Normal to a-b plane (along c-axis)
λ, A	270	1800
ξ, A	16 - 30	2 - 4
J_c, A/cm^2	$\geq 10^7$	10^4 - 10^5

These considerations demonstrate the need for oriented, epitaxial oxide superconductor films with high quality interfaces which can be best satisfied by an in-situ approach to fabrication and processing.

3. APPARATUS AND PROCESS SEQUENCES

The multi-chamber UHV closed system shown schematically in Fig. 2 was originally developed and used for in-situ studies of epitaxial films and layered film devices of LTS materials, especially of Nb, NbN, and A15 structure compounds such as Nb_3Sn, Nb_3Al and Nb_3Ge.[4] To our knowledge, this has been the most complete deposition and analytical facility ever used for superconductor fabrication. Two separate deposition chambers, one for co-evaporation from e-gun and effusion cell sources and another for magnetron sputtering, permitted us to grow multilayered epitaxial film samples combining layers deposited by both methods. The separate surface analysis chamber has been used to determine surface structures by low energy electron diffraction (LEED) and compositions by secondary electron spectroscopy (XPS and AES) after each deposition step. High-energy electron diffraction (RHEED) made it possible to monitor crystallinity directly in the growth chamber. The introduction (lock) chamber has been used for degassing, ion-beam cleaning and oxidation of surfaces. In the UHV environment, all heaters and thermal shields were made of tantalum, electron and ion gun filaments of tungsten and substrate blocks of molybdenum. The whole system is oil-free, pumped by cryopumps, ion pumps and titanium sublimation pumps. In the evaporation chamber, pumping is also assisted by extensive liquid nitrogen cryopaneling. Single-crystal quality of evaporated, epitaxial LTS films and of stable oxide tunnel barriers, such as MgO and Al_2O_3, has been attained due to excellent background vacuum, in the 10^{-10} to low 10^{-11} torr range, which insured high surface atom mobility.[1,5] The sputtering chamber had a background pressure in the 10^{-8} to 10^{-9} torr range. Sputtering in Ar, or in Ar with N_2 and CH_4 admixtures, with total gas pressure of the order of 10^{-3} torr, produced lesser but satisfactory quality epitaxial oxides or nitrides, respectively.[5]

The advent of HTS oxides imposed an additional and, in part, conflicting set of system requirements. While UHV is still required for high-temperature substrate cleaning and for surface analysis, moderate to high oxygen pressures are necessary for the deposition and post-deposition annealing of superconducting YBCO and other HTS films. Figure 3 shows a diagram of alternative in-situ routes which can be used for YBCO film fabrication by sputtering. The diagram describes our own procedures presently in use when sputtering from separate metal targets. Processing steps involving heating in one atmosphere of oxygen are destructive to all Ta, W and Mo heated parts and even moderate partial pressures of oxygen $p(O_2) > 3 \times 10^{-4}$ torr can reduce considerably their useful life. Consequently, the system was modified as follows: we replaced Ta-heaters with Pt-heaters thus accepting the penalty of reduced maximum temperature. A 3 kW battery of quartz-halogen lamps was installed in the introduction chamber to permit fast heating up to T > 1000°C at 1 atm O_2.

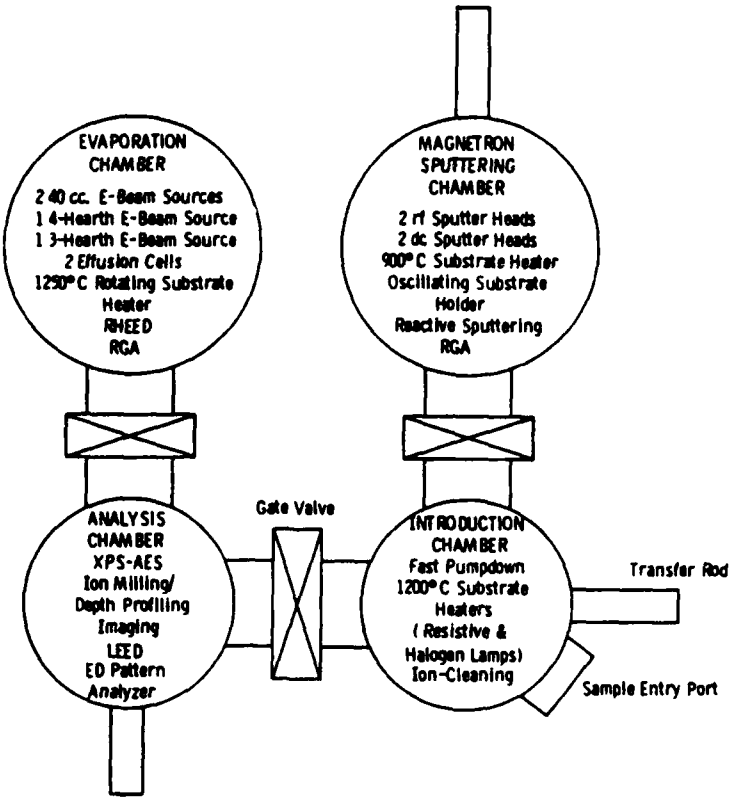

Figure 2. The UHV closed system for deposition and in-situ analysis of superconducting films and layered device structures.

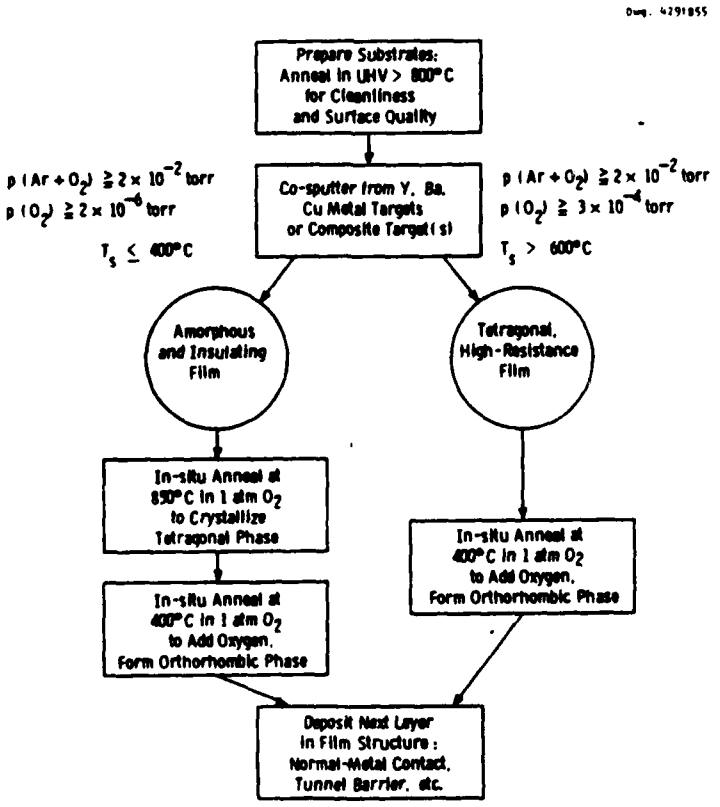

Figure 3. Diagram of alternative in-situ fabrication routes for YBCO films.

Ta shields were replaced with stainless steel shields. The substrate holder Mo-blocks and hot manipulator parts were replaced with blocks machined from Haynes alloy No. 230 which resists oxidation at high temperatures but, unfortunately, has a low thermal conductivity, a great detriment to the temperature uniformity of substrates clamped on the block.

4. FILM DEPOSITION

A systematic description of the film deposition process is beyond the scope of this paper. We will only address questions directly linked to the in-situ approach.

The left branch of Fig. 3 represents the sequence of processing steps and parameter ranges which, in the ex-situ version, are typical for early (1987) successful YBCO film fabrication activities:[6] films were deposited at low temperatures as amorphous, partly oxidized mixtures (or even as metallic components), ex-situ oxidized, annealed at up to 900°C in pure O_2 (the compound formation/crystallization step) and again oxidized at 500 to 400°C or slowly cooled in O_2 (the oxygen intercalation step) to transform from tetragonal to orthorhombic structure and attain optimum superconducting properties.

Early observations by many groups, including ours, indicated that films deteriorated at both interfaces. On one side, interdiffusion and reaction with typical non-epitaxial (Si, sapphire) and epi-substrates ($SrTiO_3$, MgO, ZrO_2) was seen, while on the other the free film surface was found non-superconducting to depths of 100 to 1000 Å. This has been generally ascribed to reactions with moisture and CO_2 in the ambient atmosphere. In an attempt to minimize these reactions, we initially implemented an in-situ pre-annealing step, at 400 to 450°C in 1 atmosphere of O_2, and eventually reached the complete in-situ process depicted in the left branch of Fig. 3.[2] Results of our in- and ex-situ surface and interface investigation of films deposited in an amorphous state are summarized in the next section. The best superconducting transition temperature and critical current density data reported in the literature are still predominantly those obtained in ex-situ crystallized films. These best results have been a consequence of obtaining a composition sufficiently close to the stoichiometric $YBa_2Cu_3O_7$ (or $REBa_2Cu_3O_7$ where RE is another rare earth) in an epitaxial film sufficiently thick to minimize effects of surface/interface degradation.[1]

The right branch of Fig. 3 is representative of many, perhaps most, recent reports on YBCO film deposition. To grow directly, i.e. in-situ, a crystalline deposit, the partial pressure of oxygen during deposition must be sufficiently high, $p(O_2) \geq 3 \times 10^{-4}$ torr, and preferably in 10^{-3} to 10^{-1} torr range. While this approach was pioneered early,[7,8] albeit with an additional ex-situ crystallization step, it has been more difficult to implement. In sputter-deposition, the negative oxygen ion and energetic neutral formation increases with $p(O_2)$, possibly causing differential or even total sputter-removal of the deposit[9] and resulting in prohibitively low deposition rates. In reactive co-evaporation at high $p(O_2)$, the useful life of e-gun filaments and/or effusion cell heaters is shortened dramatically and the automatic control of e-gun rates becomes erratic. In addition, the incorporation of molecular oxygen is difficult, hence the need for post-crystallization.[8]

With gradually improved understanding of underlying processes, partial remedies to the problems listed above are being found. Negative ion/neutral effects can be reduced by: (1) a high degree of thermalization, i.e by the use of high sputter gas pressures in the range of 0.1 to several torr,[10,11] (2) delivery of oxygen to the immediate vicinity of the substrate (effective only at very high pumping rates), and (3) altering the sputtering geometry. Examples of the third approach are the use of a hollow cathode sputter gun,[10] and placement of the substrate either far away from the plasma (in the 10^{-2} torr total pressure range) or very close to the target (in the 10^{-3} torr range).[12]

The last example has the possible advantage of easy incorporation of oxygen, due to ionization which is not always adequate near substrates far away from the plasma.[7] In reactive co-evaporation, differential pumping of the chamber can enhance the filament/heater life span and reduce the rate control problem.[13] The rf-plasma ionization of oxygen near the substrate appears to facilitate the O-incorporation so that a relatively low background pressure $p(O_2) = 10^{-5}$ torr can be employed without the need for additional crystallization annealing.[14,2] While an optimized approach has yet to evolve, it is clear that both of the deposition methods discussed are suitable for in-situ growth of crystalline, epitaxial YBCO films, monolayer-by-monolayer and without an additional crystallization step. At relatively low deposition temperatures for crystalline layers, between 550 and 700°C, the substrate/film interdiffusion is limited, even in the absence of a diffusion buffer layer.[10] The oxygen intercalation step still has to be done in-situ to avoid surface reactions and/or adsorbate formation. This relatively low-temperature step, however, can be more easily implemented than the in-situ post-deposition crystallization in oxygen.

5. RESULTS OF IN-SITU PROCESSING AND CHARACTERIZATION

5.1. Substrates and Nucleation

The best substrate choice found so far for epitaxial growth of YBCO films is $SrTiO_3$ in either a (100) or (110) orientation. Another substrate that has produced highly textured films is MgO(100). For films grown with an amorphous structure and crystallized at ~850°C, there is a sufficient interdiffusion of $SrTiO_3$ and YBCO that the preparation of the $SrTiO_3$ surface for epitaxial growth is not important. There are indications that careful $SrTiO_3$ surface preparation is similarly unimportant for deposition of crystalline films at ~600°C, since many laboratories have succeeded in growing epitaxial YBCO without attributing significance to their substrate preparation. However, we have found that films less than 100 Å thick grown on a clean, ordered $SrTiO_3$(100) surface exhibited crystallinity and textured growth in a RHEED pattern, whereas 100 Å thick films deposited on a disordered surface were amorphous.

The $SrTiO_3$(100) substrate surfaces were prepared by several different techniques: ion milling at various beam energies and substrate temperatures, and annealing in vacuum. Vacuum annealing resulted in the best surface properties. XPS showed that all residual carbon was removed from the surface after an 800°C anneal. Electron diffraction spots observed with LEED showed that the crystalline order on the surface improved as a function of annealing temperature up to 1100°C. The quality of RHEED patterns was independent of temperature for annealing temperature > 800°C. Within the precision of XPS, no oxygen was lost from the $SrTiO_3$ surface up to the maximum attainable temperature of 1250°C. Figure 4(a) is a typical LEED pattern from a substrate annealed at 1100°C.

Measurements were made on 40 Å and 100 Å thick YBCO films grown on (1) substrates annealed at 1100°C, and (2) ion-milled substrates which exhibited RHEED – but no LEED – patterns. For both types of substrates, no diffraction patterns were observed for 40 Å thick films. Only the 10 nm thick films grown on suitably prepared substrates were, at least in part, crystalline as shown by the RHEED pattern in Fig. 4(b). The thickness of the film in Fig. 4(b) was increased to 3500 Å and the crystal structure was identified as tetragonal $Y_1Ba_2Cu_3O_6$ with the c-axis in the plane of the film.

XPS measurements made on the 40 Å and 100 Å thick films gave no indication of chemical reaction between YBCO and the $SrTiO_3$ substrate. A high ratio of photoelectron counts from Y, Ba, and Cu compared to Sr and Ti indicated that there was little interdiffusion of substrate material into the film and that the film was relatively smooth and continuous.

5.2. Surface Atomic Segregation

We believed initially that the generally observed degradation of YBCO film surfaces is due entirely to reactions with moisture and CO_2 in the ambient atmosphere which can occur once the film is removed from the deposition system. However, the XPS in-situ analysis of surfaces and AES compositional depth profiles of our films have indicated that there is also an additional cause of nonsuperconducting film surface layers. In stoichiometric films which were amorphous as-deposited, the in-situ thermal oxidation at 400-500°C, i.e. prior to crystallization, caused the Ba and, to lesser extent, Y atoms to migrate to the surface which, consequently, became depleted in Cu. This is illustrated by Table 3 which presents a summary of XPS data obtained on the same specimen after several in-situ and ex-situ processing steps. The depletion also was observable in as-deposited films. The in-situ XPS spectra of those films deposited at the lowest oxygen pressures, $p(O_2) < 2 \times 10^{-6}$ torr,

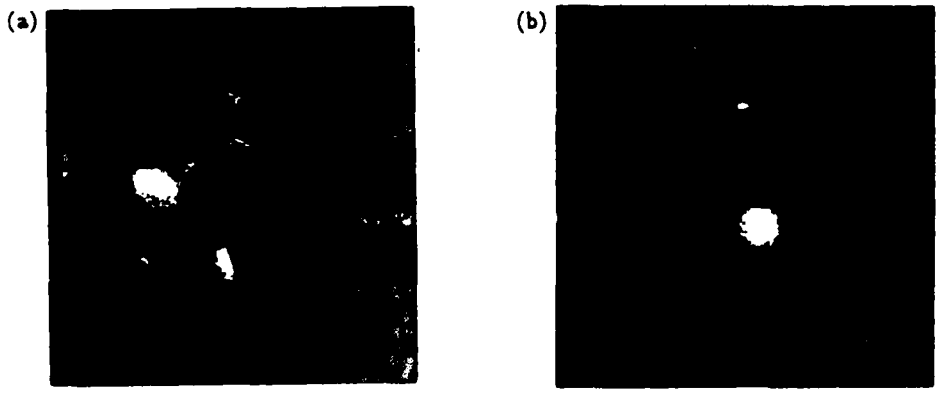

Figure 4. The in-situ RHEED patterns of $SrTiO_3$ substrate and 10 Å epitaxial YBCO film deposited at 650°C.

Table 3 The YBCO Surface Composition Determined by XPS

Treatment	Temperature, °C	Y at. %	Ba at. %	Cu at. %
As-deposited	400	18	33	50
In-situ anneal	500	21	66	13
Ex-situ anneal	850	22	41	37
Ion-milled 150V	20	50	24	26
Ion-milled 300V	20	35	29	35
In-situ anneal (10°C/sec ramp)	850	20	32	48

did not contain any signature of copper, as shown in Fig. 5. The AES depth profiles obtained after crystallization of such films revealed segregated layers much thicker than those in films deposited at higher oxygen pressures. The profiles are compared in Fig. 6.[15] Average compositions of these films were close to stoichiometric, as determined by calibrated energy-dispersive X-ray spectroscopy (EDS) and electron microprobe. After the films were crystallized, a much weaker segregation effect could also be observed by in-situ XPS to occur in the oxygen intercalation stage at 400°C (data not included in Table 3). All these results suggested that the segregation is an oxygen surface-charge-driven nonlinear diffusion process analogous to that observed in A15-structure intermetallics where atoms having a stronger affinity to oxygen migrated preferentially to the film surface to form oxides.[1] Attempts to remove the segregated near-surface layer by low-energy argon ion-beam milling using a Kauffman gun were not successful, as the surface became depleted in both Cu and Ba (Table 3). Our tentative interpretation was that these atoms were removed preferentially and we did not pursue this approach further.

A relatively efficient way to minimize atomic segregation in amorphous films is to deposit the films at the highest possible oxygen pressure, and to increase the in-situ annealing temperature relatively quickly to the maximum crystallization temperature. This process, referred to as the Rapid-Ramp Thermal Process (RRTP), produced results described in the next section. The last line of Table 3 gives an in-situ XPS analysis of a film which was fabricated by RRTP and, indeed, retained a nearly stoichiometric surface composition.

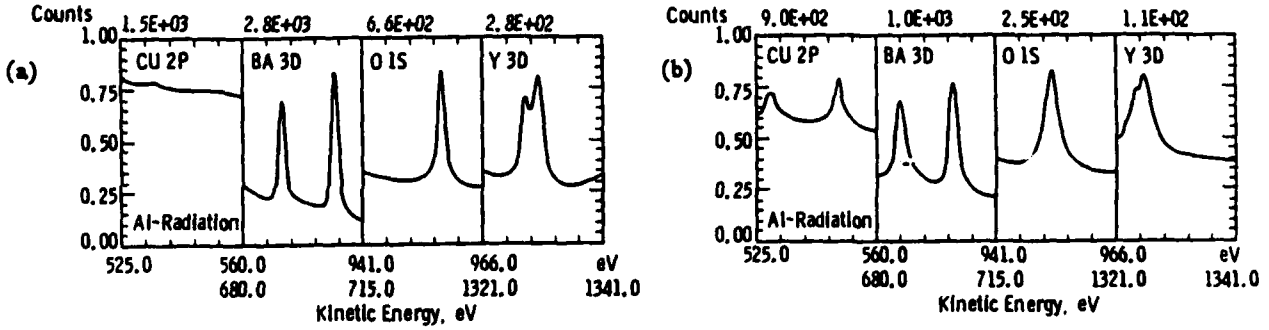

Figure 5. Comparison of raw in-situ XPS spectra of surfaces of amorphous film surfaces after sputter-deposition at two different oxygen pressures: (a) 2 x 10^{-6} torr, and (b) 8 x 10^{-6} torr.

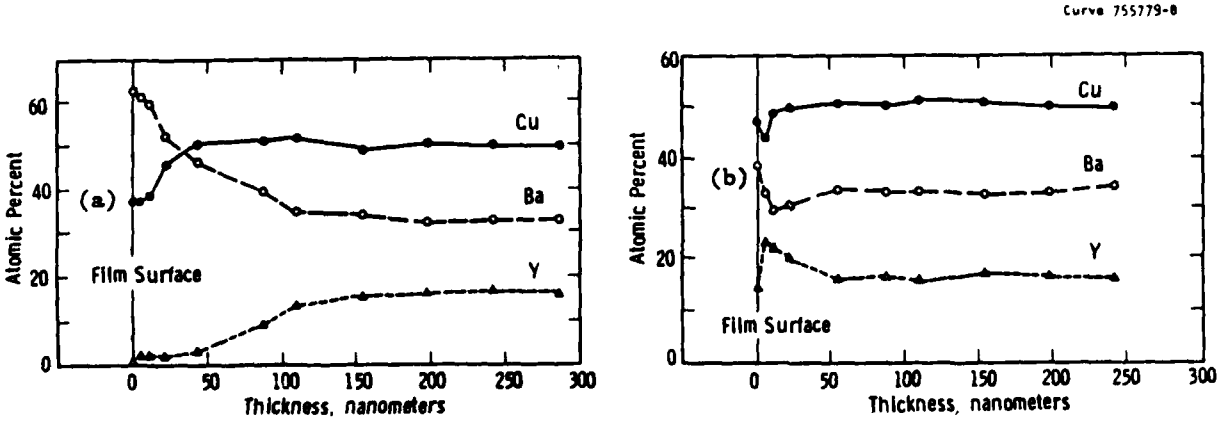

Figure 6. Comparison of calibrated AES depth profiles of crystalline YBCO films which were sputter-deposited at two different oxygen pressures in amorphous form and then annealed at 850°C (a) $p(O_2) < 10^{-10}$ torr, and (b) $p(O_2) = 3 \times 10^{-6}$ torr.

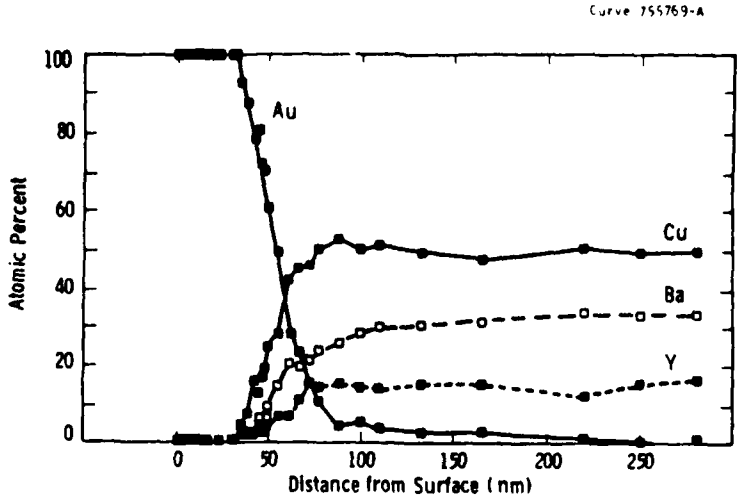

Figure 7. AES Depth Profile of a Low-Contact-Resistance Film with Au overlayer 500 Å thick.

It can be expected that films deposited in crystalline form (right branch of Fig. 3) will exhibit lesser surface segregation. Data in hand are insufficient to make a meaningful comparison. However, some surface segregation in such films was found by in-situ XPS to occur in the oxygen intercalation step.

5.3. Surface Electrical Properties

For electrical evaluation, fresh surfaces of films fabricated by RRTP were coated with an overlayer of gold evaporated in-situ at room temperature. In contrast to other reports,[16] these layers were not heated above room temperature. Figure 7 shows an AES profile of a YBCO/Au bilayer. No significant surface segregation is seen in this profile. To determine whether the YBCO surface is superconducting or highly resistive, we measured contact resistances and I-V characteristics of cross-strip junctions formed on such bilayers by depositing Nb counterelectrodes. For the contact resistance measurement, Nb cross-strips 2000 Å thick were deposited on 200-500 Å of Au. This step was performed ex-situ by sputtering Nb at room temperature through a multiple aperture mask. Subsequently, all the uncoated gold and part of Nb strips were removed by ion-milling to leave YBCO/Au/Nb contacts, each having an area of 10^{-2} cm^2. For I-V measurements, similar junctions were fabricated on very thin, 10-50 Å, and probably discontinuous gold overlayer. In this case, however, a 30 Å thick MgO barrier was evaporated on Au, again at room temperature, prior to depositing Nb. The intent was here to fabricate large area YBCO/Au/MgO/Nb proximity tunnel junctions.

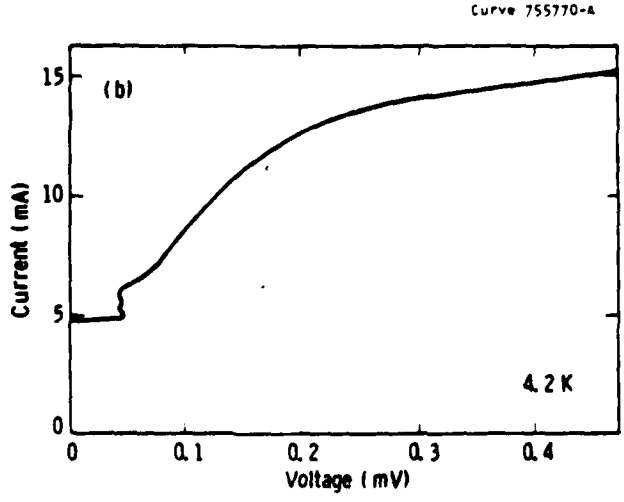

Figure 8. Current-voltage characteristics of YBCO/Au/MgO/Nb cross-junctions fabricated on RRTP films.

Measurement of contact resistance by the four-point method at 4.2K gave a value $R_c < 4 \times 10^{-10}$ Ω-cm², lower than the limit of the apparatus sensitivity. The surface contact resistance obtained by RRTP was thus clearly low enough for microelectronic applications, even if not necessarily zero. In contrast, a reference cross-strip sample, where Au was evaporated on an ex-situ annealed YBCO film surface, had a contact resistance $R = 2 \times 10^{-4}$ ohm-cm², six orders of magnitude higher.

Measurements of YBCO/Au/MgO/Nb junction I-V characteristics have been, thus far, disappointing in that the intended tunnel junctions were either resistive or shorted due to the discontinuous, "patchy" MgO overlayer. However, the formation of a superconducting short having the I-V characteristic at 4.2K shown in Fig. 8 is the nonambiguous indication that at least some areas on YBCO surface are, indeed, superconducting when fabricated by RRTP.

We regard the results shown above as preliminary and at this writing the junction fabrication and measurements are continuing.

6. CONCLUSION

We have demonstrated that the in-situ approach is capable of producing superconducting or highly conducting surfaces of epitaxial YBCO films deposited in amorphous form and subsequently crystallized by annealing. Our experience indicates that some form of in-situ processing will be necessary to successfully fabricate low resistance contacts and junctions on surfaces of YBCO films which were deposited in either amorphous or crystalline form. The in-situ approach should also make it easier to fabricate microwave YBCO components having low surface losses at the free surface. Surface properties of films of other HTS compounds, such as the Bi-Sr-Ca-Cu oxide should be evaluated to determine whether the need for in-situ processing also exists.

7. ACKNOWLEDGEMENTS

We thank D. Detar for the ex-situ AES depth profiling and Mrs. M. B. Cross for the preparation of the manuscript.

8. REFERENCES

1. A. I. Braginski, J. R. Gavaler, M. A. Janocko, and J. Talvacchio, "New Materials for Refractory Tunnel Junctions: Fundamental Aspects," in: SQUID '85 - Superconducting Interference Devices and Their Applications," H. D. Hahlbohm and H. Luebbig, eds., pp. 591-629, W. de Gruyter, Berlin, 1985.

2. At a temperature $T \ll T_c$ and well below the gap frequency.

3. J. P. Carini, A. M. Awasthi, W. Beyermann, G. Gruener, T. Hylton, K. Char, M. R. Beasley, and A. Kapitulnik, "Millimeter Wave Surface Impedance Measurements," Phys. Rev. B 37 (1988) in print.

4. J. Talvacchio, M. A. Janocko, J. R. Gavaler, and A. I. Braginski, "UHV Deposition and In-Situ Analysis of Thin-Film Superconductors," in Advances in Cryogenic Engineering - Materials, R. P. Reed and A. F. Clark, eds., pp. 527-541, Plenum, New York, 1986.

5. J. Talvacchio, J. R. Gavaler, and A. I. Braginski, "Epitaxial Niobium Nitride/Insulator Layered Structures," in: Metallic Multilayers and Epitaxy, M. Hong, S. A. Wolf, and D. U. Gubser, eds., pp. G1-G26, TMS-AIME, Pittsburgh, 1988.

6. R. M. Silver, J. Talvacchio, and A. L. de Lozanne, "Sputter Deposition of $YBa_2Cu_3O_7$ Thin Films," Appl. Phys. Lett. 51, 2149 (1987).

7. Y. Enomoto, T. Murakami, M. Suzuki, and K. Moriwaki, "Largely Anisotropic Critical Current in Epitaxially Grown $Ba_2YCu_3O_{7-y}$ Thin Film," Jpn. J. Appl. Phys. 26(7), L1248-L1250 (1987).

8. D. K. Lathrop, S. E. Rusek, and R. A. Buhrman, "Production of $YBa_2Cu_3O_{7-y}$ Superconducting Thin Films In-Situ by High-Pressure Reactive Evaporation and Rapid Thermal Annealing," Appl. Phys. Lett. 51(19), 1554-1556 (1987).

9. S. M. Rossnagel and J. J. Cuomo, "Negative Ion Effects during Magnetron and Ion Beam Sputtering of $YBa_2Cu_3O_x$," J. Vac. Sci. (1988), in print.

10. X. X. Xi, H. C. Li, J. Geerk, G. Linker, O. Meyer, B. Obst, F. Ratzel, R. Smithey, and F. Weschenfelder, "Growth and Properties of YBaCu-Oxide Superconducting Thin Films Prepared by Magnetron Sputtering," Physica C (1988), in print.

11. U. Poppe, J. Schubert, and W. Evers, "Preparation of $YBa_2Cu_3O_{7-y}$ Thin Films at Low Temperatures," Physica C (1988), in print.

12. H. Adachi, K. Hirochi, K. Setsune, M. Kitabake, and K. Wasa, "Low-Temperature Process for the Preparation of High T_c Superconducting Thin Films," Appl. Phys. Lett. 51(26), 2263-2265 (1987).

13. R. M. Silver, A. B. Berezin, M. Wendman, and A. L. de Lozanne, accepted for publication in Appl. Phys. Lett. (1988).

14. T. Terashima, K. Iijima, K. Yamamoto, Y. Bando, and H. Mazaki, "Single Crystal $YBa_2Cu_3O_{7-x}$ Thin Films by Activated Reactive Evaporation," Jpn. J. Appl. Phys. 27(1) L91-L93 (1988).

15. J. R. Gavaler and A. I. Braginski, "Near Surface Atomic Segregation in YBCO Thin Films," Physica C (1988), in print.

16. J. W. Ekin, A. J. Panson, and B. A. Blankenship, "Effect of Oxygen Annealing on Low Resistivity Contacts for High-T_c Superconductors," in: High Temperature Superconductors, edited by M. B. Brodsky, H. L. Tuller, R. C. Dynes, and K. Kitazawa, MRS Soc. Symp. Proc. 99, 283-286, MRS, Pittsburgh (1988).

CRITICAL CURRENTS OF 85 K Bi-Sr-Ca-Cu-O ☆

G.R. WAGNER, J. TALVACCHIO and A.J. PANSON
Westinghouse R&D Center, Pittsburgh, PA 15235, USA

Received 28 April 1988

We report critical current densities of pressed and sintered pellets of Bi-Sr-Ca-Cu-O measured by transport current and magnetometer. For a sample sintered at 860°C, the critical current density inferred from the magnetization was 40 times greater than the measured transport current density. This result and comparisons with the magnetization of a crushed pellet indicate that the effects of granularity are as severe as in polycrystalline $YBa_2Cu_3O_7$.

Pressed and sintered samples of $YBa_2Cu_3O_7$ have self-field transport critical current densities in the range of 10^3 A/cm^2 [1] at 4.2 K, which is three to four orders of magnitude lower than in single crystals [2] or epitaxial thin films [3] oriented for current flowing in the *a–b* planes. We previously determined [4] critical current densities of pressed and sintered $YBa_2Cu_3O_7$ from magnetization measurements and found that the critical current density, $J_c \approx 5\times10^3$ A/cm^2, if the pellet radius of 1.5 mm is used in the calculation. However, powder specimens had nearly the same magnetization as pellets. If the grain size of ≈ 10 μm is used in the calculation of J_c, then

$$J_c = 5\times10^3\ (1.5\ \text{mm}/5\ \mu\text{m}) \approx 10^6\ \text{A/cm}^2,$$

in agreement with single crystals. Similar results have been reported by others [5,6].

The origin of weak coupling between grains in $YBa_2Cu_3O_7$ is not well understood but is thought to be related to the loss of oxygen or reaction with CO_2 or water vapor on grain surfaces. The stability of Bi-Sr-Ca-Cu-O in air, even at high temperature, opens the possibility that grains in a pressed and sintered pellet of this recently discovered [7] high-T_c superconductor, would be strongly coupled together, yielding a higher transport current density. To determine this, we have measured transport critical current densities in pressed and sintered pellets and have calculated the J_c from magnetization data obtained in both the sintered pellets and crushed sintered pellets prepared with the composition Bi:Sr:Ca:Cu = 5:3:2:5.

The resistivity versus temperature for a pellet sintered at 860°C is shown in fig. 1. It was fully superconducting at 81 K with a midpoint T_c of 85 K and no indication of superconductivity above 100 K.

Transport critical current density was measured at 4.2 K in a bar sample 1×2×10 mm immersed in liquid helium. Current and voltage contacts were applied to the sample by sputtering 2 μm of silver on the surface and soldering copper leads to the silver. The sample voltage versus current is shown in fig. 2. The critical current density of 160 A/cm^2 was determined at a resistive voltage of 0.1 μV (our min-

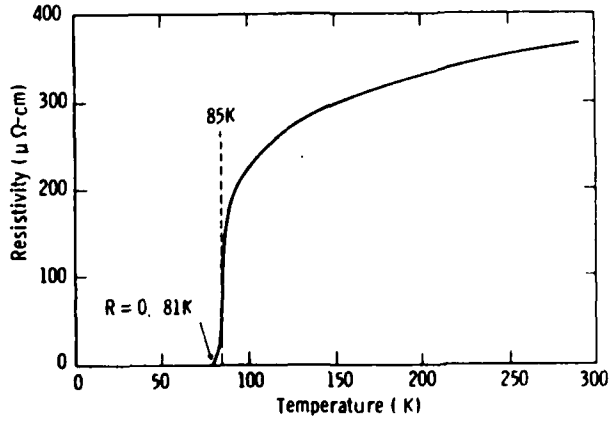

Fig. 1 Resistivity plotted as a function of temperature for a Bi-Sr-Ca-Cu-O pellet sintered at 860°C.

☆ Supported in part by AFOSR Contract No. F49620-88-C-0039.

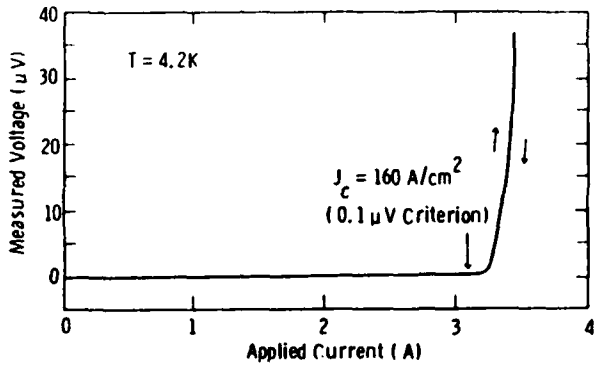

Fig. 2. Sample voltage plotted as a function of applied current for a 1×2×10 mm bar of Bi-Sr-Ca-Cu-O immersed in liquid helium which was used to determine the transport critical current density.

imum detectability) with the voltage leads separated by 5 mm. No heating effects were observed and the entire curve was retraceable for increasing or decreasing current.

The magnetization of the 3 mm diameter × 1 mm thick sintered pellet from which the bar was cut is shown as the solid curve in fig. 3. The pellet was subsequently crushed into approximately 25 pieces and remeasured. The magnetization of the crushed pellet pieces is shown as a dashed curve in fig. 3. The magnetization of the crushed pellet is approximately half that of the original, indicating that the diameter of the circulating current loops were not significantly smaller in the crushed sample.

The critical current densities calculated from the magnetization data are plotted in fig. 4. Curve A is the J_c of the sintered pellet calculated using the 3 mm

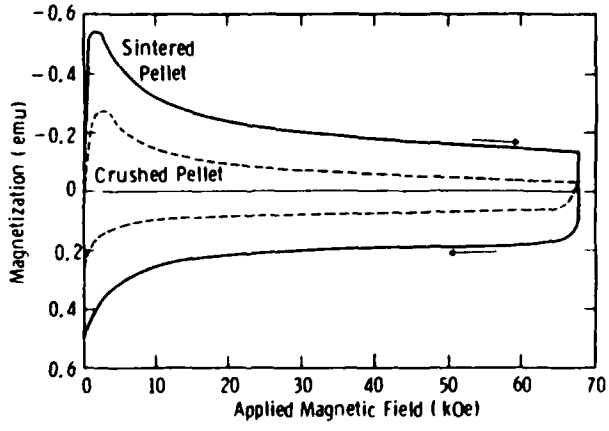

Fig. 3. The magnetization at 4.2 K of a pressed and sintered pellet (solid line) and the same sample measured after crushing (dashed line).

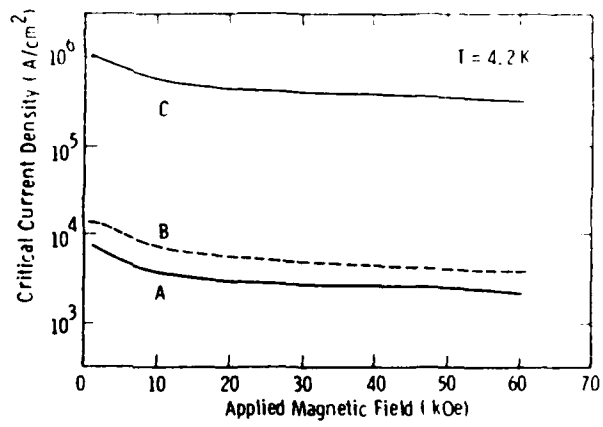

Fig. 4. Critical current density calculated from the magnetization data in fig. 3. (A) The J_c of the sintered pellet before crushing calculated using the 3 mm pellet diameter. (B) The J_c of the crushed pellet calculated with an average of measured diameters of the multi-crystal chunks. (C) Critical current density calculated from the same magnetization data as used for (A), but an average grain size of 10 μm was assumed.

diameter. Curve B is the J_c of the crushed pellet calculated with an average of measured diameters of the pieces. Curve C is the J_c of the pellet calculated using an average grain size of 10 μm.

The low value of transport critical current compared to magnetization critical current (even when calculated in the most conservative way), and the relatively small change in magnetization when the sample was crushed, indicate the granular nature of this type of Bi-Sr-Ca-Cu-O sample with weak coupling between grains.

The granularity is completely analogous to pressed and sintered $YBa_2Cu_3O_7$ pellets, since each grain appears to have an intrinsically high J_c, perhaps as large as 10^6 A/cm^2 at 4.2 K, but with surface degradation limiting the coupling between grains. The inferred intragrain current is consistent with values of 10^5 A/cm^2 measured at 77 K for Bi-Sr-Ca-Cu-O single crystals [8], and at 61 K for films [9].

References

[1] J.W. Ekin, Advan. Ceram. Mater. 2 (1987) 586.
[2] T.K. Worthington, W.J. Gallagher, T.R. Dinger and R.L. Sandstrom, in: Novel superconductivity, eds. S.A. Wolf and V.Z. Kresin (Plenum Press, New York, 1987) p. 781.
[3] P. Chaudhari, R.H. Koch, R.B. Laibowitz, T.R. McGuire and R.J. Gambino, Phys. Rev. Letters 58 (1987) 2684.

[4] A.J. Panson, A.I. Braginski, J.R. Gavaler, J.K. Hulm, M.A. Janocko, H.C. Pohl, A.M. Stewart, J. Talvacchio and G.R. Wagner, Phys. Rev. B 35 (1987) 8774.

[5] A. Ghosh, M. Suenaga and A. Moodenbaugh, in: Novel superconductivity, eds. S.A. Wolf and V.Z. Kresin (Plenum Press, New York, 1987) p. 762.

[6] I. Apfelstedt, R. Flükiger, H. Küpfer, R. Meier-Hirmer, B. Obst, C. Politis, W. Schauer, F. Weiss and H. Wühl, Japan. J. Appl. Phys. Suppl. 26-3 (1987) 1181.

[7] H. Maeda, Y. Tanaka, M. Fukutomi and T. Asano, Japan. J. Appl. Phys. 27 (1988) L209.

[8] R.B. van Dover, L.F. Schneemeyer, E.M. Gyorgy and J.V. Waszczak, Appl. Phys. Letters (1988), submitted for publication.

[9] M. Hong, J. Kwo and J.J. Yeh, Appl. Phys. Letters (1988), submitted for publication.

5th International Workshop on Future Electron Devices — High Temperature Superconducting Electron Devices -- (FED HiTcSc-ED WORKSHOP), June 2-4, 1988, Miyagi Zao pp. 171-179

PROSPECTS FOR THIN-FILM ELECTRONIC DEVICES OF HIGH-T_c SUPERCONDUCTORS*

A. I. BRAGINSKI, M. G. FORRESTER, J. TALVACCHIO and G. R. WAGNER
Westinghouse R&D Center, Pittsburgh, PA 15235, USA

ABSTRACT

Passive electronic devices show promise for early applications of high-T_c oxide films at radio and microwave frequencies. Weak link or microbridge SQUID's and radiation detectors show potential provided that low frequency noise can be reduced. Progress will depend upon control of film surfaces and interfaces, maximization of flux pinning and elimination of localized electron states from weak links.

INTRODUCTION

Prospects for electronic applications of high-T_c oxide superconductors (HTS) are largely dependent upon attainable material properties or, more precisely, the feasibility of fabricating thin films and layered film structures with required surface, interface, and substrate properties. This is in contrast to applications of conventional, low temperature superconductors (LTS) which are limited by either cryogenic or circuit characteristics. Reviews of material requirements and problems encountered in electronic applications of LTS can be found in the literature.[1-3] In this paper, we evaluate the device prospects from the HTS materials point of view.

At present, all high temperature superconductors which have a critical temperature $T_c > 30K$ are alkaline-earth cuprates i.e. oxide compounds of copper, an alkaline-earth metal and other elements. The number of cuprate superconductors is growing due to a very high level of worldwide research. The record T_c is presently 125K, in a thallium (Tl)-based cuprate, but the most researched material to date is $YBa_2Cu_3O_7$ (YBCO) and its derivatives, where Y is replaced by other rare-earth elements. Their common T_c is 90-95K. Here, we discuss prospects for devices based on YBCO, assuming that this is, presently, a generic, representative material. Indeed, all HTS cuprates known are brittle ceramic materials, exhibiting a varying degree of environmental instability. The cuprate HTS materials have other common characteristics. All crystallize into layered crystal structures which are related to the mineral, perovskite. The crystals exhibit strongly anisotropic electronic properties and, at low temperatures, $T << T_c$, the ability to sustain extremely high magnetic fields without loss of superconduction.

We believe that the HTS materials offer prospects for application in electronics which are considerably shorter-term than those for large scale, power applications. The main reasons are: (1) The cuprate brittleness is not a problem when the material is used to form a layered thin-film structure typical of electronic devices and circuits. (2) Usually required self-field critical current densities, $J_c = 10^5$ to 10^7 A/cm^2 at temperatures up to 77K, are readily achievable in epitaxial films, either in the film plane or in a plane normal to the film. (3) Weak coupling between grains of polycrystalline and granular films can be directly exploited in active, nonlinear devices.

CHARACTERISTIC LENGTH SCALES

Almost all electronic applications are based on the use of superconducting thin films and layered film structures which, in addition to superconductors, must incorporate insulating, normal metallic and/or semiconducting films. In LTS technology, the two most representative device types are: a high-frequency (microwave) transmission strip line,

---

*Supported in part by AFOSR Contract No. F49620-88-C-0039.

resonator or inductor, generally a linear, passive component, and a Josephson tunnel junction (nonlinear, active). In functional electronic circuits, both types are integrated with normal, resistive elements. Large scale integration of such multi-layered circuits has been amply demonstrated.

Integration of HTS into layered film structures must be attained without degradation of superconducting (bulk) properties at surfaces and interfaces with the other, nonsuperconducting materials. In a superconducting microwave transmission line or resonator, the characteristic depth scale for the required film perfection is set by the magnetic field penetration depth, λ, which is shorter than the skin depth in normal metals.[4] In a tunnel junction, the superconducting coherence length, ξ, sets the scale since the junction characteristics are defined by the superconductor properties within a distance of order ξ from the tunnel barrier. This means that at a distance from an interface much shorter than λ or ξ, respectively, the film must have the properties assumed in device design. However, one should bear in mind that some interfacial degradation of superconducting properties should always be expected as a consequence of deleterious physico-chemical processes occurring during the multiple fabrication steps. Interdiffusion with other layers which results from thermal treatments, interfacial disorder, free surface reactions with processing atmospheres, and interfacial strains are examples of degrading effects. Problems of surface/interface degradation appear to be less severe for applications which use granular films than for applications which require epitaxial deposits. However, resistance of ohmic contacts to granular films will increase with degradation. Performance of radiation (infrared) detectors made of granular films may also be impaired by absorption in a degraded surface layer.

The coherence length and penetration depth in cuprate crystals are anisotropic. Table 1 shows ranges of values of λ, ξ, and also the maximum J_c in YBCO, based on several recent estimates. Only epitaxial films with the c-axis in the film plane can be considered for tunneling. In this case ξ is roughly comparable to that in Nb_3Sn into which tunneling has been demonstrated. The penetration depth is rather high along the c-axis of YBCO and comparable to that in LTS NbN which is usable in electronics. The immediate inference is that passive components impose less stringent requirements on oxide film interface perfection than do tunnel junctions.

Table 1. Anisotropy of λ and ξ in YBCO, $T \ll T_c$

Parameter	In a-b plane	Normal to a-b plane (along c-axis)
λ, Å	270	1800
ξ, Å	16 - 30	2 - 4
J_c, A/cm^2	$> 10^7$	10^4 - 10^5

We believe that the need for oriented, epitaxial oxide superconductor films with high-quality interfaces can be best satisfied by an in-situ approach to fabrication and processing. In the case of granular films, in-situ fabrication is advantageous for low-noise contact formation. Indeed, using an in-situ process, we obtained nearly-zero contact resistances, R_c, between YBCO film surfaces and a gold overlayer deposited at room temperature without any post-annealing. An upper limit for R_c of 4×10^{-10} ohm-cm^2 at 4.2K was determined by the sensitivity limit of the measurement. In contrast, in an ex-situ process, the contact resistance between the gold overlayer and YBCO film was 2×10^{-4} ohm-cm^2.

FABRICATION ISSUES

The relevant length scales in high-T_c superconductors are sufficiently short that interfaces in multilayer devices must be formed by successive depositions of thin films. The status and prospects for deposition of YBCO films are discussed with reference to the most commonly used case of sputter deposition in the two alternative processes shown in Fig. 1. The first process (historically), shown in the left-hand side of Fig. 1, uses a

low substrate temperature, ≤450°C, to deposit an insulating, amorphous oxide, which must be post-annealed in oxygen at 800-900°C to form the $YBa_2Cu_3O_7$ superconductor. The other process employs a substrate temperature of ~600°C to directly form a crystalline film of $YBa_2Cu_3O_{7-\delta}$ ($\delta < 1$). The crystalline film might still require an anneal in oxygen at ~400°C to decrease δ. The significant advantage of the latter process is that the maximum processing temperature, ~600°C, is lower.

The two process alternatives shown in Fig. 1 apply much more generally than just to the case of sputter deposition. Even for sputtering, either process can be used with elemental metal targets, composite metal targets, or composite oxide targets, and with planar diode or magnetron sputtering. With any method, the correct cation stoichiometry must be obtained. The relative merits of other deposition techniques - such as co-evaporation, laser ablation, ion-beam sputtering, or chemical vapor deposition - depend primarily on their compatibility with the higher oxygen pressure, $>10^{-3}$ torr, that must be available to form crystalline $YBa_2Cu_3O_{7-\delta}$ in the lower temperature process. Lower oxygen pressures have successfully been used to grow crystalline films at ~600°C when the oxygen was ionized.[5]

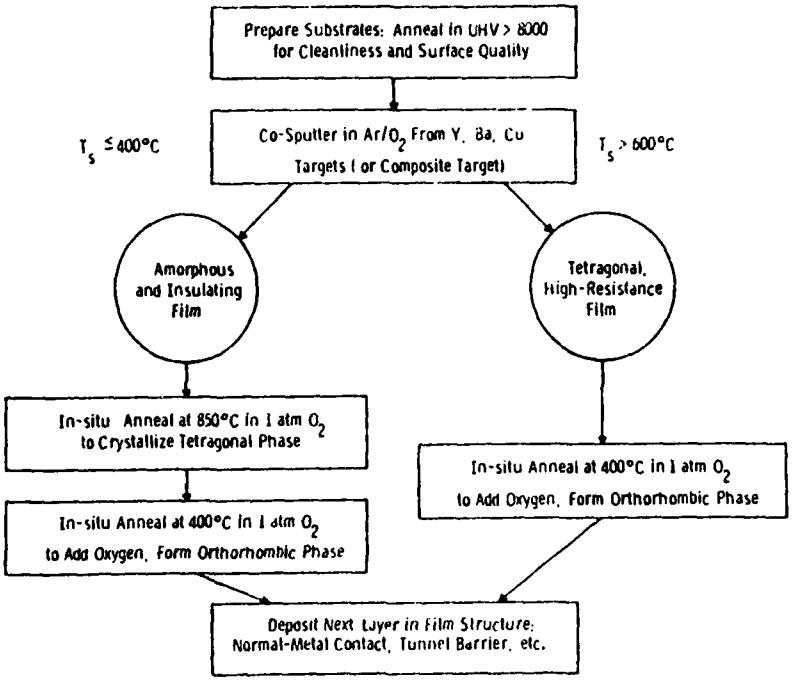

Figure 1 - Diagram of alternative processes used for YBCO film fabrication.

The commonly-used substrates for YBCO film growth, in order of increasingly deleterious reaction between film and substrate, are: $SrTiO_3$, MgO, cubic ZrO_2, α-Al_2O_3 (sapphire), and Si. In all of these cases, the reaction at the substrate/film interface can be reduced by employing the lower-temperature process. For Si substrates, superconducting films have been fabricated in many laboratories only by using the lower-temperature process. The interdiffusion between Si and YBCO creates a high contact resistance that prevents the current deposition technology from being used to fabricate interconnects between Si devices. For $SrTiO_3$ substrates, we have observed that a non-superconducting, Ba-rich layer as thick as 100 nm forms at the substrate/film interface in the 800-900°C process. Crystalline film growth at 600°C results in a Ba-rich interface layer only 10 nm thick.[6]

The choice of substrates for growth of YBCO films is determined by device applications. Epitaxial films can be grown on $SrTiO_3$ or MgO single crystals, which have a 0.5% and 8% lattice mismatch, respectively, with YBCO. For high Q microwave applications, neither $SrTiO_3$ or MgO is a suitable substrate due to high dielectric losses. Epitaxial buffer layers on low loss sapphire substrates must be developed for this purpose.

The last process step shown in Fig. 1, the deposition of the next layer in a device structure, is as important as the YBCO film growth. There is no process available for restoring a degraded YBCO surface that is compatible with electronic device processing (scraping and in-situ fracture are the methods preferred for preparing YBCO for surface-sensitive measurements). Therefore, it is crucial that all annealing and subsequent deposition steps are performed without exposing the surface to air. We have found that in-situ annealing is necessary, but not sufficient, to prevent the formation of a Ba-rich layer at the surface of films fabricated by the first process. A rapid heating rate of 10°C/sec up to the crystallization temperature is necessary to prevent surface segregation.[7]

PASSIVE DEVICES

Ultra-low surface resistance and lack of dispersion in transmitting rf signals make superconductors extremely attractive for use in passive microwave devices, high speed transmission lines and semiconductor interconnects. Cavities made of low T_c superconductors (LTS) such as Nb and Pb have achieved quality factors, $Q_c > 10^9$, when operated well below their T_c. Also, strip-line resonators[8] of LTS materials achieve Q's many orders of magnitude greater than those of normal metals. Picosecond pulses are transmitted on superconducting transmission lines with little dispersion or attenuation.[9] Only those frequencies near the gap frequency are affected.

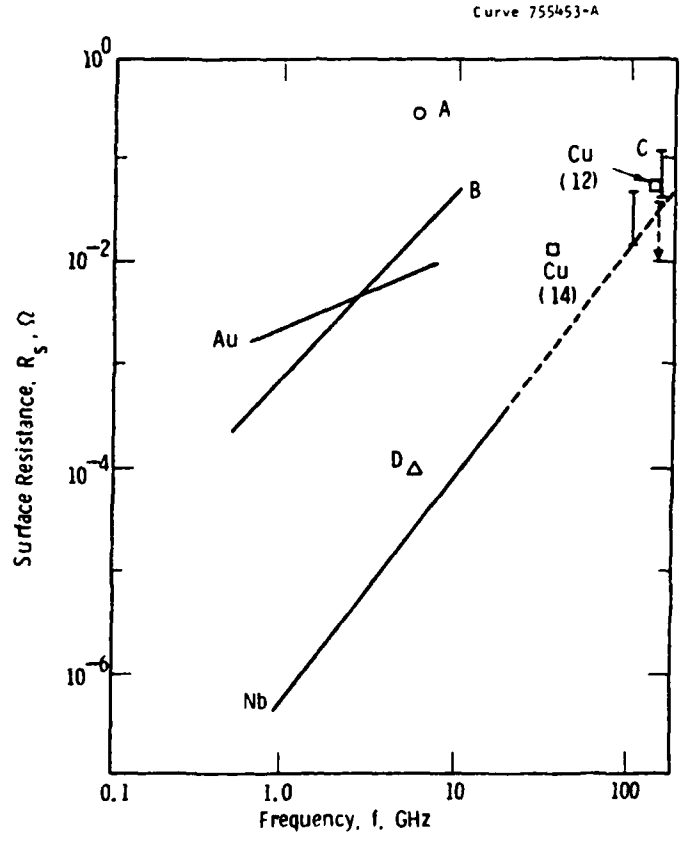

Figure 2 - Surface resistance of YBCO versus frequency at 4.2K for: (A) a polycrystalline aggregate,[10] (B) a polycrystalline film,[11] (C) bracketed estimates for epitaxial films with c-axis orientation,[12] and (D) a single-crystal platelet with the c-axis normal to the plane.[13] Experimental data for Au and Nb are from Ref. 11. The references for Cu data are indicated in the figure.

While the surface losses of LTS materials are fairly well understood on the basis of the BCS theory, such is not the case for HTS at present.

For $T < 0.5\ T_c$ a BCS type superconductor is expected to have a surface resistance given by:

$$R_s = R_{res} + A \exp(-\Delta/kT)$$

where $A \propto \omega^2$ and depends also on the penetration depth, λ and the coherence length, ξ. The term R_{res} is a residual resistance which may be temperature independent if it is due to normal material on the surface, but temperature dependent if it is due to a degraded superconducting layer with a reduced gap. Either case would vary as ω^2.

Figure 2 shows a composite of some surface resistance values for YBCO which have been reported to date, as a function of frequency, at 4.2K.[10-13] The experimentally determined values of R_s of Cu,[11,12,14] Au,[11] and Nb[11] are shown for comparison. The lowest values, which are found in epitaxial films, are slightly lower than in Nb and show roughly an ω^2 dependence. Calculations based on the BCS theory predict[15] that R_s for YBCO should be many orders of magnitude lower than Nb at 4.2K. The R_s values indicated by C and D in Fig. 2 are adequately low for useful devices if they could be obtained at higher temperatures. Preliminary data of R_s = 1 mΩ at 77K and 6 GHz obtained by Rubin et al. in single crystals grown at AT&T appear very promising.[16]

The dependence of R_s on film surface orientation is not clear. The two fluid model predicts $R_s \propto \lambda^3$, so that a-axis films would be preferred since $\lambda_c/\lambda_a \simeq 7$. However, the dependence on λ in the Mattis-Bardeen formalism is not as clear, since R_s depends on $\eta = \lambda/\xi$, where ξ is also anisotropic. In YBCO, $\eta >> 1$, and for that case, Halbritter[17] has shown that $R_s \propto \lambda\eta$. Recently reported[12] R_s values for a- and c-axis films at 100-150 GHz show higher losses for the a-axis orientation. However, neither orientation had the temperature dependence expected by the BCS theory.

To obtain the intrinsically low R_s expected for YBCO, the material must have undegraded superconducting properties to within tens of angstroms of the surface. This is clearly not the case for the samples measured so far. However, much progress has been made toward achieving these requirements in films produced by the <u>in-situ</u> technique.[5]

Operation of semiconductor devices at low temperatures leads to an improvement in speed and a reduction in noise. Computers operating at 77K are already commercially available and other cryogenic applications of semiconductors are of high interest. The use of HTS materials as interconnects between devices on chip would lead to an increase in speed. However, that improvement would be only about 20% over copper at 77K for CMOS because the major contribution to the RC time constant is the output impedance of the semiconductor device.[18] However, a significant advantage would be obtained by using HTS for longer interconnects between chips and for bus bars.

High Q microwave devices will require high quality epitaxial films on low-loss buffered sapphire substrates. The progress made so far in the understanding of epitaxial film growth, surface degradation, and substrate contamination leads to the expectation that the first practical use of the high T_c materials will be in passive devices and high speed lines.

ACTIVE DEVICES

<u>Granular Films</u>

In contrast to the passive component domain, where epitaxial HTS films offer good prospects for a multitude of device applications, prospects for active devices are linked to polycrystalline, largely equiaxial, granular films. Grain boundary regions can act as normal (N) or insulating (I) links between superconducting (S) grains and form S-N-S or S-I-S, boundary Josephson junctions (BJJ's). The early film and bulk dc SQUID demonstrations used these natural junctions.[19] Some of these devices operated up to 60-77K. In each case, the weakest inter-granular links in both branches of the SQUID loop were responsible for the quantum interference. A major problem with such devices is that the voltage versus applied flux characteristics are usually hysteretic, i.e. not single

valued, due to magnetic flux trapping. The related 1/f noise is high and dominates the white noise over a wide range of frequencies. Another source of noise might be the localized electron states at grain boundaries. Figure 3 is a composite of flux noise power data vs frequency obtained by Koch et al. in polycrystalline YBCO thin film SQUID's.[20] Two bulk YBCO SQUID data points are also given.[21,22] For reference, noise power vs frequency dependences typical for commercial rf SQUID's and representative IBM dc SQUID's operating at 4.2K are drawn schematically. The lowest noise data at 77K for thin film and bulk devices are comparable. It should be noted that the film device had a small, 40 x 40 μm loop. While the white noise in YBCO is sufficiently low for applications at 77K, the 1/f noise power is presently four to six orders of magnitude higher than in SQUID's operating in liquid helium. Better understanding of noise mechanisms in granular YBCO is required as a first step to noise reduction. Noise levels will determine future applicability limits for SQUID's made of such films.

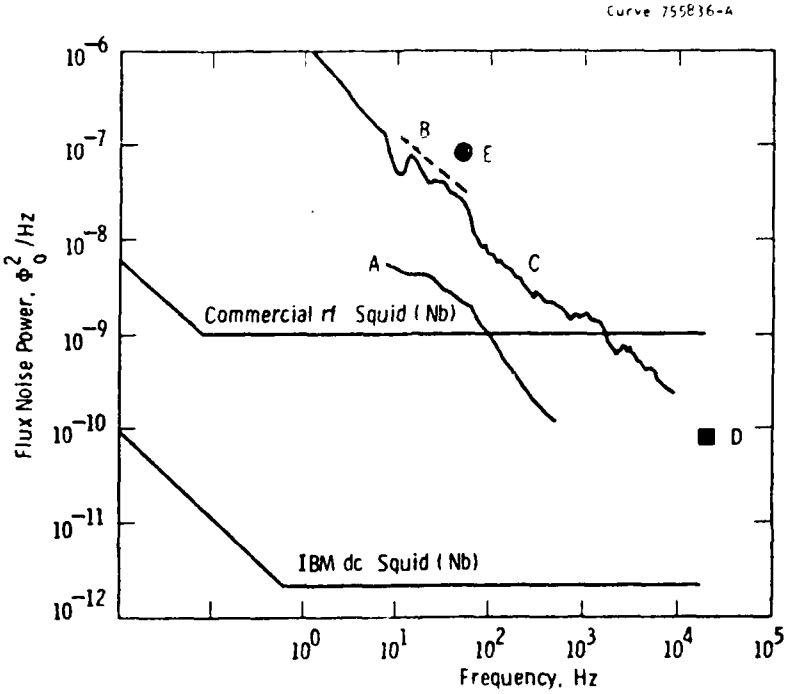

Figure 3 - The noise power density versus frequency for YBCO SQUID's fabricated from: (A) a polycrystalline film measured at 41K,[20] (B) a polycrystalline film measured at 77K,[20] (C) a single grain boundary,[20] (D) bulk material measured at 77K (best data),[21] and (E) bulk material measured at 4.2K.[22] The reference data for Nb SQUID's were measured at 4.2K.

Polycrystalline, granular films can be viewed as random arrays of BJJ's. Such arrays can be used for detection of electromagnetic radiation. Detection at visible and infrared wavelengths has been demonstrated in granular films of both LTS and HTS, including $BaPb_{1-x}Bi_xO_3$,[23] NbN/BN,[24] and YBCO[25]. The detection mechanism in such films is an optically induced phase-slip process in which photons with energy, $E>2\Delta$, break Cooper pairs, produce a nonequilibrium excess of quasiparticles, and thereby reduce the critical current of the BJJ's. A film biased sufficiently close to or above its critical current will then exhibit a voltage pulse in response to incident radiation, with a response time determined by the quasiparticle recombination time, which may be as short as 10^{-12} sec in a strong coupling superconductor. BJJ's arranged in series may contribute coherently to the signal, but incoherently to the noise, so that the signal to noise ratio will go as $1/\sqrt{N_s}$ where N_s is the number of junctions in series. Using granular HTS films, one thus has the potential for an extremely sensitive, broad-band, high-speed detector, with undemanding cryocooling requirements.

Results obtained to date for granular YBCO films are severely limited by noise. This limits their detectivity D^* (which quantifies sensitivity as well as minimum detectable signal) to 10^8 cm$\sqrt{\text{Hz}}$/W.[26] This is three to four orders of magnitude below the state of the art in semiconductor detectors. The mechanism of noise is thought to be the same as in granular SQUID's.

Epitaxial Films

As stated in Section 3, a Josephson tunnel device, the workhorse of LTS digital and analog circuits, should be easiest to fabricate using epitaxial films with c-axis in the plane. Indeed, reported attempts to fabricate thin film counterelectrode junctions on polycrystalline YBCO base electrodes have not been very successful. Most convincing were the results of Nakayama et al. who have observed Josephson current, hysteresis and Fiske steps in the I-V curve of YBCO/AlO_x/Nb junctions and presented some evidence that tunneling was occurring through the oxidized Al layer, which was deposited on a polished bulk YBCO surface.[27] We have fabricated YBCO/Au/MgO/Nb junctions on epi-films with the a-axis normal to the plane. The YBCO/Au/MgO trilayer was fabricated by an in-situ process. The I-V characteristics have been, thus far, disappointing in that the intended tunnel junctions were either resistive or shorted due to the discontinuous, "patchy" MgO overlayer.[5] However, the formation of superconducting shorts was a nonambiguous indication that at least some areas on YBCO surface were, indeed, superconducting and thus amenable to a junction formation. While it is hard to predict what gap voltages and subgap conductances can be attained, prospects for in-situ fabrication of epitaxial thin film tunnel junctions with LTS counterelectrodes are reasonably good. It is not clear whether or not HTS counterelectrodes are feasible, since they must be deposited at high temperatures which are likely to destroy the tunnel barrier. Usefulness in applications at temperatures well above 4.2K thus cannot be predicted at this time.

In the absence of HTS tunnel junctions, it is important to explore microbridge and SNS devices using epitaxial films. One can expect that artificial junctions may exhibit lower 1/f noise than those naturally present in granular films. Contrary to earlier observations,[28] YBCO single crystals do not contain intrinsic weak links along the c-axis which could be exploited for device functions. Occasional weak-link behavior is due to faults or defects in the specimen. Indeed, Koch et al. found that SQUID loops patterned in epitaxial films without T_c degradation do not exhibit voltage modulation by flux.[20] Similarly, in epitaxial films patterned into 10 μm wide microbridge and meander line detectors we have found only a bolometric response at 0.63 and 10.6 μm incident radiation wavelengths. The detectivity of such detectors was 10^8-10^9 cm$\sqrt{\text{Hz}}$/W and the response time constants were between 10^{-6} and 10^{-3} sec. Bolometric detector behavior of epitaxial films, which indicated the absence of sufficiently weak links, was also reported by Murakami and Enomoto.[29]

Device-quality weak links or S-N-S junctions in epitaxial films must, therefore, be fabricated. Local damage induced by laser patterning of a very narrow bridge in the material was found effective in creating a weak link and obtaining SQUID behavior in patterned loops.[20] Such results are not quite yet reproducible.

Prospects for three-terminal field-effect devices based on YBCO are not clear but may be somewhat brighter than in LTS if, indeed, the gap voltage, V_g is high. High $V_g \propto I_c R_n$, where I_c is the critical current and R_n the normal resistance, could make some voltage gain feasible.[30] In addition, the carrier density is relatively low, in the 10^{21} cm^{-3} range, and can be controlled by adjusting the oxygen content, albeit to the detriment of T_c. Extremely thin, undamaged YBCO films can already be fabricated. For example, we have deposited 40 Å thin epitaxial films of YBCO without indications of interdiffusion with the $SrTiO_3$ substrate.[5]

CONCLUSIONS

1. Passive electronic devices based on epitaxial HTS films show the most promise for near-term electronic applications, especially at UHF and lower microwave frequencies.

2. Weak link or microbridge electronic devices, mainly SQUID's and radiation detectors, utilizing granular and/or epitaxial HTS films, will show good near-term prospects provided that the 1/f noise can be significantly reduced.
3. Progress in passive and active device properties will depend largely upon effective control of surfaces and interfaces of HTS films. Noise reduction will require strong flux pinning and elimination of localized electron states from weak links.
4. Evaluation of device usefulness of cuprate films other than YBCO should emphasize the aspects listed in (3).

ACKNOWLEDGEMENTS

We thank R. H. Koch from IBM T. J. Watson Research Center, H. Padamsee from Cornell University, and T. Hylton of Stanford University for the communication of unpublished data and useful discussions. We also acknowledge the fruitful collaboration and discussions with J. R. Gavaler and thank Mrs. M. B. Cross for the preparation of this manuscript.

REFERENCES

1. M. R. Beasley and C. J. Kircher, in: Superconductor Materials Science, eds. S. Foner and B. B. Schwartz (Plenum Press, NY 1981), pp. 605-684.
2. S. I. Raider, IEEE Trans. Magn. MAG-21, 110 (1985).
3. A. I. Braginski, J. R. Gavaler, M. A. Janocko, and J. Talvacchio, in: SQUID '85 - Superconducting Quantum Interference Devices and their Applications, eds. H. D. Hahlbohm and H. Luebbig (W. de Gruyter, Berlin, 1985), pp. 591-629.
4. At a temperature T << T_c and well below the gap frequency.
5. A. I. Braginski, J. Talvacchio, J. R. Gavaler, M. G. Forrester, and M. A. Janocko, to appear in SPIE Proceedings Vol. 948, High-T_c Superconductivity: Thin Films and Devices, edited by R. B. van Dover and C. C. Chi (SPIE, Bellingham, Washington, 1988).
6. X. D. Wu and T. Venkatesan, to appear in SPIE Proceedings Vol. 948, High-T_c Superconductivity: Thin Films and Devices, edited by R. B. van Dover and C. C. Chi (SPIE, Bellingham, Washington, 1988).
7. J. R. Gavaler and A. I. Braginski, Physica C (1988), in print.
8. A. J. DiNardo, J. G. Smith, and F. R. Arams, J. Appl. Phys., 42: 186 (1971).
9. W. J. Gallagher, C. C. Chi, I. N. Duling III, D. Grischkowsky, N. J. Halas, M. B. Ketchen, and A. W. Kleinsasser, Appl. Phys. Lett. 50, 350 (1987).
10. L. Cohen, I. R. Gray, A. Porch, and J. R. Waldram, J. Phys. F 17: L179 (1987); M. Hagen, M. Hein, N. Klein, A. Michalke, G. Mueller, H. Piel, R. W. Roeth, F. M. Mueller, H. Scheinberg and J. L. Smith, J. Magnetism and Mag Matls. 68: L1 (1987).
11. M. S. DiIorio, A. C. Anderson, and B.-Y. Tsaur, Phys. Rev., B37 (1988), in print.
12. J. P. Carini, A. M. Awasthi, W. Beyermann, G. Gruener, T. Hylton, K. Char, M. R. Beasley, and A. Kapitulnik, Phys. Rev., B37 (1988), in print; T. Hylton (Stanford Univ.), private communication.
13. D. L. Rubin, K. Green, J. Gruschus, J. Kirchgessner, D. Moffat, H Padamsee, J. Sear, and Q. S. Shu, Phys. Rev., B37 (1988), in print.
14. J. Benard, N. H. El Minyawi, and N. T. Viet, Rev. Phys. Appl., 12: 483 (1978).
15. H. Padamsee, K. Green, J. Gruschus, J. Kirchgessner, D. Moffat, D. L. Rubin, J. Sears, Q. S. Shu, R. Buhrman, D. Lathrop, T. W. Noh, S. Russek, and A. Sievers (Cornell University), Preprint No. CLNS88/835, April 1988.
16. H. Padamsee, (Cornell University), private communication.
17. J. Halbritter, Z. Physik, 266: 209 (1974).
18. A. P. Malozemoff, Physica C (1988), in print.
19. R. H. Koch, C. P. Umbach, G. J. Clark, P. Chaudhari, and R. B. Laibowitz, Appl. Phys. Lett. 51, 200 (1987); H. Nakane,

Y. Tarutani, T. Nishino, H. Yamada, and U. Kawabe, Jpn. J. Appl. Phys. 26, 70 (1987); J. E. Zimmerman, J. A. Beall, M. W. Cromar, and R. H. Ono, Appl. Phys. Lett. 51, 617 (1987) and other papers.
20. R. H. Koch, C. P. Umbach, M. M. Oprysko, J. D. Mannhart, B. Bumble, G. J. Clark, W. J. Gallagher, A. Gupta, A. Kleinsasser, R. B. Laibowitz, R. B. Sandstrom, and M. R. Scheuermann, Physica C (1988), in print; R. H. Koch (IBM Watson Research Center), private communication.
21. D. Robbes, Y. Monfort, M. Lam Chok Sing, D. Bloyet, J. Provost, B. Raveau, M. Doisy, and R. Stephan, Nature 331, 151 (1988).
22. J. E. Zimmerman, J. A. Beall, M. W. Cromar, and R. H. Ono, Appl. Phys. Lett. 51, 617 (1987).
23. Y. Enomoto and T. Murakami, J. Appl. Phys. 59, 3807 (1986).
24. M. Leung, U. Strom, J. C. Culbertson, J. H. Claassen, S. A. Wolf, and R. W. Simon, Appl. Phys. Lett. 50, 1691 (1987).
25. M. Leung, P. R. Broussard, J. H. Claassen, M. Osofsky, S. A. Wolf, and U. Strom, Appl. Phys. Lett. 51, 2046 (1987).
26. S. A. Wolf (Naval Research Laboratory), private communication.
27. A. Nakayama, A. Inoue, K. Takeuchi, and Y. Okabe, Jpn. J. Appl. Phys. 26, L2055 (1987).
28. Y. Enomoto, T. Murakami, M. Suzuki, and K. Moriwaki, Jpn. J. Appl. Phys. 26, L1248 (1987).
29. T. Murakami (NTT), presentation of Y. Enomoto's paper at the 1988 HTSC-M^2 Interlaken Meeting.
30. A. W. Kleinsasser and T. N. Jackson, Jpn. J. Appl. Phys. 26-3, 1545 (1987).

Electrical Contact to Superconductors

JOHN TALVACCHIO

Abstract—**Electrical contacts to conventional superconductors and high-temperature oxide superconductors are reviewed. The technologically important conventional superconductors are Nb and its alloys and compounds. The oxide superconductors are typified by $YBa_2Cu_3O_7$. Three distinct forms in which the superconductor can be fabricated are considered: thin films for electronics applications, multifilamentary wires for magnets and large-scale applications, and monofilaments or tapes for measurements of the current-carrying capability of a superconducting material. The fundamental physics of current transfer to a superconductor involves the proximity effect for normal metal (nonsuperconducting)/superconductor interfaces, tunneling for cases where a thin insulating layer has formed in the interface, and the formation of a Schottky barrier at semiconductor/superconductor interfaces. Materials issues arise, in part, because the characteristic length scales are different for each superconductor and for each type of interface. Contacting the high-temperature oxide superconductors is difficult not only because the characteristic lengths are short, 0.1 to 10 nm, but because they are strongly dependent on crystal orientation and the oxides tend to be chemically unstable within that distance of the surface.**

I. Introduction

SINCE THE DISCOVERY of superconductivity in mercury in 1911—occurring at a temperature less than the critical temperature T_c of 4 K—a search has been made for the occurrence of superconductivity at higher temperatures. Among the chemical elements, the highest T_c, 9.2 K, occurs in niobium. Until 1986, a series of alloys and compounds of Nb held the record for highest T_c. The last breakthrough in that series was made in 1973 with the stabilization in thin films of A15-structure Nb_3Ge which had $T_c = 23$ K [1].

In 1986, Bednorz and Müller initiated a series of discoveries of new high-T_c oxide superconductors when they found $T_c \simeq 30$ K in $La_{1.85}Ba_{0.15}CuO_4$ [2]. The current (June 1988) highest T_c compound is in the Tl-Ba-Ca-Cu-O system where the transition to zero resistance occurs at 125 K [3]. The technologically important conventional superconductors and representative oxide superconductors are listed in Table I. The former category consists primarily of Nb and its alloys and compounds. The latter category includes compounds discovered in 1988 in three different materials systems. It appears that the relevant properties of the Bi-Sr-Ca-Cu-O and Tl-Ba-Ca-Cu-O sets of compounds are similar to those of the rare-earth Ba-Cu oxides, typified by $YBa_2Cu_3O_7$ (YBCO), so YBCO will be used to represent the high-T_c oxide superconductors. Too little is known about the third new superconductor, $Ba_{0.6}K_{0.4}BiO_3$, except that—unlike the higher T_c compounds—it has a cubic structure and (presumably) isotropic properties [4].

This paper will review the requirements and properties of interfaces with superconductors through which current is transferred. Most of the requirements for electrical contact to superconductors depend on whether the superconductor contacts a normal metal, an insulator, a semiconductor, or another superconductor. Fundamental and common requirements are that both a) the superconducting properties out to the surface of the superconductor, and b) the desired electrical properties of the contacting material must not be degraded by the process of forming an interface. Section II will be used to discuss the physics of interfaces with superconductors and length scales on each side of the interface over which degradation of the material will affect the performance of the contact. Applications will be discussed in Sections III to V.

Manuscript received April 7, 1988; revised October 27, 1988. This paper was presented at the 34th Meeting of the IEEE Holm Conference on Electrical Contacts, San Francisco, CA, September 26-29, 1988. This work was partially supported by AFOSR under Contract F49620-88-C-0039.

The author is with Westinghouse R&D Center, Pittsburgh, PA 15235.

IEEE Log Number 8825832.

II. Physics of Superconductor Interfaces

Superconductor/Superconductor Interfaces

Table I lists two of the characteristic lengths for superconductors, the coherence length ξ_s, and the penetration depth λ. The coherence length is the minimum distance between superconducting and nonsuperconducting regions. More rigorously, it is the decay length for the quantum-mechanical wave function created by the formation of Cooper pairs. The penetration depth characterizes the minimum distance needed for a shielding current to oppose penetration of magnetic field into a superconductor. At RF frequencies, λ has the role of the skin depth in normal metals. With the exception of Pb, all of the superconductors in Table I have $\xi < \lambda$. It will be shown that the short coherence lengths of many of the important superconductors—1 to 20 times the separation between atoms—limit current transfer between superconductors.

Contacts to a superconductor are characterized by a resistivity. Contacts between two superconductors are also characterized by a critical current density $J_c(T, H)$ below which, there is zero resistance,[1] and a critical magnetic field H_{c2}. The critical field is defined by $J_c(T < T_c, H = H_{c2}) = 0$. For currents greater than J_c, the resistivity is usually very high because most useful superconductors have high resistivities in their normal state.

Superconductors can carry sufficiently high current densities, as shown in Table II, to be used in their zero-resistance state ($J < J_c$). In Table II, a reduced temperature $t = T/T_c$ and a reduced magnetic field $h = H/H_{c2}$ are introduced.

[1] An upper limit of 3×10^{-18} Ω·cm for current flow at a density of 100 A/cm² and at a temperature of 77 K has been measured in a YBCO ring [14].

0148-6411/89/0300-0021$01.00

TABLE I
CHARACTERISTIC LENGTHS OF TECHNOLOGICALLY IMPORTANT CONVENTIONAL SUPERCONDUCTORS AND REPRESENTATIVE OXIDE SUPERCONDUCTORS AT TEMPERATURE, $T << T_c$

Material	Nominal T_c (K)	Coherence Length, ξ_s (nm)	Penetration Depth, λ (nm)	Superconductivity Discovered	Application
Pb	7.2	90	40	1913	laboratory circuit development
Nb	9.2	40	60	1930	most important electronic material
Nb-(46-50 wt %) Ti	9.2	7	150	1960	most important conductor material
NbN	16	4	200	1941	>10 K electronics
Nb_3Sn	18	3	80	1961	>10 T conductors
Nb_3Ge	23	3	~100	1973 [1]	—
$BaPb_{0.7}Bi_{0.3}O_3$	13	6	500	1975 [5]	—
$Ba_{0.6}K_{0.4}BiO_3$	29	—[a]	—	1988 [6]	—
$La_{1.85}Sr_{0.15}CuO_4$	40	3.7, 0.7 [7][b]	80, 430	1986 [8]	—
$YBa_2Cu_3O_7$	95	3.1, 0.4 [9]	27, 180 [9]	1987 [10]	—
Bi-Sr-Ca-Cu-O	80-115	3.8, 0.16 [11]	25, 500 [11]	1988 [12]	—
Ti-Ba-Ca-Cu-O	125	(2.6) [13]	(220) [13]	1988 [3]	—

[a] Not available.
[b] For anisotropic superconductors, values are listed for the directions parallel and perpendicular to the Cu-O planes, respectively, or for an average over all directions.

TABLE II
CRITICAL CURRENT DENSITY OF SUPERCONDUCTORS, J_c (A/cm^2)

	Nb-Ti (46.5% Ti)	Nb_3Sn	NbN	$YBa_2Cu_3O_7$
Environmental (T = 4.2 K, H = 0)	$> 5 \times 10^6$ (wire)	$\geq 1 \times 10^7$ (wire)	$> 3 \times 10^6$ (film)	10^7 (film, Cu-O plane)
Experimental (t = 0.5 h, h = 0.5)	$\sim 5 \times 10^5$ (wire)	$\sim 5 \times 10^5$ (wire)	$\sim 5 \times 10^5$ (film)	—
Experimental (t = 0.85, H = 0)	—	$\leq 10^6$ (film)	—	$> 10^6$ (film, Cu-O plane)
Theoretical ("depairing") limit (T = 0, H = 0)	2×10^8	1×10^9	1×10^8	3×10^8

The critical current is a monotonically decreasing function of t and h, and is zero at $t = 1$ or $h = 1$. The dependence of J_c on materials defects will be ignored here ([15] is a standard text on the subject).

The role of the coherence length in the spatial dependence of T_c and J_c is shown schematically in Fig. 1(a) for two superconductors, S joined by a degraded superconducting region S'. The degradation leading to a lower T_c in the S' region can be due, for example, to crystalline disorder, presence of impurities, or strain at the interface. In Fig. 1(a), the degraded region is larger than ξ_s, so the critical current density of the contact is determined by the properties of the degraded region. If the extent of the degraded region were smaller than the coherence length, no reduction of J_c would occur.

In YBCO, degradation at grain boundaries limits the current transfer between grains in all samples except for thin films and single crystals. In most grain boundaries, the degradation has resulted in a normal metal, insulating, or semiconducting layer. Even the cleanest high-angle grain boundaries, with the Cu-O planes aligned, have a reduction in critical current by a factor of 50 [16]. The problem is that the coherence length is sufficiently short that disorder in a few unit cells—or strain

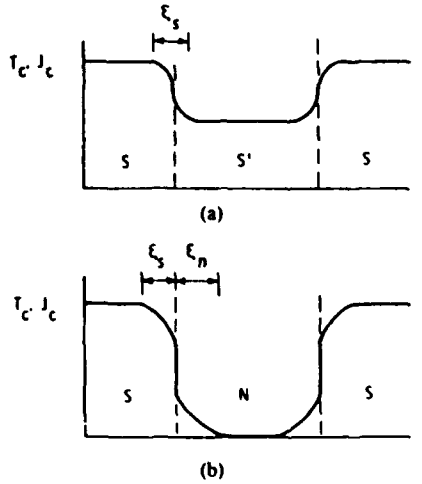

Fig. 1. Schematic of the spatial dependence of T_c and J_c for (a) an S-S'-S and (b) an S-N-S contact. The ordinate is the superconducting pair potential or wavefunction. Although T_c cannot be strictly defined locally, both T_c and J_c scale monotonically with the pair potential and are labeled for pedagogic reasons. Not shown in (a) is the fact that ξ_s will be even shorter in the degraded region S' than in the rest of the superconductor.

TABLE III
NORMAL-METAL COHERENCE LENGTHS

Metal	ξ_n (nm) Calculated	ξ_n (nm) Experimental
Au (4.2 K)	160	70 [19]
Au (77 K)	65	—
Cu (4.2 K)	200	100 [19]
Cu (77 K)	80	—
Mo (4.2 K)	16	—

fields associated with dislocations—can create a degraded region larger than ξ_s. The best YBCO wires have J_c(77 K, H = 1 T) = 10^3 A/cm^2 [17]—three orders of magnitude lower than the intragranular J_c—due to poor intergranular coupling. The coherence lengths in Nb and Nb-Ti are larger than the extent of typical interfacial defects and do not hinder the performance of superconductor/superconductor contacts.

Superconductor/Normal Metal Interfaces

The spatial dependence of T_c and J_c are shown in Fig. 1(b) for two superconductors joined by a normal metal—an S-N-S configuration. The diagram in Fig. 1(b) is for idealized S-N interfaces without chemical reaction, interdiffusion, strain, etc. A real configuration would have an S-S'-N-S'-S structure. The so called proximity effect, due to diffusion of superconducting (paired) electrons and normal electrons across the interface, creates a weakly superconducting layer in the normal metal over a thickness defined as the normal-metal coherence length ξ_n.

The normal-metal coherence length is a function of the Fermi velocity, v_F, and the electronic mean free path l [18].

$$\xi_n = \begin{cases} \dfrac{\hbar v_F}{2\pi k_B T}, & \text{clean limit, } l > \dfrac{\hbar v_F}{k_B T} \\ \left(\dfrac{\hbar v_F l}{6\pi k_B T}\right)^{1/2}, & \text{dirty limit, } l < \dfrac{\hbar v_F}{k_B T}. \end{cases} \quad (1)$$

Values of ξ_n for several commonly used normal metals are shown in Table III. The values derived from experiment are probably smaller than those calculated with (1) because electronic mean free paths near an interface are shorter than typical bulk values.

A generalization to be made from Table III is that ξ_n is large enough that contact resistances cannot be increased by alloy formation at interfaces that only extend a few monolayers into the normal metal. The effects of alloying are more deleterious on the superconductor side of the interface, since in most cases $\xi_s << \xi_n$. It will be shown in the next section that the characteristic lengths associated with thin insulating layers are $<< \xi_n$, so formation of an ultrathin insulating layer at an interface has a greater impact on contact resistance than a relatively thick alloyed layer.

A second generalization based on Table III concerns fabrication of S-N-S Josephson junctions. For the purposes of this paper, it is sufficient to identify a Josephson junction as any weak link between two superconducting electrodes [20]. In Fig. 1(b), a weak link can be established by an overlap between the superconducting wavefunctions induced in the normal metal at each interface with a superconductor. Practical considerations of current density and junction resistance require that the separation between superconductors must be on the order of ξ_n, and the cross-sectional dimensions of the normal metal must be comparable to the separation, respectively. The fact that ξ_n is always much less than dimensions obtained with conventional lithography techniques has limited the development of S-N-S Josephson-junction circuits.

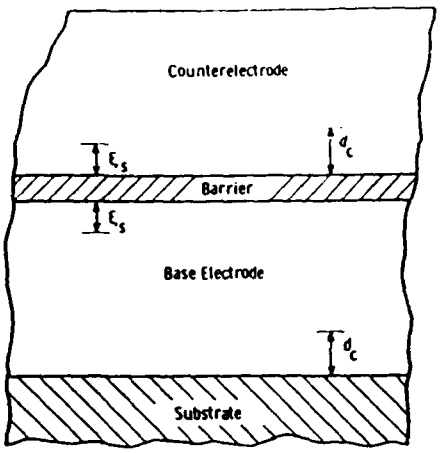

Fig. 2. Schematic cross section of an S-I-S Josephson tunnel junction. The minimum film thickness needed to obtain a T_c greater than 75 percent of the bulk T_c is shown as d_c.

Superconductor/Insulator Interfaces

It is not obvious that a discussion of interfaces with insulators is necessary in a paper on electrical contacts. However, currents transferred through thin insulating layers by tunneling are important to the technology of superconductors in two different ways. Thin insulating layers are present either as the undesirable result of an unsuccessful attempt to form a clean S-N or S-S interface, or as the mechanism for deliberately creating a weak link between superconductors in an S-I-S Josephson tunnel junction. Tunnel junctions are the most widely used type of Josephson junction in circuit applications because they can be made reproducibly (although reproducibility is a significant problem to be discussed) with high enough current densities to switch from zero resistance to a voltage state in approximately a picosecond.

The geometry of an S-I-S tunnel junction is shown schematically in Fig. 2. Two length scales affect the properties of the tunneling current, the barrier (insulator) thickness s and the superconductor's coherence length ξ_s. The small values required for s mandate that vertical integration (multilayer film deposition) must be used to form a device. The tunneling current density as calculated by Simmons using a WKB approximation is [21]

$$I \propto 1/R \propto e^{-\alpha s\sqrt{\phi}} \quad (2)$$

where $\alpha \simeq 0.1$ (eV)$^{-1/2}$/nm, the effective barrier height, ϕ is approximately equal to the energy gap between the valence and conduction bands, and R is the junction resistance. Typical values for ϕ are 1 to 3 eV as shown in Table IV for the most widely used tunnel barriers.

Table IV contains a list of barrier thicknesses needed to pro-

TABLE IV
PROPERTIES OF PRACTICAL TUNNEL BARRIERS FOR J_c = 2000 A/cm^2
(Barrier heights are from [23].)

Insulator	Barrier Height (eV)	Typical Thickness (nm)	Δs for 10× Lower Current
Al_2O_3	2.0	0.6	0.15
MgO	2.0	0.6	0.15
Nb_2O_5	0.25	1.4	0.4
—	0.02	3.4	1.4

duce junctions with J_c = 2000 A/cm^2 in the zero-resistance state, and resistances of 10^{-6} $\Omega \cdot cm^2$ in the voltage state, where both are standard values for high-speed circuits. Since the current and resistance depend exponentially on s, small changes Δs can result in 1000-percent changes in junction properties (Table IV). Typical circuit design rules require ±2-3-percent tolerances on J_c and R. Such tolerances can be obtained in state-of-the-art Nb/oxidized Al/Nb tunnel junctions which operate at ~4.2 K. However, poor reproducibility in junction properties—even across a single wafer—has prevented widespread use of NbN/MgO/NbN tunnel junctions [22], which can be operated at 10 K—the lowest temperature obtainable with relatively small, reliable, and portable refrigerators. Barriers with lower $\bar{\phi}$, perhaps small-bandgap semiconductors, would have a greater tolerance for fluctuations in barrier thickness, as indicated in the last line of Table IV. However, structural and temperature-stability constraints, to be considered next, severely constrain the selection of possible barrier materials.

The constraint imposed by the superconductor coherence length is that the maximum operating temperature of a Josephson tunnel junction is determined by the T_c of a layer of thickness ξ_s on each side of the barrier (see Fig. 2). Degradation of the top surface layer of the base electrode and the initially deposited layer of the top electrode can result in an S-S'-I-S'-S structure where S' indicates the presence of an interface layer with a T_c less than in the rest of the film.

For high-T_c oxide superconductors, the formation of a free surface with properties comparable to the bulk is a subject of current interest that will be discussed in Section III. For conventional superconductors, the top layer of a sufficiently thick base electrode has properties equivalent to bulk samples. In cases where an artificial oxide is used as a tunnel barrier, the barrier is deposited without exposing the base electrode to an atmosphere that would form a layer of native oxide. Generally, the other S' layer—the initially deposited layer of the top electrode—has a lower T_c which determines the maximum operating temperature for tunnel junctions made from conventional superconductors.

The low T_c found in the initial deposit of a superconductor film is usually due to reaction/interdiffusion with the substrate or to crystalline disorder. Table V contains the deposition temperatures used to grow representative superconducting films (or fabrication temperatures for cases where amorphous films are crystallized at high temperatures). In the third and fourth columns of Table V are the minimum film thicknesses d_c, needed to obtain a T_c which is ≥75 percent of the T_c of bulk material. For Pb or Nb, ξ_s is sufficiently large compared to d_c that Pb or Nb junctions can carry Josephson currents at practically any temperature less than the T_c of bulk material.

TABLE V
MINIMUM THICKNESS d_c REQUIRED FOR NONEPITAXIAL AND EPITAXIAL FILMS TO OBTAIN ≥75 PERCENT OF THE T_c FOUND IN BULK SAMPLES

Superconductor	Required Fabrication Temp. (°C)	d_c (nm) (Nonepitaxial)	d_c (nm) (Epitaxial)
Pb	20	3 [24]	—
Nb	20-800	25 [25]	5 [25], [26]
NbN	50-700	15 [27]	<1 [28]
Nb_3Sn	750-950	25 [29]	8 [29]
YBCO	~600-900	~400 [30]	200 [31]
Bi-Sr-Ca-Cu-O	870	—	—

In the case of NbN, $d_c > \xi_s$ for nonepitaxial growth and $d_c < \xi_s$ for epitaxial growth. The only tunnel barriers used with NbN to obtain Josephson currents near T_c are MgO or $Mg_{1-x}Ca_xO$ [22] since they have the same crystal structure as NbN and a close lattice match (exact lattice match for x = 27 at % Ca). The advantages of using the tunnel barrier as a substrate for epitaxial growth of the top electrode are present even when the NbN base electrode is polycrystalline. The alignment of each grain of the tunnel barrier and top electrode with a grain in the base electrode is sometimes called polycrystalline epitaxy.

For Nb_3Sn, $d_c \simeq 2\xi_s$ even for epitaxial film growth. An additional problem is that at the high temperature needed to obtain crystalline order (~850°C), reaction and interdiffusion between the tunnel barrier and superconductor will not only degrade the superconductor but also destroy the barrier. The highest temperature used successfully for top electrode growth, 700°C, was for a single-crystal superlattice of NbN/MgO/NbN where the absence of grain boundaries in the barrier presumably limited interdiffusion [22].

There are formidable obstacles to making tunnel junctions from high-T_c superconductors. First, $d_c >> \xi_s$, even for epitaxial growth. Secondly, high deposition or annealing temperatures are needed to make films by currently available techniques. Clearly, any progress to be made in developing high-T_c tunnel junctions will require single-crystal films and epitaxial multilayers.

Superconductor/Semiconductor Interfaces

The physics of superconductor/semiconductor contacts is generally the same as for normal metal/semiconductor contacts. That is, Schottky barrier formation requires that thermally activated and tunneling currents must be maximized. Ohmic contacts to superconductors are more difficult to obtain than to normal metals due to the constraints of low operating temperatures and a more limited selection of metals.

There are currently no commercial applications of superconductivity that require contact between superconductors and semiconductors (Sc). Three potential applications are S-Sc-S Josephson junctions, three-terminal hybrid devices (such as superconducting FET's), and superconductor transmission striplines in semiconductor circuits. These will be described in more detail.

The semiconductor layer in the simplest *S-Se-S* structure is a tunnel barrier. The potential barrier can be formed by the bandgap or a Schottky barrier (for a sufficiently thick, degenerate semiconductor). The advantage of a semiconductor tunnel barrier is that the lower barrier height permits thicker barriers with greater margins for variation in barrier thickness (last line of Table IV). The materials technology of Nb/Si/Nb tunnel junctions is quite advanced [32], and such junctions could compete with Nb/oxidized Al/Nb for LSI or VLSI where junction uniformity becomes a limiting factor. A semiconductor with a negative Schottky barrier height, n-InAs, has been used to make Josephson junctions with *S-N-S* properties [33]. Using a free electron model and (1), the coherence length in a semiconductor $\xi_n \propto n^{1/3}$, where n is the carrier density [34]. For $n = 2.6 \times 10^{18}$ cm^{-3}, ξ_n in InAs is ~250 nm—higher than in normal metals as indicated in Table III, but still requiring submicrometer lithography.

Among the concepts for three-terminal superconductor/semiconductor hybrid devices [35], [36] is a "superconducting FET." It can be made if ξ_n is large enough to pattern a gate electrode on the semiconductor link of a device with *S-N-S* characteristics. Devices have been fabricated with ohmic contacts to superconducting source and drain regions [37], [38]. However, the voltage generated across one device appears to be fundamentally limited below the gate voltage needed in the next stage [39].

Another application where contact must be made between superconductors and semiconductors is in the proposed use of high-T_c superconductors as passive transmission lines connecting active semiconductor components on or between chips at 77 K. A number of papers have been written in which the potential advantages of superconductors over normal metallization interconnects are assessed [40], [41]. The objective here is to assess whether contacts can be made without degrading the properties of either the superconductor or the semiconductor, and without restricting current flow. Deposition temperatures for YBCO are in the range ≥600°C (Table V). Since GaAs starts to decompose at 580°C, only interconnection of Si devices can be considered at this time.

As shown in Table V, even epitaxial YBCO films grown on $SrTiO_3$ substrates must be 200 nm thick to obtain $T_c \geq 0.75 \times T_{c(\text{bulk})}$. The interface layer is insulating and much too thick to obtain measurable tunneling currents (see Table IV). Films grown on Si substrates must be substantially thicker due to reaction between Si and YBCO [42]. The most promising approaches are to use a normal-metal buffer layer (thinner than ξ_n) which forms an ohmic contact with Si, and to develop lower temperature YBCO deposition techniques. The standard metal for ohmic contact to Si is Al, but it reacts strongly with YBCO [43]. Noble metals react least with YBCO, so Ag is a good candidate [44]. Noble-metal/silicide compounds, such as Pt-Si or Ir-Si might be sufficiently stable to be used as buffer layers. Lower deposition temperatures will decrease the tendency for reaction between YBCO and the buffer layer, but will decrease crystalline order. The challenge will be to provide the energy needed to crystallize YBCO in some form other than thermal energy provided by the substrate.

III. Contacts to Thin Films

This section will address the practical issues in making low-resistance and high-current-carrying contacts to thin films of Pb, Nb, and YBCO superconductors. Electronic circuits based on thin films of Pb and its alloys, such as Pb-In-Au and Pb-Bi, are primarily of historical interest, although some laboratories use a Pb-based technology to fabricate prototype circuits. IBM developed Pb-based circuitry during its Josephson computer program [45]—discontinued in 1983. The disadvantage of using Pb alloys is in their lack of mechanical and chemical stability. Repeated temperature cycling from 300 K to 4.2 K or long-term storage at 300 K (< 1 year) will destroy the Pb oxide tunnel barrier [18].

Most of the current Josephson circuit development [46] and commercially available products based on superconducting electronics,[2] are based on Nb/oxidized Al/Nb tunnel junctions. The important contacts are between two Nb films, Nb and a normal-metal resistor, and Nb and contact pads for wire bonds. Both Pb and Nb have large coherence lengths compared with the thickness of degraded surface layers caused by contamination, ion-cleaning damage, etc., and compared to substrate/superconductor interface thicknesses ($\xi_s >> d_c$). Therefore, the only impediment to making contacts comes from oxidation of free surfaces where even a few monolayers of insulation can reduce current densities by several orders of magnitude (compare Tables II and III). These oxides can easily be removed by back-sputtering or ion-milling and the surface protected from re-oxidation prior to deposition of Nb (or Au or resistor) by combining the cleaning and deposition processes in the same vacuum chamber. For Nb/Nb or Pb/Pb layers, the resulting contacts can safely be assumed to have zero resistance and to carry the same current density as the film. In the case of normal metal contacts to Nb or Pb, the proximity effect makes the contact resistance zero for low current densities, and less than the resistance of the normal-metal film at current densities up to the critical current of the superconductor (Table II).

At present, films of YBCO are always contacted on the top surface to avoid the thick degraded layer at the interface between the film and substrate ($d_c >> \xi_s$). Contacts to the top surface of YBCO films are hindered by several processes which lead to the formation of a nonsuperconducting layer on the surface of YBCO films and bulk samples. The most obvious process is the reaction of YBCO surfaces with water and carbon dioxide in the atmosphere to form hydroxides and carbonates of Ba and, possibly, Y [48], and deplete the surface concentration of Cu [49].

The formation of contacts to the surfaces of YBCO films and sintered pellets is summarized in Table VI. It is difficult to establish a requirement for specific resistivity (the product of contact resistance and area ρ_c) that can cover all thin-film superconductor applications. For semiconductor circuits, a specification for ρ_c is on the order of 10^{-4}-10^{-5} Ω·cm^2

[2] Examples of the commercial use of Nb/oxidized Al/Nb junctions are Hypres, Inc.'s sampling oscilloscope and time-domain reflectometer, and Cryogenic Consultants Limited's *SQUID* systems.

TABLE VI
FORMATION OF CONTACTS TO THE SURFACES OF YBCO FILMS AND SINTERED PELLETS

Reference	Superconductor	Normal-Metal Contact	Processing Temperature (°C)	Measurement Temperature (K)	ρ_c ($\Omega \cdot cm^2$)
[50]-[52]	YBCO films or pellets	Ag paste, In solder, direct wire bonds, pressure contacts	20-100	77	10^{-2}-10
Iye *et al.* [53]	YBCO single crystal	spark-bonded Au wire	800	100	10^{-4}
Kusaka *et al.* [50]	YBCO pellet	evaporated Pt film	~100	80	3×10^{-4}
Kusaka *et al.* [50]	YBCO pellet	evaporated Au film	500	80	2×10^{-5}
Caton *et al.* [51]	YBCO pellet	sputtered Au film	20	77	2×10^{-7}
Caton *et al.* [51]	YBCO pellet	melted Au bead	1065	77	5×10^{-7}
Wieck [54]	YBCO pellet	pressed and sintered Au bead	950	<20	4×10^{-7}
van der Maas [55]	YBCO pellet	annealed Ag epoxy	900	77	$< 10^{-7}$
Sugimoto *et al.* [56]	$ErBa_2Cu_3O_7$	evaporated Au film	300	77	$< 7 \times 10^{-8}$
Tzeng *et al.* [57]	YBCO pellet	evaporated Au film	~100	77	6×10^{-6}
Tzeng *et al.* [57]	YBCO pellet	evaporated Au film	500	77	4×10^{-8}
Tzeng [58]	YBCO pellet	melted Ag bead	970	77	$< 10^{-8}$
Ekin *et al.* [52]	sputter-etched YBCO pellet	sputtered Ag film	20	77	10^{-5}
Ekin *et al.* [59]	sputter-etched YBCO pellet	sputtered Ag film	500	77	$< 2 \times 10^{-9}$
Ekin *et al.* [59]	sputter-etched YBOC pellet	sputtered Au film	600	77	$< 4 \times 10^{-10}$
Mizushima *et al.* [60]	YBCO film	evaporated Au film	850	4.2	$< 10^{-8}$
Gavaler *et al.* [61]	YBCO film	*ex situ* evaporated Au film	20	10	2×10^{-4}
Gavaler *et al.* [61]	YBCO film	*in situ* evaporated Au film	20	10	$< 4 \times 10^{-10}$

[62]. For Josephson-junction circuits, where junctions in their voltage state have a resistance of $\sim 10^{-6}$ $\Omega \cdot cm^2$, the contact resistance must be $\leq 10^{-8}$. On the other hand, $\rho_c \simeq 1$ $\Omega \cdot cm^2$ is adequate for characterization of the resistive properties of YBCO films in a four-point measurement. Based on these requirements, the following generalizations can be made concerning the data in Table VI:

1) With the exception of the work by Gavaler *et al.*—which will be considered separately—a high-temperature (300-1065°C) anneal is needed to diffuse the contacting normal metal through the insulating surface layer to where it can make contact to superconducting YBCO.

2) The anneal must be performed in pure oxygen to maintain the oxygen stoichiometry of YBCO. To prevent oxidation of the contacting normal metal, one of the noble metals must be used. Silver, gold, and, to a lesser extent, Pt, have been successful because they do not react readily with YBCO.

3) The best contacts have values of ρ_c less than the minimum detectable resistance 10^{-8}-10^{-10} $\Omega \cdot cm^2$. The calculated value of ρ_c for a pure noble metal in contact with a superconductor is $\sim 10^{-12}$ $\Omega \cdot cm^2$—well below measurement resolution [59].

4) Similar results have been obtained on either polycrystalline YBCO films or pressed and sintered pellets. A relatively poor contact was made to a single crystal, despite the use of an 800°C anneal [53]. It is probable that the absence of grain boundaries impeded diffusion of Au from the bonded wire. The same difficulties could be expected for contacts to single-crystal films.

5) In the work reported by Ekin *et al.*, a 20-200-nm-thick surface layer was removed by back-sputtering just prior to depositing a Au or Ag film [52], [59]. The ρ_c of the as-formed contact (20°C processing temperature) was 10^{-5} $\Omega \cdot cm^2$—approximately the same as contacts made in [50], [57], or [61] without a sputter-etch. The back-sputtering does not appear to have exposed a superconducting surface.

TABLE VII
YBCO SURFACE COMPOSITION DETERMINED BY XPS

Film Treatment	Process Temperature	Y at %	B at %	Cu at %
Film 1				
as-deposited (amorphous oxide)	400°C	17	33	50
in situ O_2 anneal	500°C	21	66	13
ex situ O_2 anneal	850°C	22	41	37
ion-milled, 150 eV	20	50	24	26
ion-milled, 300 eV	20	35	29	35
Film 2				
as-deposited (crystalline)	650°C	20	29	51
in situ O_2 anneal	500°C	32	50	18
Film 3				
as-deposited (amorphous oxide)	400°C	19	33	48
in situ O_2 anneal (10°C/s ramp)	850°C	21	33	46

The work of Gavaler *et al.* [61], [63] is an exception to these generalizations because normal metal contacts were deposited both *ex situ* and *in situ*, that is, without exposing the film's surface to air. All of the other Ag or Au films deposited in the work summarized in Table VI were deposited *ex situ*.

The *in situ* approach to multilayer superconductor film deposition and surface analysis has been described elsewhere [64], [65]. Table VII contains some of the results of *in situ* X-ray photoelectron spectroscopy (XPS) of YBCO films. The

relative count rates of Y_{3d}, Ba_{3d}, and Cu_{2p} photoelectrons were used to obtain the cation composition of a surface YBCO layer approximately 2 nm thick. The as-deposited composition of one of the amorphous films deposited at low temperature was used for calibration—in reasonable agreement with other calibration techniques.

Film 1 of Table VII was deposited by sputtering in an Ar–O_2 gas mixture with a substrate temperature of 400°C [66], and the as-deposited surface had a stoichiometric composition. After annealing in a full atmosphere of oxygen *in situ* at 500°C (< crystallization temperature), and after an *ex situ* anneal at 850°C, the surface became Ba-rich. Ion-milling with Ar and Ar–O_2 at various energies is not sufficient to restore the composition of the surface which became Y-rich. Film 2, deposited at 650°C to grow in a crystalline, tetragonal structure, is included in Table VII to show that the segregation of Ba to the surface during O_2 annealing is not restricted to amorphous films.

Film 3 was annealed with a rapid ramp to 850°C at a rate of 10°C/s. The soak duration at 850°C does not appear to be important. The effect of the rapid ramp may have been to kinetically limit Ba diffusion until the YBCO surface was fully oxidized.

Additional evidence that the driving force for Ba segregation is related to oxygen deficiency can be found in the Auger spectroscopy depth profiles in Fig. 3. The film used for Fig. 3(a) was deposited (without oxygen) as an amorphous metal at 400°C, and post-annealed at 850°C in an O_2 atmosphere. The Ba-rich surface layer thickness was ~100 nm. The film in Fig. 3(b) was grown as an amorphous oxide and post-annealed. The thickness of the Ba-rich surface layer was reduced to ~10 nm. The film in Fig. 3(c) was an amorphous oxide post-annealed *in situ* with a rapid ramp rate. It was cooled and then coated with a 50-nm-thick Au film deposited by evaporation at 20°C. The ratio Y:Ba:Cu was 1:2:3 at all distances from the interface with the Au overlayer. The contact resistance of this type of interface, shown in the last line of Table VI, was $< 4 \times 10^{-10}\ \Omega\cdot cm^2$—without annealing the contact.

The significance of this technique extends beyond the need to make low-resistance contacts to Au or Ag. A trivial extension is that other normal metals could be used. Most importantly, surfaces prepared by this technique meet the requirements for the top surface of a Josephson junction base electrode as shown in Fig. 2. Tunneling experiments using YBCO base electrodes and Nb top electrodes are described in [67].

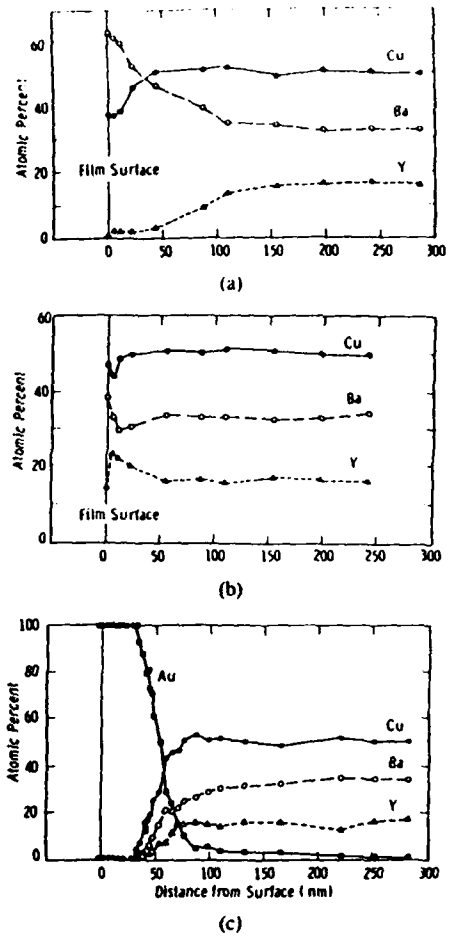

Fig. 3. Auger spectroscopy depth profiles of YBOC films which where amorphous as-deposited and re-crystallized in an O_2 atmosphere at 850°C. (a) Amorphous metal film grown in $< 10^{-7}$ Pa O_2 and annealed with a slow ramp to 850°C. (b) Amorphous oxide film grown in 4×10^{-3} Pa O_2; annealed with a slow ramp. (c) Film grown in 4×10^{-3} Pa O_2 which was annealed with a 10°C/s ramp rate to 850°C, cooled, and then coated with 50 nm of evaporated Au at 20°C.

IV. Contacts to Practical Wires

Practical superconducting wires generally consist of as many as thousands of fine filaments of Nb–Ti or, for very high magnetic field applications, Nb_3Sn, embedded in a matrix of high-purity copper [46]. The multifilamentary design provides dynamic stability in ac operation. (Reference [68] contains a collection of reviews on conductor design.)

The most important applications of superconducting wire are in magnets. Although the first unit was installed only in 1981, the largest commercial application of superconductivity is in magnets for nuclear magnetic resonance imaging (MRI) systems [69]. Among the specifications for contacts to be considered in this section are the particular requirements for MRI magnets. Magnets in rotating machinery do not have to be considered separately because brushes in these applications always employ normal metals. This section will not describe each of the possible joining techniques which have been reviewed elsewhere [69], [70], instead, it will show how the principals developed in Section II relate to applications of superconducting magnets. The latter part of this section will discuss the origins of the poor intergranular contacts in YBCO that are preventing the development of practical high-T_c conductors.

Two types of contacts are present in magnets. The first is the contact from copper leads bringing current from a room-temperature power supply to the superconducting wire. Since the superconductor filaments are embedded in a Cu matrix, it is simply a Cu–Cu joint that must be made. Usually, a lap joint is used. Under most conditions—quantified in the next section—power dissipation will be much greater in the Cu leads than at the contact. Sufficient cooling must be provided

for the leads to prevent them from warming the superconductor. The tradeoff between thermal conductivity and Joule heating is the central engineering problem in the design of leads [71].

The second contact to be considered is the joint between lengths of superconducting wire. Usually, a butt joint is required to maintain a constant conductor diameter. The simplest approach is to bond the Cu matrices by any one of a number of techniques—such as resistance welding, ultrasonic welding, soldering, or cold welding—to form an *S–N–S* structure with a critical current density much lower than the rest of the conductor. This approach is satisfactory in cases where current is continually provided by a room-temperature power supply and the heat generated at the joint can be dissipated without overheating the superconductor. For example, the 5-MVA superconducting generator field winding and 300-kJ pulsed energy coil made at Westinghouse used In-soldered lap joints clamped by Cu plates [70]. The Nb_3Sn LCP coil produced by Westinghouse had a resistance butt-welded Cu-Cu joint with $\rho_c \simeq 10^{-9}\ \Omega\cdot cm^2$ [70].

The requirements are more stringent for a magnet operated in persistent mode, that is, with the superconductor forming a closed loop [69]. Some MRI magnets are designed so the Cu leads to "charge" the magnet can be unplugged and withdrawn from the dewar to eliminate a major thermal link to the room [72]. Dissipation due to joint resistance causes a decay of the magnetic field and, in MRI, the resonance frequency which is proportional to the magnetic field. Typical specifications for magnetic field stability are <0.1 ppm/h [69]. In such cases, contact must be made between Nb–Ti filaments on each side of the joint. For the dc operation needed for MRI, conductors are used which have relatively large and few filaments. The Cu matrix is etched away and individual filaments crimped in Cu sleeves [73], electron-beam welded [74], or joined by any number of similar but proprietary techniques, in an effort to form an *S–S′–S* structure. Typical values for the specific resistance of such joints are $\rho_c < 10^{-11}\ \Omega\cdot cm^2$.

In contrast to conventional superconductors, many significant problems must be solved to make practical high-T_c superconducting wires. Single-filament [75] and, in one report [76], multifilamentary wires modeled after Nb–Ti conductors have been produced. However, as discussed in Section II, polycrystalline bulk samples carry several orders of magnitude lower currents in zero applied magnetic field than bulk single crystals and polycrystalline films due to poor contact between grains. In an externally applied magnetic field, the relative performance of bulk composite samples is even worse [17].

There is no agreement on which mechanism is responsible for isolating grains in bulk YBCO. Auger spectroscopy [77] and XPS measurements [78] of fracture surfaces have detected the presence of carbon and barium carbonate similar to that found on the surface of thin films exposed to air. Barium carbonate is an insulator that could form a tunneling barrier that would effectively decrease critical currents. The origin of the carbon is either from carbonate starting materials or carbon dioxide in the atmosphere. A number of laboratories have attempted to avoid these sources of carbon by using barium peroxide rather than barium carbonate powder as a starting ingredient and processing samples in a controlled atmosphere. Although XPS data indicate that $BaCO_3$ at grain boundaries is reduced [79], no J_c data are available on such samples.

Some analyses indicate that the presence of intergranular carbon may be due to microcracks which lie parallel to the Cu-O planes [80], [81]. The cracks are thought to result from strain due to anisotropic thermal expansion [82] or the tetragonal-to-orthorhombic structural transformation which occurs during cooling at ~750°C (in an O_2 atmosphere) [83]. They could form a vacuum tunneling barrier to current transport and open grain boundaries to contamination from CO_2 in the atmosphere.

Normal-metal or insulating layers at grain boundaries can also be created by compositional variations. The transition temperature of $YBa_2Cu_3O_{7-x}$ is very sensitive to oxygen composition in the range $0 \le x \le 0.75$ [84]. Particularly in the direction perpendicular to the Cu-O planes where $\xi_s = 0.4$ nm, a partial loss of oxygen in even one monolayer will reduce J_c. The techniques commonly used for analysis of composition at grain boundaries, scanning Auger microscopy, and analytical transmission electron microscopy, are probably not sensitive enough to detect such a small change in oxygen. Some grain boundary regions enriched in Cu have been observed by both techniques [85], [86]. There is too little work in which both analytical and electrical properties of grain boundaries are directly correlated for any of these possible mechanisms of isolating grains to be ignored, and it is likely that all of these contribute to lowering J_c.

Some of the problems with high-T_c conductors are only related indirectly to the coupling between grains. They affect the prospects for YBCO wires even if long, single-crystal fibers could be grown. One is the brittleness of ceramics. A ceramic wire could not survive the strain created by winding a magnet. Wind-and-react techniques have been developed for brittle Nb_3Sn conductors, but at a high cost. Other difficulties are intrinsic to operation at temperatures on the order of 77 K. The electrical conductivity of a stabilizing normal-metal matrix at 77 K is much lower than at 4.2 K and less effective—although the stability is helped somewhat by a greater heat capacity [87]. The shorter mean free path l at 77 K decreases ξ_n (1) and therefore decreases the coupling between filaments that is provided by the matrix.

V. Contacts for Critical Current Measurements

This section is concerned with contacts to bulk superconductors which have been fabricated for measurements of superconducting properties or in more primitive forms of conductors than considered in Section IV. Typical sample shapes for conventional superconductors in this category are monofilamentary wires, foils, and tapes made from thick film deposits on a flexible substrate. For high T_c oxide superconductors, samples are in the form of pressed and sintered rods or pellets, and thick-film tapes. Contacts are important in the measurement of critical current density J_c. Measurements of J_c are normally made by slowly increasing the current flowing through a superconductor until a nonzero voltage is measured across a separate pair of contacts. Attempts have been made to

establish a particular voltage or electric field as the "critical" level [88], but most experiments simply choose a voltage near their minimum detectable level.

Thin films can be patterned using conventional photolithography techniques to obtain small cross-sectional areas A of the superconductor. Even for films which have large critical current densities, typical measurement currents are small. For example, a typical value for the critical current is $J_cA = 2\,\mu m \times 0.5\,\mu m \times 10^6$ A/cm^2 = 10 mA. Contact areas can be much greater than the film's cross-sectional area, and the power dissipated even by relatively poor contacts can be heat-sunk by the substrate anchored to a temperature-controlled block.

Those samples for which cross-sectional areas cannot be made arbitrarily small require low-resistance contacts to prevent heat from the contacts from raising the sample temperature. The power generated at a simple lap joint between Cu and a superconductor (equipotential) surface has been calculated following Wilson [47]

$$P_{\text{contact}} = I^2 \sqrt{\rho_c R_\square}/w \; f(R_\square L^2/\rho_c) \qquad (3)$$

where I is the measurement current, w and L are the width and length of the lap joint, ρ_c is the specific resistance of the contact, and $R_\square$ is the sheet resistance of the Cu (units of ohm per square). The function $f(R_\square L^2/\rho_c)$ is a monotonically decreasing function of its argument and reaches a constant value of $f = 1$ for $R_\square L^2 > \rho_c$. The power generated in the same length L of the Cu current lead is

$$P_{\text{lead}} = I^2 R_\square L/w. \qquad (4)$$

A reasonable criterion for a "good" contact is that $P_{\text{lead}} \geq P_{\text{contact}}$. From (3) and (4), this criterion reduces to $R_\square L^2 \geq \rho_c$. Consider a lap joint made with 0.010-in-thick Cu on a YBCO sample at 77 K using the data in Table VI. For an In-solder or Ag-paste contact ($\rho_c \simeq 10^{-2}\ \Omega\cdot$cm^2), the length of the joint would have to be ~50 cm—much greater than typical dimensions of laboratory samples. For Cu bonded to an evaporated Au contact pad, the joint length could be three orders of magnitude smaller, $L \simeq 0.5$ mm.

VI. Conclusions

Electrical contact to the technologically important superconductors, primarily Nb and Nb-Ti, is relatively straightforward. The only short length scales involved are the thicknesses of insulating tunnel barriers. Insulating surface layers—usually formed by the native oxide—must be completely removed in the process of making a contact. The coherence lengths of Nb and Nb-Ti are sufficiently long that oxide layers can be removed or dissolved without creating a degraded layer on the surface of the superconductor. Not only does this result in low contact resistances, but critical current density is in the vicinity of the contact remain comparable to values in bulk superconductors.

Another length scale of importance in superconductor/normal metal and superconductor/semiconductor interfaces is the normal-metal coherence length ξ_n. Although $\xi_n > \xi_s$ for most normal metals, semiconductors, and superconductors, ξ_n is too small for optical lithography to be used to pattern reproducible and high-current S-N-S and three-terminal S-Se-S structures.

Electrical contact to high-T_c oxide superconductors is much less straightforward. Many of the issues involved are likely to be the cause of poor current transfer between adjacent grains in bulk samples: chemically unstable surfaces, short coherence lengths, sensitivity to oxygen loss, mechanical strains, and contamination from the atmosphere. In the case of YBCO thin films, samples have been prepared by a rapid-ramp thermal treatment and *in situ* encapsulation which exhibited superconducting properties at all distances from the surface. For bulk samples, diffusion of noble-metal contact layers into the surface at ≥300°C forms sufficiently good contacts to permit the measurement of critical current densities without overheating.

Acknowledgment

The author wishes to acknowledge the assistance of P. W. Eckels and G. R. Wagner in gathering reference material for this review and the willingness of J. R. Gavaler and M. G. Forrester to share unpublished data.

References

[1] J. R. Gavaler, "Superconductivity in Nb-Ge films above 23K," *Appl. Phys. Lett.*, vol. 23, pp. 480-482, Oct. 173.

[2] J. G. Bednorz and K. A. Müller, "Possible high-T_c superconductivity in the Ba-La-Cu-O," *Z. Phys. B*, vol. 64, pp. 189-192, 1986.

[3] S. S. P. Parkin, V. Y. Lee, E. M. Engler, A. I. Nazzal, T. C. Huang, G. Gorman, R. Savoy, and R. Beyers, "Bulk superconductivity at 125 K in $Tl_2Ca_2Ba_2Cu_3O_x$," *Phys. Rev. Lett.*, vol. 60, pp. 2539-2542, June 1988.

[4] R. J. Cava, B. Batlogg, J. J. Krajewski, R. Farrow, L. W. Rupp Jr., A. E. White, K. Short, W. F. Peck, and T. Kometani, "Superconductivity near 30 K without copper: The $Ba_{0.6}K_{0.4}BiO_3$ perovskite," *Nature*, vol. 332, pp. 814-816, Apr. 1988.

[5] A. W. Sleight, J. L. Gillson, and P. E. Bierstedt, "High-superconductivity in the $BaPb_{1-x}Bi_xO_3$ system," *Solid State Commun.*, vol. 17, pp. 27-28, 1975.

[6] L. F. Mattheiss, E. M. Gyorgy, and D. W. Johnson Jr., "Superconductivity above 20 K in the Ba-K-Bi-O system," *Phys. Rev. B*, vol. 37, pp. 3745-3746, Mar. 1988.

[7] M. Suzuki, Y. Enomoto, K. Moriwaki, and T. Murakami, "Anisotropic properties of superconducting $La_{1-x}Sr_{x2}CuO_4$ single-crystal thin films," *Japan J. Appl. Phys.*, vol. 26, pp. L1921-L1924, Nov. 1987.

[8] R. J. Cava, R. B. van Dover, B. Batlogg, and E. A. Rietman, "Bulk superconductivity at 36K in LaSrCuO," *Phys. Rev. Lett.*, vol. 58, pp. 408-410, Jan. 1987.

[9] W. J. Gallagher, "Studies at IBM on anisotropy in single crystals of the high-temperature oxide superconductor $YBa_2Cu_3O_{7x}$," *J. Appl. Phys.*, vol. 63, pp. 4126-4219, Apr. 1988.

[10] M. K. Wu, J. R. Ashburn, C. J. Torng, P. H. Hor, R. L. Meng, L. Gao, Z. J. Huang, Y. Q. Wang, and C. W. Chu, "Superconductivity at 93 K in a new mixed-phase Y-Ba-Cu-O compound system at ambient pressure," *Phys. Rev. Lett.*, vol. 58, pp. 908-910, Mar. 1987.

[11] T. T. M. Palstra, B. Batlogg, L. F. Schneemeyer, R. B. van Dover, and J. V. Waszczak, "Angular dependence of the upper critical field of $Bi_{2.2}Sr_2Ca_{0.8}Cu_2O_{8+\delta}$," *Phys. Rev. B*, vol. 38, pp. 5102-5105, Sept. 1988.

[12] H. Maeda, Y. Tanaka, M. Fukutomi, and T. Asano, "A new high T_c oxide superconductor without rate earth element," *Japan J. Appl. Phys.*, vol. 27, pp. L209-L210, Feb. 1988.

[13] H. Kumakura, K. Togano, K. Takahashi, H. Shimizu, M. Uehara, H. Maeda, and M. Nakao, "Magnetic properties and upper critical fields of sintered Tl-Ca-Ba-Cu-O superconductors," *Japan J. Appl. Phys.*, vol. 27, pp. L857-L860, May 1988.

[14] E. M. Gyorgy, G. S. Grader, D. W. Johnson Jr., L. C. Feldman, D. W. Murphy, W. W. Rhodes, R. E. Howard, P. M. Mankiewich,

and W. J. Skocpol, "Persistent currents in ceramic and evaporated thin-film toroids of $B_2YCu_3O_7$," *Appl. Phys. Lett.*, vol. 52, pp. 328-330, Jan. 1988.

[15] H. Ullmaier, *Irreversible Properties of Type-II Superconductors*. New York, NY: Springer-Verlag, 1975.

[16] D. Dimos, P. Chaudhari, J. Mannhart, and F. K. LeGoues, "Orientation dependence of grain boundary critical currents in $YBa_2Cu_3O_{7-\delta}$ bicrystals," *Phys. Rev. Lett.*, vol. 61, pp. 219-222, July 1988.

[17] S. Jin, T. H. Tiefel, R. C. Sherwood, R. B. van Dover, M. E. Davis, G. W. Kammlott, and R. A. Fastnacht, "Melt-textured growth of polycrystalline $YBa_2Cu_3O_{7-\delta}$ with high transport J_c at 77 K," *Phys. Rev. B*, vol. 37, pp. 7850-7853, May 1988.

[18] M. R. Beasley and C. J. Kircher, "Josephson junction electronics: Materials issues and fabrication techniques," in *Superconductor Materials Science*, S. Foner and B. B. Schwartz, Eds. New York: NY: Plenum, 1981, pp. 605-684.

[19] R. B. van Dover, A. de Lozanne, and M. R. Beasley, "Superconductor-normal-superconductor microbridges: Fabrication, electrical behavior, and modeling," *J. Appl. Phys.*, vol. 52, pp. 7327-7343, Dec. 1981.

[20] For a complete review of Josephson junction properties and applications, see T. Van Duzer and C. W. Turner, *Principles of Superconductive Devices and Circuits*. New York, NY: Elsevier, 1981.

[21] J. G. Simmons, "Low-voltage current-voltage relationship of tunnel junctions," *J. Appl. Phys.*, vol. 34, pp. 238-239, Jan. 1963.

[22] J. Talvacchio, J. R. Gavaler, and A. I. Braginski, "Epitaxial niobium nitride/insulator layered structures," in *Proc. TMS-AIME: Metallic Multilayers and Epitaxy*, M. Hong, S. A. Wolf, and D. U. Gubser, Eds. Pittsburgh, PA: TMS-AIME, 1987, pp. 109-134.

[23] A. I. Braginski, J. R. Gavaler, M. A. Janocko, and J. Talvacchio, "New materials for refractory tunnel junctions: Fundamental aspects," in *SQUID 85-Superconducting Quantum Interference Devices and their Applications*, H. D. Hahlbohm and H. Lubbig, Eds. Berlin, FRG: Walter de Gruyter, 1985, pp. 591-631.

[24] M. Strongin, R. S. Thompson, O. F. Kammerer, and J. E. Crow, "Destruction of superconductivity in disordered near-monolayer films," *Phys. Rev. B*, vol. 1, pp. 1078-1091, Feb. 1970.

[25] J. Kodama, M. Itoh, and H. Hirai, "Superconducting transition temperature versus thickness of Nb films on various substrates," *J. Appl. Phys.*, vol. 54, pp. 4050-4053, July 1983.

[26] S. I. Park, A. F. Marshall, R. H. Hammond, T. H. Geballe, and J. Talvacchio, "The role of ion-beam cleaning in the growth of strained-layer epitaxial thin transition metal films," *J. Mater. Res.*, vol. 2, pp. 446-455, July 1987.

[27] M. Igarashi, M. Hikita, and K. Takei, "Barrier/electrode interface structure and I-V characteristics of NbN Josephson junctions," in *Advances in Cryogenic Engineering-Materials*, vol. 30, A. F. Clark and R. P. Reed, Eds. New York, NY: Plenum, 1984, pp. 535-546.

[28] A. Shoji, M. Aoyagi, S. Kosaka, and F. Shinoki, "Temperature-dependent properties of niobium nitride Josephson tunnel junctions," *IEEE Trans. Magn.*, vol. MAG-23, pp. 1464-1471, Mar. 1987.

[29] J. Talvacchio, J. R. Gavaler, M. A. Janocko, and A. I. Braginski, unpublished.

[30] K. Hirochi, H. Adachi, K. Setsune, O. Yamazaki, and K. Wasa, "Thickness dependence of superconductivity in As-sputtered Er-Ba-Cu-O thin films," *Japan J. Appl. Phys.*, vol. 26, pp. L1837-L1838, Nov. 1987.

[31] H. Akoh, F. Shinoki, M. Takahashi, and S. Takada, "Thickness dependence of superconductivity in RF-sputtered Y-Ba-Cu-O thin films," *Appl. Phys. Lett.*, vol. 52, pp. 1732-1734, May 1988.

[32] L. N. Smith, H. Kroger, and D. W. Jillie, "Uniformity and stability of Nb/aSi/Nb "SNAP" Josephson tunnel junctions," *IEEE Trans. Magn.*, vol. MAG-19, pp. 787-790, May 1983.

[33] T. Kawakami and H. Takayanagi, "Single crystal n-InAs coupled Josephson junctions," *Appl. Phys. Lett.*, vol. 46, pp. 92-94, Jan. 1985.

[34] J. Seto and J. Van Duzer, "Theory and measurements on lead-tellurium-lead supercurrent junctions," in *Low Temperature Physics, LT-13*, vol. 3, K. D. Timmerhaus, W. J. O'Sullivan, and E. F. Hammel, Eds. New York, NY: Plenum, 1974, pp. 328-333.

[35] W. J. Gallagher, "Three-terminal superconducting devices," *IEEE Trans. Magn.*, vol. MAG-21, pp. 709-717, Mar. 1985.

[36] D. J. Frank and A. Davidson, "Prospects for high-T_c superconductor/semiconductor transistor-like devices," in *Proc. 5th Int. Workshop on Future Electron Devices* (Miyagi-Zao, 1988), pp. 313-321.

[37] T. Nishino, E. Yamada, and U. Kawabe, "Carrier-concentration dependence of critical superconducting current induced by the proximity effect in Si," *Phys. Rev. B*, vol. 33, pp. 2042-2045 Feb. 1986.

[38] K. Inoue and T. Kawakami, "Self-field effects in Josephson junctions coupled with n-InAs and the surface inversion layer on p-InAs," *Japan J. Appl. Phys.*, suppl. 26-3, pp. 1665-1666, 1987.

[39] A. W. Kleinsasser and T. N. Jackson, "Superconductivity and field-effect transistors," *Japan J. Appl. Phys.*, suppl. 26-3, pp. 1545-1546, 1987.

[40] A. P. Malozemoff, "Computer applications of high temperature superconductivity," *Physica C*, vol. 153-155, pp. 1049-1054, 1988.

[41] L. A. Hornak, S. K. Tewksbury, and M. Hatamian, "The impact of high-T_c superconductivity on system communications," in *Proc. 38th Electronic Components Conf.* (Los Angeles, CA, 1988), pp. 152-158. Also, *IEEE Trans. Comp. Hybrids, Manuf. Technol.*, vol. 11, no. 4, pp. 412-415, Dec. 1988.

[42] H. Myoren, Y. Nishiyama, H. Nasu, T. Imura, Y. Osaka, and H. Fukumoto, "Preparation of Ba-Y-Cu-O films on epitaxial ZrO_2/Si," in *Proc. 5th Int. Workshop on Future Electron Devices* (Miyagi-Zao, 1988), pp. 31-88.

[43] T. Siegrist, L. F. Schneemeyer, J. V. Waszczak, N. P. Singh, R. L. Opila, B. Batlogg, L. W. Rupp, and D. W. Murphy, "Aluminum substitution in $Ba_2YCu_3O_7$," *Phys. Rev. B*, vol. 36, p. 8365-8368, Dec. 1987.

[44] M. Gurvitch and A. T. Fiory, "Preparation and substrate reactions of superconducting Y-Ba-Cu-O films," *Appl. Phys. Lett.*, vol. 51, pp. 1027-1029, Sept. 1987.

[45] H. H. Zappe, "Josephson computer technology," in *Advances in Superconductivity*, B. Deaver and J. Ruvalds, Eds. New York, NY: Plenum, 1983 pp. 51-127.

[46] See for example, *IEEE Trans. Magn.*, vol. MAG-23, pp. 329-1763 (Proc. Applied Superconductivity Conf., J. F. Schooley *et al.*, Eds.), Mar. 1987.

[47] M. N. Wilson, "Practical superconducting materials," in *Superconductor Materials Science*, S. Foner and B. B. Schwartz, Eds. New York, NY: Plenum, 1981, p. 124.

[48] G. F. Holland, R. L. Hoskins, M. A. Dixon, P. D. VerNooy, H.-C. zur Loye, G. Brimhall, D. Sullivan, R. Cormia, H. W. Zandbergen, R. Gronsky, and A. M. Stacy, "Interplay of synthesis, structure, microstructure, and superconducting properties of $YBa_2Cu_3O_7$," in *Chemistry of High-Temperature Superconductors*, D. L. Nelson, M. S. Whittingham, and T. F. George, Eds. Washington, DC: Am. Chem. Soc., 1987, pp. 102-113.

[49] H. W. Zandbergen, R. Gronsky, and G. Thomas, "Surface decomposition of superconducting $YBa_2Cu_3O_7$," *Phys. Status Solidi a*, vol. 105, pp. 207-218, 1988.

[50] T. Kusaka, Y. Suzuki, T. Yotsuya, S. Ogawa, T. Aoyama, and H. Imokawa, "Contact formation to $Y_1Ba_2Cu_3O_{7-\delta}$ ceramics," in *Proc. 5th Int. Workshop on Future Electron Devices* (Miyagi-Zao, 1988), pp. 205-208.

[51] R. Caton, R. Selim, A. M. Buoncristiani, and C. E. Byvik, "Rugged low-resistance contacts to $YBa_2Cu_3O_x$," *Appl. Phys. Lett.*, vol. 52, pp. 1014-1016, Mar. 1988.

[52] J. W. Ekin, A. J. Panson, and B. A. Blankenship, "Effect of Oxygen annealing on low-resistivity for high-T_c superconductors," in *MRS Vol. 99: High-Temperature Superconductors*, M. B. Brodsky, H. L. Tuller, R. C. Dynes, and K. Kitazawa, Eds. Pittsburgh, PA: Materials Res. Soc., 1988, pp. 283-286.

[53] Y. Iye, T. Tamegai, H. Takeya, and H. Takei, "A simple method for attaching electrical leads to small samples of high-T_c oxides," *Japan J. Appl. Phys.*, vol. 27, pp. L658-L660, Apr. 1988.

[54] A. D. Wieck, "Vanishing contact resistance on polycrystalline $YBa_2Cu_3O_{7-x}$," *Appl. Phys. Lett.*, vol. 52, pp. 1017-1019, Mar. 1988.

[55] J. van der Maas, V. A. Gasparov, and D. Pavuna, "Improved low contact resistance in high-T_c Y-Ba-Cu-O ceramic superconductors," *Nature*, vol. 328, pp. 603-604, Aug. 1987.

[56] I. Sugimoto, Y. Tajima, and M. Hikita, "Low resistance ohmic contact for the oxide superconductor $EuBa_2Cu_3O_y$," *Japan J. Appl. Phys.*, vol. 27, pp. L864-L866, May 1988.

[57] Y. Tzeng, A. Holt, and R. Ely, "High performance silver ohmic contacts to $YBa_2Cu_3O_{6+x}$ superconductors," *Appl. Phys. Lett.*, vol. 52, pp. 155-156, Jan. 1988.

[58] Y. Tzeng, "Fabrication of electrical contacts to $YBa_2Cu_3O_{7-x}$ superconductor by molten silver processing," *J. Electrochem. Soc.*, vol. 135, pp. 1309-1310, May 1988.

[59] J. W. Ekin, T. M. Larson, N. F. Bergren, A. J. Nelson, A. B. Swartzlander, L. L. Kazmerski, A. J. Panson, and B. A. Blankenship, "High T_c superconductor/noble-metal contacts with surface resistivities in the 10^{-10} Ω-cm^2 range," *Appl. Phys. Lett.*, vol. 52, pp. 1819-1821, May 1988.

[60] K. Mizushima, M. Sagoi, T. Miura, and J. Yoshida, "Electric properties of the $YBa_2Cu_3O_{7-\delta}$/Au interface," *Appl. Phys. Lett.*, vol. 52, pp. 1101-1103, Mar. 1988.

[61] J. R. Gavaler, A. I. Braginski, J. Talvacchio, M. A. Janocko, M. G. Forrester, and J. Greggi, "Fabrication of high-T_c superconducting $YBa_2Cu_3O_7$ films," in *MRS Vol. EA-14: High-Temperature Superconductors II*, D. W. Capone II, W. H. Butler, B. Batlogg, and C. W. Chu, Eds. Pittsburgh, PA: Mater. Res. Co., 1988, pp. 193-196.

[62] J. W. Ekin, A. J. Panson, and B. A. Blankenship, "Method for making low resistivity contacts to high-T_c superconductors," *Appl. Phys. Lett.*, vol. 52, pp. 331-333, Jan. 1987.

[63] J. R. Gavaler and A. I. Braginski, "Near-surface atomic segregation in YBCO thin films," *Physica C*, vol. 153-155, pp. 1435-1436, 1988.

[64] J. Talvacchio, M. A. Janocko, J. R. Gavaler, and A. I. Braginski, "UHV deposition and analysis of thin-film superconductors," in *Advances in Cryogenic Engineering-Materials, Vol. 32*, A. F. Clark and R. P. Reed, Eds. New York, NY: Plenum, 1986, pp. 527-541.

[65] A. I. Braginski, J. Talvacchio, J. R. Gavaler, M. G. Forrester, and M. A. Janocko, "*In situ* fabrication, processing, and characterization of superconducting oxide films," in *SPIE Proceedings Vol. 948, High-T_c Superconductivity: Thin Films and Devices*, R. B. van Dover and C. C. Chi, Eds. Bellingham, WA: SPIE, 1988, pp. 89-97.

[66] R. M. Silver, J. Talvacchio, and A. L. de Lozanne, "Sputter deposition of $YBa_2Cu_3O_{7-y}$ thin films," *Appl. Phys. Lett.*, vol. 51, pp. 2149-2151, Dec. 1987.

[67] J. R. Gavaler, A. I. Braginski, M. G. Forrester, and J. Talvacchio, "Optimization of YBCO surfaces for tunnel junctions," in *Proc. 1988 Applied Superconductivity Conf.*, to be published in *IEEE Trans. Magn.*, vol. 25, Mar. 1989.

[68] S. Foner and B. B. Schwartz, Eds., *Superconductor materials Science*. New York, NY: Plenum, 1981.

[69] R. E. Schwall, "MRI—Superconductivity in the marketplace," *IEEE Trans. Magn.*, vol. MAG-23, pp. 1287-1293, Mar. 1987.

[70] R. D. Blaugher, "Recent developments in methods for superconductor joining," in *Advances in Cryogenic Engineering—Materials*, vol. 28, A. F. Clark and R. P. Reed, Eds. New York, NY: Plenum, 1982, pp. 689-700.

[71] G. Bogner, "Transmission of electrical energy by superconducting cables," in *Superconducting Machines and Devices*, S. Foner and B. B. Schwartz, Eds. New York, NY: Plenum, 19873, pp. 401-547.

[72] G. R. Morrow and C. H. Rosner, "Superconducting magnets for magnetic resonance imaging applications," *IEEE Trans. Magn.*, vol. MAG-23, pp. 1294-1298, Mar. 1987.

[73] M. J. Leupold and Y. Iwasa, "Superconducting joint between multifilamentary wires: 1. Joint making and joint results," *Cryogenics*, vol. 16, pp. 215-216, Apr. 1976.

[74] G. Luderer, P. Dullenkopf, and G. Laukien, "Superconducting joint between multifilamentary wires," *Cryogenics*, vol. 14, pp. 518-519, Sept. 1974.

[75] K. Noto, "Present status of development in J_c and other characteristics of oxide superconductors in Japan," in *Proc. 5th Japan-US Workshop on High-Field Superconducting Materials for Fusion*, 1988.

[76] H. Sekine, K. Inoue, H. Maeda, K. Numata, K. Mori, and H. Yamamoto, "Fabrication of multifilamentary Y-Ba-Cu-O oxide superconductors," *Appl. Phys. Lett.*, vol. 52, pp. 2261-2263, June 1988.

[77] S. Nakahara, G. J. Fisanick, M. F. Yan, R. B. van Dover, and T. Boone, "On the defect structure of grain boundaries in $Ba_2YCu_3O_{7-x}$," *J. Cryst. Growth*, vol. 85, pp. 639-651, 1987.

[78] A. G. Schrott, S. L. Cohen, T. R. Dinger, F. J. Himpsel, J. A. Yarmoff, K. G. Frase, S. I. Park, and R. Purtell, "Photoemission study of grain boundary segregation in $YBa_2Cu_3O_7$," in *Thin Film Processing and Characterization of High-Temperature Superconductors* (Proc. No. 165), J. M. E. Harper, R. J. Colton, and L. C. Feldman, Eds. New York, NY: Amer. Inst. of Physics, 1988, pp. 349-357.

[79] A. F. Hepp, P. R. Aron, J. R. Gaier, D. K. Wheeler, and R. G. Garlick, "Characterization of $Ba_2YCu_3O_{7-x}$ prepared in an inert atmosphere," in *MRS Vol. EA-14: High-Temperature Superconductors II*, D. W. Capone II, W. H. Butler, B. Batlogg, and C. W. Chu, Eds. Pittsburgh, PA: Mater. Res. Soc., 1988, pp. 183-186.

[80] J. D. Verhoeven, A. J. Bevolo, R. W. McCallum, E. D. Gibson and M. A. Noack, "Auger study of grain boundaries in large grained $YBa_2Cu_3O_x$," *Appl. Phys. Lett.*, vol. 52, pp. 745-747, Mar. 1988.

[81] G. J. Fisanick, P. Mankiewich, W. Skocpol, R. E. Howard, A. Dayem, R. M. Fleming, A. E. White, S. H. Liou, and R. Moore, "Microstructural characterization of $Ba_2YCu_3O_7$ films produced by co-evaporation," in *MRS Vol. 99: High-Temperature Superconductors*, M. B. Brodsky, H. L. Tuller, R. C. Dynes, and K. Kitazawa, Eds. Pittsburgh, PA: Mat. Res. Soc., 1988, pp. 703-706.

[82] T. H. Tiefel, S. Jin, R. C. Sherwood, R. A. Fastnacht, S. Nakahara, G. Fisanick, and T. Boone, "Effect of temperature cycles on the critical current density of $YBa_2Cu_3O_{7-\delta}$," in *MRS Vol. 99: High Temperature Superconductors*, M. B. Brodsky, R. C. Dynes, K. Kitazawa, and H. L. Tuller, Eds. Pittsburgh, PA: Mater. Res. Soc., 1988, pp. 365-369.

[83] I. K Schuller, D. G. Hinks, M. A. Beno, D. W. Capone II, L. Soderholm, J.-P. Locquet, Y. Bruynsersede, C. U. Segre, and K. Zhang, "Structural phase transition in $YBa_2Cu_3O_{7-\delta}$: The role of dimensionality for high temperature superconductivity," *Solid State Commun.*, vol. 63, pp. 385-389, Aug. 1987.

[84] R. J. Cava, B. Batlogg, C. H. Chen, E. A. Riteman, S. M. Zahurak, and D. Werder, "Single phase 60 K bulk superconductor in annealed $Ba_2YCu_3O_{7-\delta}$ ($0.3 < \delta < 0.4$) with correlated oxygen vacancies in the Cu-O-chains," *Phys. Rev. B*, vol. 36, pp. 5719-5722, Oct. 1987.

[85] D. M. Kroeger, A. Choudhury, J. Brynestad, R. K. Williams, R. A. Padgett, and W. A. Coghlan, "Grain-boundary compositions in $YBa_2Cu_3O_{7-x}$ from Auger electron spectroscopy of fracture surfaces," *J. Appl. Phys.*, vol. 64, pp. 331-335, July 1988.

[86] S. E. Babcock, T. F. Kelly, P. J. Lee, J. M. Seuntjens, L. A. LaVanier, and D. C. Larbalestier, "Investigation of composition variations near grain boundaries in high-quality sintered samples of $YBa_2Cu_3O_{7-\delta}$," *Physica C*, vol. 152, pp. 25-38, 1988.

[87] E. W. Collings, "Design of cryostable conductors for 80 K," in *Advances in Cryogenic Engineering—Materials*, vol. 34, A. F. Clark and R. P. Reed, Eds. New York, NY: Plenum, 1988, pp. 639-646.

[88] H. R. Segal, Z. J. J. Stekly, and T. A. de Winter, "Development of critical current standards," *IEEE Trans. Magn.*, vol. MAG-17, pp. 73-76, Jan. 1981.

Proc. 1988 Applied
Superconductivity Conf.
(IEEE Trans. Magn.
MAG-25, 1989)

SUPERCONDUCTING STRIPLINE RESONATOR PERFORMANCE

B. R. McAvoy, G. R. Wagner, J. D. Adam, and J. Talvacchio*
Westinghouse Research and Development Center
1310 Beulah Rd.
Pittsburgh, PA 15235
and
M. Driscoll
Westinghouse Electronics System Group
Baltimore, MD 21203

Summary

Reliable techniques for evaluating the microwave
operties of superconductors are essential in providing
librated data for exchange between laboratories and for
veloping practical device designs. We are examining the
chniques which utilize microwave stripline resonators.
iese resonators provide for the rapid measurement of
crowave parameters in a repeatable fashion with minimal
nstraints on processing. Sandwiched microstrip line
sonators are used to compare the performance at 4.2°K of
FHC copper and superconducting films of Pb, Nb, and
$Ba_2Cu_3O_7$ (YBCO) at C-band and X-band. Typical results
r the Nb resonators show a loaded Q_L of about 8×10^4
ith a transmission insertion loss of 5 dB at 3 GHz. Initial
sults on a YBCO a-axis film used as a ground plane in
e Nb resonator yield a surface resistance value of about
$^{-3}$ Ω at 2.8 GHz. Preliminary results on the phase noise
rformance of a Nb resonator at 2.9 GHz are presented.

Experimental

ripline Design

The various approaches to planar microwave line
ometry are depicted in Fig. 1., where A and B are
icrostrip configurations, while C and D, with a ground
ane at top and bottom, are referred to as stripline. Slot
e and coplanar line are shown in E and F, respectively.
nfigurations A and B will have lower attainable Q than C
d D due to higher radiation losses. The suspended
bstrate configuration (D) has the advantage that very thin,
gher loss substrates such as $SrTiO_3$ or MgO may be used
to facilitate epitaxial film growth of YBCO for the strip
conductor without causing substantial dielectric loss. A
difficulty with this approach is the means of suspension to
provide for reproducible mechanical positioning and for
vibration immunity. By using sapphire to fill the voids and
a thin buffer layer on which to deposit the YBCO as the
suspended layer, the option is essentially that of
configuration C. Accordingly, we have chosen this option as
the most promising to explore.

An exploded view of the resonator structure is shown in
Fig. 2. A brass mounting block, shown to the right in Fig.
3, receives a sapphire substrate which has a superconducting
ground plane and a superconducting stripline resonator[1] (half
wavelength) pattern on the top surface as shown in Fig. 2.
The spacer or upper substrate has small portions of each
end removed by ultrasonic machining to provide space for
the flat pins of the 3 mm coaxial connectors. Figure 4
shows this feature in detail together with evaporated gold
contact strips along the sides to facilitate ground current
return and subsequent reduction of radiation losses. The
goal of such a design is the achievement of consistent
results with repeated assembly and disassembly.

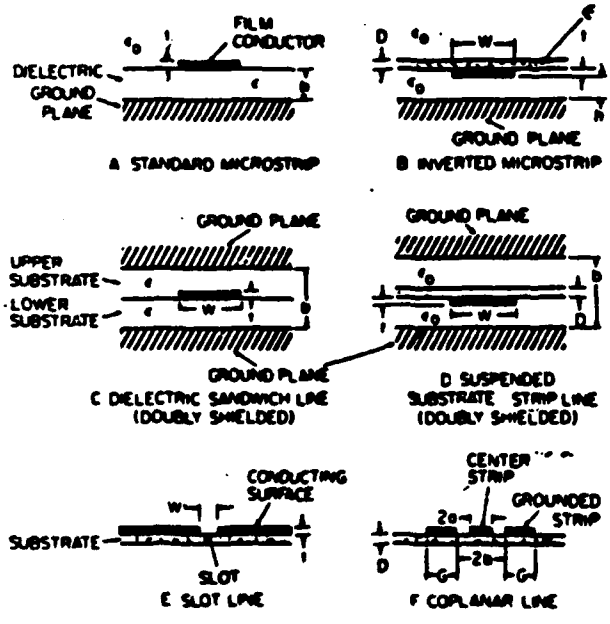

g. 1. Planar microwave line configurations.

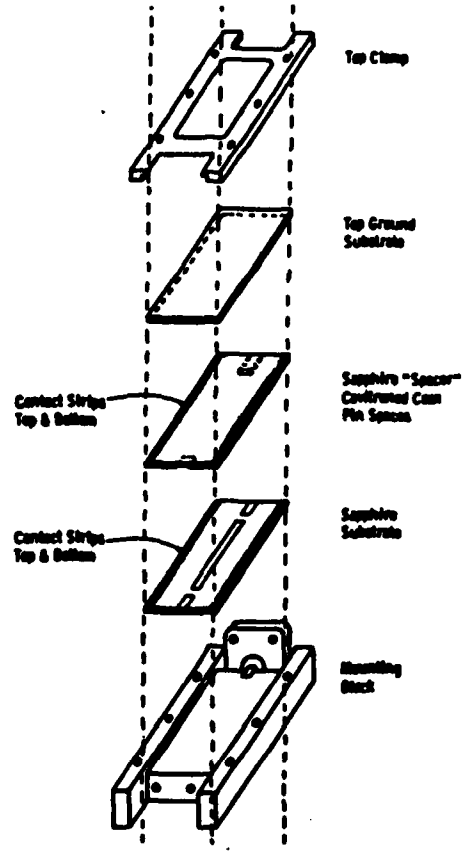

Fig. 2. Dielectric sandwich line (stripline) showing placement of sapphire spacer and top ground substrate.

Supported in part by AFOSR Contract F49620-88-C-0039
anuscript received August 22, 1988.

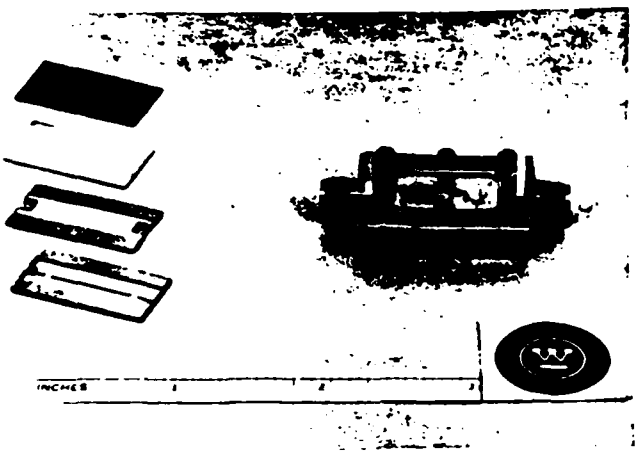

Fig. 3. At left bottom is a Nb stripline resonator with a sapphire spacer above it. At left top is a polished Cu upper ground and a Pb coated Cu plate. Assembled resonator is to the right.

Fig. 4. End of sapphire spacer substrate showing accommodation for rf connecting pins.

The resonator assembly is cooled by immersion in liquid helium. Electrical input and output lines are 3 mm, flexible coaxial cable (Sucoflex 104) for transmission measurements.

Superconductor Film Preparation

The high purity Nb films were deposited epitaxially on sapphire by evaporation in a UHV system[2] which had a background pressure of 10^{-10} torr during deposition. With a substrate temperature during deposition of 700°C, films are produced with a typical residual resistance ratio (RRR) of 50 and some as high as 100. These higher values of RRR are limited by the film thickness.[3] Typical thicknesses are 300 nm. Approximately 100 nm of Au was evaporated on the Nb ground planes without breaking vacuum. This ensures good electrical contact for returning the ground currents. The resonator strips were patterned by reactive ion etching.

The lead films were deposited by evaporation in a separate system and patterned by wet etching.

The YBCO film was deposited[4] by sputtering from three separate metal targets onto a 2.54 x 1.27 cm rectangular substrate of $SrTiO_3$ (100). The film as deposited was amorphous. Following an in-situ oxygen anneal at 500°C, the film was ex-situ annealed in oxygen at 850°C and finally at 400°C. Test samples which were deposited and annealed at the same time showed resistive T_c's (R = 0) of about 65°K.

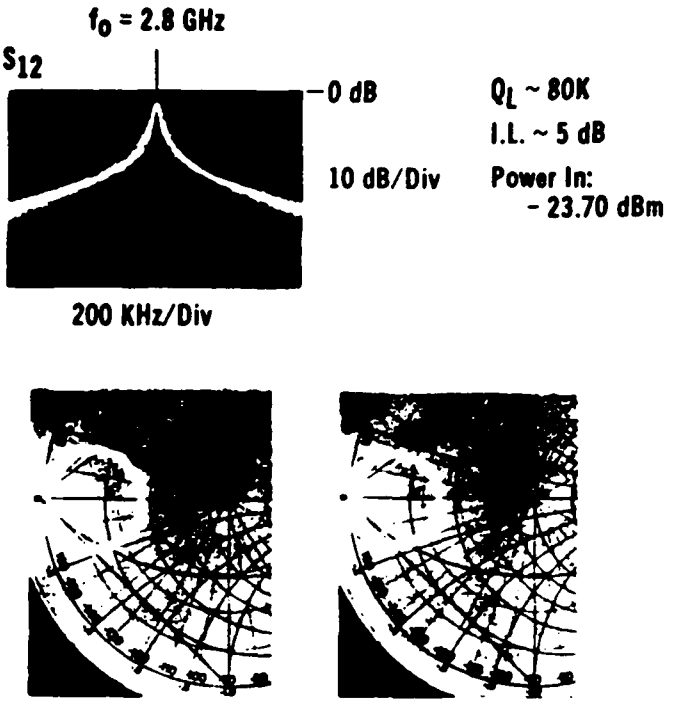

Fig. 5. Network analyzer results for a Nb stripline resonator film on sapphire at 4.2°K.

Experimental Results

Figure 5 shows a typical result for microwave transmission obtained on a network analyzer. Transmission measurements afford an expeditious evaluation of Q_L from the frequency width at the half power points. This, together with an accurate measure of the insertion loss at resonance, provides the unloaded Q_U value.[5] The state of the coupling to the resonator is provided by the reflection measurements (S_{11} and S_{22}).

Figure 6 summarizes the result of a series of measurements. In block No. 1, highly polished OFHC copper is used as the top ground plane. Three runs at the niobium stripline resonant frequency of 2.8 GHz are listed. The data for the four runs in block No. 2 characterize a top ground plane of lead-coated copper used with a niobium stripline resonator. The values of Q_L and Q_U obtained for the different runs in each case are quite consistent. Between each run the resonator was reassembled and the results verify the repeatably with which the resonator can be constructed. Block No. 3 shows the results for a niobium resonator with a niobium film on sapphire forming the top ground plane. The importance of returning the top ground plane current, i.e., sealing, is evident in the factor of nearly two in measured Q's. Block No. 4 shows an all Pb resonator at higher frequency. Block No. 5 shows preliminary results for an a-axis film of YBCO on $SrTiO_3$. The film is clamped against a sapphire spacer in similar fashion to the methods of No. 1 and No. 2.

Preliminary results have been obtained for the noise performance of a Nb resonator of the type shown in block No. 3 of Fig. 6 suspended on a semi-rigid probe in a dewar of liquid helium. The measurements were made with a Hewlett-Packard HP 3048A Phase Noise Test System and an HP 8672 Generator. The results are shown in Fig. 7 where the noise power per unit frequency is plotted as a function of the difference frequency from the carrier. Also shown are the calculated noise level due to FM noise level of the synthesizer and the measured noise level of the amplifier. These must be subtracted from the measured total result to obtain the resonator noise. Below 1 KHz they contribute little. The resonator had $Q_L = 5 \times 10^4$ and IL = 11 dB.

		Q_L (K)	IL (dB)	Q_U* (K)
#1 – Cu WITH MIRROR FINISH	Fo= 2.8GHz			
COPPER / SAPPHIRE / Nb / SAPPHIRE / Nb/Au	RUN 1	11	12	15
	RUN 3	12	16	14
	RUN 2	12	12	14
#2 – LEAD ON COPPER	Fo= 2.8GHz			
COPPER / Pb / SAPPHIRE / Nb / SAPPHIRE / Nb/Au	RUN 1	38	3.2	122
	RUN 2	35	2	175
	RUN 3	38	2.0	190
	RUN 4	38	2.2	170
#3 – Nb/Au ON SAPPHIRE	Fo= 2.8GHz			
Nb/Au / SAPPHIRE / Nb / SAPPHIRE / Nb/Au	UNSEALED	45	6.0	90
	SEALED	77	5.2	177
#4 – Pb/Au ON SAPPHIRE	Fo= 7.6GHz			
Pb/Au / SAPPHIRE / Pb / SAPPHIRE / Pb/Au	RUN 1	27	0.4	590
#5 – YBCO ON $SrTiO_3$	Fo= 2.8GHz			
$SrTiO_3$ / YBCO / SAPPHIRE / Nb / SAPPHIRE / Nb/Au	RUN 1	9.5	10.0	14
	RUN 2	6.6	13.4	9
	RUN 3	12.9	9.8	19
	RUN 4	10.6	9.8	16
	RUN 5	12.8	8.5	21

ig. 6. Summary of Q_L, IL and Q_U values for Nb, Pb and YBCO resonators.

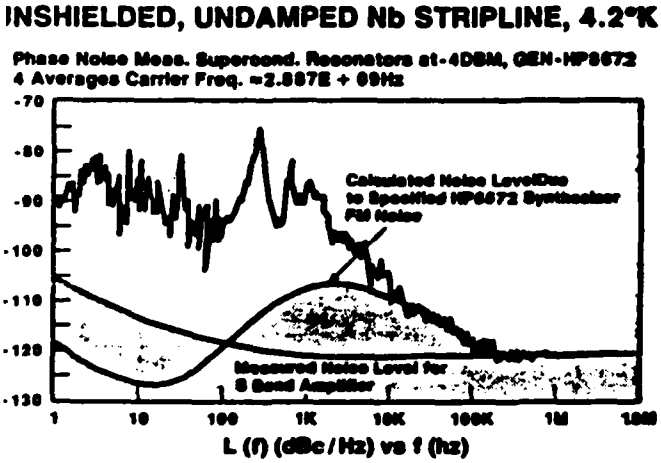

ig. 7. Self noise measurement of Nb stripline resonator at2.9 GHz.

Discussion of Results

To our knowledge, the values of Q_L obtained for the Nb esonators at 2.8 GHz are the highest ever reported.[6] The nportance of proper sealing of the device for ground current eturn and elimination of radiation losses is evident. In ddition, the combination of high vacuum and elevated ubstrate temperature during deposition yields extremely high uality epitaxial Nb films[3] and thus low microwave loss.

The preliminary results on the YBCO film indicate that, s expected from the low T_c, it is not of high quality. A urface resistance value of 10^{-3} Ω is obtained from the Q easurement when compared to that of copper.[7] This is approximately half that reported[7] for polycrystalline films at 3 GHz, but about 100 times higher than reported[8] for a c-axis single crystal at 5.95 GHz. The ex-situ annealing technique is known to produce films with surface degradation.[4] Films produced by our in-situ process have been shown[4] to be superconducting at the surface and will be used in future experiments.

The phase noise measurements indicate that below 1 KHz the noise is comparable to that obtained in acoustic devices where the fundamental frequency of operation (~100 MHz) is multiplied to C-band for radar applications. However, the excessive noise near the carrier seen in Fig. 7 is currently attributed to mechanical vibrations and helium bubbling. Whether it is due to resonator self noise,[9] as in quartz piezoelectric resonators and high overtone bulk acoustic resonators, will be studied in more detail later.

Acknowledgements

The authors are pleased to acknowledge the assistance of Dr. J. X. Przybysz, D. Watt, S. Pieseski, J. Buttyan, and J. C. Brown in the fabrication, H. C. Pohl and R. L. Grassel in the film growth, and G. Draper in the microwave measurements.

References

[1.] A. J. DiNardo, J. G. Smith, and F. R. Arams, J. Appl. Phys. 42, 186 (1971).
[2.] J. Talvacchio, M. A. Janocko, J. R. Gavaler, and A. I. Braginski, Proc. of ICMC, Adv. in Cryogenic Engineering, 32, 527 (1986).
[3.] A. I. Braginski and J. R. Gavaler, Ibid, p. 585.
[4.] J. R. Gavaler, A. I. Braginski, M. G. Forrester, J. Talvacchio, and J. Greggi, paper EB-3, this conference, and references therein.
[5.] L. Ginzton, Microwave Measurements, McGraw-Hill, New York, 1957.
[6.] A. C. Anderson, R. S. Withers, and G. L. Fitch, M. I. T. Lincoln Labs Quarterly Technical Report, Solid State Research, 1985:2
[7.] M. S. Dilorio, A. C. Anderson, and B. Y. Tsaur, Phys. Rev. B, to be publ.
[8.] D. L. Rubin, K. Green, J. Gruschus, J. Kirchgessner, D. Moffat, H. Padamsee, J. Sears, and Q. S. Shu, preprint.
[9.] H. L. Salvo, Jr. et al., 41st Annual Frequency Control Symposium Proceedings, IEEE 87CH2427-3 (1987), p. 388.

Superconductivity Conf.
(IEEE Trans. Magn. MAG-25, 1989)

COMPARISON OF $YBa_2Cu_3O_7$ FILMS GROWN BY SOLID-STATE AND VAPOR-PHASE EPITAXY

J. Talvacchio,* J. R. Gavaler,* J. Greggi,*
M. G. Forrester,** and A. I. Braginski*
Westinghouse R&D Center
Pittsburgh, Pennsylvania 15235

Abstract

Epitaxial films of $YBa_2Cu_3O_7$ (YBCO) have been grown on single-crystal $SrTiO_3$ and MgO substrates by two different routes using rf and dc magnetron co-sputtering. In the first case, amorphous oxide films were deposited at a substrate temperature of 400°C and the crystalline film grew by solid-state epitaxy in an *in-situ* post-anneal at ~850°C. In the second case, a substrate temperature of 600-650°C was used which was sufficient to crystallize the film as it was deposited from the vapor-phase. Reaction with the substrate was less for the films grown by vapor-phase epitaxy – even when they were annealed at 850°C – as shown by the transition temperatures of very thin films, Auger depth profile measurements, *in-situ* XPS analysis and transmission electron microscopy. XPS was used to show that segregation of Ba at the free surface can occur in either type of film. The relative merits of each growth process are discussed for microwave applications and tunnel junction fabrication.

1. Introduction

The formation of all vapor-deposited YBCO thin films can be categorized as either a reaction of solid-state precursors or direct condensation from the vapor phase into the perovskite-related structure (tetragonal or orthorhombic) of $YBa_2Cu_3O_{7-x}$. The former category currently includes all techniques in which a substrate temperature, T_s, ≤400°C is used, the source of Ba is BaF_2,[1] layered structures of Y, Ba, Cu (or their oxides) are deposited,[2] or a solution of nitrates or metallorganic precursor compounds are dried on a substrate.[3,4] As-deposited crystalline films can be produced if sufficient oxygen – or sufficiently active oxygen – is available during deposition to be incorporated into the film. Most as-deposited crystalline films have been prepared by magnetron or diode sputtering and the necessary deposition conditions will be examined as part of this work (Table 1). However, co-evaporation,[5-7] laser ablation,[8,9] plasma spraying,[10] and ion-beam sputtering[11] have also been used successfully to grow such films.

This paper will discuss film properties that affect microwave applications and tunnel-junction development of high-transition-temperature (T_c) superconductors. The important length scale for microwave applications is the magnetic penetration depth, λ. For $T<<T_c$, λ_{ab}(parallel to Cu-O planes) ≃ 27 nm and λ_c ≃ 180 nm.[12] For tunneling, the important length scale is the coherence length: ξ_{ab} ≃ 3.1 nm, ξ_c ≃ 0.4 nm.[12] These length scales define the thickness of the layer of superconductor adjacent to the film's free surface and the interface with the substrate which must have optimized superconducting properties.

Some film deposition techniques appear to be inappropriate for these applications. For example, all solution-deposited films produced to date have low critical current densities. Films reacted in the solid state from layered structures, fluorides, or an amorphous metal undergo a volume change during reaction that leads to rough surfaces. Therefore, the films reported here in which YBCO is formed in a solid-state reaction were deposited as amorphous oxides.

Specific film properties which will be compared are: reaction with the substrate and composition of the film adjacent to the substrate, microstructure and surface roughness, surface composition, and dc resistivity.

2. Fabrication of YBCO Films

All films were deposited by magnetron sputtering in an apparatus described elsewhere.[13] Briefly, Y, Ba, and Cu were deposited from metallic targets in an Ar/O_2 atmosphere in sub-monolayer layers onto a substrate holder which oscillated to face the targets in sequence at 8 cycles/min. Argon was introduced to the chamber from the dark-space shield of the Ba sputter gun and oxygen was introduced at the substrates. The deposition rates at three vibrating crystal rate monitors were fed back to the sputtering power supplies to control composition much more reproducibly than possible with constant sputtering power. The composition was uniform across a 2-inch diameter substrate holder within the precision of electron microprobe measurements. Samples were generally annealed *in-situ* – that is, without exposure to air – in an O_2 atmosphere.[14] *Ex-situ* anneals were used for some films when surface-sensitive properties were not being measured.

Several deposition parameters were set differently for the two alternative fabrication routes. The most important, the substrate temperature, T_s, was 400°C for amorphous film growth and 600-650°C for crystalline films. The Cu deposition rate had to be increased by 80% to maintain stoichiometry in the films deposited at higher T_s. Deposition rates were a sensitive function of oxygen partial pressure for more than 0.3 mtorr O_2, so a lower oxygen pressure – usually 0.03 mtorr – was used for amorphous film growth. For crystalline growth, the highest practical oxygen pressure was used. Before sputtering, the oxygen pressure was set to ~0.6 mtorr. During sputtering, the pressure could be increased to ~3 mtorr. At higher pressures, the surface of the Ba target oxidized, indicated by a change in the plasma color from green to purple. The Ba deposition rate decreased dramatically, and indications appeared of oxygen ion sputtering of the substrate holder.[15] Ion sputtering of the substrate holder was always present to some degree and all holders were pre-coated with YBCO to prevent contamination of the films by molybdenum from screws and clamps.

As-deposited amorphous films were annealed 30 min to 1 hr at 850°C and 30 min-1 hr at 400°C. As-deposited crystalline films grown on (1120) sapphire were identified as having a tetragonal structure by the relative intensities of (013), (103), and (110) x-ray diffraction peaks. Films grown on $SrTiO_3$(100) or MgO(100) substrates were always sufficiently textured that x-ray diffraction could not distinguish between tetragonal and orthorhombic structures. A mixture of the two structures was most likely obtained. Although as-deposited films were not superconducting, their room-temperature resistivity was as low as 2 mΩ-cm.[16]

Table 1 is a summary of the deposition conditions used by a number of researchers who have obtained as-deposited crystalline films by sputtering. The significance of this table is that it shows a lack of consensus regarding target composition and placement, and sputter-gas pressures. The common deposition conditions are rather trivial: T_s ≃ 550-700°C, oxygen must be added to the sputter gas (in addition to oxygen from the target), and non-stoichiometric targets must have extra Cu to compensate for re-sputtering effects. The critical deposition issues are often not addressed. In particular, the effects of target-to-substrate distance should be reported since it determines the extent of re-sputtering of the film surface. The severity of this problem for planar sputtering geometries can be inferred from

* Supported in part by AFOSR Contract F49620-88-C-0039.
** Supported by AFOSR Contract F49620-88-C-0030.
Manuscript received August 22, 1988.

the references in Table 1 in which substrates are placed perpendicular to the target. Our own experience with a single $YBa_2Cu_3O_7$ target in a planar geometry is that re-sputtering of the substrates and substrate holder contaminated our films even without O_2 added to the sputtering gas for an Ar pressure in the range of 5 to 100 mtorr.

A lack of consensus is also apparent in Table 1 for the annealing temperature needed to transform tetragonal films to the orthorhombic structure. Part of the disparity can be attributed to the facts that T_c measurements can be dominated by a minority phase and the tetragonal and orthorhombic structures cannot be distinguished in standard "2θ" x-ray diffraction scans on textured films. Our highest T_c's were obtained from films post-annealed in an O_2 atmosphere at 850°C.

3. Electrical Properties – Ultrathin Films

Examples of resistivity plotted as a function of temperature are shown in Fig. 1 for two of our YBCO films. Important differences in the temperature dependence of resistivity of amorphous and crystalline as-deposited films were evident in very thin films. Crystallized amorphous films 100 nm thick were semiconducting. Data presented in Sec. 4 and documented in many other reports show that there is significant reaction and interdiffusion between the film and substrate. However, as-deposited crystalline films 100 nm thick were superconducting after a post-anneal and had positive temperature coefficients of resistivity for $T>T_c$ – even for films annealed at 850°C. Films 100 nm thick deposited on MgO(100) also had T_c (zero resistance) = 30-35K. The T_c's of 100 nm thick films are slightly higher but in reasonable agreement with the T_c's of films deposited at 600-650°C reported in references 17, 18, and 19, but much lower than values obtained in ultrathin films by Bando et al.[6] Epitaxial growth of YBCO at a substrate temperature of 630°C is shown in the RHEED patterns of Fig. 2 to be clearly established at a film thickness of 10 nm. *In-situ* annealed 10 nm thick films deposited at 400°C, did not exhibit a RHEED pattern. XPS measurements of the 10 nm solid-state epitaxial films showed that the major source of contamination was Ti diffusion from the substrate.

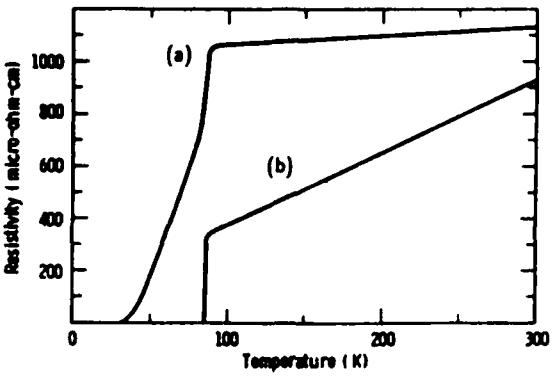

Fig. 1 - Resistivity versus temperature for (a) a 100 nm thick film which was crystalline as-deposited, and (b) a 500 nm thick film which was amorphous as-deposited. Both films were annealed in an O_2 atmosphere at 850°C for 1 hr.

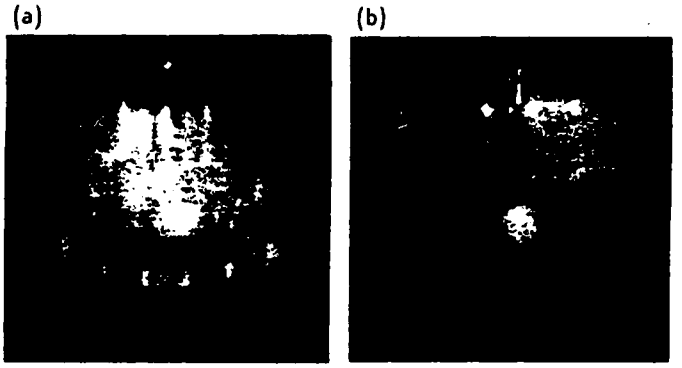

Fig. 2 - 9 kV RHEED patterns from (a) a $SrTiO_3$(100) substrate at a [011] azimuth, and (b) a 10 nm thick film deposited at 630°C. Extra spots in (b) are similar to spots obtained from the 2x2 reconstruction of $SrTiO_3$(100), but relative Y_{3d}, Ba_{3d}, Cu_{2p}, Ti_{2p}, and Sr_{3d} photoelectron counts confirmed that the film was ≃10 nm thick.

Table 1. Fabrication of as-deposited crystalline YBCO films by sputtering.

First Author (Laboratory)	Sputtering Technique	Targets (Composition)	Ar / O_2 (mtorr)	T_s (°C)	Distance (cm)	Rate (nm/min)	Thickness (microns)	Substrates	As-deposited Structure, T_c	T_{anneal} T_c (K)
This work	2 rf, 1 dc magn.	Y,Ba,Cu	20/3	600-630	11	3-4.5	0.1-0.8	$SrTiO_3$	tetragonal	850°C, 80K
Miura (Toshiba)[20]	rf magnetron	Y,Ba_2CuO_3,Cu	2.5/2.5	560	-	2.2	0.4	$SrTiO_3$	80K	
Hirochi (Matsushita)[18]	rf magnetron	ErBCO=1:2:4.5:x	1.5/1.5	650	2.5-3.5	4-8	1.0	Al_2O_3	80K	
Itozaki (Sumitomo)[21]	rf magnetron	HoBCO=1:2.2:3.4	80%/20%	600	-	2-5	0.7	MgO	tetragonal	920°C, 84K
Myoren (Hiroshima)[22]	rf magnetron	YBCO=1:2:3:7	2-12/3-18	600-700	7.5	2	0.1-0.3	Si/ZrO_2	tetragonal	700°C, 82K
Michikami (NTT)[23]	rf magnetron	YBCO=1:6:10:x	10/10	580	-	5	0.2-0.5	Al_2O_3	40K	
Tsuda (Fuji Elec.)[24]	rf magnetron	YBCO=1:2.6:6:x	37/37	650	-	3.3	0.4	MgO	tetragonal	930°C, 80K
Tonouchi (Osaka U.)[25]	rf magnetron	YBCO=1:3:9:x	18/12	670	-	12	0.7	$SrTiO_3$, MgO	20	900°C, 80K
Takagi (Hitachi)[26]	rf magnetron	YBCO=1:2:3:7	-/-	750	-	-	-	$SrTiO_3$	50	800°C, 80K
Sandstrom (IBM)[27]	rf magnetron	YBCO=1.06:1.86:3[a]	6/0.1	640-650	(90°)	7-10	0.4	MgO	74K	
Lee (IBM)[28]	dc magnetron	YBCO=1:2:3:7[b]	4/0.4	650	-	4	2.0	Si	76K	
Li (Karlsruhe)[29]	dc magnetron	YBCO=1:2:3:7[c]	400/200	770	-	30	1.5	Al_2O_3	tetragonal	430°C, 83K
Matsuda (U. Hokkaido)[30]	rf diode	YBCO=1:6:18:x	--/60%	650	2.5	3	0.7	Al_2O_3 $SrTiO_3$	-	650°C, 72K
Terada (ETL)[31]	rf diode	YBCO=1:2:3:x[a]	30/30	580	(90°)	-	0.4	MgO, $SrTiO_3$	82K	
Yamamoto (Nihon U.)[32]	rf diode	Y_2O_3,BaO,Cu	80/20	550	2.5	0.03	0.2	MgO	tetragonal	-
Poppe (Julich)[33]	dc diode	YBCO=1:2:3:7[c]	0/2500	670	-	6	0.1-0.5	$SrTiO_3$	81K	
Kawasaki (U. Tokyo)[34]	dc diode	(2)YbBCO=1:2:3:x[a]	150/17	640	(90°)	1.6	0.5	YSZ	66K	
Lin (ITRI)[35]	dc diode	YBCO=1:2:3:x	500/-	370	2	12	0.8	Si	-	270°C, 56K

[a] Substrates perpendicular to target.
[b] Bias sputtering.
[c] Sputtering from inside edge of annular target.

4. Film/Substrate Reaction

The reaction between $SrTiO_3$ substrates and YBCO films ıs studied by Auger spectroscopy depth profiles. Figure a) is a profile of an as-deposited amorphous film after ınealing at 850°C. The ~100 nm thick BaO layer which rmed at the interface was also observed in a TEM ıalysis. The TEM analysis showed that the BaO layer ınsisted of randomly-oriented and equi-axed crystalline ains. The presence of this disordered layer apparently did ɔt interfere with the nucleation of an epitaxial film (Sec. 5) ıring solid-state crystallization, so we speculate that the Ba ıgregation to the interface must have occurred after the BCO crystalline structure formed. The data in Fig. 3(a) e nearly identical to Auger depth profiles reported by Wu al. for annealed YBCO films which had been amorphous ı-deposited by laser ablation.[36] The thickness of the ansition layer between the part of the film with Y:Ba:Cu = 2:3 and the BaO interface layer is comparable to the agnetic penetration depth. For microwave applications, the sses in this transition layer and dielectric losses in the aO layer are expected to be very high. Considerations of electric losses also mandate that MgO substrates should be ɜed rather than $SrTiO_3$.[37]

Figure 3(b) shows that the film/substrate interface is ıuch sharper for a YBCO film deposited at 600°C and ınnealed at 850°C. A ratio, Y:Ba:Cu ≃ 1:2:3 is maintained ıroughout the film. We have obtained similar depth profile ata (not shown) for films grown on MgO at 600°C and ost-annealed at 850°C. Wu et al. showed a similar result ɔr laser-ablated films which were crystalline as-deposited on rTiO3.[8]

5. Microstructure

X-ray diffractometer data from YBCO films crystallized ɔm the vapor phase or from an amorphous oxide indicated hat the film texture was the same for either fabrication ɔute. Most grains in the films were oriented with the a-xis, [100], parallel to the growth direction and a smaller mount of c-axis, [001], growth. Figs. 4(a) and (b) show ypical results for "a>c" growth, and exclusively a-axis rowth, respectively. The highest critical current densities, J_c, are obtained for c-axis growth.[12] The highest J_c's

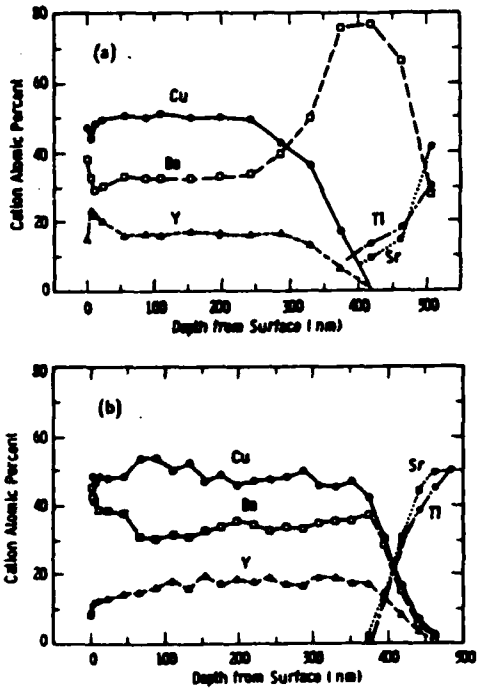

ig. 3 Auger spectroscopy depth profiles for YBCO films annealed at 850°C: (a) amorphous as-deposited, and (b) crystalline as-deposited.

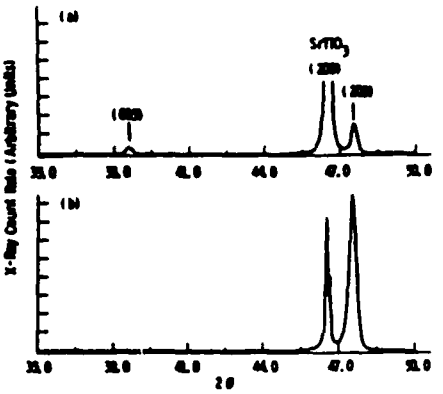

Fig. 4 - Portions of x-ray diffractometer scans showing (a) predominantly a-axis growth, and (b) exclusively a-axis growth.

measured in these predominantly a-axis films were 5×10^5 A/cm^2 at 4.2K and 2×10^4 at 77K. However, for planar tunneling, a-axis growth is clearly preferable to have the benefit of a longer coherence length. For microwave applications, it is not clear which orientation is better. Preliminary measurements published in Ref. 38 found lower surface resistances in c-axis films. Surface resistance measurements of our films are reported in Ref. 39.

The x-ray diffractometer scans shown in Fig. 4 only identified growth *texture*. TEM data showed that the films were both polycrystalline and epitaxial. That is, a mosaic structure formed in which (almost) all grains were oriented with respect to the $SrTiO_3$(100) substrate, but the c-axes of individual grains could lie parallel to [010] or [001] directions in the $SrTiO_3$.

Figure 5 contains two TEM micrographs which show that the mosaic structure was common to both solid-state and vapor-phase epitaxial growth. Differences were observed in grain size and shape. Films crystallized in the solid state had roughly equiaxial grains 0.5 to 1.0 μm wide. The grains in as-deposited crystalline films had an aspect ratio of ~4:1 with a 0.5 μm longer edge and the c axis parallel to the shorter edge. Figure 5(b) shows an example, found in both types of films, of a grain oriented 45° away from the others.

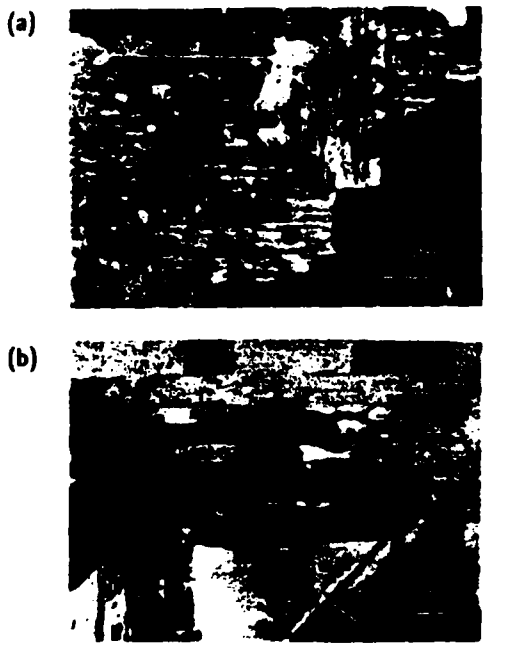

Fig. 5 - TEM micrographs showing characteristic grain sizes, shapes, and orientation for post-annealed films which had been crystallized (a) from an amorphous oxide, and (b) during deposition.

6. Surface Composition and Structure

It is well known that exposure to air will degrade the surface of YBCO to a depth greater than the coherence length - the critical length for tunneling. We have shown in an earlier publication that the surface is degraded during crystallization of an amorphous film – even for completely *in-situ* processing – by segregation of Ba to the surface.[40] The same phenomenon has since been observed for films deposited at 600-650°C during post-annealing in O_2 at 600°C. Barium segregation can be avoided by using a rapid-ramp anneal.[40] The segregation appears to be driven by oxygen deficiency. In as-deposited crystalline films, either the oxygen-deficiency of the tetragonal structure or the presence of some amorphous oxide must be invoked to explain the segregation.

Surface morphology is also important for fabrication of planar tunnel junctions. Films grown by solid-state epitaxy had smoother surfaces - usually featureless at 10^5 magnification in an SEM. The surfaces of as-deposited crystalline films 0.5 μm thick had a dense "basket-weave" appearance with feature sizes and orientations which were the same as observed by TEM. Local variations in film thickness due to this structure were approximately 100 nm.

Conclusions

As-deposited crystalline films clearly form better film/substrate interfaces than films crystallized in the solid state, and are the better fabrication alternative for thin-film microwave applications. The improved interfaces with the substrate are related to the chemical stability of the crystalline phase and not simply due to reduced processing temperatures. Either fabrication alternative could be used as base electrodes for high-T_c tunnel-junction development, although crystallized amorphous films are smoother. Only general and rather trivial deposition conditions needed for growing crystalline YBCO films can be specified at this time.

Acknowledgments

The authors acknowledge the assistance of H. C. Pohl, A. M. Stewart, R. F. Farich, D. Detar, T. Mullen, and R. T. Blackham.

References

1. P. M. Mankiewich, J. H. Scofield, W. J. Skocpol, R. E. Howard, A. H. Dayem and E. Good, Appl. Phys. Lett. 51, 1751 (1987).
2. C.-A. Chang, C. C. Tsuei, C. C. Chi, and T. R. McGuire, Appl. Phys. Lett. 52, 72-74 (1987).
3. S. A. Kramer, G. Kordas, J. McMillan, G. C. Hilton, and D. J. Van Harligen, Appl. Phys. Lett. 53, 156 (1988).
4. R. L. Henry, H. Lessoff, E. M. Swiggard, and S. B. Qadri, J. Cryst. Growth 85, 615-618 (1987).
5. D. K. Lathrop, S. E. Russek, and R. A. Buhrman, Appl. Phys. Lett. 51, 1554-1556 (1987).
6. Y. Bando, T. Terashima, K. Iijima, K. Yamamoto, K. Hirata, and H. Mazaki, Proc. 5th Intl. Workshop on Future Electron Devices (Miyagi-Zao, 1988), p. 11.
7. R. M. Silver, A. B. Berezin, M. Wendman, and A. L. de Lozanne, Appl. Phys. Lett. 52, 2174 (1988).
8. X. D. Wu, A. Inam, T. Venkatesan, C. C. Chang, E. W. Chase, P. Barboux, J. M. Tarascon, and B. Wilkens, Appl. Phys. Lett. 52, 754-756 (1988).
9. S. Witanachchi, H. S. Kwok, X. W. Wang, and D. T. Shaw, Appl. Phys. Lett. 53, 234-236 (1988).
10. K. Terashima, K. Eguchi, T. Yoshida, and K. Akashi, Appl. Phys. Lett. 52, 1274 (1988).
11. T. Yotsuya, Y. Suzuki, S. Ogawa, H. Kuwahara, K. Otani, T. Emoto, and J. Yamamoto, Proc. 5th Intl. Workshop on Future Electron Devices (Miyagi-Zao, 1988), p. 57.
12. W. J. Gallagher, J. Appl. Phys. 63, 4216 (1988).
13. R. M. Silver, J. Talvacchio, and A. L. de Lozanne, Appl. Phys. Lett. 51, 2149 (1987).
14. A. I. Braginski, J. Talvacchio, J. R. Gavaler, M. G. Forrester, and M. A. Janocko, to appear in SPIE Proc. Vol. 948, High-T$_c$ Superconductivity: Thin Films and Devices (SPIE, Bellingham, Washington, 1988).
15. S. M. Rossnagel, and J. J. Cuomo, AIP Conf. Proc. No. 165, 106-113 (1988).
16. R. J. Cava, B. Batlogg, C. H. Chen, E. A. Rietman, S. M. Zahurak, and D. Werder, Phys. Rev. B 36, 5719 (1987).
17. H. Akoh, F. Shinoki, M. Takahashi, and S. Takada, Appl. Phys. Lett. 52, 1732 (1988).
18. K. Hirochi, H. Adachi, K. Setsune, O. Yamazaki, and K. Wasa, Jpn. J. Appl. Phys. 26, L1837-L1838 (1987).
19. T. Murakami, Y. Enomoto, and M. Suzuki, Physica C 153-155, 1690 (1988).
20. T. Miura, Y. Terashima, M. Sagoi, and K. Kubo, Proc. 5th Intl. Workshop on Future Electron Devices (Miyagi-Zao, 1988), p. 75.
21. H. Itozaki, S. Tanaka, K. Harada, K. Higaki, N. Fujimori, and S. Yazu, Proc. 5th Intl. Workshop on Future Electron Devices (Miyagi-Zao, 1988), p. 149.
22. H. Myoren, Y. Nishiyama, H. Nasu, T. Imura, Y. Osaka, and H. Fukumoto, Proc. 5th Intl. Workshop on Future Electron Devices (Miyagi-Zao, 1988), p. 31.
23. O. Michikami, H. Asano, Y. Katoh, S. Kubo, and K. Tanabe, Jpn. J. Appl. Phys. 26, L1199-L1201 (1987).
24. K. Tsuda, M. Muroi, T. Matsui, Y. Koinuma, M. Nagano, and K. Mukae, Physica C 153-155, 788 (1988).
25. M. Tonouchi, Y. Yoshizako, M. Iyori, and T. Kobayashi, Proc. 5th Intl. Workshop on Future Electron Devices (Miyagi-Zao, 1988), p. 68.
26. K. Takagi, M. Hirao, M. Hiratani, H. Kakibayashi, T. Aida, and S. Takayama, in MRS Vol. 99: High Temperature Superconductors (Matls. Res. Soc., Pittsburgh, 1988), pp. 647-650.
27. R. L. Sandstrom, W. J. Gallagher, T. R. Dinger, R. H. Koch, R. B. Laibowitz, A. W. Kleinsasser, R. J. Gambino, B. Bumble, and M. F. Chisholm, Appl. Phys. Lett. 53, 444 (1988).
28. W. Y. Lee, J. Salem, V. Lee, T. Huang, R. Savoy, V. Deline, and J. Duran, Appl. Phys. Lett. 52, 2263 (1988).
29. H. C. Li, G. Linker, F. Ratzel, R. Smithey, and J. Geerk, Appl. Phys. Lett. 52, 1098 (1988).
30. M. Matsuda, A. Matachi, and S. Kuriki, 5th Intl. Workshop on Future Electron Devices (Miyagi-Zao, 1988), p. 287.
31. N. Terada, H. Ihara, M. Jo, M. Hirabayashi, Y. Kimura, K. Matsutani, K. Hirata, E. Ohno, R. Sugise, and F. Kawashima, Jpn. J. Appl. Phys. 27, L639 (1988).
32. H. Yamamoto, Y. Morikawa, H. Okukawa, and M. Tanaka, Proc. 5th Intl. Workshop on Future Electron Devices (Miyagi-Zao, 1988), p. 105.
33. U. Poppe, J. Schubert, R. R. Arons, W. Evers, C. H. Freiburg, W. Reichert, K. Schmidt, W. Sybertz, and K. Urban, Solid State Commun. 66, 661 (1988).
34. M. Kawasaki, S. Nagata, Y. Sato, M. Funabashi, T. Hasegawa, K. Kishio, K. Kitazawa, K. Fueki, and H. Koinuma, Jpn. J. Appl. Phys. 26,L738-L740 (1987).
35. R. J. Lin, J. H. Kung, and P. T. Wu, Physica C 153-155, 796-797 (1988).
36. X. D. Wu, D. Dijkkamp, S. B. Ogale, A. Inam, E. W. Chase, P. F. Miceli, C. C. Chang, J. M. Tarascon, and T. Venkatesan, Appl. Phys. Lett. 51, 861 (1987).
37. A. I. Braginski, M. G. Forrester, J. Talvacchio, and G. R. Wagner, Proc. 5th Intl. Workshop on Future Electron Devices (Miyagi-Zao, Japan 1988), pp. 171-179.
38. J. P. Carini, A. M. Awasthi, W. Beyermann, G. Gruner, T. Hylton, K. Char, M. R. Beasley, and A. Kapitulnik, Phys. Rev. B 37, 9726 (1988).
39. B. R. McAvoy, J. D. Adam, and G. R. Wagner, "Superconductor Stripline Resonator Performance," this volume.
40. J. R. Gavaler, and A. I. Braginski, Physica C 153-155, 1435 (1988).

Proc. 1988 Applied
Superconductivity Conf.
(IEEE Trans. Magn.
MAG-25, 1989)

OPTIMIZATION OF YBCO SURFACES FOR TUNNEL JUNCTIONS*

J. R. Gavaler, A. I. Braginski, M. G. Forrester,
J. Talvacchio, and J. Greggi
Westinghouse R&D Center
1310 Beulah Road
Pittsburgh, Pennsylvania 15235

Abstract

We have established that in $YBa_2Cu_3O_7$ films, pared by annealing amorphous oxide deposits, Ba regation in the amorphous phase and YBCO omposition after crystallisation are the major ses of surface degradation. We have grown films, by irely in-situ processing, in which these effects are imised. These films were epitaxially grown on (100) iO_3 substrates with the a-axis normal to the film ne. Both structural and chemical analyses indicated t they were homogeneous and have proper ichiometry up to their surfaces. At 4.2K, contact istivities below 4×10^{-10} ohm-cm^2 were obtained h gold overlayers. Junctions have been formed by positing thin Au proximity layers over the YBCO films lowed by MgO barriers and Nb counterelectrodes. In ie of the junctions weak-link shorts were observed viding unambiguous evidence that the growth cedures used can produce films that are erconducting up to their surfaces.

Introduction

One of the more important potential applications r the new high-T_c oxide superconductors is in nneling devices. For any practical tunneling device e superconductor must be prepared in thin film form. reported in the voluminous literature on the oxide perconductors, the capability for depositing these terials as thin films with T_c's close to that of the lk is already well developed. It is well recognised, wever, that obtaining a high critical temperature in film does not necessarily insure its usefulness in a nnel junction. The electrons which can tunnel are ly those which are within a distance from the surface proximately equal to the coherence length. This fact aces very stringent demands on the near-surface ality of a thin film to be used for tunneling. In $a_2Cu_3O_7$ (YBCO) for example, depending on orientation, e coherence length is either 0.4 nm (normal to the axis) or 2-3 nm (parallel to the c-axis).[1] Thus for YBCO film to be useful for tunneling it must retain s superconducting properties to within these stances from the surface.

There have been a wide variety of techniques ported for depositing YBCO films. One of the iginal methods involves the deposition of an orphous film which is then annealed in oxygen to form e orthorhombic "1:2:3" structure compound. Although ere are many workers who have used this method to epare YBCO films there are, as of this writing, no ports of the successful use of one of these films as electrode in a tunnel junction. Undoubtedly one of e reasons for this is the difficulties encountered in eparing films which have the required near-surface operties. We have been investigating this growth thod to determine whether it can ever be optimised fficiently to permit the growth of films which would usable in tunnel junctions. In this paper we mmarise the results of these studies.

pported in part by AFOSR Contract No.
49620-88-C-0039.
nuscript received August 22, 1988.

Experimental Procedure

The films were sputtered in a UHV deposition and analytical facility which has been described previously.[2] The specific apparatus and procedures have also been reported.[3] The films were deposited from three elemental targets at a substrate temperature of 400°C. The Ba and Y were sputtered with rf magnetron guns and the copper with a dc magnetron gun. During sputtering the total argon-oxygen sputtering gas pressure was kept at 3 Pa. The partial pressure of the oxygen was 4×10^{-4} Pa. The sputter guns are mounted along a 180°C arc and point to the center of the chamber. During deposition the substrate holder, mounted on a manipulator in the center of the chamber, is rotated back and forth to face the three guns sequentially. The time in front of each gun is less than required to deposit one monolayer. The total deposition rate was 3 nm/min and film thickness, 350 nm. All of the films were deposited on single crystal (100) $SrTiO_3$.

Following deposition the films were annealed using either one of two procedures. Our early films were first annealed in-situ for 20 minutes at 500°C. They were then removed from the system and annealed in a quartz tube at a maximum temperature of 850°C for one hour. In both cases the annealing was done in one atmosphere of oxygen. After the 850°C anneal the films were cooled to room temperature at 5°C/min. The intermediate 500°C in-situ anneal was instituted because of the reactivity of the as-deposited films with room air. This anneal was found to be sufficient to stabilize the surfaces of the films so they could be safely removed from the system without any discernible (by XPS) reaction with the water or carbon dioxide in the air.

The ex-situ anneal was required because our in-situ annealing apparatus initially was not capable of operating at temperatures as high as 850°C in one atmosphere of oxygen. After the necessary modifications were made to allow this type of operation, all films were annealed entirely in-situ at various temperatures up to 950°C for, typically, 20 minutes. This annealing was done using a platinum wire heater located immediately behind the substrate holder and a bank of five 0.5 kW quartz lamps which was situated approximately 2 cm from the films during the annealing. After the high-temperature anneal the films were held at 600°C for approximately 30 minutes and then allowed to cool to room temperature. The in-situ cooling rate was high, of the order of 25°C/min. The film temperature was determined by clamping a thermocouple to the substrate surface. The reading from this thermocouple was correlated to the reading from a second thermocouple located inside the substrate holder. During the actual film processing, only the latter thermocouple was used. Structural analyses of the films were made by in-situ reflection high energy electron diffraction (RHEED), X-ray diffraction, transmission electron microscopy (TEM), and by scanning electron microscopy (SEM). Chemical analyses were by in-situ X-ray photoelectron spectroscopy (XPS), and Auger Electron spectroscopy, and energy dispersive X-ray spectroscopy (EDS). Critical temperatures were measured resistively by the standard four-point van der Pauw method.

Results and Discussion

All of the films sputtered under the conditions described were amorphous as-deposited. We will discuss here only those films which, based on EDS and XPS analyses, had the proper 1-2-3 ratio of metallic elements. When these were annealed using either of the two annealing procedures, X-ray analyses showed that the orthorhombic structure had formed and that it had grown epitaxially on the (100) substrates with the a-axis normal to the substrate surface. The T_c onsets of these films were 88-90°C and they became completely superconducting between 80 and 85°C.

We have previously reported on the near-surface degradation of films, prepared by this technique, which was due to the diffusion of Ba toward the surface during annealing before the films reached the crystallization temperature.[4] This was documented by XPS data showing non-stoichiometric compositions near surfaces of amorphous films which had been heated to 500°C. To obtain more information on the distribution of the 1:2:3 phase in these films, a TEM study was done as a function of thickness. Three regions of a representative film are shown in Figure 1: (a) a region immediately below the surface, (b) at a depth of approximately 50 nm from the surface, and (c) in the center of the 350 nm film. As indicated in Figure 1(c), the center portion of the film contains single phase YBCO. The TEM analysis shows that the 1:2:3 phase in the film grew epitaxially on the $SrTiO_3$ substrate with the a-axis normal to the film surface in a "checkerboard" type microstructure. This type of epitaxial growth has been discussed previously.[5] The TEM analysis also shows that as one moves away from the center of the film the quality deteriorates. This is illustrated by the other two photographs in this figure. At approximately 50 nm from the film surface (b), there is clear evidence of polycrystalline second phase (2:1:1) growth interspersed among the YBCO. In the near-surface region (a) the 1:2:3 phase has completely disappeared and only the polycrystalline 2:1:1 material remains. These TEM data indicate that the surface quality of the film would make it useless for any tunnel junction application. Tunnel junctions which had been made with this type of film were in fact found to be ohmic even when no barrier layer was deposited. The only positive aspect of this film with respect to tunneling is its a-type epitaxy. Because the c-axis is parallel to the film surface, the coherence length normal to the surface is the larger of the two possible values.

Following the necessary modifications to the annealing apparatus, all films were processed entirely in-situ. We had already established that at least part of the near-surface degradation occurred because of Ba segregation during the annealing process prior to the crystallization of the 1:2:3 phase. Therefore to minimize this Ba diffusion, the temperature was ramped to 850°C as quickly as possible, at rates of up to 10°C/min.

To try to gain some insight into the cause of the formation of the 2:1:1 phase on the film surface [Figure 1(a)], a series of films were annealed at temperature between 800 and 950°C. We found that anneals done only 20-30°C lower than our 850°C standard produced films with high resistivities and degraded T_c's. This was due to an incomplete crystallisation of the 1:2:3 phase. However annealing at temperatures above 850°C also produced a deleterious effect on the quality of the films. Figure 2 shows SEM photographs of a film which was annealed at 900°C for 20 min. It can be seen that at this temperature copper has precipitated on the surface leaving behind a material which, from EDS analysis, has the 2:1:1 composition. This result shows that at a temperature not far removed from the minimum usable crystallization temperature, 1:2:3 phase decomposition occurs. Since a temperature not significantly less than 850°C is required to crystallize YBCO from the amorphous phase (at least in the time scale discussed here), it appears that only a very narrow temperature window can be used which will not result in surface degradation of the YBCO films. That such a window exists is demonstrated by electrical measurements made on films processed under our optimum conditions. Contact resistance between a gold overlayer and YBCO was measured to be less than 4×10^{-10} ohm-cm^2 which is the sensitivity limit of the apparatus. This is about six orders of magnitude lower than the value obtained with earlier films.

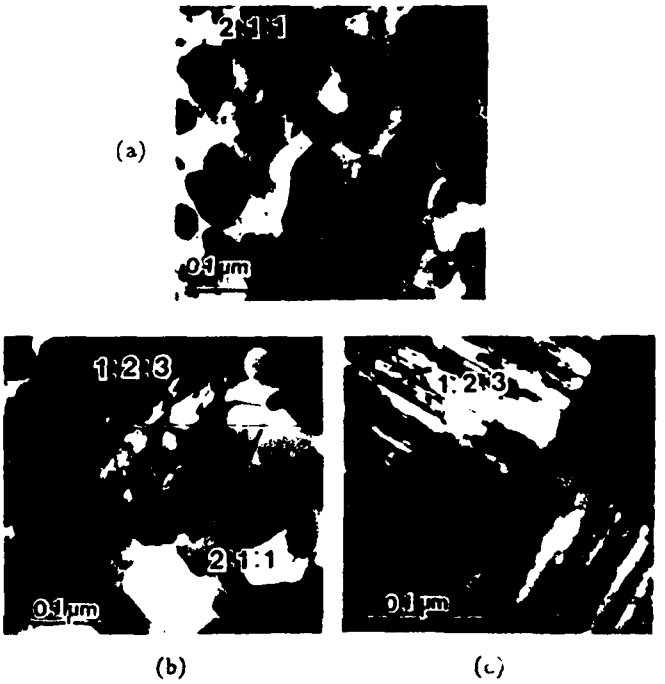

Figure 1. Photomicrographs of three regions of a YBCO film: (a) immediately below the surface, (b) at a depth of approximately nm from the surface, and (c) in the center of the film.

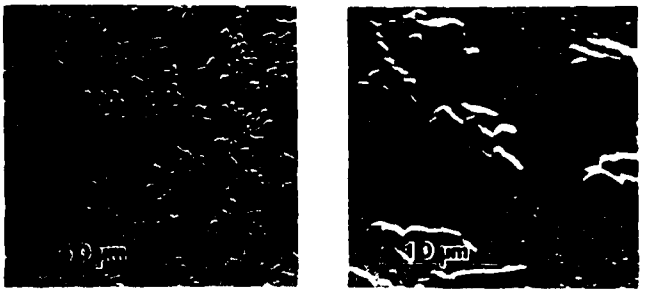

Figure 2. SEM pictures of the surface of a film which had been annealed at 900°C for 20 minutes.

We have made tunnel junctions using such films. A 2 nm gold layer and a 2 nm MgO layer were evaporated on a YBCO film, at room temperature. This trilayer was deposited in-situ. A Nb counterelectrode was then evaporated at room temperature. Although many of the junctions prepared in this way were resistive, in some cases I-V curves as shown in Figure 3 were obtained. As can be noted this junction shows a superconducting short between the two electrodes. Although disappointing with respect to the goal of producing a working tunnel junction, this result is significant in that it provides unambiguous evidence that the growth

iod can indeed prepare YBCO films which are
erconducting up to the surface.
difficulties in reproducibly obtaining high-quality
faces, however, reinforce our belief that the
aling temperature must be rapidly ramped to a
cisely-maintained maximum temperature.

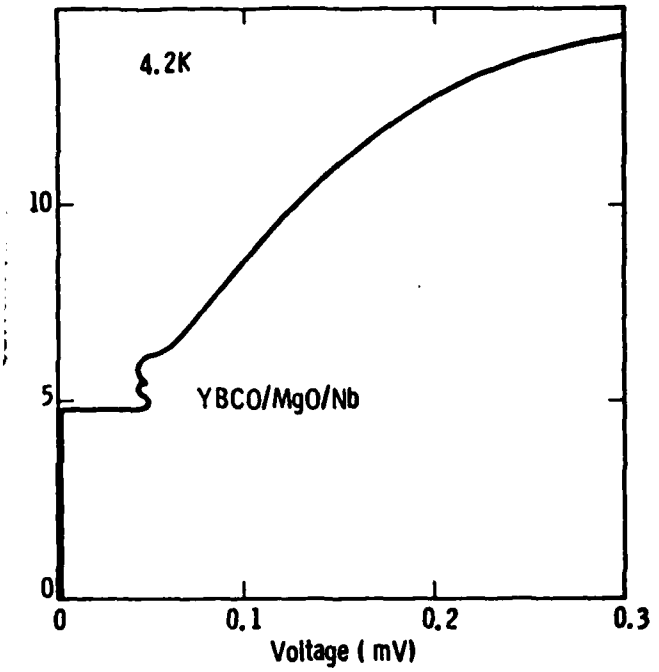

gure 3. I-V curve of a YBCO/MgO/Nb junction showing superconducting short between the two electrodes.

Acknowledgments

We thank T. Mullen, H. C. Pohl, A. L. Foley, and T. Blackham for their valuable technical assistance d Mrs. M. B. Cross for her help in preparing the nuscript.

References

[1] W. J. Gallagher, "Studies at IBM on Anisotropy in Single Crystals of the High-Temperature Oxide Superconductor $YBa_2Cu_3O_{7-x}$," J. Appl. Phys. 63, 4216 (1988).

[2] A. I. Braginski, J. Talvacchio, J. R. Gavaler, M. G. Forrester, and M. A. Janocko, "In-situ Fabrication, Processing, and Characterization of Superconducting Oxide Films," to appear in SPIE Proceedings Vol. 948, High-T_c Superconductivity: Thin Films and Devices, edited by R. B. van Dover and C. C. Chi (SPIE, Bellingham, Washington, 1988).

[3] R. M. Silver, J. Talvacchio, and A. L. de Lozanne, "Sputter Deposition of $YBa_2Cu_3O_{7-y}$ Thin Films," Appl. Phys. Lett. 51, 2149 (1987).

[4] J. R. Gavaler, and A. I. Braginski, "Near-Surface Atomic Segregation in YBCO Thin Films," Physica C 153-155, 1435 (1988).

[5] J. R. Gavaler, A. I. Braginski, J. Talvacchio, M. A. Janocko, M. G. Forrester, and J. Greggi, "Fabrication of High-T_c Superconducting $YBa_2Cu_3O_7$ Films," in MRS Vol. EA-14: High-Temperature Superconductors II, ed. by D. W. Capone II, W. H. Butler, B. Batlogg, and C. W. Chu (Mater. Res. Soc., Pittsburgh, 1988) pp. 193-196.

CHAPTER 8

"MBE" Growth of Superconducting Materials

A.I. BRAGINSKI*
and
J. TALVACCHIO
Westinghouse Science & Technology Center
Pittsburgh, Pennsylvania

1. Introduction

Recent attempts to fabricate superconducting devices of refractory low temperature superconductors (LTS) led to the exploratory use of film growth by "molecular beam epitaxy". We use this term and its acronym (MBE) in quotes since it represents a widely accepted but unfortunate misnomer. Molecular beams are really not employed to attain epitaxial growth of crystalline superconductors by physical vapor deposition (PVD). The ultra-high-vacuum growth apparatus and methodology are analogous to MBE as it is often used to fabricate semiconducting materials and devices. However, to evaporate refractory, high melting and boiling point materials—such as Nb, Mo, or Y—electron-beam heated sources are necessary. Sputtering and ion sources are also employed to deposit films. The analogies and distinctions

* Present address: ISI, Kernforschungsanlage Juelich, D-5170 Juelich, FRG.

between methods of superconductor and semiconductor growth will be reviewed in Section 2.

We assume that at this point the reader is familiar with basic concepts of superconducting electronic devices and circuits. The two most basic components of these circuits are the Josephson junction, an active nonlinear device, and a passive superconducting transmission line. By far the most widely used type of Josephson device—at least until the present time—is the tunnel junction. Practically all components and integrated circuits are now being fabricated exclusively by thin-film techniques typical of large-scale integration (LSI). As in the case of semiconductor technology, the component and circuit geometries are obtained by depositing multi-level layered film structures and, at various levels, patterning the circuit elements by photolithography. In these structures, superconducting films must interface with thin and thick insulators, normal metals, and, possibly, also semiconductors. In practical devices, the structures included, until recently, only polycrystalline superconductor films. The other materials were either amorphous or polycrystalline. The reader can find an extensive discussion of pertinent material problems in a review by Beasley and Kircher [1]. Update review articles concentrating on refractory materials have also been published [2,3].

The rationale for "MBE" growth of films of conventional superconductors is related to the length scales for superconductor perfection set by the two characteristic lengths: the superconducting coherence length ξ and the magnetic penetration depth λ. In superconductor–insulator–superconductor (SIS) tunnel junctions, the probed superconductor properties that define the junction characteristics are those within a depth of the order of the superconducting coherence length ξ from each interface with the barrier. Within this depth, the superconductor properties, i.e., the critical temperature T_c and the energy gap Δ, should be those of the bulk of the film. However, at interfaces between films of various materials some degradation of properties is usually unavoidable. Causes of the degradation can be many, for example, an interdiffusion and chemical reaction between the films or chemical reaction of one superconducting film with the ambient atmosphere prior to the deposition of a subsequent layer. Even if these effects are negligible, interfacial structural disorder will reduce T_c and Δ. The resulting depth of degradation observed in conventional polycrystalline superconductors d_c is on the order of 10 to 100 nm, in reasonably optimized processing conditions. When d_c is comparable to or greater than ξ, the junction characteristics are also degraded. The probed proximity layer in each electrode has now a lower T_c or may even be nonsuperconducting by itself. Consequently, the sumgap voltage V_g and also the critical current I_c are reduced [4], while the subgap conductance $1/R_s$ and

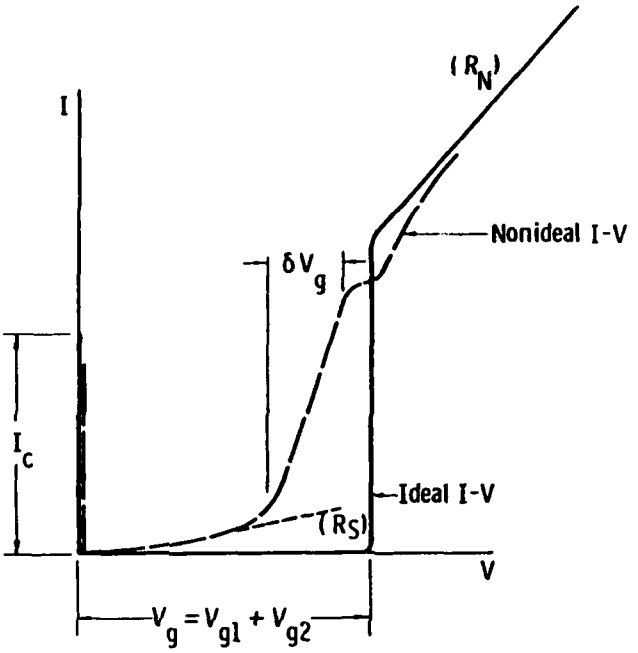

Fig. 1. Comparison of ideal tunnel junction $I-V$ curves with typical non-ideal characteristics.

the leakage current below the gap voltage are higher. The width of transition at the gap voltage δV_g (from the subgap to normal conductance $1/R_n$) broadens, and a proximity-effect knee appears. These deviations from an ideal, low temperature ($t = T/T_c < 0.5$) current–voltage ($I-V$) tunnel junction characteristic are shown in Fig. 1. The barrier non-ideality also increases $1/R_s$. Finally, the highest possible temperature of operation T_{op}, usually $T_{op} = 0.5\ T_c$, is defined by the lowest value of T_c near an interface with the barrier.

In a transmission line, surface and interface perfection of the superconductor within λ from the boundary is required to insure the lowest possible rf or microwave surface resistance and losses at a given frequency and temperature.

Junctions with Type I superconductor electrodes, having ξ of the order of 100 nm, are readily fabricated with nearly ideal $I-V$ characteristics at low t without much concern for interfacial degradation. In the case of Type II superconductors, where $\lambda \gg \xi$, it is usually much more difficult to fabricate high-quality tunnel junctions than to attain low rf surface losses in transmission lines. Table I includes representative examples of characteristic length scales of polycrystalline Type II superconductors listed in order of increasing T_c and decreasing ξ. Film thicknesses necessary to attain $> 75\%$ of bulk T_c are also indicated. Obviously, the sensitivity of SIS junction characteristics to interfacial degradation must increase with the T_c of electrodes. In the new, highest-T_c oxide superconductors (HTS), this sensitivity must be extreme.

Table 1. Representative Parameters of Important Superconductor Films

Superconductor	Nominal transition temperature (K)	Coherence length ξ (nm) (‖Cu-O, ⊥)	Penetration depth λ (nm) (‖Cu-O, ⊥)	Required film fabrication temp. (°C)	Thickness for ≥75% T_c d_c (nm) (Non-epitaxial)	Thickness for ≥75% T_c d_c (nm) (Epitaxial)
Pb	7.2	90	40	20	3	—
Nb	9.2	40	85	20–800	25	5
Mo-Re (bcc, A15)	12, 15	20, —	70, —	20, 800	—	10
NbN	16	4	300	50–700	15	<1
Nb_3Sn	18	3	65	750–950	25	8
Nb_3Ge	23	3	90	>850	130	40
$La_{1.85}Sr_{0.15}CuO_4$	40	3.7, 0.7	80, 430	800–900	—	—
YBCO	92	3.1, 0.4	27, 180	~550–900	~200	5
Bi-Sr-Ca-Cu-O	85–110	3.8, 0.16	25, 500	870	≫100	≫100
Tl-Ba-Ca-Cu-O	108–125	⟨2.6⟩	⟨220⟩	850	≫100	≫100

Epitaxial, single crystal tunnel devices were first proposed mainly to solve the problem of stresses in soft alloy electrodes and to eliminate device failures resulting from thermal cycling [5]. Other possible advantages, however, were also mentioned by the proponents. There was, however, no further activity in this area until the early 1980s. We then realized that this approach could eliminate or minimize the degradation of T_c and Δ due to crystalline disorder near the electrode/barrier interfaces. In addition, it became clear that the *in-situ* fabrication of all or the most critical layers in an enclosed high- or ultra-high-vacuum (HV or UHV) system should minimize the contamination of free surfaces prior to the next layer deposition. These considerations led us to the exploration of "MBE" growth of refractory superconductors such as Nb, NbN, and Nb_3Sn. The next logical step was to attempt fabrication of epitaxial bi- and trilayers with insulating tunnel barriers. Both, single-crystal and polycrystalline epitaxy have proven effective. A new impetus, however, toward the use of "MBE" was provided by the advent of electronically anisotropic materials (HTS). Deposition of epitaxial films is necessary to obtain—in the plane of the film—the requisite high critical current density, $J_c = 10^5$ to 10^6 A/cm^2 at the temperature of possible utilization. Tunneling into films with parameters well defined by crystalline orientation imposed by epitaxy will probably become a necessity although at this writing technologically meaningful tunneling characteristics have not yet been demonstrated in layered film structures incorporating HTS.

2. "MBE" Apparatus for Superconductor Growth

2.1. Analogy with Semiconductor MBE Systems—Requirements

Considerations that led to the development of MBE growth of semiconductors [6] are also applicable to epitaxial superconductor growth. Most important are the abilities to

(1) Attain and maintain cleanliness of epitaxial substrate and film surfaces (e.g., absence of water and organic adsorbate layers) for periods of time long enough to make possible the storage between processing steps and surface characterization of the crystalline structure, composition, and contaminants prior to the subsequent processing step.

(2) Sequentially deposit epitaxial layers of similar and dissimilar materials while meeting the first requirement at all fabrication stages.

(3) Co-deposit alloys and compounds from multiple sources while maintaining a precise composition control and uniform coating thickness.

(4) Deposit at low growth rates, typically between 0.01 and 1 nm/sec to promote crystalline perfection without incorporating background impurities into the film.

(5) Maintain an acceptable throughput in the system.

To meet requirements (1) and (2), and also (4), a UHV environment must usually be employed, especially for single-crystal LTS epitaxy. Oil-free pumping methods are preferred over diffusion and turbomolecular pumps when carbon contamination is to be avoided. Cryopumping insures quick pumpdowns to 10^{-7} to 10^{-9} torr. This makes it particularly convenient for lock-chamber evacuation and degassing of sources and specimens. Pumping down further, to 10^{-10} to 10^{-11} torr, is then achieved by an ion pump, possibly assisted by a titanium sublimation pump (TSP). The UHV system should be bakeable to a temperature defined by the type of gaskets, at least 150 to 200°C. Pumps must be capable of handling the degassing load created during the bakeout.

Sequential deposition and analysis are most conveniently attained in a closed, multi-chamber system where relatively incompatible functions or fabrication methods can be grouped and separated by gate valves. Suitable manipulators and linear transfer mechanisms are installed for transporting the substrate wafers or specimens between chambers without exposure to ambient atmosphere. Prior to inserting into the system, these wafers and specimens are mounted or clamped on transfer holders or blocks that are compatible with the transfer mechanism. The manipulator in a deposition chamber is often equipped with a rotary feedthrough permitting one to rotate or oscillate the holder in the flux path of evaporant(s) to improve the deposit uniformity.

Essential for an acceptable throughput (requirement (5)) is a lock (introduction) chamber that permits one to maintain the UHV environment for many fabrication cycles without the necessity of a long-duration pumpdown and bakeout for each material batch. The throughput is also enhanced by the possibility of simultaneously carrying out different processing and analytical steps in separate, gated chambers, thus permitting the user a parallel fabrication and characterization of several batches.

Growth of epitaxial and single-crystalline layers usually requires heating the substrate to a well-defined temperature in order to clean it, attain an adequate atomic surface mobility during growth, and also carry out processes such as a bulk interdiffusion, homogenization, grain growth, chemical reactions, etc. In typical MBE systems, the maximum temperature attainable does not exceed 800°C. Higher temperatures, up to 1200°C, are necessary for

substrate cleaning and deposition or processing of A15 structure superconductors and some oxide insulators. Such high temperatures can be attained by flat strip tantalum resistive heaters. The wafers or specimens are heated by either direct thermal radiation or by contact anchoring to the thermally irradiated holder/block. Surface irradiation by halogen lamp heaters can also be employed. Small area surface heating by electron beam can be attained if temperatures in excess of 1200°C are required.

The problem of accurate temperature measurement and control on the surface of the substrate is a difficult one. Proper instrumentation of a transferable and rotatable holder is virtually impossible. The temperature of a solid block is best monitored by a thermocouple seating in a well formed in the center backside of the block. Calibration of this thermocouple to the sample surface temperature can be performed by a variety of methods including melting point observation, optical pyrometry, comparison with temporary thin film thermocouple data, etc. The uncertainty of measurement depends on the quality of thermal anchoring, with ± 20°C being a typical figure.

A block diagram of the "MBE" system used by the authors for epitaxial superconductor and layered film growth is shown in Fig. 2 [7]. Figure 3 shows

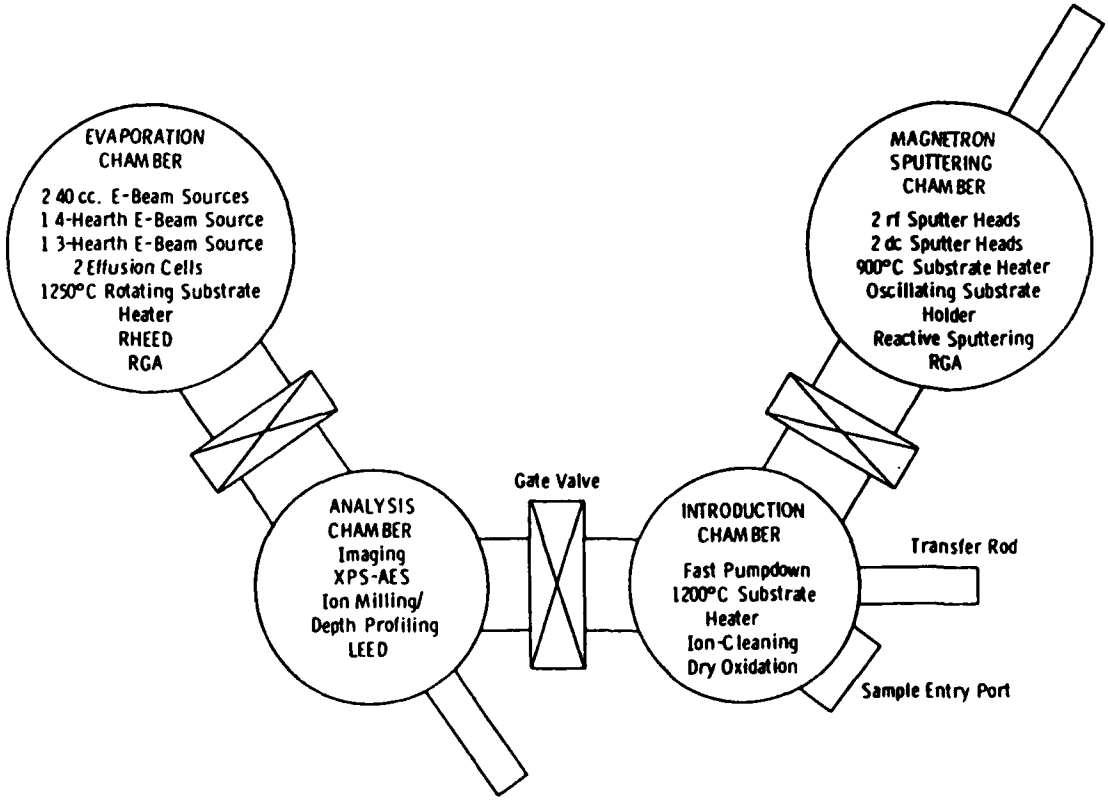

Fig. 2. Schematic of the deposition and analysis facility used at Westinghouse for "MBE" growth of superconductor films.

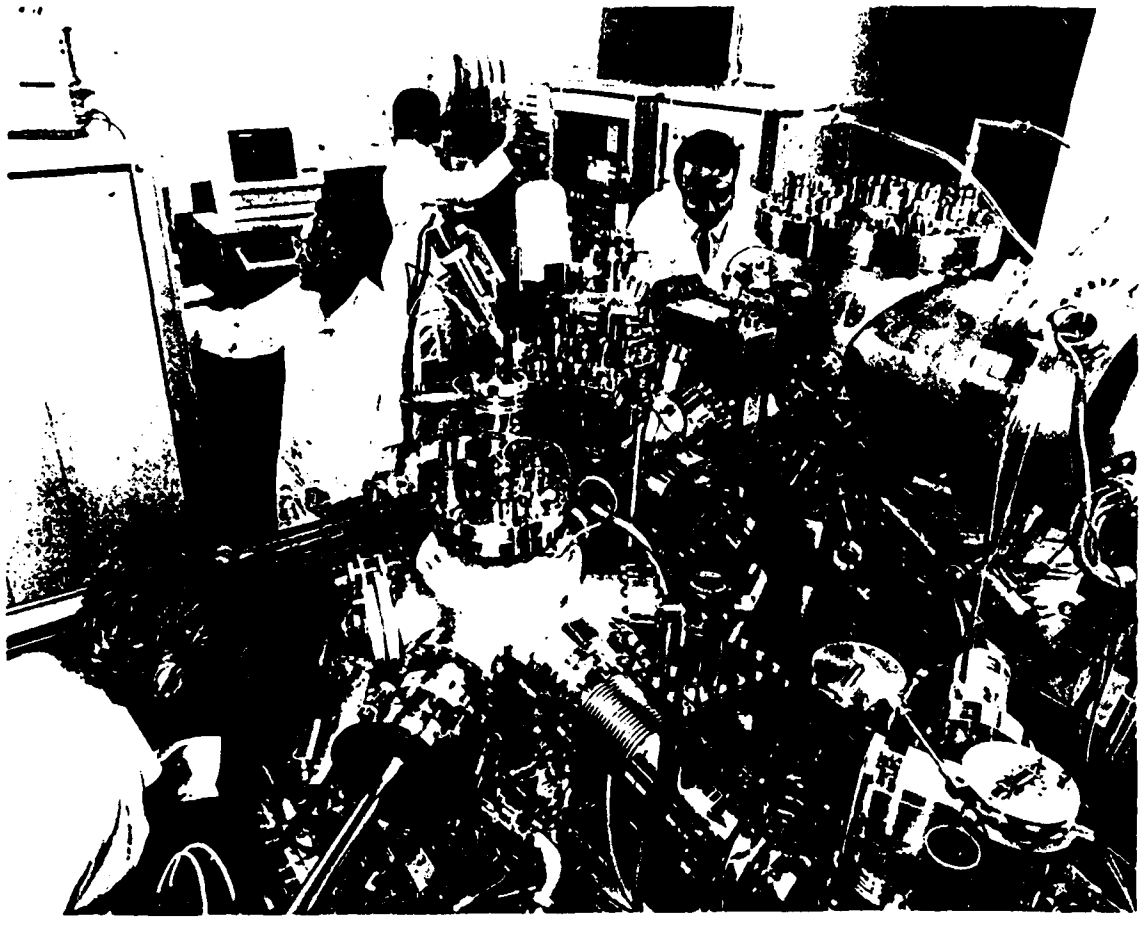

Fig. 3. Photograph of the Westinghouse deposition and analysis chambers.

the general view of the facility. This oil-free system meets satisfactorily the requirements discussed above and is equipped with most of the features reviewed in this and following sections. The advent of oxide superconductors necessitated an adaptation of the apparatus to the growth and processing in the presence of dry oxygen partial pressures ranging from 10^{-7} torr to 1 atmosphere. Obviously, the need to use UHV techniques appears questionable in this case. In our case, the first level of adaptation consisted of replacing tantalum heaters and shields with platinum, halogen lamp, and Kanthal heaters and stainless steel shields. Molybdenum transfer blocks and heater support elements were replaced with equivalents fabricated from Haynes alloy No. 230 (Haynes International, Inc., Kokomo, Indiana 46902), which resists oxidation at high temperatures. Unfortunately, it has a low thermal conductivity – detrimental to temperature uniformity of substrates clamped to the block. These changes permitted us to deposit YBCO films at

partial pressures of oxygen up to 10^{-2} torr and to *in-situ* oxidize and react (anneal) the deposits in 1 atmosphere of O_2 at temperatures up to 900°C.

2.2. *Sources and Deposition Rate Control*

Deposition of various materials may lead to the use of various source types and deposition rate control methods. For example, in semiconductor fabrication the co-evaporation of low-melting-point Ga, As, and Al can be conveniently performed from resistively heated Knudsen and effusion cells where a high-precision rate and deposit composition control (requirement (3)) can be attained by means of electronic temperature controllers. Evaporation of epitaxial silicon and of refractory metals or compounds usually requires an electron-beam-heated source due to the evaporants' high melting point. In this case, a rate control apparatus monitors the evaporant flux and uses a rate-proportional signal in a feedback loop to control the power and focus of a stationary electron beam or sweep amplitude of a scanning beam on the surface of an evaporant charge. The control of power results in a long response time, of the order of 1 sec. Much faster fluctuations of rate may occur in molten pools of refractory material and this necessitates using an additional feedback scheme acting on the sweep amplitude or beam focus with a time constant of much less than 0.1 sec [8]. However, even such elaborate rate control schemes are usually less precise than the resistive heater temperature control.

The choice of an e-beam gun rate control method is dictated by the vacuum environment and the type of material to be deposited. In a HV environment, rotating choppers can be used to generate an ac signal proportional to the flux of evaporant(s), which can be sensed by one or several ion gauge sensors suitably positioned in the chamber to monitor the temporal and spatial variation of flux [8]. Unfortunately, UHV-compatible chopper motors have not been readily available and, until the present, sensors different from ion gauges have been used. For certain elements, such as Si or Cu, electron impact emission spectroscopy (EIES) can be used to attain a rate control within $\pm 2\%$ [9]. For some other elements, and especially Nb, the EIES signal-to-noise ratio is too low to permit the rate control to better than ± 5–10%. Good success with short-term Nb rate control was obtained using a cross-beam mass spectrometer as a sensor [10]. Independent of the method of film deposition and growth rate control, an "MBE" growth chamber should be equipped with multiple vibrating crystal thickness monitors for absolute rate calibration. For co-depositions, the crystals should be positioned such that rate calibration is

possible for individual sources and that accumulation on the substrate block can be independently measured.

The deposition of refractory materials is rarely required in semiconductor fabrication so that sources of different types are rarely grouped in the same deposition chamber. In contrast, co-evaporation of compound superconductors typically involves both high-melting-temperature T_m (Nb, V, Y) and low-T_m (Sn, Ga, Al, Ge, Ba, Sr, Bi, etc.) sources. Consequently, evaporator chambers may incorporate both e-beam guns and effusion cells. Sputtering or ion-beam deposition of epitaxial, single crystal layers is, *a priori*, less desirable than co-evaporation since the surface mobility of deposited atoms is reduced in the relatively high-pressure inert gas environment, the probability of gas impurity incorporation is augmented and bombardment by energetic particles is likely to occur, all leading to a reduced crystalline perfection. Nevertheless, crystals of superconductors and insulators incorporating gaseous components, such as NbN or oxide compounds, are conveniently grown by reactive sputtering or reactive ion beam deposition. The incorporation of the gaseous component species (N, O) is effectively done during growth, even when using a metallic source(s). The need to co-deposit or integrate dissimilar materials in one layered film structure may lead, therefore, to the incorporation of sources employing various deposition principles into either a common chamber of a UHV system or separate but interconnected chambers. This latter alternative was adopted in the "MBE" system shown in Figs. 2 and 3. A specific discussion of various deposition methods is included in Section 3.

2.3. *Surface Analysis*

Analytical tools that might be installed in a superconductor "MBE" system are similar to those in use for semiconductors. Only surface-sensitive techniques need to be considered. In the case of analytical tools that probe length scales on the order of typical electronic film thicknesses, 0.1 to 1.0 μm, such as x-ray diffraction, Rutherford backscattering (RBS), or electron microprobe, films can generally be removed from vacuum and transferred to a dedicated analytical machine without compromising the measurement. Similarly, surface-sensitive measurements that involve the removal of the contaminated surface layer can be performed *ex-situ*, such as secondary ion mass spectroscopy (SIMS), Auger depth profiling, or surface analysis by laser ionization (SALI) [11].

The remaining surface-sensitive techniques can be categorized by their utility for structural or chemical analysis. In the former category are reflection

high-energy electron diffraction (RHEED), low-energy electron diffraction (LEED), and scanning tunneling microscopy (STM). The most common techniques in the latter category are x-ray photoelectron spectroscopy (XPS or, sometimes, ESCA) and Auger electron spectroscopy (AES). An additional technique, ellipsometry, measures optical properties determined by both surface composition and structure. All of these techniques are sensitive to surface contamination or reaction with background gases in the vacuum system. Ultra-high vacuum conditions are therefore necessary as much for *in-situ* analysis as for film growth. To allow for no more than 0.1 monolayers of contamination in the one hour time that is typically needed for analysis, one should operate in a pressure $< 10^{-10}$ torr [12].

Most analytical tools are installed in MBE systems in a chamber adjoining the growth chamber—not in the growth chamber. The exceptions are RHEED and ellipsometry [13] because the grazing angle incidence on the film and the high energy of the incident beam (10–100 keV electrons for RHEED) permit the beam source and the detector—usually a phosphor screen for RHEED—to be placed far from the sample where they do not obstruct the substrate and are not coated during deposition. The advantage of incorporating RHEED into an MBE growth chamber is that monolayer-by-monolayer growth of some semiconductor films can be monitored in real time [14]. The intensity oscillations of RHEED beams associated with monolayer growth have not been observed during superconductor growth. One reason is that most epitaxial superconducting films are composed of at least one refractory element. The black-body spectrum of the evaporating refractory source contains enough visible light to mask the RHEED pattern on a phosphor screen. Secondary electrons from the electron-beam sources that must be used with refractory materials would presumably lead to similar problems for other types of RHEED detectors. A more fundamental reason why RHEED oscillations have never been observed in superconductor film growth is that the oscillations are related to a step-propagation growth mode that may simply not occur in any of the superconducting materials. In conclusion, RHEED has generally been used to study the surface of epitaxial superconductors after film growth has stopped so there is no major advantage to having the technique available in the growth chamber.

For superconducting films, the only information gained from RHEED has been qualitative: indications of surface smoothness [7,15], evidence that some regions of the film have grown epitaxially [16,17], and the observation of reconstructed surfaces [18]. The depth scale from the surface that is probed by RHEED depends on surface roughness and varies from a few monolayers for

smooth films to hundreds of nanometers for surfaces that are rough on that scale. General reviews of the merits and applications of RHEED have been published by Lagally [19] and Cohen *et al.* [14].

In contrast to RHEED, there is no reason why LEED cannot be used in a quantitative way with epitaxial superconductor films. Qualitatively, LEED has been used to indicate that some regions of the surface of a superconductor have a periodic structure related to the substrate [20], much in the same way as RHEED. Unlike RHEED, the depth from the surface that is probed is reliably known to be a few monolayers, independent of surface roughness. Quantitative LEED analysis involves the collection of diffracted beam intensity as a function of incident beam energy (LEED $I-V$ curves) [21]. The $I-V$ curves can be compared with a series of curves generated from structural and electronic models of the surface in a way that is widely used in other fields but has only recently been applied to superconducting film surfaces [22]. The only applications of LEED $I-V$ curves to the study of multilayer superconducting film structures have been measurements of the lattice constants of artificial tunnel barriers [23].

No other structural surface analysis techniques have been used for *in-situ* characterization of superconductors. The structure of the surfaces of superconductors have been studied by scanning tunneling microscopy (for example, [24]) and by field ion microscopy (for example, [25]). The apparatus for either of these measurements could be attached to a deposition chamber to study as-deposited surfaces.

The most common analysis techniques for obtaining *in-situ* information about surface composition and chemistry are XPS and AES. The usual advantage of AES is the small area that can be analyzed. The area on which an electron beam can be focussed is on the order of 1 μm^2, compared to typical x-ray beam diameters of several millimeters. However, for *in-situ* analysis of the surface of films that have been deposited over an entire wafer or chip that has dimensions that exceed a few millimeters, the chemical-shift information that can be obtained with XPS makes it the more useful technique. The chemical shift of XPS peak energies is due to the formal valence state of the atom from which a photon has been emitted and the atomic environment [26]. An example of its utility is the distinct separation that can be seen between the energies of photoelectrons emitted from oxidized metal overlayers used as artificial tunnel barriers, and from any part of the metallic overlayer that remained unoxidized [27]. Too many applications of the *in-situ* analysis of superconductor film structures have been published to list them here, but some examples are discussed in Section 3. For a detailed treatment of the relative merits and applications of XPS and AES, see Briggs and Seah [28].

3. Materials Systems

3.1. *Substrates for Epitaxial Growth*

Table 2 contains a complete list of substrates used for epitaxial growth of important superconductors. Some of the superconductor films listed in Table 2 are epitaxial but not single-crystal. In those cases, the symmetry of the substrate surface is higher than the symmetry of a parallel plane in the film. The film can nucleate in more than one equivalent orientation. For example, α-$Al_2O_3(11\bar{2}0)$ has two-fold symmetry and NbN(111) has three-fold symmetry. There are two distinct orientations in which NbN(111) will nucleate and the resulting grains will be separated by stacking faults. The references cited in Table 2 are intended to be either the first or the most complete description of a particular epitaxial relationship.

At least one of the faces of sapphire (single-crystal α-Al_2O_3) is a suitable epitaxial substrate for all of the conventional (non-oxide) superconductors listed in Table 2. It is a particularly useful substrate material since it is readily available, has good mechanical and thermal properties, and has low dielectric losses at rf frequencies. Sapphire has the most complex crystal structure of the substrates considered here, so the relative orientations of the film and substrate are not obvious and have been, therefore, listed in Table 3. Table 3 contains the growth direction of the film, the indices of the parallel planes that contain the growth direction, and the lattice mismatches in two orthogonal directions. The orientations of Mo, MgO, and Si films grown on sapphire are included for reference.

The listing of lattice mismatches in Table 3 invites predictions by numerology of when epitaxy will occur. At one time, a mismatch of $\geq 15\%$ was thought to eliminate any possibility of epitaxial growth [49]. The data in Table 3 confirms the common wisdom that a "critical lattice mismatch" is an inadequate criterion for epitaxy. Although there is no adequate set of criteria for predicting epitaxial relationships, the important issue in cases where there is a large misfit is not so much whether epitaxial growth occurs, but whether the resulting strain or dislocation density in the film proves to be detrimental to technological applications. This issue has been most thoroughly examined for the Si-on-sapphire system, and only tentatively approached for epitaxial superconductor films.

Substrate preparation is one of the most important factors in determining the structural properties of epitaxial films. The surfaces of oriented and polished substrates generally have a layer of contamination and crystalline disorder due to adsorbed gases from the air, which, additionally, may react with the surface. Absorbed carbon and other organic contamination can

Table 2. Summary of Substrates for Epitaxial Superconductor Films

Epitaxial superconductor	Single-crystal substrate	Film orientation	Reference
Nb	α-$Al_2O_3(0001)$	(111) (110)[a]	[29]
Nb	α-$Al_2O_3(11\bar{2}0)$	(110)	[29]
Nb	α-$Al_2O_3(1\bar{1}02)$	(100) (110)	[30]
Nb	α-$Al_2O_3(10\bar{1}0)$	(211)	[31]
Nb	α-$Al_2O_3(21\bar{1}3)$	(113)	[32]
Nb	MgO(100)	(100)	[33]
Nb	MgO(111)	(111)	[32]
Nb	GaAs(100)	(100)	[34]
Mo-Re	α-$Al_2O_3(11\bar{2}0)$	bcc-(110)	[35]
Mo-Re	α-$Al_2O_3(0001)$	bcc-(111)	[35]
Mo-Re	α-$Al_2O_3(11\bar{2}0)$	A15-(100)	[35]
NbN	MgO(100)	(100)	[36]
NbN	MgO(110)	(110)	[37]
NbN	MgO(111)	(111)	[37]
NbN	α-$Al_2O_3(0001)$	(111)	[38]
NbN	α-$Al_2O_3(11\bar{2}0)$	(111)	[38]
NbN	α-$Al_2O_3(1\bar{1}02)$	(135)	[38]
NbN	α-$Al_2O_3(10\bar{1}0)$	(110)	[38]
NbN	α-$Al_2O_3(2\bar{1}\bar{1}3)$	(113)	[32]
Nb_3Sn	α-$Al_2O_3(0001)$	(100)	[32]
Nb_3Sn	α-$Al_2O_3(11\bar{2}0)$	(100)	[32]
Nb_3Sn	α-$Al_2O_3(1\bar{1}02)$	(100)	[39]
Nb_3Ge	$Nb_3Ir(100)$	(100)	[40]
Nb_3Ge	$Nb_3Ir(110)$	(110)	[40]
Nb_3Ge	$Nb_3Ir(111)$	(111)	[40]
Nb_3Ge	$Nb_3Sn(100)$	(100)	[40]
Nb_3Ge	α-$Al_2O_3(11\bar{2}0)$	(100)	[41]
Nb_3Ge	α-$Al_2O_3(1\bar{1}02)$	(100)	[41]
Nb_3Ge	$ZrO_2(100)$[b]	(100)	[42]
Nb_3Ge	$ZrO_2(111)$[b]	(111)	[40]
$La_{1.85}Sr_{0.15}CuO_4$	$SrTiO_3(100)$	(100)	[16]
$La_{1.85}Sr_{0.15}CuO_4$	$SrTiO_3(110)$	(110)	[43]
$YBa_2Cu_3O_7$	$SrTiO_3(100)$	(100) (001)	[44]
$YBa_2Cu_3O_7$	$SrTiO_3(110)$	(110)	[17]
$YBa_2Cu_3O_7$	$LaAlO_3(100)$	(001)	[45]
$YBa_2Cu_3O_7$	$LaGaO_3(100)$	(001)	[46]
$YBa_2Cu_3O_7$	$KTaO_3(100)$	(001)	[47]
$YBa_2Cu_3O_7$	$LiNbO_3(2\bar{1}\bar{1})$	(001)	[48]

[a] More than one orientation grown depending on substrate surface preparation, deposition temperature, or other factors.

[b] Yttria-stabilized cubic zirconia

Table 3. Summary of Experimentally Obtained Crystallographic Orientations of Superconductor Films Deposited on Sapphire Substrates (Mo, MgO, and Si Included for Reference).[a]

Material	Structure	Lattice constant, Å	Sapphire Orientation					
			c (0001)	*r* ($1\bar{1}02$)	*a* ($11\bar{2}0$)	*m* ($10\bar{1}0$)	*r'* ($10\bar{1}2$)	*n* ($2\bar{1}\bar{1}3$)
$Mo_{.65}Re_{.35}$	bcc	3.13	111	—	110	—	—	—
			$11\bar{2}\|\|10\bar{1}0$	—	$001\|\|1\bar{1}02$	—	—	—
			7.5%	—	11%	—	—	—
			7.5%	—	15%	—	—	—
Mo	bcc	3.15	111 (110)	100	—	—	221	—
			$11\bar{2}\|\|10\bar{1}0$	$011\|\|11\bar{2}0$	—	—	$1\bar{1}0\|\|11\bar{2}0$	—
			6.8%	6.4%	—	—	6.4%	—
			6.8%	6.4%	—	—	6.4%	—
Nb	bcc	3.30	111 (110)	100 (110)	110	211	—	113
			$11\bar{2}\|\|10\bar{1}0$	$011\|\|11\bar{2}0$	$001\|\|1\bar{1}02$	$1\bar{1}0\|\|1\bar{2}10$	—	$\bar{1}2\bar{1}\|\|01\bar{1}0$
			2.0%	2.0%	5.4%	1.0%	—	2.0%
			2.0%	9.4%	9.4%	2.0%	—	9.4%
MgO	B1	4.21	—	100	111	110	—	—
			—	$010\|\|11\bar{2}0$	$1\bar{1}0\|\|0001$	$001\|\|1\bar{2}10$	—	—
			—	13%	6.6%	13%	—	—
			—	21%	9.2%	9.2%	—	—
NbN	B1	4.38	111	135	111	110	—	113
			$\bar{1}10\|\|10\bar{1}0$	$21\bar{1}\|\|\bar{1}104$	$1\bar{1}0\|\|0001$	$1\bar{1}0\|\|0001$	—	$1\bar{1}0\|\|01\bar{1}0$
			−11%	−3.9%	2.2%	4.8%	—	−3.8%
			−11%	−11%	4.8%	−8.6%	—	−11%

(continues)

Table 3. (*continued*)

Material	Structure	Lattice constant, Å	Sapphire Orientation					
			c (0001)	*r* ($1\bar{1}02$)	*a* ($11\bar{2}0$)	*m* ($10\bar{1}0$)	*r'* ($10\bar{1}2$)	*n* ($2\bar{1}\bar{1}3$)
$Mo_{.65}Re_{.35}$	A15	4.96	poly	—	100 (210)	—	—	—
			—	—	010‖$1\bar{1}00$	—	—	—
			18%	—	11%	—	—	—
			18%	—	−13%	—	—	—
Nb_3Ir	A15	5.14	poly	100	100	poly	—	—
			—	001‖$11\bar{2}0$	010‖$1\bar{1}00$	—	—	—
			6.9%	−0.7%	6.9%	−7.4%	—	—
			6.9%	−7.4%	−16%	−16%	—	—
Nb_3Ge	A15	5.14	poly	100	100	poly	—	—
			—	001‖$11\bar{2}0$	010‖$1\bar{1}00$	—	—	—
			6.9%	−0.7%	6.9%	−7.4%	—	—
			6.9%	−7.4%	−16%	−16%	—	—
Nb_3Sn	A15	5.29	100	100	100,201	poly	—	—
			001‖$10\bar{1}0$	001‖$11\bar{2}0$	010‖$1\bar{1}00$	—	—	—
			3.9%	−3.5%	3.9%	−10%	—	—
			−10%	−10%	−18, 10%	−18%	—	—
Si	diamond	5.43	111	100	111	—	—	111
			$11\bar{2}$‖$1\bar{1}00$	001‖$11\bar{2}0$	$11\bar{2}$‖$1\bar{1}04$	—	—	$1\bar{1}0$‖$01\bar{1}0$
			24%	−6.0%	6.8%	—	—	7.2%
			24%	−12%	13%	—	—	28%

[a] The growth direction for the primary epitaxial orientation is listed in the first row of each entry and an alternative relationship, if any, is shown in parentheses. Planes in sapphire and the film are listed in the second row that are parallel to each other but perpendicular to the plane of the substrate surface. The third and fourth rows show the lattice mismatch in two orthogonal directions in the plane of the film.

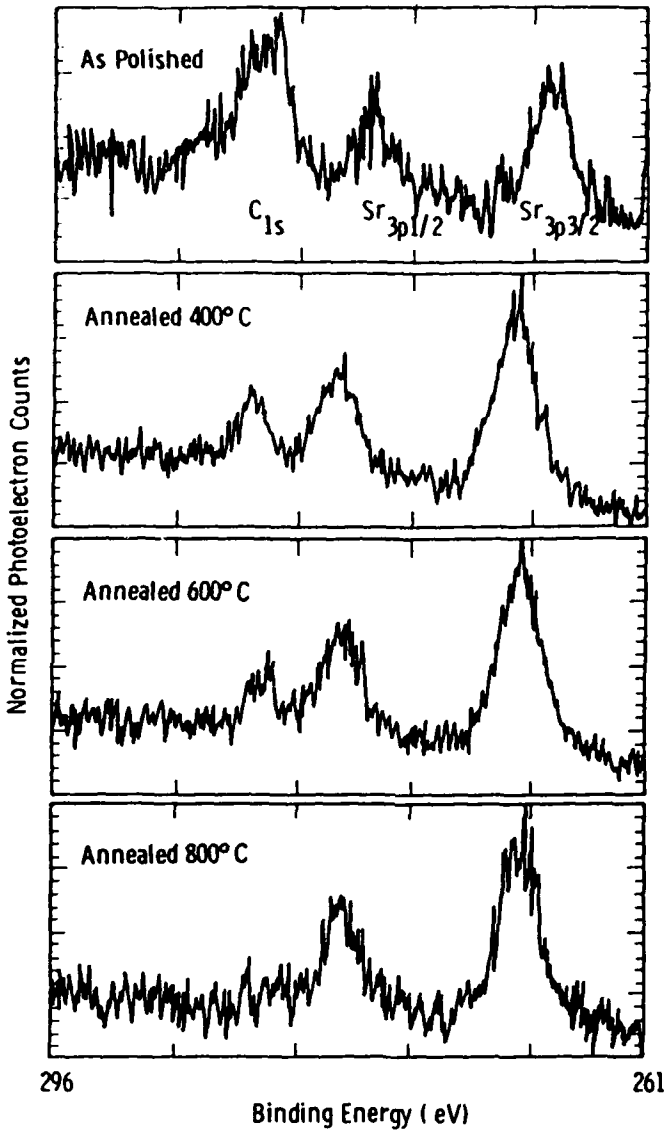

Fig. 4. *In-situ* XPS spectra centered on the energy of C_{1s} photoelectrons obtained from the surface of a $SrTiO_3(100)$ substrate after annealing at a series of temperatures in UHV.

usually be removed with an anneal in UHV just prior to film deposition. The temperatures needed for cleaning sapphire and MgO are 1250°C and 900°C, respectively. Figure 4 contains XPS data for annealed $SrTiO_3(100)$, showing that all traces of carbon disappear after an 800°C anneal.

In the case of α-$Al_2O_3(1\bar{1}02)$ substrates annealed at 800°C, Park *et al.* [15] found that a remaining sub-monolayer of carbon adversely affected both the structural and superconducting properties of epitaxial ultra-thin (< 5 nm) Nb and V films. Argon ion-milling was effective in removing the carbon and improving the Nb and V film quality.

In some cases, the process needed to remove surface contaminants does not maintain crystalline order in the substrate's surface layer. For Nb_3Ir, a simultaneous combination of ion-milling and elevated temperature were needed to obtain clean surfaces that exhibited sharp LEED patterns [50].

3.2. Nb-Based Structures

Reports of the epitaxial growth of Nb films by vapor-phase deposition—primarily on MgO or α-Al_2O_3 single-crystal substrates—have been published for more than twenty years (see Table 2). Epitaxial Nb films have been used mainly for basic physics or materials science studies and currently do not have technological importance. The successful application of randomly oriented polycrystalline films can be attributed to superconducting length scales, ξ and λ, which are much greater than the scales of d_c, typical crystal defects, damaged surfaces due to ion-milling, etc. Possible applications where single-crystal films will be needed are in those microwave devices that are limited in performance by the surface resistance of polycrystalline Nb films.

A simple characteristic often used to compare the quality of Nb films is the resistance ratio, RR = ρ(300 K)/ρ(10 K). For high-purity epitaxial films, a limit for RR based on an electronic mean-free path comparable to the film thickness has been inferred from a roughly linear dependence of RR on thickness with a slope of 0.5 nm^{-1} for RR $\leq$ 170. [51]. Since Nb is a refractory element, "MBE" growth requires the use of an electron-beam evaporation source. However, epitaxial Nb films sputtered in a UHV chamber can have equally high RR values. This section will describe the following properties of films produced by either growth technique: film/substrate epitaxial relationships, effects of film thickness, surface resistance, tunneling into single-crystal Nb films, epitaxial tunnel junctions (trilayers), and multilayer structures.

The orientation of epitaxial Nb films grown on sapphire is summarized in Table 3. As discussed by Claassen *et al.* [52], the sapphire/Nb registry is three dimensional. That is, the relative crystal orientation is the same regardless of which plane forms the interface between Nb and sapphire crystals. The registry is shown in Fig. 5 where stereographic projections for sapphire and Nb are overlayed corresponding to the relative crystal orientations found experimentally. Figure 5 shows that the three-dimensional orientation relationship leads to the 2.6° misorientation observed for Nb(110) grown on α-$Al_2O_3(1\bar{1}02)$ [53].

The structure of sapphire is such that there is no difference in the surface positions of oxygen ions between the $(1\bar{1}02)$ and $(10\bar{1}2)$ orientations. On the

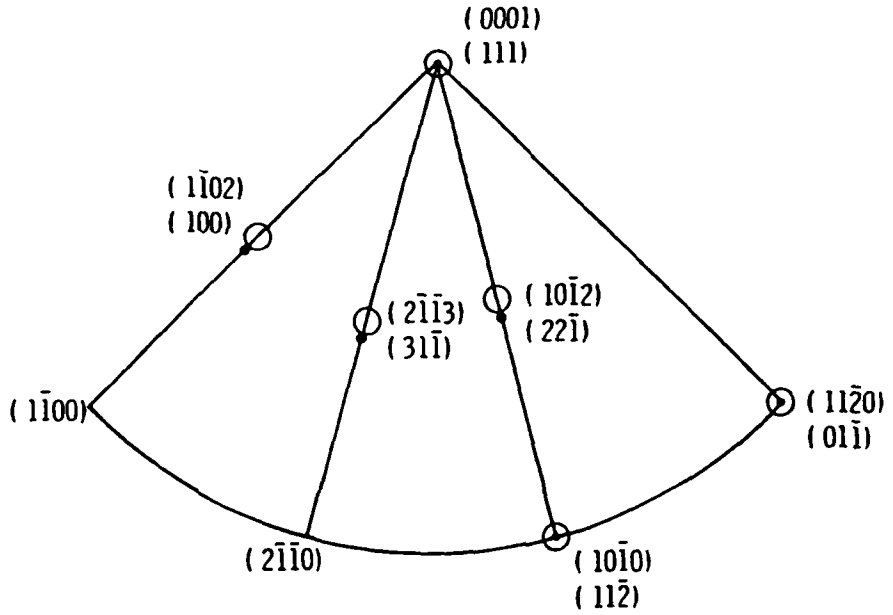

Fig. 5. Stereographic projections of α-Al_2O_3 and Nb crystals to show the relative orientation of an epitaxial film.

other hand, the two-dimensional unit cell defined by Al ions is three times larger for the latter surface. No data is available for the growth orientation of Nb deposited on α-$Al_2O_3(10\bar{1}2)$. However, a Nb(22$\bar{1}$) growth orientation can be predicted based on the 3-D registry of Nb and in analogy with the data of O'Neal and Rath [54] for the epitaxial growth of Mo on sapphire (see Table 3). The combined data for Nb and Mo growth on sapphire support the model that the initial monolayer of deposited Nb (or Mo) ions occupy sites on the surface of sapphire that would be occupied by Al ions in an extension of the bulk sapphire structure. The positions of Nb ions have no simple correlation with sapphire's oxygen sites. It will be shown in Section 3.4 that a similar empirical result relating to Al ion sites holds for the orientation of A15 compounds grown on sapphire.

Niobium-based tunnel junctions are affected by the use of epitaxial films in the base electrode, the tunnel barrier, and the counterelectrode. The first reports of tunneling into single crystal Nb(110) and (111) base electrodes, and the use of the native oxide grown on a single-crystal film as a tunnel barrier, were contained in a paper by Laibowitz and Cuomo [29]. Later tunneling measurements of single-crystal Nb films were performed by Durbin *et al.* [55] who observed an anisotropic product of the electron-phonon coupling function $\alpha^2(\omega)$ and the phonon density of states $F(\omega)$ between $\langle 110 \rangle$ and $\langle 111 \rangle$ directions.

The thermal oxides of polycrystalline Nb have made poor tunnel barriers even when used with Pb-alloy or other soft top electrode materials—due to the formation of conductive suboxides at the Nb/Nb_2O_5 interface [56] and to the structure of Nb_2O_5 [57]. Oxidation by an rf plasma forms a satisfactory low-leakage tunnel barrier due to the properties of a buried Nb-C-O layer [58], rather than those of the native oxide. In contrast to the polycrystalline case, the thermal oxide of epitaxial Nb(110) [59] or Nb(111) [29] formed low-leakage tunnel barriers. Another advantage of the oxidized single-crystal Nb was found by Celaschi *et al.* [59], who measured a reduced specific capacitance corresponding to $\varepsilon = 5-6$, compared with $\varepsilon = 29$ for oxidized polycrystalline Nb [60]. These results would seem to make the use of single-crystal Nb base electrodes preferable to polycrystalline films. However, no variation of Nb_2O_5 tunnel barriers has been found to be chemically stable during the deposition of a Nb counterelectrode. The technological state of the art employing all-Nb junctions with artificial tunnel barriers has obviated any advantages found in using the native oxide of single-crystal Nb base electrodes.

Other potential advantages of using epitaxial Nb films in tunnel junctions concern the uniformity of epitaxial artificial barriers and the gap energy of the top Nb electrode within a coherence length of the barrier/electrode interface. Epitaxial Al(111) has been grown on Nb(110) by Durbin *et al.* [55] and Braginski *et al.* [61] and subsequently oxidized. In the latter case, evaporated Nb counterelectrodes also grew epitaxially. However, the subgap leakage currents were much higher than for junctions formed with Pb top electrodes on the same type of base/barrier structure. This was interpreted as the result of non-uniform coverage by the Al layer that left pinholes in the artificial barrier filled by Nb_2O_5. The conclusion to which we are led by that singular study of epitaxial Nb/oxidized Al/Nb tunnel junctions is that randomly oriented, fine-grained Al deposited on polycrystalline Nb can provide better coverage than the epitaxial Al overlayer deposited on single-crystal Nb.

As shown in Table I, very thin Nb films, $\leq \xi$, can have transition temperatures approaching 9 K whether the film is epitaxial [110] or not [62]. Therefore, the same contribution to the gap voltage of a tunnel junction can be obtained for a polycrystalline Nb top electrode as for one that is grown epitaxially with a suitable epitaxial tunnel barrier acting as a substrate. In contrast, Table I shows that NbN films thinner than ξ can have a T_c approaching that of a much thicker film only when they are grown on a suitable epitaxial substrate.

The most likely practical application for "MBE"-grown Nb films is in analog signal processing at microwave frequencies where the surface re-

sistance of polycrystalline Nb films could limit device performance. Such devices (see, for example, [63]) have not, in general, been optimized in other ways so losses may be dominated by radiation or by dissipation in dielectrics rather than by the superconductor's surface resistance. No detailed comparisons have been made between single-crystal and polycrystalline Nb films for this application, and most devices that have been tested used polycrystalline films. In one example that is available, however, the highest-Q Nb thin-film resonator reported, which had a loaded $Q = 4 \times 10^5$ at 3 GHz and 4.2 K, was made from epitaxial films [64].

Another use for epitaxial Nb films has been in the study of metallic multilayer superlattices. The first superlattices in which three-dimensional coherence was observed were Nb(110)/Ta multilayers grown by "MBE" on α-$Al_2O_3(1\bar{1}02)$ [31]. The epitaxial Nb layers stabilized the formation of the metastable bcc Ta phase. The bcc phase is superconducting and a similar use was made [65] of an epitaxial Nb layer on sapphire to grow Ta/Ta_2O_5/Pb-Bi tunnel junctions. These junctions have a particularly sharp nonlinearity at the gap voltage that makes them useful as quasiparticle mixers for heterodyne detection of millimeter waves. Another high-quality superlattice system, Gd(0001)/Y, makes use of an epitaxial Nb(110) layer as a diffusion barrier between sapphire and Gd or Y [111].

In conclusion, the "MBE" growth of Nb has yet to make a significant impact on modern superconducting device development—despite the fact that Nb/oxidized Al/Nb tunnel junctions represent the state of the art for circuit development. The primary reason is that the coherence length of Nb is larger than the polycrystalline film thicknesses needed to obtain ~9 K transition temperatures. However, the relative ease of growing a single-component single-crystal film makes it likely that epitaxial Nb films will be implemented in other applications as small advantages over polycrystalline films are found.

3.3. NbN-Based Structures

The first epitaxial NbN films were grown by CVD on MgO(100) substrates [36]. Magnesium oxide and NbN both have a B1 structure and a lattice mismatch of only 4%, so MgO was a natural candidate for an epitaxial substrate. Single-crystal films were later deposited by reactive sputtering on MgO(100) [66], and on a number of different sapphire surfaces [38]. In some cases where polycrystalline substrates were used, the concept of polycrystalline epitaxy, in which each crystallite in the film aligns with one in the

substrate, has been invoked to explain higher T_c's measured for NbN films grown on oxidized Mg substrates, compared with films grown on other oxide substrates [41,67].

The only all-NbN Josephson tunnel junctions reported to date with gap voltages $V_g \geq 5$ mV have used MgO tunnel barriers (for example, [67,68]). The significance of a 5 mV gap voltage at 4.2 K is the likelihood that such a junction can operate with a closed-cycle refrigerator at ~ 10 K [116]. Since the tunnel barrier is the substrate for counterelectrode formation, the junction results suggest that polycrystalline epitaxy was responsible for a substantial contribution to V_g from the energy gap of the NbN counterelectrode. The difference in the energy gap of NbN counterelectrodes formed on substrates that promote epitaxial growth and those that do not, is summarized in Table 1. Only in the case of epitaxial growth does the T_c of NbN films thinner than a coherence length approach the T_c of bulk NbN.

Despite the technological importance of polycrystalline NbN/MgO/NbN structures, the remainder of this section will focus on the "MBE growth" of single-crystal epitaxial NbN films and multilayers. In contrast to all of the other superconductor material systems described in this chapter, epitaxial NbN films have never been produced by evaporation. Typically, such films are produced by reactive sputtering of Nb in an Ar/N_2 sputtering gas which may also contain a source of carbon (e.g., CH_4, [113]) to stabilize the superconducting phase and increase T_c from ~ 15 K to 17 K. The best epitaxial films have been produced in the range of substrate temperatures between 500 and 700°C.

A unique property of epitaxial NbN films—in comparison with polycrystalline NbN—is a resistivity ratio, $\rho(300\,\text{K})/\rho(100\,\text{K})$, greater than unity [37]. This metallic characteristic of the normal-state resistivity is even observed for epitaxial NbN grown on sapphire. These films generally grow in a direction with a different symmetry than the substrate surface (see Table 3). Planar defects—grain boundaries, twin boundaries, or stacking faults—must form at the boundary of grains that nucleated on rotationally equivalent sites on the substrate, which are not rotationally equivalent in the film [38,20].

Low-energy electron diffraction (LEED) patterns of an α-Al_2O_3(0001) surface and a subsequently deposited NbN(111) film are shown in Figs. 6(a) and 6(b). Figures 6(c) and 6(d) contain LEED patterns obtained from an MgO(111) tunnel barrier deposited on the first NbN(111) film and from a NbN(111) counterelectrode, respectively. Figure 6 shows that an orientation relationship was maintained in the plane of the films throughout the thickness of the trilayer, and that a periodic structure was maintained in the top 1–2

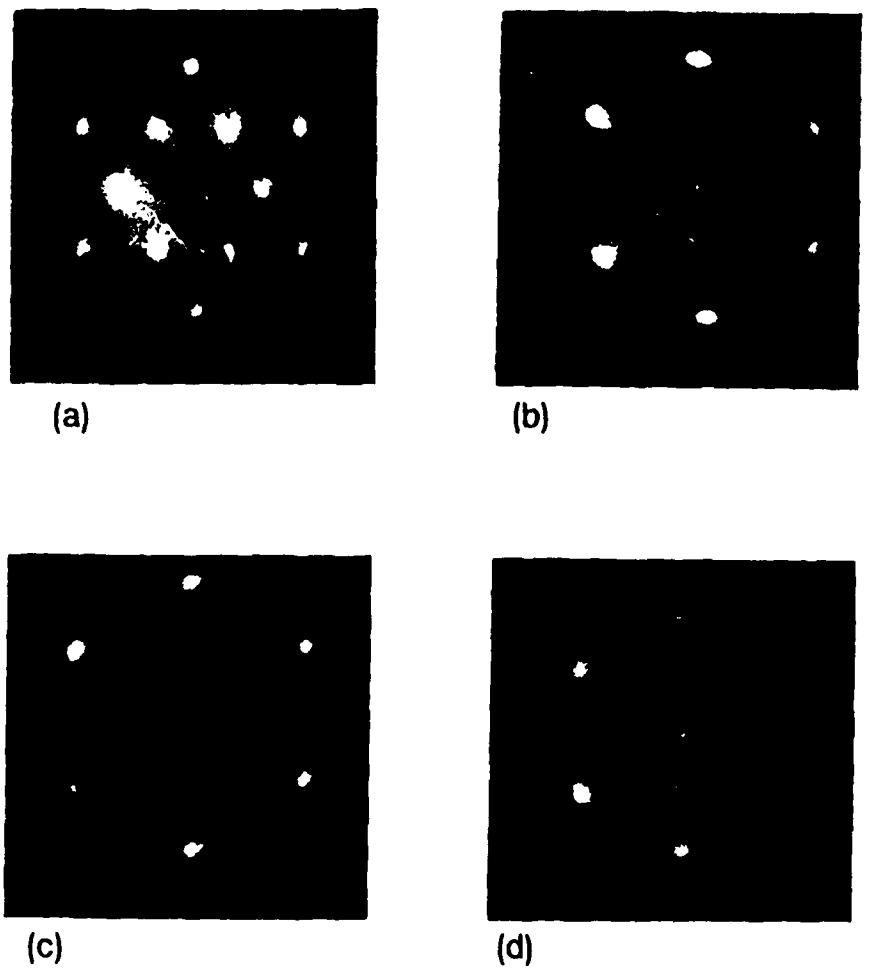

Fig. 6. LEED patterns from the surfaces of a NbN(111)/MgO/NbN epitaxial tunnel junction: (a) α-Al_2O_3(0001) substrate, electron beam voltage = 103 V; (b) 50-nm thick NbN(111) base electrode, 81 V; (c) 0.7-nm thick MgO barrier, 72 V; (d) 50-nm thick NbN top electrode, 88 V.

monolayers. The extreme surface-sensitivity of LEED was particularly important in the analysis of the structure of tunnel barriers (Fig. 6c) since, in many cases, they were only a few monolayers thick. Electrical measurements of tunnel junctions patterned from epitaxial trilayers showed that coverage by these thin MgO barriers was (nearly) complete so a pattern such as the one in Fig. 6(c) is truly a measurement of MgO and not the underlying NbN.

Typical quasiparticle $I-V$ curves for two orientations of epitaxial NbN-based tunnel junctions are shown in Fig. 7. A complete review of epitaxial NbN junction properties has been published [20]. The junctions in Fig. 7 had resistances at 6 mV less than 10^{-4} Ω-cm^2 and critical current densities on the order of 100 A/cm^2. The $I-V$ characteristics were strongly influenced by the deposition temperature of the top electrode. For the junctions shown in Fig. 7,

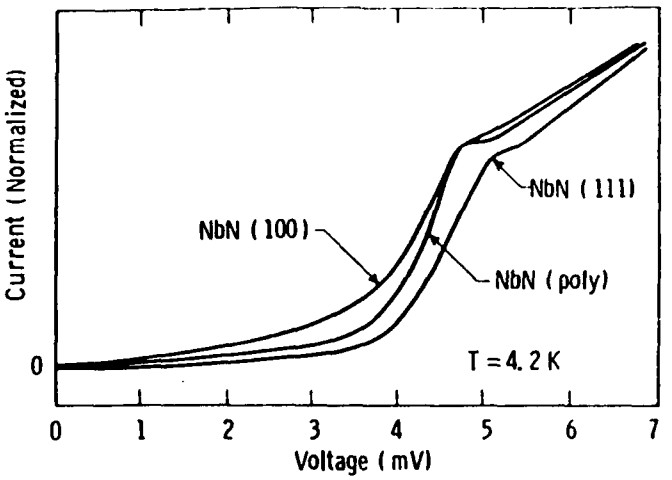

Fig. 7. Comparison of quasiparticle $I-V$ curves for NbN/MgO/NbN tunnel junctions made with single-crystal and polycrystalline electrodes.

the counterelectrode was grown at 150°C. Higher deposition temperatures, as high as 750°C, were used without significantly degrading the epitaxial barriers. Junctions with polycrystalline barriers—such as the one used for a reference curve in Fig. 7—were shorted during the process of counterelectrode deposition at such high temperatures. The epitaxial junctions formed at high temperatures had higher gap voltages, higher critical current densities, and higher subgap conductance than those completed at 150°C.

Tunnel barriers for epitaxial junctions were deposited at 700°C to obtain sharp LEED and RHEED spots indicative of good crystalline order, although low-temperature depositions provide more uniform coverage. In cases where the tunnel barriers were deposited in pure Ar, pinholes in the barrier were plugged by niobium oxide. Although Pb-alloy counterelectrodes deposited on these NbN/MgO bilayers resulted in low-leakage junctions, NbN counterelectrodes reduced the oxide in the pinholes and led to shorts through the barrier. XPS studies of NbN/MgO bilayers indicated that 1% methane added to the sputter gas during tunnel barrier deposition led to the formation of a niobium carbo-oxide in the pinholes that was more chemically stable and solved the problem [20].

A study was performed to determine whether the elimination of the 4% mismatch between NbN and MgO and, therefore, tensile stress in barriers, could lead to improved junction characteristics [20]. Figure 8 shows the lattice constant and equilibrium phase boundaries of solid solutions in the MgO-CaO pseudo-binary system as a function of CaO content. Metastable solid solutions were successfully formed in either sputtered or evaporated MgO-

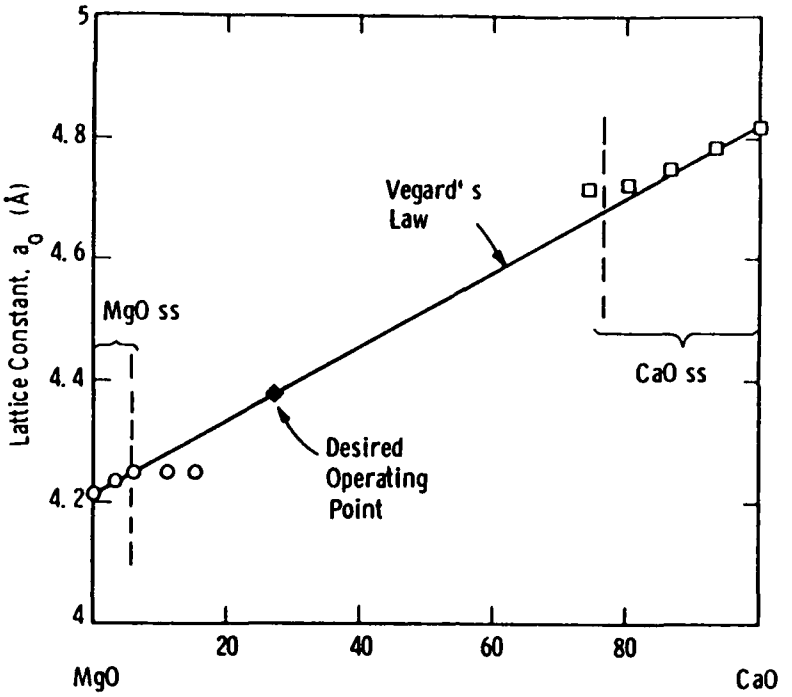

Fig. 8. Variation of lattice constants as a function of CaO content in the MgO–CaO pseudo-binary system. The desired operating point—the lattice constant of NbN—falls outside the equilibrium solid-solution phase fields.

CaO epitaxial films grown on NbN throughout the range of tensile-stress, lattice-matched, or compressive-stress solid solutions. Based on Vegard's Law, the lattice-matched composition was assumed to be 27 mole percent CaO.

Evidence that a single-phase MgO-CaO solid solution was obtained is presented in Figure 9, which shows the kind of quantitative LEED data that was discussed in Section 2.3. Ignoring dynamical diffraction effects, a lattice constant for the 7 nm thick, 50%-CaO film in Fig. 9 was found from the spacing between 00n Bragg peaks to be 0.439 nm. In contrast, reference LEED data for an MgO crystal was best fit by a lattice constant of 0.425 nm.

However, thinner MgO-CaO overlayers ($\sim$1 nm), had a lattice constant that matched NbN regardless of CaO content. The misfit strain that was evidently present in the tunnel barriers had a negligible effect on the electrical properties of epitaxial NbN junctions. The I–V curves presented in Fig. 7 were from junctions with barriers made at the lattice-matched composition, but had gap voltages and subgap conductances comparable to junctions made with pure MgO barriers.

The discovery of HTS oxides has sidetracked the development of NbN-based circuits capable of operation at 10 K, pending the outcome of efforts to make HTS junctions that could operate at much higher temperatures. As

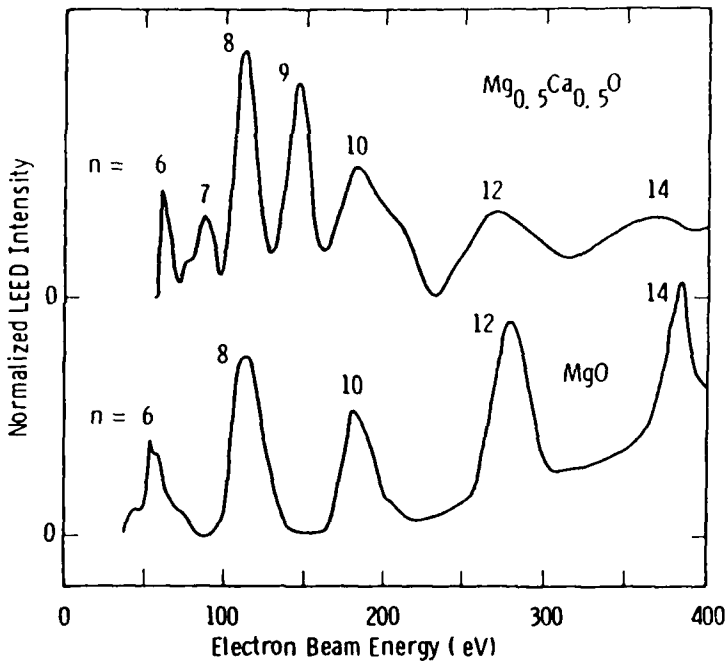

Fig. 9. LEED intensity plotted as a function of incident beam energy for the (0,0) beam: (a) a 7-nm thick $Mg_{0.5}OCa_{0.5}O(100)$ film deposited on NbN(100); (b) an MgO(100) crystal.

attention is shifted back to NbN, the most important issue in making junctions will be to obtain reproducible critical current densities. If polycrystalline NbN/MgO/NbN junctions cannot be made reproducibly, epitaxial junctions may become a practical alternative rather than simply model systems for materials studies.

An alternative to MgO or MgO-CaO epitaxial tunnel barriers, wurtzite-structure AlN(0001) grown epitaxially on NbN(111), has been used in a preliminary manner to fabricate junctions [117]. Although the junction quality was poor, the chemical compatibility of an epitaxial nitride insulator on a nitride superconductor should provide a motivation for further work. The epitaxial NbN/AlN/NbN system is also significant as a predecessor to current activity in the fabrication of the epitaxial oxide structure, $YBCO/PrBa_2Cu_3O_7/YBCO$ [115,114]. The successful formation of epitaxial NbN/MgO/NbN junctions at temperatures as high as 750°C is also an important indicator of what is possible in HTS junction development.

3.4. A15 Superconductors

3.4.1. "MBE" of A15 Superconductors

The UHV "MBE" of A15 superconductors was motivated by the interest in properties of epitaxial thin films and tunneling structures (Section 1). Prior

investigations of homo- and hetero-epitaxial effects in films of high-T_c A15's have been performed mostly in conjunction with the problem of high-T_c Nb_3Al, Nb_3Ga, Nb_3Ge, and Nb_3Si phase stabilization. In almost all cases, these films were deposited, by co-evaporation or sputtering, in HV systems having background pressures in the 10^{-5} to high 10^{-8} torr range. Below, we limit our attention to those A15's that were also grown by "MBE."

3.4.2. Mo-Re Films and Tunneling Structures

Bulk solid solution alloys of Mo-Re having the α-Mo structure are superconducting with a maximum $T_c = 12$ K at approximately 40 at.% Re, the boundary of this phase stability field [69]. A metastable A15 structure was observed in sputtered [70] and e-beam evaporated [71] polycrystalline thin films with compositions between 25 and 40 at.% Re. A maximum $T_c = 15$ K was observed in mostly A15 films containing 38 at.% Re [70] and in films having an unresolved structure and a composition Mo–(62 at.%) Re [72].

Interest in the use of Mo-Re films for tunneling structures and also microwave cavities was stimulated by the coherence length in the α-Mo phase, $\xi = 20$ nm, much longer than in other superconductors of comparable T_c, and by the low solubility of oxygen in Mo-Re alloys [73]. Superconductor surface and interface degradation could thus have a lesser effect on the tunnel junction gap voltage and subgap conductance or on the cavity losses than in the case of B1 and A15 structure films. Interest in the unresolved issue of the Mo-Re A15 phase stabilization mechanism (by impurities versus epitaxy?) also motivated the only "MBE" study by Talvacchio *et al.* [35], which is summarized below.

The "MBE" system of Fig. 3 was used for film and tunnel junction fabrication and analysis. Thin Mo–(25 to 40 at.%)Re films were e-beam co-evaporated on $(11\bar{2}0)$ and (0001) sapphire substrates. At low deposition temperature of $T_s = 100°C$, the films were polycrystalline with α-Mo structure. At higher temperatures, however, epitaxial deposits were obtained with orientations indicated in Table 2. The crystalline quality was relatively high, with the x-ray rocking curve width of 0.4 degrees of arc. At $T_s = 800°C$, the structure was still α-Mo, while at 1000°C predominantly A15. The conditions of deposition were otherwise identical and the very low background pressure of impurities, 1×10^{-10} torr or less, made the impurity-stabilization of A15 phase very unlikely and stabilization by epitaxy probable. Due to the absence of impurities, the film T_c was independent of the deposition temperature and also of film thickness, in a marked contrast to analogous films sputtered in the presence of impurities. Figure 10 compares the T_c and residual resistivity ratio vs. thickness dependences in these two types of films.

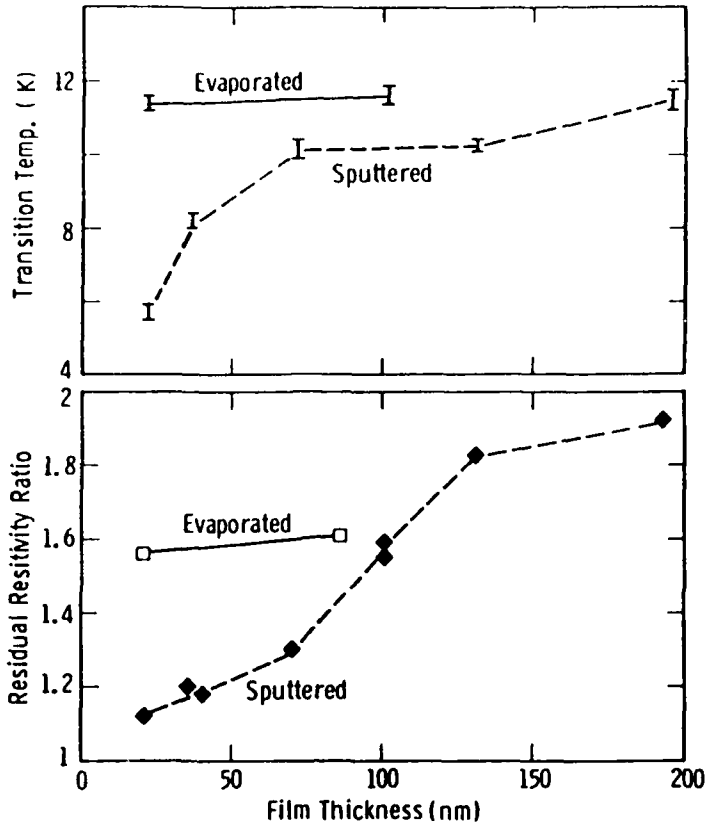

Fig. 10. Critical temperature and residual resistivity vs. thickness of sputtered and "MBE" co-evaporated Mo-Re films.

In co-evaporated films, the compositional dependence of T_c was that of the bulk α-Mo phase with a maximum T_c of 12 K, almost independent of the crystal structure. The higher $T_c = 15$ K that was obtained by sputtering was not reproduced.

The *in-situ* XPS analysis of film surfaces confirmed that Mo-Re is much less susceptible to oxidation than either Mo or Re. Due to the thinness of the native Mo-Re oxide—only 0.5 nm—a complete coverage of the Mo-Re base electrode by an artificial Al-Al_2O_3 barrier was necessary to obtain low subgap conductance tunnel junctions with Pb or Mo-Re counterelectrodes. The all-Mo-Re tunnel junctions had a low "junction T_c" temperature of only 8 K. This indicated that the counterelectrode was amorphous at the interface with crystalline Al_2O_3, in contrast to films on sapphire that were crystalline even when only one coherence length thick.

In conclusion, the available "MBE" results documented the epitaxial film growth of both α-Mo and A15 phases and the ability to fabricate all-Mo-Re tunnel junctions. The mechanism of A15 Mo-Re stabilization, however, was

not revealed. It appears that epitaxy may stabilize an A15 phase with a T_c lower than that of films stabilized by impurities present in sputtering. The technological usefulness of Mo-Re for higher-T_c tunnel junctions remains in doubt since epitaxial growth of counterelectrodes was not attained.

3.4.3. Nb-Sn Films and Tunneling Structures

In the Nb-Sn binary system, the A15 structure is stable between 18 and 25 at.% Sn. A nonequilibrium phase diagram useful as a guide for Nb-Sn film deposition was proposed by Rudman *et al.* [74] and is shown in Fig. 11. Stoichiometric Nb_3Sn deposits can be conveniently obtained without a very accurate deposition rate control by co-evaporating the two constituents with some, relatively arbitrary excess of tin at substrate temperatures near 900°C. This temperature is high enough for the excess of Sn to re-evaporate as Nb_6Sn_5. The "composition-locked" field, where stoichiometric Nb_3Sn can be obtained, is shown in the phase diagram. Within the A15 stability field, some

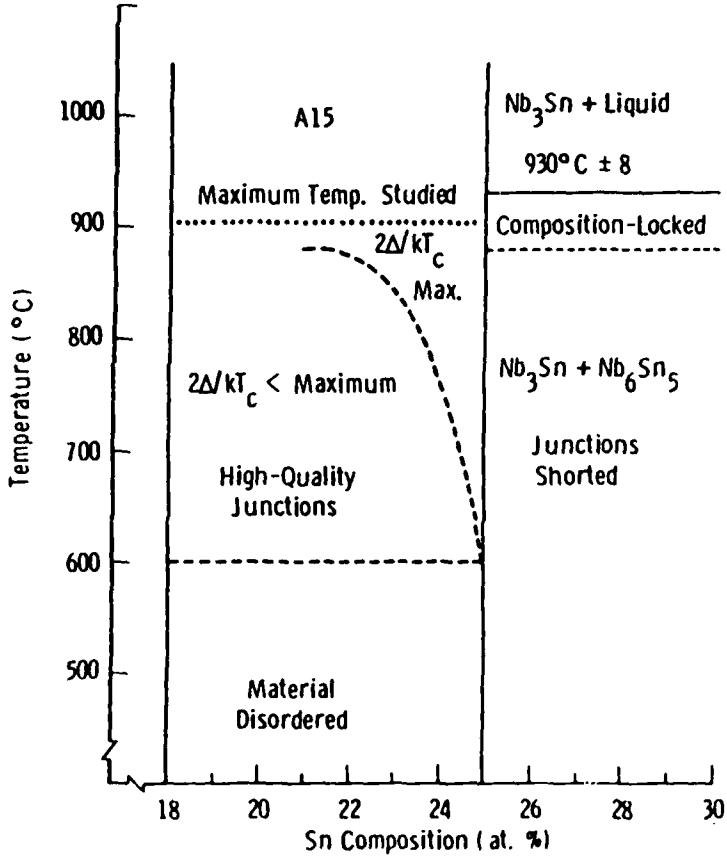

Fig. 11. The nonequilibrium phase diagram for Nb-Sn thin film growth [75].

tendency exists to segregate into two A15's differing in the tin concentration [75]. This is the cause of the observed broadening of the superconducting transition.

Epitaxial growth of (100) Nb-Sn on $(1\bar{1}02)$ sapphire substrates was first observed and investigated by TEM in thick deposits that were e-beam co-evaporated in HV at substrate temperatures up to 900°C [39]. While nucleation on the substrate was preferentially (100), grains of other orientations were also nucleated so that the deposits were oriented but polycrystalline through the first 100 nm. With the increasing film thickness, random orientations became overgrown by $\langle 100 \rangle$ regions and the crystalline quality improved. However, even in films thicker than 1 micron, some domains misoriented within 5 degrees were present and separated by end-on dislocation boundaries. In addition, especially at $T_s < 900$°C, domains having another epitaxial relationship, tilted by 30 and 60 degrees with respect to the matrix, were also present. Marshall *et al.* [39] analyzed the observed epitaxial relationship, where the cube axes of Nb_3Sn align along the twofold symmetry orthogonal axes in the $(1\bar{1}02)$ face of sapphire, and suggested that the small misorientations were related to the different symmetries of the substrate and film.

In the only "MBE" deposition study, Sn was evaporated from an effusion cell and Nb from an e-gun (Talvacchio *et al.* [76,7]). The main difference, when compared with Marshall *et al.* [39], was a much lower background pressure of impurities, $< 1 \times 10^{-10}$ torr. Films were grown in the "composition-locked" regime, simultaneously on sapphire of several orientations listed in Table 2. The deposit crystallinity was determined by *in-situ* RHEED and LEED. Substrate orientations where the minimum lattice parameter mismatch along one cube axis did not exceed $+4\%$ permitted the film to grow epitaxially with a (100) and (201) orientation. The epitaxial relationships are shown in Fig. 12. On sapphire $(10\bar{1}0)$, where the minimum mismatch was approximately -10%, the films were polycrystalline. The LEED pattern of films only 6 to 10 nm thick is shown in Fig. 13. It indicates that "MBE" films have nucleated in highly epitaxial form. These films attained a high degree of perfection at a thickness of only 100 nm (Fig. 13), in contrast to the films grown in HV [39]. The x-ray rocking curve linewidth was only 0.4 degrees. However, the "MBE" films were not truly single crystals, as they contained two growth orientations with (100) and (201) planes tilted by about 30 degrees of arc. This was revealed by x-ray Weissenberg camera results [77] and confirmed by x-ray diffractometer data, which indicated that the two habits were present in approximately equal proportion. No TEM results were obtained. However, the narrow x-ray rocking curve suggested that the concentration of low-angle boundaries was

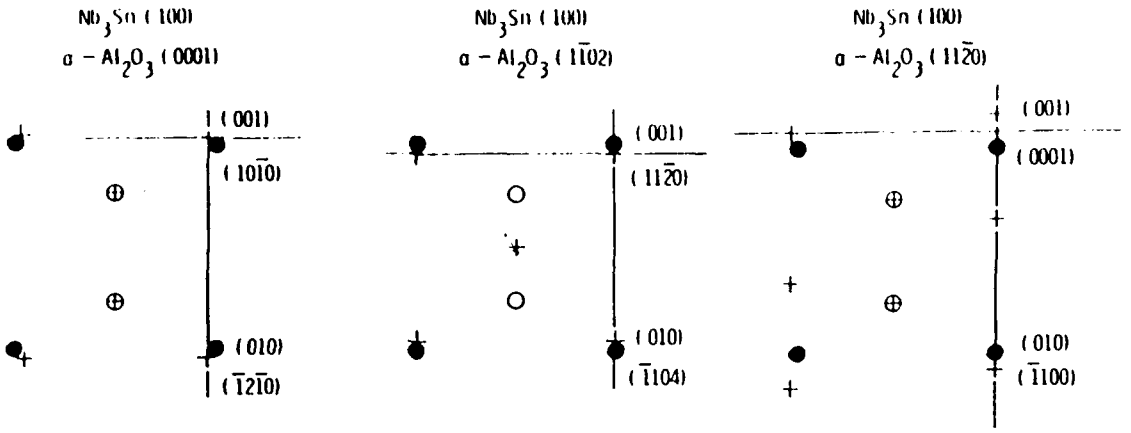

Fig. 12. Epitaxial relationships between $Nb_3Sn(100)$ and three different sapphire faces showing that Nb(○) and Sn(●) occupy sites that would be occupied by Al(+) if one more layer of the sapphire structure were added.

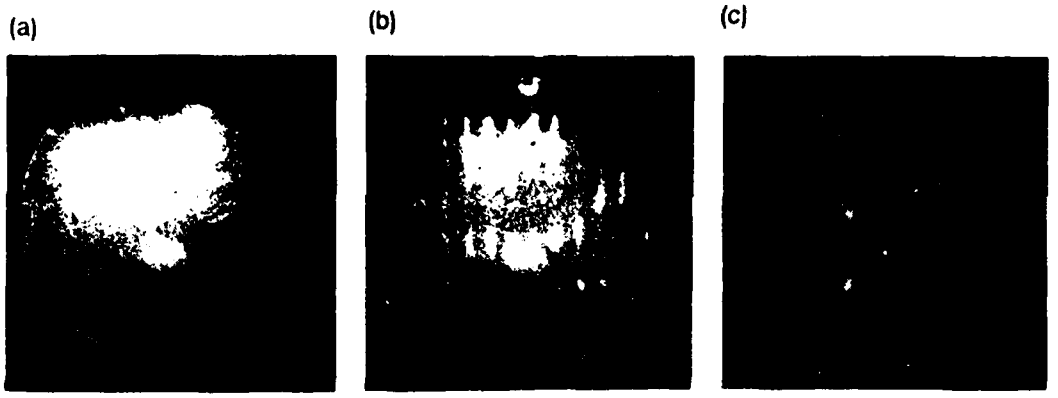

Fig. 13. Electron diffraction patterns—RHEED and LEED, respectively—of $Nb_3Sn(100)$: (a) 6-nm thick film; (b), (c) 100-nm thick.

low. The polycrystalline nucleation and gradual overgrowth observed by Marshall *et al.* [39] were thus due to background impurities. The alternative growth habits in "MBE" films were different than in non-"MBE" films but could also be due to differences in the film and substrate symmetry, as suggested by Marshall *et al.*

Similarly to the case of NbN, the ability to grow reasonably high quality Nb_3Sn films by "MBE" made it possible to investigate growth of epitaxial Nb_3Sn/insulator bilayers and trilayers with Nb_3Sn and NbN counterelectrodes. The insulators were (1) e-beam evaporated and sputtered Al overlayer thermally or ion-beam oxidized after deposition, Al-Al_2O_3; (2) e-beam evaporated Al_2O_3; (3) thermally evaporated/sublimated CaF_2; and (4) thermally evaporated SrO. These overlayers were deposited at room temperature, except for SrO. The Al overlayer was epitaxial and the thin thermal

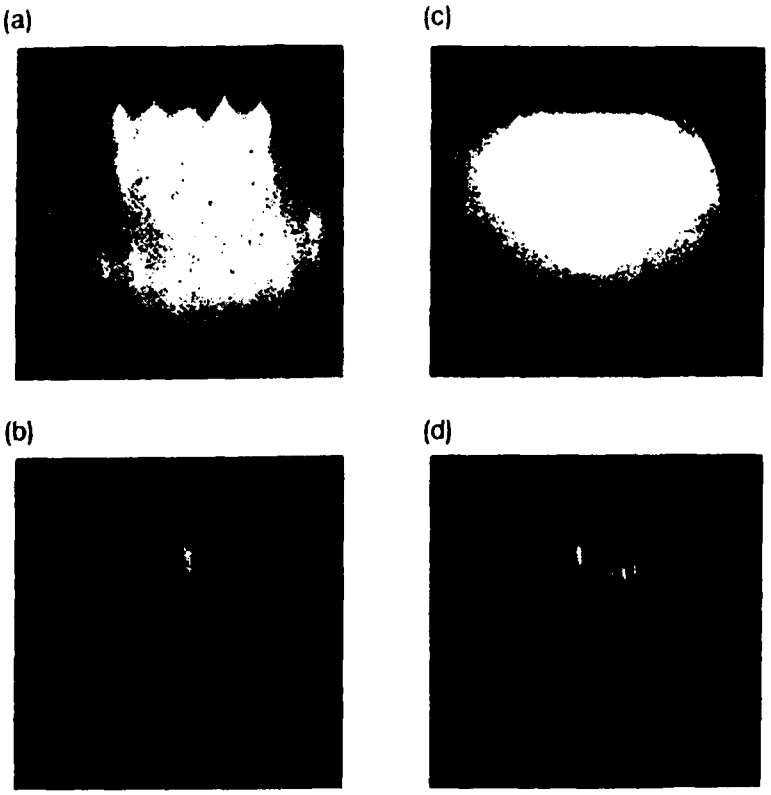

Fig. 14. RHEED patterns of (a) epitaxial Al on Nb_3Sn, (b) oxidized Al–Al_2O_3, (c) evaporated Al_2O_3 and (d) SrO tunnel barriers.

oxide was in epitaxial relationship with the metal, as shown by RHEED patterns in Fig. 14a,b. The evaporated Al_2O_3 was also epitaxial (Fig. 14c). The CaF_2 and SrO overlayers (Fig. 14d) contained random crystallites in an epitaxial matrix.

The $I-V$ characteristics of bilayers with Pb-Bi electrodes (Fig. 15a) showed low subgap conductance and high gap voltage when barrier pinholes were sealed by the native Nb-Sn oxide. This observation was first made by Rudman *et al.* [74]. In contrast, $I-V$ characteristics indicating microshorts in the barrier were obtained with NbN counterelectrodes deposited near room temperature. The microshorts presumably occurred at the native-oxide-sealed pinholes. Ion-beam oxidation of Nb_3Sn/Al-Al_2O_3 was reasonably effective in sealing these pinholes but a rise in conductance at the NbN gap indicated ion-beam-induced damage in Nb_3Sn (Fig. 15b). In the case of CaF_2 and SrO, barrier microshorts were always present.

Fabrication of all-Nb_3Sn junctions required depositing or annealing the counterelectrode at temperatures above 600°C, sufficient for Nb_3Sn formation. In trilayers with Al_2O_3, the counterelectrode deposited at ≥ 700°C was

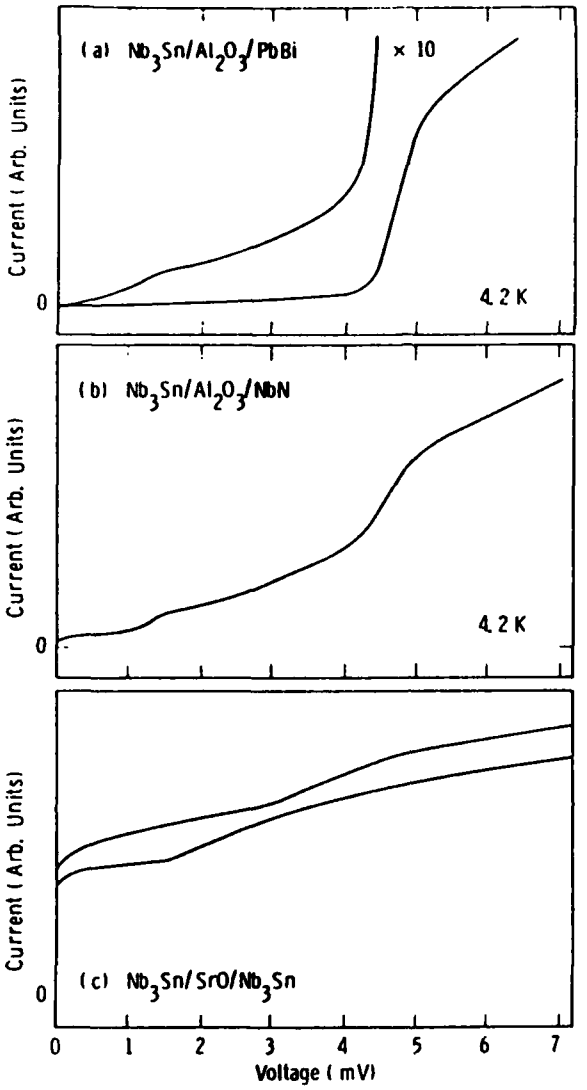

Fig. 15. (a) The $I-V$ characteristics of tunneling into an epitaxial $Nb_3Sn(100)/Al_2O_3$ bilayer using a Pb-Bi counterelectrode. For comparison, characteristics of (b) $Nb_3Sn/Al_2O_3/NbN$ and (c) $Nb_3Sn/SrO/Nb_3Sn$ are also plotted.

epitaxial, according to RHEED, but the reactions at pinholes and Al_2O_3 interfaces were severe enough to result in complete shorts. In one case of a textured SrO barrier, the top Nb_3Sn layer was co-evaporated at ambient temperature and then flash annealed at 650°C. This counterelectrode was polycrystalline by RHEED with no evidence of texturing. The resulting junction contained microshorts and was extremely leaky but a low sumgap voltage of, approximately, 4 meV could be estimated at 4.2 K (Fig. 15c). This suggested that all-Nb_3Sn junctions could be feasible with further process refinements.

In conclusion, the "MBE" approach permitted the authors to grow epitaxial

Nb_3Sn of relatively high quality. It appears that the key unresolved issue in all-Nb_3Sn epitaxial tunnel junction fabrication is the presence of pinholes and/or thin areas in the barrier. High gap voltage Nb_3Sn trilayers would be viable if a very smooth single-crystal base electrode and a completely continuous Al_2O_3 barrier could withstand processing temperatures high enough to obtain epitaxial top layers of Nb_3Sn.

3.4.4. Nb-Ge Films

In the Nb-Ge binary system, the A15 structure is stable between 18.5 and 20 at.% Ge at 900°C [78]. The critical temperature of the stable phase is only 6.5 K, approximately, and the large lattice parameter, $a_0 \geq 0.517$ nm, is typical of anti-site disorder. Even at the peritectic solidus temperature of 1865°C the phase boundary was determined to be substoichiometric, at 23 ± 1 at.% Ge [78]. The nearly stoichiometric, high-T_c A15 phase has been obtained only in the form of films where the presumably metastable material was stabilized. High-T_c film deposition was first achieved by sputtering [79] and later also by co-evaporation and CVD. The highest-T_c films consisted of nearly single A15 phase having $a_0 = 0.512$ to 0.514 nm but often contained small admixtures of the tetragonal or hexagonal Nb_5Ge_3 phase. The mechanism of the metastable Nb_3Ge stabilization, a subject of numerous studies, has not been elucidated satisfactorily. It was, however, observed by Gavaler *et al.* [80] and confirmed by many authors that either incorporation of some oxygen or the presence of a low partial pressure of oxygen (or another impurity) during the deposition was necessary to stabilize the stoichiometric phase. The typical oxygen partial pressure required was found to be in the range of 10^{-6} to 10^{-7} torr.

Dayem *et al.* [81] were the first to observe polycrystalline epitaxial growth of high-T_c Nb-Ge on isomorphic A15 Nb_3Ir polycrystalline films having a matching, adjustable lattice parameter. Figure 16 shows their data of a_0 and T_c vs. at.% Ge. The A15 phase boundary appeared to have shifted to 26.3 at.% Ge and T_c's were much higher than in the same deposition conditions but without Nb_3Ir substrate. This was an indication that epitaxy can contribute to the stabilization of the metastable Nb-Ge phase, at least at background impurity pressures of high 10^{-7} to 10^{-8} torr, which were typically obtained without intentional additions of oxygen. Gavaler *et al.* [82] observed $T_c = 20$ K even in the thinnest (< 20 nm) films co-sputtered on Nb-Ir. On sapphire, however, deposition of a layer at least 100 nm thick was necessary to attain this critical temperature. Evidently, the high-T_c phase was directly nucleated on the Nb-Ir

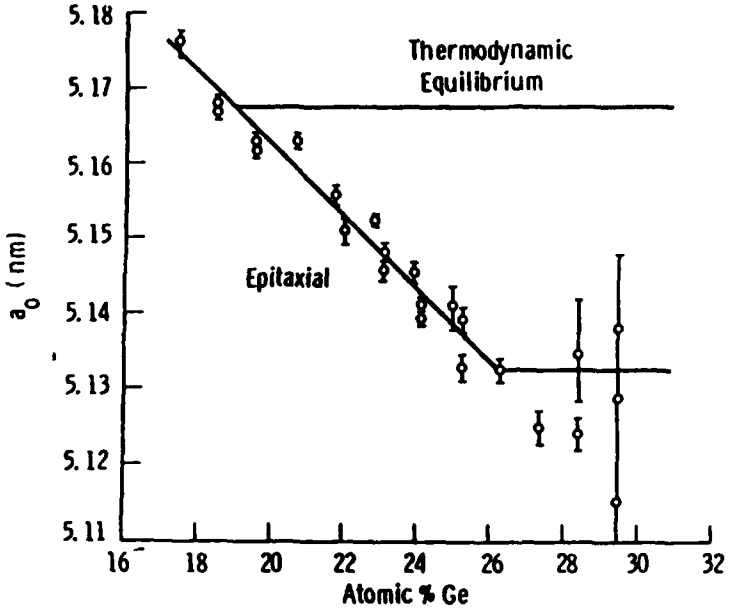

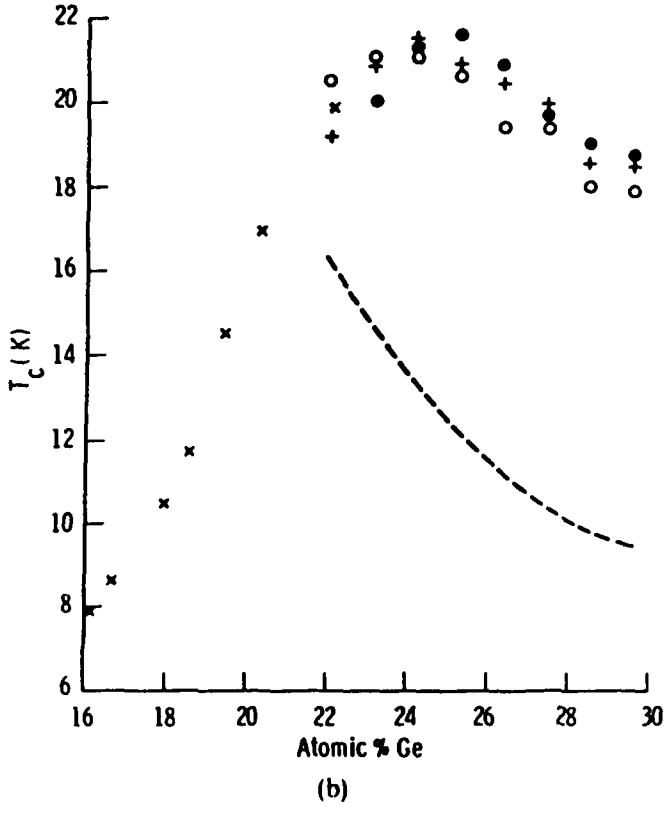

Fig. 16. (a) Lattice parameter and (b) T_c vs. at.% Ge in Nb-Ge films co-evaporated epitaxially on $NbIr$ [81]. The dotted line represents T_c onset in the absence of epitaxy.

substrate, rather than formed as a result of a gradual, homoepitaxial overgrowth.

Kuwasa and Nakano [83] have shown that in UHV of 10^{-8} to 10^{-9} torr (during co-evaporation) the homoepitaxial, polycrystalline nucleation of Nb_3Ge was assisted by the presence of oxygen in the Nb-Ge substrate layer. Subsequent UHV growth produced a phase having T_c's higher than on oxygen-free Nb-Ge but lower than typically obtained in HV deposition.

Asano *et al.* [42] reported heteroepitaxial growth of textured Nb_3Ge films on cubic, yttria stabilized, zirconia (YSZ) single crystals with (100) orientation and $a_0 = 0.512$ to 0.516 nm. Films were magnetron-sputtered simultaneously on both YSZ and $(1\bar{1}02)$ sapphire substrates, presumably in a HV system. The x-ray diffractometer traces indicated that polycrystalline epitaxy occurred with the orientation A15 $Nb_3Ge(100)||$ YSZ(100). Diffraction data for films on sapphire were not given. Figure 17 shows T_c vs. the film thickness for YSZ and sapphire substrates. Indeed, in very thin films, higher T_c (and lower a_0) obtained on YSZ confirmed that these films were stabilized by epitaxy. However, with increasing film thickness, this beneficial YSZ substrate effect gradually disappeared, presumably due to the homoepitaxial over-growth of the higher-T_c phase.

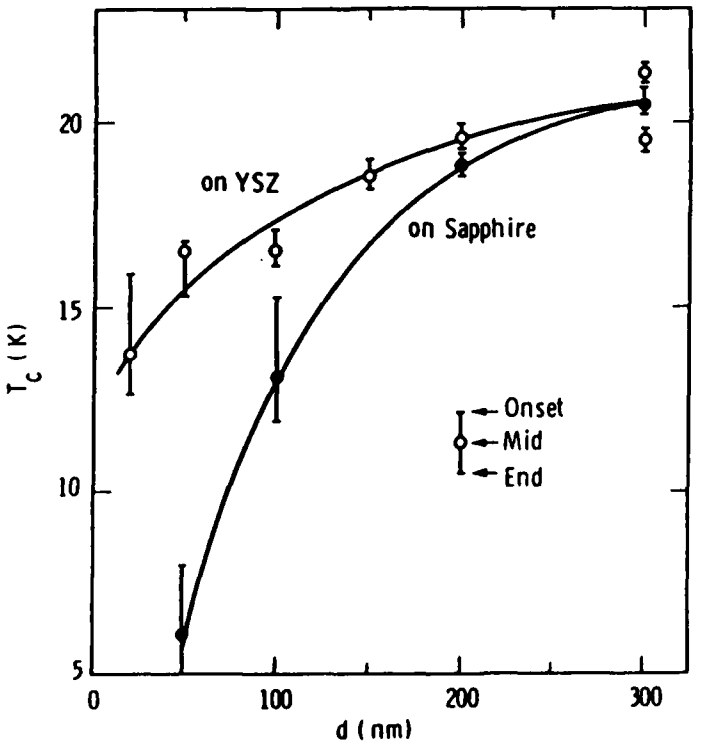

Fig. 17. T_c vs. thickness of Nb-Ge films on YSZ(100) and α-$Al_2O_3(1\bar{1}02)$ [42].

In our "MBE" experiments, Ge was evaporated from an effusion cell and Nb from an e-gun, as in the case of Nb_3Sn [84]. The substrate temperatures were in the range between 820 and 920°C, optimally 880°C. The background pressure was extremely low, 5×10^{-11} torr, and it was possible to deposit films at various low partial pressures of oxygen, up to 2×10^{-9} torr, bled deliberately into the chamber in the proximity of the substrate holder. The *in-situ* electron diffraction (LEED and RHEED) of films 50 to 200 nm thick confirmed that in UHV the A15 Nb-Ge phase can grow epitaxially on a variety of single-crystal substrates, including sapphire, as shown in Table 2.

The x-ray diffraction data were obtained by texture camera only and limited to epitaxial films on single crystal (100) Nb_3Ir [50]. The diffraction spots for the film and substrate could not be resolved well enough to obtain the film lattice parameter as a function of oxygen partial pressure during deposition. However, the T_c versus $p(O_2)$ dependence (Fig. 18), obtained by resistive measurements, showed that epitaxy alone did not stabilize the high-T_c phase. The stable, low-T_c A15 phase dominated in films deposited without oxygen injection. The T_c was increasing with $p(O_2)$ but the onsets did not attain 20 K up to $\geq 10^{-9}$ torr. Evidently, much higher oxygen partial pressures are required for stoichiometric Nb_3Ge stabilization. Only at these higher pressures, a close epitaxial lattice parameter match, obtained with Nb-Ir and

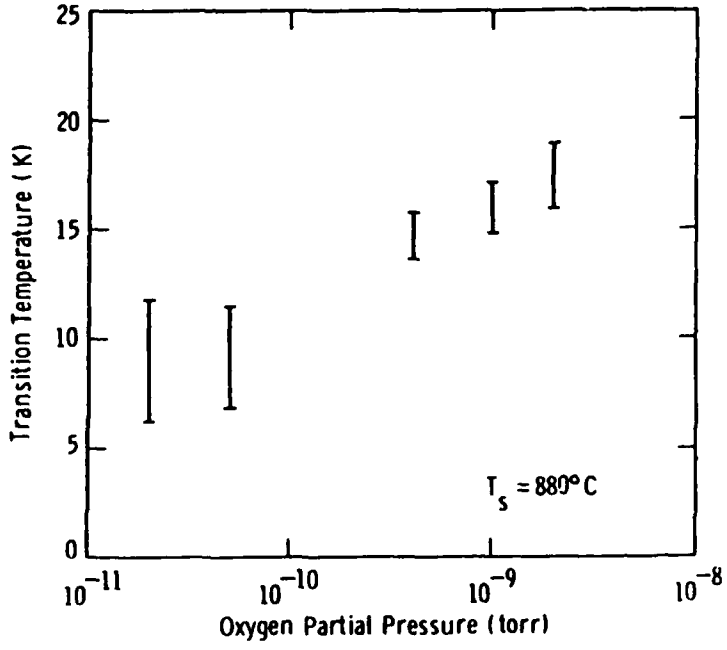

Fig. 18. The T_c of epitaxial Nb_3Ge plotted as a function of the O_2 partial pressure present during deposition.

YSZ substrates but not the sapphire, is contributing to the nucleation and growth of the metastable phase, as shown by the results of Dayem *et al.*, Gavaler *et al.*, and Asano *et al.*, which were summarized above.

In conclusion, we found the UHV "MBE" method to be rather unsuitable for growing epitaxial high-T_c Nb_3Ge films and tunneling structures.

3.5. *High-T_c Oxide Superconductors*

All high-T_c oxide superconductors (HTS) that have $T_c > 35$ K are cuprates, i.e., oxide compounds of copper, an alkaline earth metal(s), and other elements [85,86]. The number of materials and their confirmed T_c's are growing, due to a very high level of effort worldwide. The confirmed record T_c is presently 125 K, in a thallium-based cuprate, $Tl_2Ca_2Ba_2Cu_3O_y$ [87,89]. To date, the most researched material is $YBa_2Cu_3O_7$ (YBCO) and its derivatives in which Y is replaced by another lanthanide (Ln) rare-earth element. The T_c common to $LnBa_2Cu_3O_7$ is 90–95 K.

All HTS cuprates are ceramic materials, very brittle, and environmentally rather unstable. All have tetragonal or orthorhombic crystal structures which are perovskite-related. Each of the Bi- and Tl-based cuprates (BSCCO and TBCCO) crystallizes in several structures in which T_c increases with the number of Cu-O planes in the elementary cell n that are stacked along the c-axis normal to the basal plane [88,89]. The stability of these structures appears to decrease with increasing n, so that a mixture of phases with different n values is being obtained in the highest-T_c compound synthesis. In the case of TBCCO, the number of Tl planes in the unit cell can also vary [89]. At present, the LnBCO family is the most reproducible object of application studies, although the interest in applications of BSCCO and TBCCO is increasing rapidly.

At a first glance, co-evaporation in a "MBE"-type system does not appear to be a method suitable for deposition of oxide films several hundreds of nanometers thick. Sputtering and ion-beam sputtering are more typical methods of oxide deposition. However, the "MBE" hardware has been used by Chaudhari *et al.* [44] to, for the first time, co-evaporate YBCO films on $SrTiO_3$ single-crystal substrates. After their report, the "MBE" of YBCO has been pursued successfully by many experimenters. Thereafter, sputtering and laser evaporation became equally effective, as documented in a multitude of publications in the 1987–88 period. However, as it did not involve "MBE" techniques, most of that work will not be reviewed here.

The particular mode of "MBE" use has been determined by the following structural, chemical, and electronic properties, which are, at least qualitatively, common to all high-T_c cuprates.

(1) The cuprate crystalline phase(s) can, obviously, form only in the presence of oxygen. In addition, the crystal structure and electrical characteristics of the film depend strongly upon deviations of the oxygen concentration from the stoichiometric value. This effect is most pronounced in LnBCO in which oxygen atoms intercalate reversibly into the crystal lattice at relatively low temperatures. The tetragonal $LnBa_2Cu_3O_6$ crystal is an insulator. Upon oxygenation, it transforms into an orthorhombic modification at 6.3 to 6.6 oxygen atoms per unit cell, depending upon the conditions of the process and, at slightly higher oxygen contents, the c-axis lattice parameter exhibits a nonlinear reduction. At this point the crystal becomes superconducting [90]. The highest T_c and optimum superconducting properties of $LnBa_2Cu_3O_x$ are attained when approaching $x = 7.0$ oxygens per unit cell. By controlling x locally, patterned regions of a YBCO film can be easily transformed from superconductor, to semiconductor, to insulator. This may offer a unique flexibility in tailoring devices.

(2) Some constituent elements, especially Tl, have high vapor pressures and are also weakly bound in the crystal lattice. Consequently, synthesis of a stoichiometric compound is only possible at high ambient pressure of the element or with a large excess of Tl in the source. The best near-stoichiometric TBCCO films were obtained by post-annealing in sealed ampoules containing an excess amount of bulk TBCCO [91].

(3) The constituent elements, spurious phases and, to a lesser degree, the compound itself react at high temperatures with most substrate materials and with CO_2 and water vapor in the ambient atmosphere.

(4) The coherence length is extremely short and anisotropic. In these extreme type II superconductors, it decreases with increasing T_c and, along the c-axis, is comparable to the interatomic distance (Table 1). Due to this short range of superconducting interactions, atomic-scale defects disrupt superconductivity. For example, the transfer of current between crystallites in polycrystalline materials is severely limited by imperfect grain boundaries. Tunneling along the c-axis would require crystalline perfection up to the first atomic monolayer at the surface.

(5) The critical parameters, especially J_c and H_c are strongly anisotropic. While the intrinsic (depairing) J_c limit is high (in the 10^8 A/cm^2 range) and

self-field values $J_c \leq 5 \times 10^6$ A/cm^2 have been indeed obtained at 77 K in the a–b plane of nearly single-crystalline films of YBCO on $SrTiO_3$ or MgO crystal substrates, the experimental J_c's along the c-axis are lower, typically by one to two orders of magnitude.

Relatively high partial pressures of oxygen are required to deposit epitaxial cuprate oxide(s) directly from vapor phase or to oxygenate an oxygen-deficient deposit by *in-situ* post-annealing. This is a significant deviation from standard MBE practice which involves UHV. However, the rationale for "MBE" is still to maintain undegraded interfaces in multilayer deposition and *in-situ* surface/interface characterization. A low background pressure of gas-phase impurities is also a requirement well satisfied by "MBE".

Following Chaudhari *et al.* [44], some experimenters used "MBE"-type evaporation chambers to deposit epitaxial films of LnBCO from e-beam or effusion cell sources and MBE was specifically identified as the preparation method. The various film fabrication procedures, however, did not follow the "MBE" methodology, except for *in-situ* substrate characterization [92]. The range of deposition temperatures and pressures was broad. On one extreme was the co-deposition of constituent metals in UHV at temperatures between ambient and 400°C, followed by *ex-situ* oxidation, annealing in oxygen between 850 and 900°C (to crystallize the compound) and by either post-annealing at a lower temperature or cooling slowly in O_2 to approach the desired concentration of 7 oxygen atoms per unit cell [93]. On another extreme was the reactive e-beam co-evaporation on substrates hot enough to obtain a crystalline deposit: T_s = 560 to 650°C at an oxygen partial pressure so high (up to 10^{-3} torr) that the evaporation paths were no longer line-of-sight, making rate control difficult, and the lifetime of e-gun filaments limited to a few hours [94]. In the latter case, Lathrop *et al.* [94] backfilled the chamber with 1 to 20 torr of O_2 at the end of each deposition so that the deposit was slowly cooled in oxygen. Even so, an additional *ex-situ* post-anneal in O_2 was usually necessary.

Generally, in experiments involving co-evaporation from e-gun sources in the presence of oxygen, even at low partial pressures, the precision of the evaporation rate control is impaired due to the oxidation of the molten pool and a possible effect on flux sensor calibration. Specific data are scarce but Terashima *et al.* [109] reported reproducibility within $\pm 5\%$ from the YBCO stoichiometry when operating two e-guns to evaporate Y and Ba in a background pressure of 10^{-5} torr of oxygen. The common characteristic of all films processed *ex-situ* has been a resistive, nonsuperconducting surface

attributed to the interaction with CO_2 and H_2O in the ambient atmosphere. The first, to our knowledge, experiments to *in-situ* fabricate and characterize YBCO film surfaces prior to the deposition of an overlayer were performed in the system of Figs. 2 and 3. Films deposited as an amorphous phase were annealed *in-situ* in the introduction chamber at 1 atm of O_2 pressure and their surfaces characterized by XPS before and after annealing. The two main results were

(1) Oxidation of an oxygen-deficient amorphous deposit caused a segregation of Ba and Y atoms to or toward the surface, thus resulting in a non-superconducting surface layer even in the absence of reactions with H_2O or CO_2 [95]. Rapid thermal ramping to the crystallization temperature was found to minimize the segregation.

(2) Films annealed in this manner were epitaxial, with *c*-axis in the film plane, and their surfaces were at least in part superconducting [96]. Thin Au-overlayers deposited *in-situ* at room temperature after the complete annealing cycle conducted, at 4.2 K, a supercurrent between the YBCO and Nb counterelectrodes. With tunnel barriers of MgO *in-situ* evaporated on Au, unambiguous evidence of tunneling into the YBCO film surface was obtained in YBCO/MgO/Nb junctions with a YBCO gap voltage of 19 mV at 4.2 K, although device-quality junctions have not yet been obtained [97].

These experiments demonstrated again the advantages of an "MBE" approach, although the method of film synthesis by solid state epitaxy was not a desirable one. The post-deposition crystallization annealing of amorphous deposits, at temperatures $>800°C$, was promoting interdiffusion and reactions of substrate and film components. This was producing interface degradation in excess of that found in crystalline deposits (by vapor phase epitaxy), even if post-annealing at the same temperature and time was employed [32,98]. Solid state epitaxy is also unlikely to result in films having single-crystalline quality comparable to that of films deposited from vapor phase, monolayer by monolayer. Finally, the use of high oxygen pressure at high temperatures is hardly compatible with standard "MBE" equipment and requires modifying many components (Section 2) or even the deposition chamber itself. For example, Silver *et al.* [99] constructed a differentially pumped evaporation chamber shown schematically in Fig. 19.

At present, a very promising approach for "MBE", permitting the use of standard equipment, is reactive epitaxial growth from the vapor phase. It does not require high oxygen pressures due to the use of activated or atomic

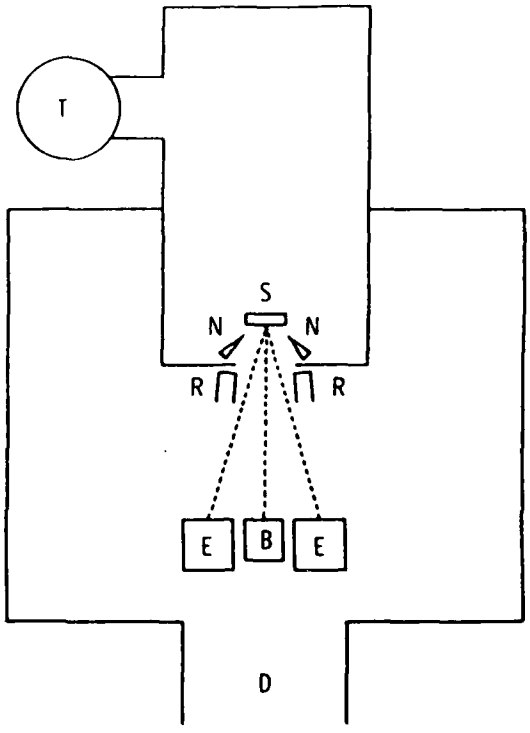

Fig. 19. Schematic of a differentially pumped evaporator [100]. The substrates (S) are in a subchamber pumped by a turbopump (T). Activated oxygen is sprayed on the substrate surface through two nozzles (N). The main part of the chamber, pumped by a diffusion pump (D), contains two e-beam sources (E), one evaporation boat (B), and rate monitors (R).

oxygen. Chamber pressures of $p(O_2) = 10^{-6}$ to 10^{-5} torr appear to be sufficient in this case. Several methods of activated or atomic oxygen generation have been reported as successful in producing YBCO films that did not require any post-annealing at a temperature higher than the deposition temperature. These are

- rf-plasma activation and atomic oxygen generation [99–103],
- atomic oxygen generation by an ozone source [104],
- atomic oxygen generation by NO cracking [105],
- low-energy ion beam generation by a Kaufman source [103] or electron cyclotron resonance (ECR) [106].

Each of the methods permitted the respective authors to deposit superconducting ($T_c \geq 80$ K, $R = 0$), highly epitaxial YBCO films at low substrate temperatures, between 450 and 650°C, either without any post-annealing or with oxygen annealing below the deposition temperature only. It is not clear yet which of these methods will turn out to be the most advantageous and, therefore, generally accepted.

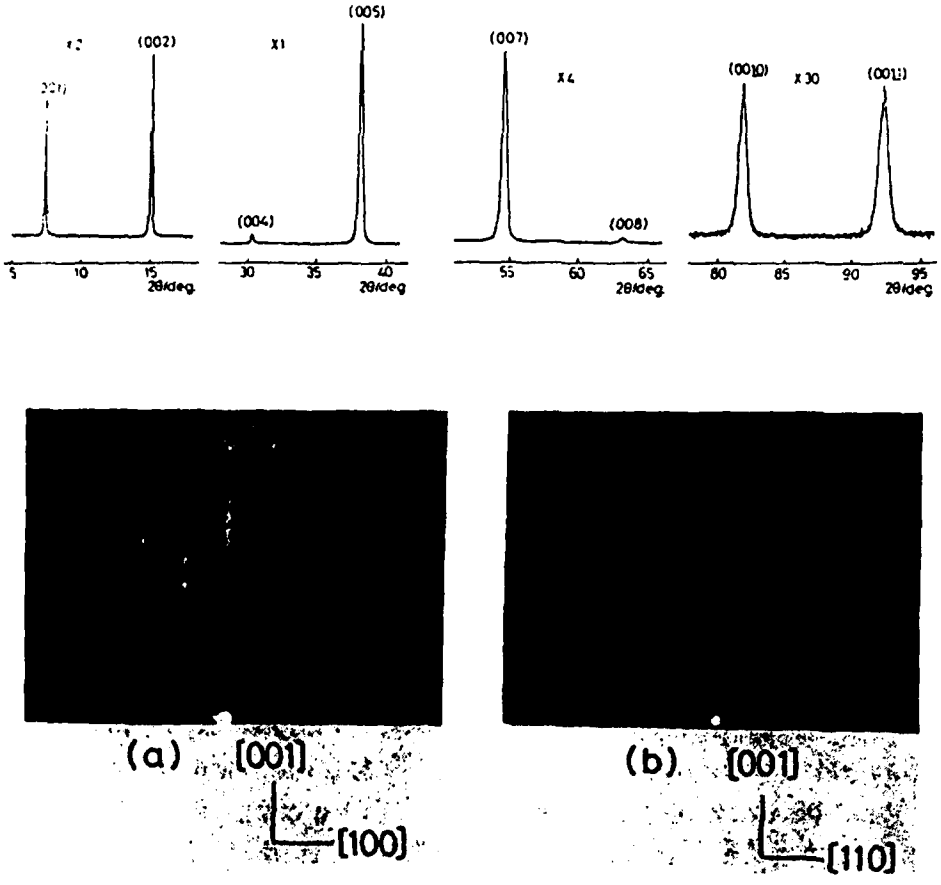

Fig. 20. RHEED and x-ray diffraction patterns for as-grown YBCO(100) 100-nm thick [100,101].

According to Bando *et al.* [100, 101] the oxygen activation by rf-plasma resulted in YBCO films that are probably the best to date, independent of the fabrication method. These films were co-evaporated from two e-guns and one thermal source on single-crystalline $SrTiO_3$ with (100) and (110) orientation and on MgO(100). The deposition temperature was $T_s = 500$ to 700°C, and the chamber pressure was 10^{-5} torr of O_2, while the local pressure of rf-plasma-activated O_2 sprayed at the substrate was 10^{-2} torr. *In-situ* post-annealing in O_2 was limited to temperatures lower than T_s. Figure 20 shows x-ray and electron diffraction patterns of 100-nm thick films deposited on (100) $SrTiO_3$ that suggest a very high degree of texturing and a relatively high surface quality. LEED patterns indicate that these films are, indeed, single crystals [107]. These films had a residual resistivity of only 63 $\mu\Omega$-cm (resistivity ratio of 3.4), were superconducting at 90 K ($R = 0$), and at 77 K exhibited a $J_c = 4 \times 10^{6}$ A/cm^2. The *in-situ* RHEED pattern of a film growing on MgO was characteristic of a perovskite at thicknesses exceeding 0.6 nm. On $SrTiO_3$, a film 10-nm thick was not only crystalline by x-ray

diffraction but had a $T_c = 82$ K ($R = 0$) after low-temperature oxidation. Data by Bando *et al.* and by other authors referenced above offer a strong argument for the use of activated oxygen in vapor-phase epitaxy of YBCO.

Progress in HTS epitaxial film growth and characterization attained by summer–fall of 1988 suggests that "MBE" employing activated oxygen sources may become a leading technique in YBCO layered film device fabrication. It is not clear yet, whether or not a similar approach will be successful with other high-T_c cuprates, and especially with TBCCO. A severe loss of Tl occurs at high temperatures while, thus far, crystallization of high-T_c phases has only been observed close to the compound's melting point.

Section 3.5 was prefaced with a brief comparison of "MBE" growth versus higher-oxygen-pressure techniques for growth of high-T_c films. The successful use of activated oxygen sources to grow epitaxial YBCO films in high vacuum has differentiated "MBE" growth from higher-pressure methods. The benefits of operation in high vacuum are those traditionally associated with MBE: high surface mobility for adatoms, long mean-free paths, and access to the growth surface by various beam techniques. Examples of the last benefit are real-time monitoring by RHEED [102,108] and ion-assisted deposition.

Perhaps the work of Fujita *et al.* [108] is an example that indicates the future direction for superconductor "MBE", although they used dual ion-beam sputtering rather than evaporation. They created artificial superlattices in the Bi-Sr-Ca-Cu-O system on an atomic scale and attempted to grow metastable structures with c-axis unit cell lengths halfway between those of $Bi_2Sr_2Ca_nCu_{n+1}O_x$ ($n = 0, 1, 2$). They failed to stabilize any new phases, but succeeded in performing growth experiments on an atomic scale. A similar approach may be the best method for growing a tunnel barrier in high-T_c Josephson junctions, creating new device structures, stabilizing single-phase films, or searching for new superconductors.

A possibly intrinsic drawback of "MBE" fabrication is the loss of oxygen from the surface of HTS films exposed to UHV and the resulting degradation of the order parameter. Such loss was observed for YBCO by List *et al.* [112]. Use of cold substrate holders may be required to minimize the degradation prior to low-temperature deposition of a protective layer.

In closing, we should note that inherently non-"MBE," high-growth-pressure methods can be incorporated into separate chambers of a "MBE" multi-chamber system, as long as these chambers can be pumped down, after the deposition, to the requisite background pressure of the system. This was demonstrated for sputtering (Fig. 2) but can be equally well done for high-oxygen-pressure laser evaporation or even CVD. The surface oxygen loss problem will persist in these cases.

4. Conclusions

This chapter would have been very brief if we had confined the discussion to a description of technologically useful superconductors grown by MBE techniques defined in a narrow, traditional sense. Instead, we defined "MBE growth" broadly so that it encompassed all growth of highly oriented superconductors that were both deposited by PVD and maintained in an environment suitable for surface analysis and subsequent deposition of oriented film layers. Within the broader scope, MBE techniques have been used successfully to address scientific issues related to electronic applications of conventional superconductors.

However, it is the short coherence lengths and anisotropic properties of HTS materials that will move the use of MBE techniques to the forefront of superconductor technology. Passive electronic devices using HTS will require highly oriented films for low dissipation, low noise, and high current densities. Active devices will require, in addition, attention to problems with surfaces and interfaces that could be ignored in cases where long-coherence-length superconductors such as Nb or Pb were used. The development of active HTS devices will employ the experimental techniques and reopen materials issues already explored for short-coherence-length conventional superconductors—NbN and the A15 compounds.

References

1. Beasley, M.R., and Kircher, C.J. Josephson junction electronics: Material issues and fabrication techniques. *In* "Superconductor Materials Science" (S. Foner and B.B. Schwartz, eds.), pp. 605–684. Plenum Press, New York, (1981).
2. Raider, S.I. Josephson tunnel junctions with refractory electrodes. *IEEE Trans. Magn.* **21**, 110–117 (1985).
3. Braginski, A.I., Gavaler, J.R., Janocko, M.A., and Talvacchio, J. New materials for refractory tunnel junctions: Fundamental aspects. *In* "SQUID '85: Superconducting Quantum Interference Devices and their Applications" (H.D. Hahlbohm and H. Luebbig, eds.), pp. 591–630. Walter de Gruyter, Berlin, 1985.
4. Gallagher, W.J. Theory of Josephson tunneling into proximity-effect sandwiches. *Physica B* **108**, 825–826 (1981).
5. Cuomo, J.J., Laibowitz, R.B., Mayadas, A.F., and Rosenberg, R. Single crystal tunnel devices. United States Patent No. 3,816,845; 1974.
6. Luscher, P.E., and Collins, D.M. Design considerations for molecular beam epitaxy systems. *In* "Molecular Beam Epitaxy" (B.R. Pamplin, ed.), pp. 15–30. Pergamon Press, Oxford, 1980.
7. Talvacchio, J., Janocko, M.A., Gavaler, J.R., and Braginski, A.I. UHV deposition and analysis of thin-film superconductors. *In* "Advances in Cryogenic

Engineering Materials, Vol. 32" (A.F. Clark and R.P. Reed, eds.), pp. 527–541. Plenum, New York, 1986.

8. Hammond, R.H. Electron beam evaporation synthesis of A15 superconducting compounds: Accomplishments and prospects. *IEEE Trans. Magn.* **11**, 201–207 (1975).
9. Bean, J.C., and Sadowski, E.A. Silicon MBE apparatus for uniform high-rate deposition on standard format wafers. *J. Vac. Sci. Technol.* **20**, 137–142 (1982).
10. Schellingerhout, J., Janocko, M.A., Klapwijk, T.M., and Mooij, J.E. Rate control for electron gun evaporation. *Rev. Sci. Instrum.* **60**, 1177–1183 (1988).
11. Becker, C.H., and Gillen, K.T. (1984). Surface analysis by nonresonant multiphoton ionization of desorbed or sputtered species. *Anal. Chem.* **56**, 1671–1674 (1984).
12. Dushman, S. "Scientific Foundations of Vacuum Technique." Wiley, New York, 1962.
13. Houdy, Ph., Sirat, J.A., Theeten, J.B., Landesman, J.P., Baudry, H., Monneraye, M., Schiller, C., and Patillon, J.N. Amorphization evidence from kinetic ellipsometry in monolayer-controlled deposition of RF sputtered YBaCuO compounds. *In* "Thin Film Processing and Characterization of High-Temperature Superconductors" (J.M.E. Harper, R.J. Colton, and L.C. Feldman, eds.), pp. 122–129. Am. Inst. of Phys., New York, 1988.
14. Cohen, P.I., Pukite, P.R., van Hove, J.M., and Lent, C.S. Reflection high energy electron diffraction studies of epitaxial growth on semiconductor surfaces. *J. Vac. Sci. Tech. A* **4**, 1251–1258 (1986).
15. Park, S.I., Marshall, A.F., Hammond, R.H., Geballe, T.H., and Talvacchio, J. The role of ion-beam cleaning in the growth of strained-layer epitaxial thin transition metal films. *J. Mater. Res.* **2**, 446–455 (1987).
16. Adachi, H., Setsune, K., and Wasa, K. Superconductivity of La-Sr-Cu-O single-crystal thin films. *Japan. J. Appl. Phys.* supp. **26-3**, 1139–1141 (1987).
17. Enomoto, Y., Murakami, T., Suzuki, M., and Moriwaki. K. Largely anisotropic superconducting critical current in epitaxially grown $Ba_2YCu_3O_{7-y}$ thin film. *Japan. J. Appl. Phys.* **26**, L1248–1250 (1987).
18. Talvacchio, J., Sinharoy, S., and Braginski, A.I. Surface stability of NbN single-crystal films. *J. Appl. Phys.* **62**, 611–614 (1987).
19. Lagally, M.G. Diffraction Techniques. *In* "Methods of Experimental Physics, Vol. 22" (R.L. Park and M.G. Lagally, eds.), p. 237. Academic Press, New York, 1985.
20. Talvacchio, J., Gavaler, J.R., and Braginski, A.I. Epitaxial niobium nitride/insulator layered structures. *In* "Proceedings TMS–AIME: Metallic Multilayers and Epitaxy" (M. Hong, D.U. Gubser, and S.A. Wolf, eds.), pp. 109–134. The Metallurgical Society, Pittsburgh, 1987.
21. Jona, F. LEED crystallography. *J. Phys. C* **111**, 4271–4306, (1987).
22. Talvacchio, J., Sinharoy, S., and Takei, K. Low-energy electron diffraction study of epitaxial NbN tunnel junctions. In preparation.
23. Talvacchio, J., and Braginski, A.I. Lattice-matched oxide barriers for NbN tunnel junctions. *In* "Proc. Intl. Superconductivity Electronics Conference" (S. Hasuo, ed.), pp. 309–312. Tokyo, 1987.

24. Laiho, R., Heikkila, L., and Snellman, H. Microstructural investigation of the high-T_c superconductor $YBa_2Cu_3O_x$ with a scanning tunneling microscope. *J. Appl. Phys.* **63**, 225–227 (1988).
25. Kellogg, G.L., and Brenner, S.S. Investigations of superconducting and non-superconducting $YBa_2Cu_3O_{7-x}$ by field ion microscopy, atom-probe mass spectroscopy and field electron emission. *J. de Phys.* **49**, C6, 465–475 (1988).
26. Siegbahn, K. "ESCA Applied to Free Molecules." North Holland, Amsterdam, 1969.
27. Kwo, J., Wertheim, G.K., Gurvitch, M., and Buchanan, D.N.E. X-ray photoelectron study of surface oxidation of Nb/Al overlayer structures. *Appl. Phys. Lett.* **40**, 675–678 (1982).
28. Briggs, D., and Seah, M.P., eds. "Practical Surface Analysis." Wiley, New York, 1983.
29. Laibowitz, R.B., and Cuomo, J.J. Tunneling sandwich structures using single-crystal niobium films. *J. Appl. Phys.* **41**, 2748–2750 (1970).
30. O'Neal, J.E., and Wyatt, R.L. Hetero-epitaxial films of niobium on sapphire. *Thin Films* **2**, 71–81 (1971).
31. Durbin, S.M., Cunningham, J.E., and Flynn, C.P. Growth of single-crystal metal superlattices in chosen orientations. *J. Phys. F: Met. Phys.* **12**, L75–L78 (1982).
32. Talvacchio, J., Janocko, M.A., Braginski, A.I., and Gavaler, J.R. Comparison of $YBa_2Cu_3O_7$ films grown by solid state and vapor-phase epitaxy. *IEEE Trans. Magn.* **25**, 2538–2541 (1989).
33. Sosniak, J. The deposition of niobium thin films by dc diode and substrate bias sputtering. *J. Appl. Phys.* **39**, 4157–4163 (1968).
34. Eizenberg, M., Smith, D.A., Heiblum, M., and Segmuller, A. Electron beam evaporation of oriented Nb films onto GaAs crystals in ultrahigh vacuum. *Appl. Phys. Lett.* **49**, 422–424 (1986).
35. Talvacchio, J., Janocko, M.A., and Greggi, J. Properties of evaporated Mo-Re thin-film superconductors. *J. Low Temp. Phys.* **64**, 395–408 (1986).
36. Oya, G., and Onodera, Y. Transition temperatures and crystal structures of single-crystal and polycrystalline NbN films. *J. Appl. Phys.* **45**, 1389 (1974).
37. Talvacchio, J., and Braginski, A.I. Tunnel junctions fabricated from coherent NbN/MgO/NbN and $NbN/Al_2O_3/NbN$ structures. *IEEE Trans. Magn.* **23**, 859–862 (1987).
38. Noskov, V.L., Titenko, Y.V., Korzhinskii, F.I., Zelenkevich, R.L., and Komashko, V.A. Heteroepitaxial layers of niobium nitride on sapphire. *Sov. Phys. Crystallogr.* **25**, 504–508 (1980).
39. Marshall, A.F., Hellman, F., and Oh, B. Epitaxy of Nb_3Sn films on sapphire. *In* "Layered Structures, Epitaxy, and Interfaces; MRS Vol. 37" (J.M. Gibson and L.R. Dawson, eds.), p. 517. Materials Research Society, Pittsburgh, 1985.
40. Janocko, M.A., Braginski, A.I., Gavaler, J.R., Talvacchio, J., and Walker, E. Properties of epitaxial Nb_3Ge films on Nb_3Ir and Nb_3Sn single crystals. *Bull. Am. Phys. Soc.* **31**, 238 (1986).
41. Gavaler, J.R., Braginski, A.I., Janocko, M.A., and Talvacchio, J. Epitaxial growth of high-T_c superconducting films. *Physica* 135B, 148–153 (1985).
42. Asano, H., Tanabe, K., Katoh, Y., and Michikami, O. Epitaxial growth of

superconducting Nb_3Ge Films on YSZ single-crystal substrates. *Japan. J. Appl. Phys.* **27**, 35–39 (1988).

43. Suzuki, M., Enomoto, Y., Moriwaki, K., and Murakami, T. Anisotropic properties of superconducting $(La_{1-x}Sr_x)_2CuO_4$ single-crystal thin films. *Japan. J. Appl. Phys.* **26**, L1921–L1924 (1987).
44. Chaudhari, P., Koch, R.H., Laibowitz, R.B., McGuire, T.R., and R.J. Gambino Critical current measurements in epitaxial films of $YBa_2Cu_3O_{7-x}$. *Phys. Rev. Lett.* **58**, 2684–2687 (1987).
45. Simon, R.W., Platt, C.E., Lee, A.E., Lee, C.S., Daly, K.P., Wire, M.S., Luine, J.A., and Urbanik, M. Low-loss substrate for epitaxial growth of high-temperature superconductor thin films. *Appl. Phys. Lett.* **53**, 2677–2679 (1988).
46. Sandstrom, R.L., Giess, E.A., Gallagher, W.J., Segmuller, A., Cooper, E.I., Chisholm, M.F., Gupta, A. Shinde, S., and Laibowitz, R.B. Lanthanum gallate substrates for epitaxial high-T_c superconducting thin films. *Appl. Phys. Lett.* **53**, 1874–1876 (1988).
47. Feenstra, R., Boatner, L.A., Budai, J.D., Christne, D.K., Galloway, M.D., and Poker, D.B. Epitaxial superconducting thin films of $YBa_2Cu_3O_{7-x}$ on $KTaO_3$ single crystals. *Appl. Phys. Lett.* **54**, 1063–1065 (1989).
48. Höhler, A., Guggi, D., Neeb, H., and Heiden, C. Fully textured growth of $YBa_2Cu_3O_{7-\delta}$ films by sputtering on $LiNbO_3$ substrates. *Appl. Phys. Lett.* **54**, 1066–1067 (1989).
49. Royer, L. Experimental research on parallel growth or mutual orientation of crystals of different species. *Bull. Soc. Fr. Mineral. Crystallogr.* **51**, 7 (1928).
50. Sinharoy, S., Braginski, A.I., Talvacchio, J., and Walker, E. A LEED, AES and XPS study of single crystal Nb_3Ir substrates. *Surf. Science* **167**, 401–416 (1986).
51. Braginski, A.I., Gavaler, J.R., and Schultze, K. Formation of A15 phase in expitaxial and polycrystalline Nb-Sn and Nb-Al diffusion couples. *In* "Advances in Cryogenic Engineering—Materials, Vol. 32" (A.F. Clark and R.P. Reed, eds.), pp. 585–592. Plenum, New York, 1986.
52. Claassen, J.H., Wolf, S.A., Qadri, S.B., and Jones, L.D. Epitaxial growth of niobium thin films. *J. Cryst. Growth* **81**, 557–561 (1987).
53. McWhan, D.B. Structure and coherence of metallic superlattices. *In* "Layered Structures, Epitaxy, and Interfaces; MRS Vol. 37" (J.M. Gibson and L.R. Dawson, eds.), p. 483. Materials Research Society, Pittsburgh, 1985.
54. O'Neal, J.E., and Rath, B.B. Crystallography of epitaxially grown molybdenum on sapphire. *Thin Solid Films* **23**, 363–380 (1974).
55. Durbin, S.M., Buchanan, D.S., Cunningham, J.E., and Ginsberg, D.M. Observation of tunneling anisotropy in superconducting niobium crystals. *Phys. Rev. B.* **28**, 6277–6280 (1983).
56. Darlinski, A., and Halbritter, J. Angle-resolved XPS studies of oxides at NbN, NbC, and Nb surfaces. *Surf. Inter. Anal.* **10**, 223–237 (1987).
57. Pollak, R.A., Stolz, H.J., Raider, S.I., and Marks, R.F. Chemical composition and interface chemistry of very thin Nb_2O_5 films prepared by rf plasma oxidation. *Oxidation of Metals* **20**, 185–192 (1983).
58. Raider, S.I., Johnson, R.W., Kuan, T.S., Drake, R.E., and Pollak, R.A.

Characterization of Nb/Nb oxide structures in Josephson tunnel junctions. *IEEE Trans. Magn.* **19**, 803–806 (1983).

59. Celaschi, S., Geballe, T.H., and Lowe, W.P. Tunneling properties of single crystal $Nb/Nb_2O_5/Pb$ Josephson junctions. *Appl. Phys. Lett.* **43**, 794–796 (1983).
60. Henkels, W.H. and Kircher, C.J. Penetration depth measurements on type II superconducting films. *IEEE Trans. Magn.* **13**, 63–66 (1977).
61. Braginski, A.I., Talvacchio, J., Janocko, M.A., and Gavaler, J.R. Crystalline oxide tunnel barriers formed by thermal oxidation of aluminum overlayers on superconductor surfaces. *J. Appl. Phys.* **60**, 2058–2064 (1986).
62. Kodama, J., Itoh, M., and Hirai, H. Superconducting transition temperature versus thickness of Nb films on various substrates. *J. Appl. Phys.* **54**, 4050–4052 (1983).
63. Reible, S.A. Wideband analog signal processing with superconductive circuits. *In* "1982 Ultrasonics Symposium Proceedings," pp. 190–201. IEEE, New York, 1982.
64. McAvoy, B.R., Wagner, G.R., Adam, J.D., and Talvacchio, J. Superconducting stripline resonator performance. *IEEE Trans. Magn.* **25**, 1104–1106 (1989).
65. Face, D.W., Prober, D.E., McGrath, W.R., and Richards, P.L. High quality tantalum superconducting tunnel junctions for microwave mixing in the quantum limit. *Appl. Phys. Lett.* **48**, 1098–110 (1986).
66. Kosaka, S. and Onodera, Y. Epitaxial deposition of niobium nitride by sputtering. *Japan. J. Appl. Phys.* Suppl. **2-1**, 613–616 (1974).
67. Yamashita, T., Hamasaki, K., and Komata, T. Epitaxial growth of NbN on MgO film. *In* "Advances in Cryogenic Engineering—Materials, Vol. 30" (A.F. Clark and R.P. Reed, eds.), pp. 616–626. Plenum, New York, 1986.
68. Shoji, A., Aoyagi, M., Kosaka, S., Shinoki, F., and Hayakawa, H. NbN Josephson tunnel junctions with MgO barriers. *Appl. Phys. Lett.* **46**, 1098–1100 (1985).
69. Knapton, A.G. The Mo-Re system. *J. Inst. Metals* **87**, 62–64 (1958).
70. Gavaler, J.R., Janocko, M.A., and Jones, C.K. A-15 structure Mo-Re superconductor. *Appl. Phys. Lett.* **21**, 179–180 (1972).
71. Postnikov, V.S., Postnikov V.V., and Zheleznyi, V.S. Superconductivity in Mo-Re system alloy films produced by electron beam evaporation in high vacuum. *Phys. Stat. Solidi* **A39**, K21–23 (1977).
72. Testardi, L.R., Hauser, J.J., and Read, M.H. Enhanced superconducting T_c and structural transformation in Mo-Re alloys. *Solid State Commun.* **9**, 1829–1831 (1971).
73. Brophy, J.H., Rose, R.M., and Wulff, J. On the solubility of interstitial elements in binary transition metal alloys. *J. Less-Common Metals* **5**, 90–91 (1963).
74. Rudman, D.A., Hellman, F., Hammond, R.H., and Beasley, M.R. A15 tunnel junction fabrication and properties. *J. Appl. Phys.* **55**, 3544–3553 (1984).
75. Hellman, F., Talvacchio, J., and Geballe, T.H. A new look at the growth of thin films of Nb-Sn. *In* "Advances in Cryogenic Engineering—Materials, Vol. 32" (A.F. Clark and R.P. Reed, eds.), pp. 593–602. Plenum, New York, 1986.
76. Talvacchio, J., Braginski, A.I., Janocko, M.A., and Bending, S.J. Tunneling and

interface structure of oxidized metal barriers on A15 superconductors. *IEEE Trans. Magn.* **21**, 521–524 (1985).

77. Schellingerhout, J. Unpublished analytical data. Technological University of Delft, Netherlands, 1986.
78. Jorda, J.L., Fluekiger, R., and Muller, J. The phase diagram of the Nb-Ge system. *J. Less-Common Metals* **62**, 25–37 (1978).
79. Gavaler, J.R. Superconductivity in Nb-Ge films above 22 K. *Appl. Phys. Lett.* **23**, 480–482 (1973).
80. Gavaler, J.R., Miller, J.W., and Appleton, B.R. Oxygen distribution in sputtered Nb-Ge films. *Appl. Phys. Lett.* **28**, 237–239 (1976).
81. Dayem, A.H., Geballe, T.H., Zubeck, R.B., Hallak, A.B., and Hull, Jr. G.W. Epitaxial growth of high T_c superconducting Nb_3Ge on Nb_3Ir. *Appl. Phys. Lett.* **30**, 541–543 (1977).
82. Gavaler, J.R., Braginski, A.I., Ashkin, A., and Santhanam, A.T. Thin films and metastable phases. *In* "Superconductivity in d- and f-Band Metals" (H. Suhl and M.B. Maple, eds.), pp. 25–36. Academic Press, New York, 1980.
83. Kuwasa, Y., and Nakano, S. Correlation of homoepitaxial growth of high-T_c A15 Nb_3Ge with characteristics of substrate surface. *J. Low Temp. Phys.* **61**, 45–53 (1985).
84. Braginski, A.I., Janocko, M.A., Gavaler, J.R., and Talvacchio, J. Unpublished results, presented at the 1987 CEC–ICMC, 1987.
85. Bednorz, J.G., and Müller, K.A. Possible high T_c superconductivity in the Ba-La-Cu-O system. *Z. Phys. B* **64**, 189–193 (1986).
86. Wu, M., Ashburn, J.R., Torng, C.J., Hor, P.H., Meng, R.L., Gao, L., Huang, Z.J., Wang, Y.Q., and Chu, C.W. Superconductivity at 93 K in a new mixed phase Y-Ba-Cu-O compound system at ambient pressure. *Phys. Rev. Lett.* **58**, 908–910 (1987).
87. Parkin, S.S.P., Lee, V.Y., Engler, E.M., Nazzal, A.I., Huang, T.C., Gorman, G., Savoy, R., and Beyers, R. Bulk superconductivity at 125 K in $Tl_2Ca_2Ba_2Cu_3O_x$. *Phys. Rev. Lett.* **60**, 2539–2542 (1988).
88. Tarascon, J.M., McKinnon, W.R., Barboux, P., Hwang, D.M., Bagley, B.G., Greene, L.H., Hull, G.W., LePage, Y., Stoffel, N., and Giroud, M. Preparation, structure and properties of the superconducting compound series $Bi_2Sr_2Ca_{n-1}Cu_nO_y$ with $n = 1,2$ and 3. *Phys. Rev. B.* **38**, 8885–8892 (1988).
89. Parkin, S.S.P., Lee, V.Y., Nazzal, A.I., Savoy, R., Beyers, R., and La Placa, S.J. $Tl_1Ca_{n-1}Ba_2Cu_nO_{2n+3}$ ($n = 1,2,3$): A new class of crystal structures exhibiting superconductivity at up to 110 K. *Phys. Rev. Lett.* **61**, 750–753 (1988).
90. Cava, R.J., Battlog, B., Sunshine, S.A., Siegrist, T., Fleming, R.M., Rabe, K., Schneemeyer, L.F., Murphy, D.W., van Dover, R.B., Gallagher, P.K., Glarum, S.H., Nakahara, S., Farrow, R.C., Krajewski, J.J., Zahurak, S.M., Waszczak, J.V., Marshall, J.H., Marsch, P., Rupp, Jr., L.W., Peck, W.F., and Rietman, E.A. Studies of oxygen-deficient $YBa_2Cu_3O_{7-\delta}$ and superconducting Bi(Pb)-Sr-Ca-Cu-O. *Physica C* **153–155**, 560–565 (1988).
91. Lee, W.Y., Lee, V.Y., Salem, J., Huang, T.C., Savoy, R., Bullock, D.C., and Parkin, S.S.P. Superconducting Tl-Ca-Ba-Cu-O thin films with zero resistance at temperatures of up to 120 K. *Appl. Phys. Lett.* **53**, 329–331 (1988).

92. Kwo, J., Hsieh, T.C., Hong, M., Liou, S.H., Davidson, B.A., and Feldman, L.C. Structural and superconducting properties of orientation-ordered $YBa_2Cu_3O_{7-x}$ films prepared by molecular-beam epitaxy. *Phys. Rev. B* **36**, 4039–4042 (1987).
93. Gavaler, J.R., and Janocko, M.A. Data quoted by Braginski A.I., Study of superconducting oxides at Westinghouse. *In* "Novel Superconductivity" (S.A. Wolf and V.Z. Kresin, eds.), pp. 935–950. Plenum Press, New York, 1987.
94. Lathrop, D.K., Russek, S.E., and Buhrman, R.A. Production of $YBa_2Cu_3O_{7-y}$ superconducting thin films *in situ* by high-pressure reactive evaporation and rapid thermal annealing. *Appl. Phys. Lett.* **51**, 1554–1556 (1987).
95. Gavaler, J.R., and Braginski, A.I. Near surface atomic segregation in YBCO thin films. *Physica C* **153–155**, 1435–1436 (1988).
96. Braginski, A.I., Talvacchio, J., Gavaler, J.R., Forrester, M.G., and Janocko, M.A. *In-situ* fabrication, processing and characterization of superconducting oxide films. *In* "SPIE Proceedings Vol. 948, High-T_c Superconductivity: Thin Films and Devices" (R.B. van Dover and C.C. Chi, eds.), pp. 89–98. SPIE, Bellingham, Washington, 1988.
97. Gavaler, J.R., Forrester, M.G., and Talvacchio, J. Properties of YBCO-based tunnel junctions. *Physica C* in press (1989).
98. Wu, X.D., Venkatesan, T., Inam, A., Chase, E.W., Chang, C.C., Yeon, Y., Croft, M., Magee, C., Odom, R.W., and Radicati, F. Versatility of pulsed laser deposition technique for preparation of high-T_c superconducting thin films. *In* "SPIE Proceedings Vol. 948, High-T_c Superconductivity: Thin Films and Devices (R.B. van Dover and C.C. Chi, eds.), pp. 50–65. SPIE, Bellingham, Washington, 1988.
99. Silver, R.M., Berezin, A.B., Wendman, M., and de Lozanne, A.L. As-deposited superconducting Y-Ba-Cu-O thin films on Si, Al_2O_3, and $SrTiO_3$ substrates. *Appl. Phys. Lett.* **52**, 2174–2176 (1988).
100. Bando, Y., Terashima, T., Iijima, K., Yamamoto, K., Hirata, K., and Mazaki, H. Single crystal $YBa_2Cu_3O_{7-x}$ thin film by activated reactive evaporation. *Physica C* **153–155**, 810–811 1988).
101. Bando, Y., Terashima, T., Iijima, K., Yamamoto, K., Hirata, K. and Mazaki, H. Single crystal $YBa_2Cu_3O_{7-x}$ thin film by activated reactive evaporation. *In* "FED-65: Extended Abstracts of Future Electron Devices Workshop," pp. 11–16. Miyagi-Zao, 1988.
102. Kwo, J., Hong, M., Trevor, D.J., Fleming, R.M., White, A.E., Farrow, R.C., Kortan, A.R., and Short, K.T. *In-situ* epitaxial growth of $YBa_2Cu_3O_{7-x}$ films by molecular beam epitaxy with an activated oxygen source. *Appl. Phys. Lett.* **53**, 2683–2685 (1988).
103. Missert, N., Hammond, R.H., Mooij, J.E., Matijasevic, V., Rosenthal, P., Geballe, T.H., Kapitulnik, A., Beasley, M.R., Laderman, S.S., Lu, C., Garwin, E., and Barton, R. *In-situ* growth of superconducting YBaCuO using reactive electron-beam coevaporation. *IEEE Trans. Magn.* **25**, 2418–2421 (1989).
104. Berkley, D.D., Johnson, B.R., Anand, N., Beauchamp, K.M., Conroy, L.E., Goldman, A.M., Maps, J., Mauersberger, K., Mecartney, M.L., Morton, J., Tuominen, M., and Zhang, Y.-J. *In situ* formation of superconducting

$YBa_2Cu_3O_{7-x}$ thin films using pure ozone vapor oxidation. *Appl. Phys. Lett.* 53, 1973–1975 (1988).

105. Evetts, J. Unpublished data (Cambridge University), 1988.
106. Moriwaki, K., Enomoto, Y., Kubo, S., and Murakami, T. As-deposited superconducting $Ba_2YCu_3O_{7-y}$ films using ECR ion beam oxidation. *Japan. J. Appl. Phys.* 27, L2075–L2077 (1988).
107. Sakisaka, Y., Komeda, T., Maruyama, T., Onchi, M., Kato, H., Aiura, Y., Yanashima, H., Torashima, T., Bando, Y., Iijima, K., Yamamoto, K., and Hiata, K. Angle-resolved photoemission investigation of the electronic band properties of $YBa_2Cu_3O_{7-x}$ (001). *Phys. Rev.* B 39, 9080–9090 (1989).
108. Fujita, J., Tatsumi, T., Yoshitake, T., and Igarashi, H. Film fabrication of artificial (BiO)/(SrCaCuO) layered structure. *In* "Science and Technology of Thin-Film Superconductors" (R. McConnell and S.A. Wolf, eds.), Plenum, New York, 175–184, 1989.
109. Terashima, T., Iijima, K., Yamamoto, K., Takada, J., Hirata, K., Mazaki, H., and Bando, Y. Formation and properties of $YBa_2Cu_3O_{7-x}$ single-crystal thin films by activated reactive evaporation. *J. Crystal Growth* 95, 617–620 (1989).
110. Park, S.I., and Geballe, T.H. Superconductive tunneling in ultrathin Nb films. *Phys. Rev. Lett.* 57, 901–904 (1986).
111. Kwo, J., Hong, M., and Nakahara, S. Growth of rare-earth single crystals by molecular beam epitaxy: The epitaxial relationship between hcp rare earth and bcc niobium. *Appl. Phys. Lett.* 49, 319–321 (1986).
112. List, R.S., Arko, A.J., Fisk, Z., Cheong, S.-W., Conradson, S.D., Thompson, J.D., Pierce, C.B., Peterson, D.E., Bartlett, R.J., Shinn, N.D., Schirber, J.E., Veal, B.W., Paulikas, A.P., and Campuzano, J.C. Photoemission from single crystals of $EuBa_2Cu_3O_{7-x}$ cleaved below 20 K: Temperature-dependent oxygen loss. *Phys. Rev. B* 38, 11966–11969 (1988).
113. Gavaler, J.R., Talvacchio, J., and Braginski A.I. Epitaxial growth of NbN films. *In* Advances in Cryogenic Engineering—Materials, Vol. 32 (A.F. Clark and R.P. Reed, eds.), pp. 627–633. Plenum Press, New York, (1986).
114. Poppe, U., Prieto, R., Schubert, J., Soltner, H., Urban, K., and Buchal C. Epitaxial multilayers of $YBa_2Cu_3O_7$ and $PrBa_2Cu_3O_7$ as a possible basis for superconducting electronic devices. *Solid State Commun.* 71, 569–572 (1989).
115. Rogers, C.T., Inam, A., Hegde, M.S., Dutta, B., Wu, X.D., and Venkatesan, T. Fabrication of heteroepitaxial $YBa_2Cu_3O_{7-x}$-$PrBa_2Cu_3O_{7-x}$-$YBa_2Cu_3O_{7-x}$ Josephson devices grown by laser deposition. *Appl. Phys. Lett* 55, 2031–2034 (1989).
116. Shoji, A., Aoyagi, M., Kosaka, S., and Shinoki, S. Temperature-dependent properties of niobium nitride Josephson tunnel junctions. *IEEE Trans. Magn.* 23, 1464–1467 (1987).
117. Song, S.N., Jin, B.Y., Yang, H.Q., Ketterson, J.B., and Schuller, I.K. Preparation of large-area NbN/AlN/NbN Josephson junctions. *Jpn. J. Appl. Phys. Suppl.* 26–3, 1615–1616 (1987).

2nd Workshop on High Temperature Superconducting Electron Devices
R&D Association for Future Electron Devices, June 7-9, 1989, in Shikabe, Hokkaido, Japan. pp

PREPARATION AND CHARACTERIZATION OF SUPERCONDUCTING SURFACES IN HIGH-T_c SUPERCONDUCTORS*

G. R. Wagner, R. M. Silver,** J. Talvacchio,
J. R. Gavaler, and A. J. Panson
Westinghouse R&D Center, Pittsburgh, PA 15235, USA

ABSTRACT

We report the results of *in-situ* XPS and UPS studies of the surface of sputtered HTS films. Stoichiometric cation composition within several lattice constants of the surface was achieved by a rapid (~10°C/min) *in-situ* anneal of YBCO films. The I-V characteristics of Nb/MgO/YBCO junctions, fabricated without exposure to the ambient, indicate that the YBCO surface is superconducting and some evidence of a gap at 20 mV. UPS studies of the rapidly annealed films show that cooling *in-situ* to 50 K in O_2 before exposure to vacuum produces a metallic surface within the escape depth of the electrons, as evidenced by a measured non-zero density of states at the Fermi edge. Subsequent warming to room temperature in vacuum produces a surface with no measurable density of states.

INTRODUCTION

The properties of S-I-S or S-N-S Josephson junctions are strongly dependent on the surface properties of the superconductor within a coherence length of the interface with an insulator or normal metal. The coherence lengths for all of the high-T_c oxide superconductors are anisotropic and small, in the range of 0.2 to 3 nm. This paper reports on the results of three complementary techniques – tunneling, XPS, and UPS – used to probe the properties of the surface layers of $YBa_2Cu_3O_7$ (YBCO) and $Tl_2Ba_2Ca_1Cu_2O_8$ (TBCCO) thin films.

The techniques used by others to prepare HTS surfaces for tunneling and photoelectron spectroscopy measurements have included: scraping, ion milling, and fracture of ceramic pellets and films; and cleavage of single crystals. All have been done in vacuum. Reviews of UPS studies of such surfaces have concluded that either the density of electronic states at the Fermi energy is zero [1] or appears to be zero [2] for intrinsic reasons. Recently, List et al. have succeeded in using UPS to observe a metallic surface layer by cleaving and analyzing a $EuBa_2Cu_3O_7$ crystal at 20 K.[3] The entirely *in-situ* approach of preparing films, cooling them to ~50 K in an oxygen atmosphere, and then evacuating the chamber to UHV for surface analysis, which we report here, is an attempt to adapt their technique to a technologically-important sample configuration.

EXPERIMENTAL

The YBCO films were grown by magnetron sputtering from three metal targets in a UHV deposition and analysis facility which has been fully described.[4] The sputtering conditions and annealing procedures have also been reported [5] and will be given only briefly here.

YBCO Junctions:

Amorphous films of YBCO were obtained on $SrTiO_3$ substrates at a temperature of 400°C by automatically rotating the substrate to face each target sequentially for a time which allowed the deposition of a monolayer, or less. An oxygen partial pressure of 10^{-6} Torr in a total argon/oxygen pressure of 15 mTorr was used. The orthorhombic superconducting phase was obtained by a rapid ramp anneal at ~10°C/sec to 850°C in 1 atm of O_2 without exposure to the ambient. The films grew epitaxially with an a-axis orientation – the orientation preferred for tunneling since it is the

*Work supported in part by AFOSR Contract No. F49620-88-C-0039.
**Permanent Address: University of Texas, Austin, TX, USA.

direction of the largest value of the anisotropic coherence length.

Junctions were fabricated using either Al_2O_3 or MgO barriers. The Al_2O_3 was formed by evaporating Al and oxidizing *in-situ* with pure O_2 for about 20 min producing about 2 nm of oxide. The MgO was e-beam evaporated to various thicknesses between 1 and 15 nm. In some junctions, Au proximity layers were e-beam evaporated on the YBCO before the insulator. The films were removed from the system to apply a shadow mask to define the Nb counter electrode which was e-beam evaporated. Except for the YBCO all depositions were done at room temperature. Although large junctions (~1 mm^2) were formed in this way, the procedure yielded a short turn-around time for the experiments.

UPS Apparatus and Samples:

The YBCO films used in the UPS experiments were magnetron-sputtered in the same system. They were grown crystalline as-deposited on MgO(100) substrates at a substrate temperature of 600°C with an oxygen partial pressure of 0.5 mTorr in a total argon/oxygen pressure of 15 mTorr. Although crystalline, the films were a tetragonal phase which requires a high temperature anneal to form the orthorhombic, superconducting phase. The rapid ramp *in-situ* anneal to 850°C was used. The resulting films were preferentially oriented with the c-axis normal to the surface and had T_c's (R = 0) of 70°K.

Following the high temperature anneal, the films were cooled to room temperature in 1 atm O_2 and transferred to the UHV analysis chamber without exposure to the ambient for UPS and XPS. The cold head of a cryocooler, installed through the wall of the chamber, was used to reduce the sample temperature to 50 K during evacuation of the chamber to 1×10^{-9} Torr (mostly He) and the subsequent UPS analysis. The evacuation of O_2 and sample cooling to <100 K were performed in a series of iterations since the cold stage warmed to ~100 K in 100 Torr of O_2. A liquid-nitrogen-cooled shield was used to reduce the radiative heat load from the room-temperature walls of the vacuum chamber. A rhodium-plated copper block was used for sample mounting to ensure good thermal contact for cooling to low temperatures while avoiding oxidation problems during the high temperature anneal. The block temperature was measured with a thermocouple clamped to its face.

Photon energies of 21 and 41 eV from a He discharge were used to obtain the UPS data. Care was taken to focus and calibrate the spectrometer in order to obtain the required resolution in the electron spectra. The UPS spectra of Au, Cu, and Ni were used as calibrations and the Ni spectrum was obtained each run as a standard.

TBCCO Samples:

Following Kang et al.,[6] the TBCCO films were grown by rf magnetron sputtering from three targets (Tl, BaCa, and Cu) on yttria-stabilized ZrO_2 at room temperature in a chamber separate from that in which the YBCO films were grown. The sputtering gas was 10 mTorr argon/5% O_2. The resulting films were wrapped in Au foil and annealed at 880°C in a sealed quartz ampule containing one atm. of O_2 and a sintered bulk pellet of TBCCO to provide the Tl vapor pressure required to prevent evaporation from the film.

RESULTS AND DISCUSSION

Junction Structures:

We have previously reported that slow annealing of the amorphous films results in a degraded layer within ~10 nm of the surface.[7] *In-situ* XPS and *ex-situ* Auger depth profiling have shown that the degradation was due to Ba diffusion to the surface which the rapid ramp anneal prevents resulting in near stoichiometric cation composition at the surface. The contact resistance of the rapidly annealed films was found to be $<10^{-10}$ Ω-cm^2 when a Au overlayer was deposited before the film was exposed to the atmosphere.[7]

Most of the junctions fabricated with either MgO or Al_2O_3 barriers on films with good near-surface stoichiometry were resistors. However, a few

have resulted in I-V characteristics which show an indication of tunneling into a superconductor. Figure 1 shows the derivative of the I-V curve for such a junction measured at 4.2 K. An energy gap of 1.5 mV is obtained for the Nb counter electrode, which agrees well with the value of 1.6 mV expected for pure Nb. The sum-gap voltage is 21 mV, indicating a gap of 19.5 mV for YBCO. The poor quality of these junctions is exemplified by a high value of sub-gap conductance and lack of a Josephson supercurrent. We felt that the junction properties are unlikely to have been due to non-stoichiometric cation composition at the surface since it was found by XPS to be at or close to 1:2:3. A likely cause, based on the UPS results discussed below, is the *loss* of oxygen at the surface before or during the barrier layer deposition. However, before the UPS results were available, we tried to inhibit the loss of oxygen by depositing a Au proximity layer on the YBCO.[8] Gold thicknesses between 1 and 20 nm were used. Junctions containing the Au layers exhibited supercurrents between the two electrodes for average barrier layer thickness in the 2-5 nm range. This provides unambiguous evidence that some fraction of the near surface of the YBCO is superconducting. Figure 2 shows a typical result for a Nb/MgO/Au/YBCO junction and the results were similar for the junctions with Al_2O_3 barriers. The curve of Fig. 2. resembles somewhat that expected for an S-N-S junction. However, the shape of the curve, especially near zero voltage, is clearly not that expected for a Josephson current. The supercurrents are probably due to direct shorts which strongly linked the electrodes. This indicates that the barrier is not continuous across the entire area of the junction. Attempts to eliminate the microshorts by using thicker barrier layers failed. Layers of Al_2O_3 were limited to about 3 nm using the technique of oxidizing Al. Layers of MgO up to 5 nm thick gave the results of Fig. 2 and thicker layers gave resistive junctions.

Junctions with very thick Au proximity layers gave some indication of tunneling between superconductors. Figure 3 is the I-V curve for a junction with a 20 nm Au layer. The I-V curve exhibits switching and hysteretic behavior indicating that at least part of the critical current may be a Josephson current.

Obviously, the large junction areas may be limiting their quality. We are currently fabricating junctions by photolithography to produce smaller areas. This technique will also allow all-*in-situ* fabrication of Nb/insulator/YBCO trilayers.

UPS Surface Studies:

UPS spectra were taken for several samples which had undergone a variety of thermal cycles in oxygen and vacuum. The most important result - shown in Fig. 4(a) - was the observation of a non-zero density of states at the Fermi edge for YBCO films annealed in O_2 at one atmosphere pressure and transferred in O_2 to a ~50 K cold stage for UPS measurements. The spectrum in Fig. 4(a) is similar to that reported by Arko, et al.[9] for a single crystal cleaved in vacuum at 20 K. It shows a peak at the Fermi edge which is about 20% of the maximum valence band intensity. The negative curvature of the trace at energies just below E_F has been reported previously only by Arko, et al. and is a clear indication of a Fermi edge. In contrast, the tail of the valence band peak which would have a positive curvature at energies close to E_F.

Figure 4(b) shows a UPS spectrum recorded after a film with a metallic YBCO surface was left on the cold stage for 48 hours at ~80 K. We believe that the change in the spectrum between 0 and 5 eV is due to a loss of oxygen within an electron escape depth, ~1 nm, of the surface. Figure 4(b) represents a rather extreme case, since we observed a significant degradation of sample surfaces after 2-3 hours storage at 50 K. Arko et al.[9] observed no significant change in the spectrum of their YBCO crystal after storage in UHV for 48 hours at 20 K but detected a "rapid" change at ~50 K.

In contrast to the experimental conditions of Arko et al., for whom the loss of oxygen at the YBCO surface was irreversible, our procedure permitted films to be degraded, re-annealed, and measured again. The spectrum in Fig. 4(a) is for an *in-situ* film that was briefly removed from the vacuum system. When it was returned to the system, it was annealed in an O_2 atmosphere at 400°C and transferred in O_2 to the cold stage for analysis. Although such experiments are preliminary, it appears that surfaces can be restored by this procedure - even with the likelihood

of some hydroxide and carbonate formation when the sample was exposed to air. We expect to be able to use core-level XPS spectra to understand the surface restoration process.

Surface Composition of TBCCO Films

We know of only two papers in the literature concerning photoelectron spectroscopy of the TBCCO superconducting compounds: An XPS study in which a ceramic pellet was scraped in vacuum at room temperature before measurement,[10] and a calculation of the photoelectron spectrum near the Fermi energy based on band-structure calculations.[11] Photoelectron studies of the TBCCO films are of scientific, as well as technological interest for two reasons: 1. Oriented thin films may take the place of single crystals which are unavailable; 2. A distinct Fermi edge has been observed in the isostructural superconductors in the Bi-Sr-Ca-Cu-O system.[12,13]

Figure 5 shows the resistivity and c-axis crystalline orientation of our annealed $Tl_2Ba_2Ca_1Cu_2O_8$ films. The "zero" resistance point in Fig. 5(a) is at 109 K. The surface cation composition was calibrated based on the assumption that the surface composition measured by XPS was representative of the bulk composition measured by EDS for as-deposited, unannealed films. Peak areas taken from XPS core-level spectra indicated that there was approximately five times as much thallium on the surface of the annealed film as measured in the bulk of the film. The chemical shift of the Tl_{4f} photoelectron line was consistent with the presence of Tl_2O_3 on the surface. The UPS spectrum from an annealed film, shown in Fig. 4(c), is clearly indicative of an insulating surface.

CONCLUSIONS

We have studied the near surface properties of YBCO films by three complementary methods employing all-*in-situ* fabrication and analysis. Tunneling experiments show that superconducting surfaces of amorphous as-deposited films may be obtained by a rapid *in-situ* anneal which provides stoichiometric cation composition. However, the junctions are of poor quality with only an indication of a Josephson current only in cases where the tunnel barrier is discontinuous. UPS studies indicate that this is very likely due to a degraded surface layer caused by loss of oxygen during exposure to vacuum at room temperature.

The observation of a non-zero density of states at the Fermi edge in films cooled in oxygen to 50 K indicates that a metallic layer is present within ~1 nm of the surface. The loss of this metallic surface by exposing it to vacuum occurs slowly at 50 K (some degradation in 3-4 hr) but very rapidly at 300 K (in minutes). Previous reports [3,9] for cleaved single crystals indicate no degradation after 48 hr at 20 K. A metallic surface may be recovered by *in-situ* annealing at 400°C after the film has been exposed to air and contaminated by reaction and adsorbed impurities.

It is obvious that junctions should be fabricated with films that are cooled in O_2 before being exposed to vacuum for deposition of the metal or insulator. The preservation of the metallic surface in this way may yield the superconducting properties required within a coherence length to produce quality Josephson devices. We are presently pursuing this approach.

XPS and UPS data taken on films of TBCCO (T_c = 109 K) which had been annealed *ex-situ* show a non metallic surface containing a segregation layer of Tl_2O_3. Although it is known that TBCCO is more stable than YBCO with regard to oxygen loss, it may be necessary to develop an all *in-situ* processing technique for film deposition and fabrication of junctions to ensure a superconducting surface at the interfaces.

ACKNOWLEDGMENTS

We are pleased to thank Dr. M. G. Forrester for his valuable experimental contributions and discussions; H. C. Pohl, J. H. Uphoff, and C. L. Jones for experimental help; and Mrs. M. B. Cross for the preparation of this manuscript.

2nd Workshop on High Temperature Superconducting Electron Devices
R&D Association for Future Electron Devices. June 7-9, 1989, in Shikabe, Hokkaido, Japan.

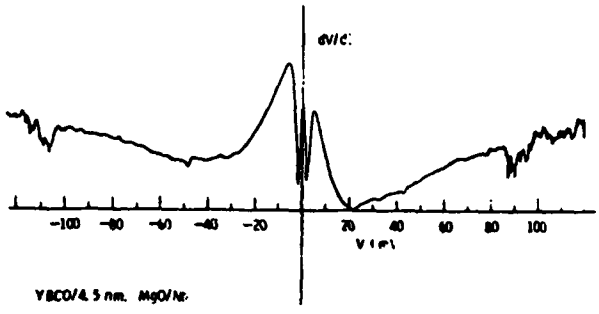

Fig. 1. Derivative of the I-V characteristic of a YBCO/MgO/Nb junction measured at 4.2 K.

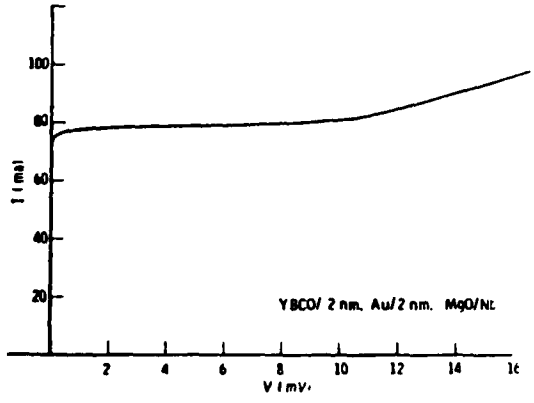

Fig. 2. The I-V curve at 4.2 K for a junction with a thin proximity layer

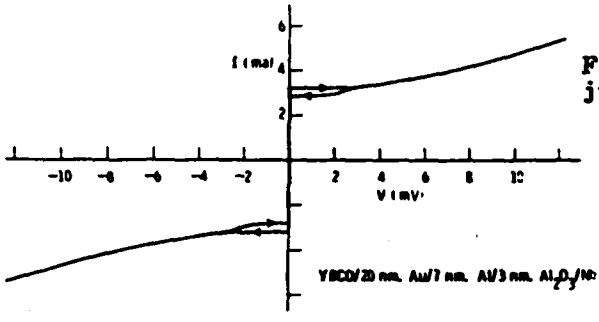

Fig. 3. The I-V curve at 4.2 K for a junction with a thick proximity layer showing hysteresis.

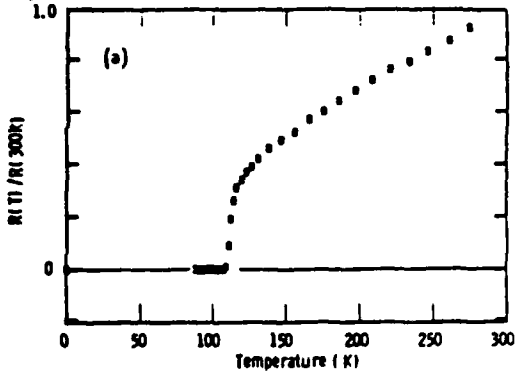

Fig. 5. (a) The resistance of a TBCCO film normalized to its value at 300 K and plotted as a function of temperature. (b) An x-ray diffractometer scan showing the c-axis orientation of a TBCCO film grown on cubic ZrO_2.

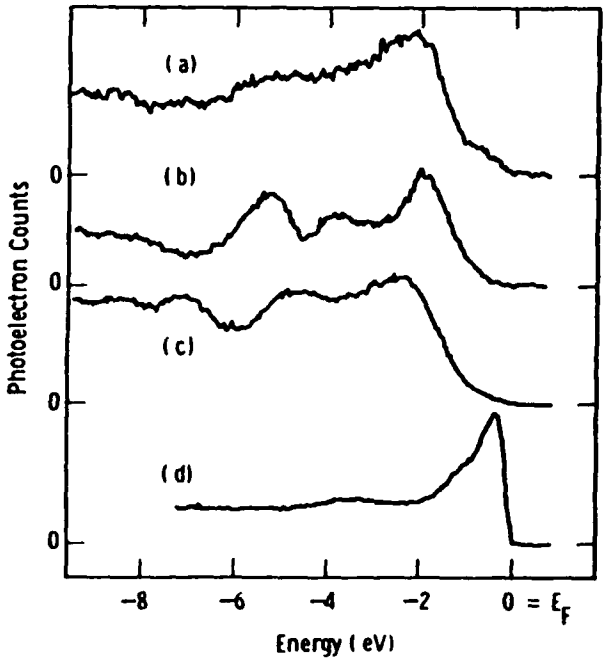

Fig. 4. UPS spectra from (a) a YBCO film annealed at 400°C in O_2 and cooled in O_2 to 50 K; (b) a YBCO film analyzed after storage in UHV at 80 K for 48 hours; (c) a TBCCO film after *ex-situ* annealing; and (d) a clean Ni standard used to calibrate the spectrometer's work function.

2nd Workshop on High Temperature Superconducting Electron Devices
R&D Association for Future Electron Devices, June 7-9, 1989, in Shikabe, Hokkaido, Japan. pp

REFERENCES

1. R. G. Egdell and W. R. Flavell, "Is the Surface of $YBa_2Cu_3O_{7-x}$ Intrinsically Non-Metallic?," Z. Phys. B - Condensed Matter 74, 279-282 (1989).
2. N. G. Stoffel, P. A. Morris, W. A. Bonner, Y. Chang, M. Tang, R. Zanoni, L. Dottl, Q. B. Chen, R. Joynt, D. L. Huber, M. Onellion, and G. Margaritondo, "Cleaved Single Crystals of High-T_c Superconductors: Electron Spectroscopy and Electron Diffraction Studies," Surf. Sci. 211/212, 1123 (1989).
3. R. S. List, A. J. Arko, Z. Fisk, S-W. Cheong, S. D. Conradson, J. D. Thompson, C. B. Pierce, D. E. Peterson, R. J. Bartlett, N. D. Shinn, J. E. Schirber, B. W. Veal, A. P. Paulikas, and J. C. Campuzano, "Photoemission from Single Crystals of $EuBa_2Cu_3O_{7-x}$ Cleaved below 20 K: Temperature-Dependent Oxygen Loss," Phys. Rev. B 38(16), 11,966 (1988).
4. A. I. Braginski, J. Talvacchio, J. R. Gavaler, M. G. Forrester, and M. A. Janocko, "In-Situ Fabrication, Processing, and Characterization of Superconducting Oxide Films," in SPIE Proceedings Vol. 948, High-T_c Superconductivity: Thin Films and Devices, edited by R. B. van Dover and C. C. Chi (SPIE, Bellingham, Washington, 1988), pp. 89-97.
5. J. Talvacchio, J. R. Gavaler, J. Greggi, M. G. Forrester, and A. I. Braginski, "Comparison of $YBa_2Cu_3O_7$ Films Grown by Solid-State and Vapor-Phase Epitaxy," IEEE Trans. Magn. 25(2), 2538 (1989).
6. J. H. Kang, R. T. Kampwirth, and K. E. Gray, "Superconductivity in Sputtered Thin Films of Tl-Ba-Ca-Cu-O," Phys. Lett. A 131(3), 208 (1988).
7. J. R. Gavaler, A. I. Braginski, J. Talvacchio, M. A. Janocko, M. G. Forrester, and J. Greggi, "Fabrication of High-T_c Superconducting $YBa_2Cu_3O_7$ Films," in MRS Vol. EA-14: High-Temperature Superconductors II, edited by D. W. Capone II, W. H. Butler, B. Batlogg, and C. W. Chu (Mater. Res. Soc., Pittsburgh, 1988), pp. 193-196.
8. Y. Gao, H. M. Meyer III, T. J. Wagener, D. M. Hill, S. G. Anderson, J. H. Weaver, B. Flandermeyer, and D. W. Capone II, "Interface Formation: High-Temperature Superconductors with Noble Metals, Reactive Transition Metals, and Semiconductors," in Thin Film Processing and Characterization of High-Temperature Superconductors, edited by J. M. E. Harper, R. J. Colton, and L. C. Feldman (Am. Inst. of Phys., New York, 1988).
9. A. J. Arko, R. S. List, R. J. Bartlett, S.-W. Cheong, Z. Fisk, J. D. Thompson, C. G. Olson, A.-B. Yang, R. Liu, C. Gu, B. W. Veal, J. Z. Liu, A. P. Paulikas, K. Vanderwoort, H. Claus, J. C. Campuzano, J. E. Schirber, and N. D. Shinn, "Large, Dispersive Photoelectron Fermi Edge and the Electronic Structure of $YBa_2Cu_3O_{6.9}$ Single Crystals Measured at 20 K," Phys. Rev. B (1989).
10. A. K. Ganguli, K. S. Nanjunda Swamy, G. N. Subbanna, M. K. Rajumon, D. D. Sarma, and C. N. R. Rao, "Superconductivity in the Tl-Ca-Ba-Cu-O System: Synthesis, Characterization and Mechanism," Mod. Phys. Lett. B 2(10), 1169 (1988).
11. P. Marksteiner, J. Yu, S. Massidda, A. J. Freeman, J. Redinger, and P. Weinberger, "Calculated Photoemission, Inverse Photoemission, and X-Ray Emission Spectra of High-T_c Superconductors: $Tl_2Ba_2CaCu_2O_8$ and $Tl_2Ba_2Ca_2Cu_3O_{10}$," Phys. Rev. B 39(4), 2894 (1989).
12. M. Onellion, M. Tang, Y. Chang, G. Margaritondo, J. M. Tarascon, P. A. Morris, W. A. Bonner, and N. G. Stoffel, "Photoemission Study of the New High-Temperature Superconductor Bi-Ca-Sr-Cu-O," Phys. Rev. B 38(1), 881 (1988).
13. T. Takahashi, H. Matsuyama, H. Katayama-Yoshida, Y. Okabe, S. Hosoya, K. Seki, H. Fujimoto, M. Sato, and H. Inokuchi, "Evidence from Angle-Resolved Resonant Photoemission for Oxygen-2p Nature of the Fermi-Liquid States in $Bi_2CaSr_2Cu_2O_8$," Nature 334, 691 (1988).

2nd Workshop on High Temperature Superconducting Electron Devices
R&D Association for Future Electron Devices, June 7-9, 1989, in Shikabe, Hokkaido, Japan pp. 313-316

PHYSICAL CHARACTERIZATION OF HTS FILMS (*Invited*)

A. I. BRAGINSKI*
Westinghouse R & D Center, Pittsburgh, PA 15235, USA

ABSTRACT

Categories of characterization methods relevant to future HTS electron devices are reviewed to indicate areas where progress in methodology is required. Difficulties in physical characterization are largely due to the surface and interface instability of HTS cuprates.

INTRODUCTION

The purpose of this introductory paper is to highlight the topic of physical characterization of high temperature superconductor (HTS) films. In this Session, a selection of physical properties is emphasized which, at present, appear particularly relevant to future electron devices. These devices fall broadly into the two categories of passive and active components of superconducting circuitry. A great majority of these will be fabricated from epitaxial thin film structures, hence the emphasis on thin film properties.

Standard methods of measuring HTS material properties: structural, chemical, thermal, mechanical and electrical must often be complemented by more refined methods capable of probing the true, undegraded properties of HTS materials. Indeed, the first general comment which should be made is that most of the results published to date on HTS properties have been flawed by the imperfection and non-representative behavior of examined samples. This is especially true in cases when HTS near-surface properties were probed.

NATURE OF CARRIERS

The determination of hole vs electron conduction is based on the sign of the Hall coefficient and the Seebeck effect in the normal state. The recent discovery of electron-pairing in HTS[1] and the speculations on the possibility of p-n junction devices make these measurements especially relevant. Luckily, bulk single crystal samples and standard procedures appear adequate for obtaining the data. However, successful fabrication of a p-n superconducting junction will require undegraded and well characterized surfaces and interfaces of epitaxially correlated p- and n-oxides.

DISSIPATION IN HTS

Dissipative effects in the superconducting state are equally important for both bulk and thin film HTS applications, albeit for different reasons. In HTS, thermal activation causes the giant flux creep/flow and vortex lattice melting which become prominent at higher reduced temperatures, t, even at relatively low reduced magnetic field intensities, h.[2] A manifestation of these effects is broadening of the superconducting transition which is observed when the measuring current or applied magnetic field increases[3] and the logarithmic decay of magnetization with time.[2] The magnitude of these effects is different for various material systems, as shown by Palstra *et al.* who compared the thermally activated resistivity in YBCO and BSCCO single crystals over a broad range of t and h.[4] Data such as[4] show that the traditional J_c criteria (e.g. the customary 1 μV/cm voltage drop) are unacceptable since a low-level dissipation persists below the "J_c". Thermal activation of fluxons poses a serious basic obstacle to the utilization of bulk HTS conductors, especially at higher temperatures. In contrast, the activated flux flow in HTS epitaxial films may offer new opportunities for electronic devices such as the vortex

* Present address: Kernforschungsanlage Juelich (KFA), D-5170 Juelich, West Germany.

memory. The importance of the whole problem is reflected by its prominent presence in the contributions to this session by the commentators.

The present electrical characterization approaches appear adequate. However, refinements in microscopic fluxon observations are desirable. While high-resolution (SEM) Bitter pattern observation[5] suggested the lattice melting effect, much finer scale microscopic examination of fluxon structures in crystals and epitaxial films, e.g. by scanning tunneling microscopy (STM), could show which defect structures are effectively pinning the extremely small vortices.

Measurements of radio-frequency losses (surface resistance, R_s) in HTS have been performed by both cavity perturbation and strip/microstrip line techniques over a broad range of microwave frequencies, 3 to 150 GHz. As predicted,[6] residual rf losses correlate with the number density of grain boundaries within the penetrated layer.[7] In low rf fields, R_s values sufficiently low for many passive electronic device applications (lower than in Nb at the same t) have already been measured at 77K in highly epitaxial YBCO films with c-axis orientation.[8] In these cavity measurements, the low R_s was characteristic of the film top surface only. The low-field rf resistance is surface sensitive but the depth scale, set by the penetration depth, λ, of the order of 100 nanometers, is more forgiving than in active devices where it is set by the coherence length, ξ.

Microwave absorption measurements vs rf and dc field intensity are capable of yielding information on flux creep/flow behavior and the usefulness of HTS for high power resonant cavities. Improvements in rf loss measurements should occur through a broader use of very high-Q superconducting cavities with controlled specimen temperature which would be capable of resolving low perturbations caused by small (e.g. single crystal) low-loss samples. Device-oriented planar resonator (e.g. strip or microstrip line) measurements of $R_s(f,T)$ should become possible with the availability of low-loss epitaxial substrates. The rf (microwave) measurements of non-dissipative properties such as the kinetic inductance and resonator phase noise are also of importance to passive devices.

SURFACE-SENSITIVE PROPERTIES AND TUNNELING

Both, passive and active electronic devices impose stringent requirements on the HTS film surface and interface perfection. However, the issue is much more critical in the latter category due to the extremely short, anisotropic coherence length in oxide superconductors. Environmental instability of known HTS imposes a broad use of *in-situ* methods of surface characterization. This instability appears to be particularly severe in compounds such as YBCO, where the activation energy for a reversible oxygen intercalation is low and the surface is prone to lose oxygen when exposed to high or ultra-high vacuum, even at ambient temperatures. The surface oxygen loss was confirmed in YBCO by *in-situ* low-temperature photoelectron spectroscopy stimulated by ultra-violet radiation, UPS.[9,10]

In a broader sense, the UPS and XPS are good tools to investigate the valence band structure for comparison with band energy calculations, to validate theories of superconductivity, and also to obtain technologically useful data on thin surface layers within the low-kinetic-energy photoelectron escape depth, which is of the order of a few angstroms.[10] However, the oxygen loss, where occurring, imposes the use of low sample temperatures during processing.

An effective route to define processing conditions for undegraded surfaces would be to couple several low-temperature *in-situ* methods, such as low-temperature UPS, quantitative low-energy electron diffraction (LEED) and STM.[11] Only after attaining relatively undegraded HTS surfaces will the tunneling spectroscopy be able to contribute to the verification of various models of HTS superconductivity.[12,13] The same requirement is essential for any practical thin-film tunneling or proximity device. To date, published experimental tunneling results have been generally unsatisfactory, with relatively most trustworthy data obtained by *in-situ* methods such as film breaking which suggested an evidence of gap anisotropy in YBCO[14] or *in-situ* bilayer fabrication.[10] It is necessary to determine whether or not the present difficulties in obtaining clean I-V and dI/dV-V characteristics are due solely to to the surface instability of

the structure or to a fundamentally new mechanism of superconductivity. Shorter term active device interests will probably concentrate on S-N-S proximity junctions so that characterization of S/N interfaces and proximity effects is important.

OPTICAL CHARACTERIZATION AND PROPERTIES

A very large number of HTS investigations have used optical methods of characterization. However, due to the HTS surface instability, only measurements of single crystals could have contributed some intrinsic data and even these were likely to be affected by surface degradation. Numerous have been studies of single crystal infrared reflectivity spectra in superconducting and normal state. From such data, inferences on the YBCO energy gap and its anisotropy were made.[15] Even more abundant have been measurements of Raman vibrational spectra in single crystals which have provided some insight into the lattice dynamics and electron-phonon coupling.[16] Unfortunately, the Raman spectroscopy is particularly sensitive to the presence of impurity phases. Neither of the above methods has, at present, any serious device implications.

Current HTS optical device interest concentrates on the question of electrical response to radiation in the visible and infrared (IR) spectrum and the suitability of HTS for IR detectors. The mechanism of detector response, bolometric vs nonequilibrium (quantum), is the subject of controversy.[17] Claims of nonequilibrium response in HTS films are generally based on an optically-induced electrical signal which either (1) exhibits a temperature dependence which deviates from that of dR/dT, possibly diverging or peaking at low temperatures, or (2) contains a fast component (~ nsec) to the response to a short laser pulse, which is claimed to be inconsistent with the known thermal properties of the detector film/substrate combination. Data in category (1) can generally be explained in terms of the temperature-dependent thermal properties of the HTS film, which make the optically-induced temperature rise a strong function of temperature. The analysis of detector response to a pulsed laser must also consider the thermal properties of the thin film (as opposed to that of the substrate) which can have an extremely short (<< nsec) thermal time constant. The convolution of a rapidly falling film temperature and a resistance which decreases rapidly with temperature can lead to extremely fast electrical response to radiation.

SUMMARY

Characterization of dissipative properties in HTS is essential for the development of conductors and passive RF devices. In the case of active HTS circuit elements, the *in-situ* structural and photoemission characterization of surface/interface layers at a depth scale of a few monolayers is the necessary prerequisite for tunneling and attaining representative electrical properties in general. For opto-electrical HTS detectors, the separation of thermal and quantum response to radiation is a major challenge in characterization. Overall, the problems of characterization are largely related to HTS surface instability.

REFERENCES

1. Y. Tokura, H. Takagi, and S. Uchida, Nature 337, 345 (1989) and H. Takagi, this Workshop.
2. Y. Yeshurun and A. P. Malozemoff, Phys. Rev. Lett. 60, 2202 (1988).
3. M. Tinkham, Phys. Rev. Lett. 61, 1662 (1988).
4. T.T.M. Palstra, B. Batlogg, R. B. van Dover, L. F. Schneemeyer, and J. V. Waszczak, Appl. Phys. Lett. 54, 763 (1989).
5. P. L. Gammel, D. J. Bishop, G. J. Dolan, J. R. Kwo, C. A. Murray, L. F. Schneemeyer, and J. V. Waszczak, Phys. Rev. Lett. 59, 2592 (1987).
6. T. L. Hylton, A. Kapitulnik, M. R. Beasley, J. P. Carini, L. Drabeck, and G. Gruener, Appl. Phys. Lett. 53, 1343 (1988).
7. J. Wosik *et al.* (Houston Univ.) unpublished data, 1989.

8. H. Chaloupka, G. Muller, U. Klein, and H. Piel, Proc. IEEE/MTT-S Int. Microwave Symp., Long Beach, CA, June 1989, to be published.
9. R. S. List, A. J. Arko, Z. Fisk, S-W. Cheong, S. D. Conradson, J. D. Thompson, C. B. Pierce, D. E. Peterson, R. J. Bartlett, N. D. Shinn, J. E. Schirber, B. W. Veal, A. P. Paulikas, and J. C. Campuzano, Phys. Rev. B 38, 11966 (1988).
10. G. R. Wagner, R. M. Silver, J. Talvacchio, J. R. Gavaler, and A. J. Panson, this Workshop.
11. A. De Lozanne *et al.*, this Workshop.
12. H. Fukuyama, this Workshop.
13. I. Iguchi, this Workshop.
14. J. S. Tsai, I. Takeuchi, J. Fujita, T. Yoshitake, S. Miura, S. Tanaka, T. Terashima, Y. Bando, K. Ijima, and K. Yamamoto, FED HiTcSc-ED 1988 Workshop extended Abstracts, FED 65, p. 219.
15. Z. Schlesinger, R. T. Collins, D. L. Kaiser, F. Holtzberg, G. V. Chandrashekhar, M. W. Shafer, and T. M. Plaskett, Physica C 153-155, 1734 (1989); and references therein.
16. D. M. Krol, M. Stavola, L. F. Schneemeyer, J. V. Waszczak, and S. A. Sunshine, J. Opt. Soc. Am. B 3, 448 (1989); and references therein.
17. A. I. Braginski, M. G. Forrester, and J. Talvacchio, Proc. ISEC 89, paper DE1-2 and references therein.

Physica C 162-164 (1989) 1051-1052
North-Holland

PROPERTIES OF YBCO-BASED TUNNEL JUNCTIONS*

J. R. Gavaler, M. G. Forrester, and J. Talvacchio

Westinghouse Science and Technology Center, Pittsburgh, PA 15235

We have made tunnel junctions with YBCO base and Nb counterelectrodes. At 4.2K an energy gap of 19.5 mV was derived for YBCO. Junctions with thick Au proximity layers showed evidence of Josephson currents in some instances.

1. EXPERIMENTAL PROCEDURE

The YBCO films were deposited, initially in the amorphous state, by sputtering onto (100) $SrTiO_3$ substrates at ≤400°C.[1] To crystallize the YBCO in-situ, fast-ramp (10°C/sec. from ambient to 850°) annealing was used. The resulting films had a near-stoichiometric cation composition at the surface, as determined by in-situ XPS.[2] When Au was deposited on such surfaces at 20°C, a contact resistance of $<10^{-10}$ Ω-cm^2 was obtained without annealing.

Al_2O_3 or MgO barriers were used. The Al_2O_3 was formed by oxidizing Al with oxygen. The MgO was evaporated to desired thicknesses. In some junctions Au layers were evaporated onto the YBCO. Films were removed from the system only to apply a mask to define the Nb counterelectrode which was e-beam evaporated. The size of the junctions was ~1 mm^2. Except for the YBCO all depositions were done at room temperature.

2. RESULTS AND DISCUSSION

The YBCO films grew with an a-axis orientation. T_c's were ~80K (R=0) and films had a near-surface stoichiometry close to 1:2:3. When incorporated into junctions with no Au and with either MgO or Al_2O_3 barriers, they were in many cases resistive. In some instances however, junctions were obtained whose I-V curves indicated tunneling into the YBCO. Figure 1 shows the derivative of the I-V curve for one such junction. This curve is reminiscent of data obtained by other workers who have investigated junctions using YBCO as the base and a conventional superconductor for the counterelectrode.[3,4] The minimum in the dV/dI curve which occurs at ±1.5 mV is the energy gap of the Nb. The gap-like structure seen at about 20 mV is similar to structure observed at a somewhat lower voltage by Geerk et al.[3] These authors argue persuasively that this structure is due to quasi-particle tunneling into the superconductor. In their case they show a gap voltage at 4.2K of 16 mV. In our junction the sum-gap voltage is 21 mV indicating an energy gap for YBCO of 19.5 mV. This value is in line with Lee et al.[4] who concluded that there was strong evidence for an energy gap of 17 to 23 mV in YBCO. Published values for the ratio $2\Delta/kT_c$ range from 4 to 7.5.[4] We calculate a value of 5.9.

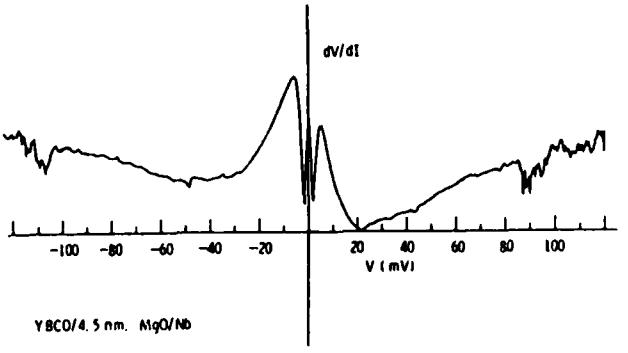

Figure 1
A YBCO/MgO/Nb junction measured at 4.2K.

*Supported in part by AFOSR Contract No. F49620-88-C-0039.

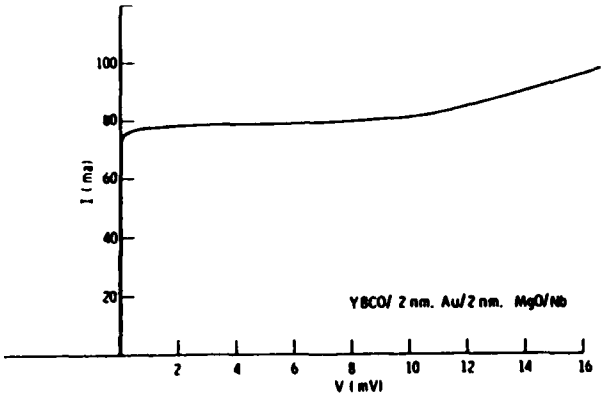

Figure 2
A junction with a thin proximity layer at 4.2K.

We have noted the similarity among data obtained in various laboratories including poor junction quality as exemplified by the absence of Josephson current and high sub-gap conductance. In the junctions discussed above made by other workers, a degraded surface layer on the YBCO served as the barrier. Based on the similarity of results it is likely that the barriers in our junctions also included degraded surface layers. From our XPS data it is unlikely that this layer is due to a non-stoichiometric cation composition. We feel that a more likely cause is oxygen deficiency. Recent UPS measurements made in our laboratory show that in vacuum at room temperature a YBCO surface changes from metallic to insulating in a matter of minutes.[5] To inhibit oxygen loss, we prepared junctions in which gold layers were deposited on the YBCO. Figure 2 shows a YBCO/Au/MgO/Nb junction. As can be noted there is a supercurrent between the electrodes in this junction. The curve is clearly not that for a junction exhibiting a Josephson current. The supercurrent is probably due to microshorts. Its presence however does provide evidence that some fraction of the YBCO near-surface region is superconducting. Attempts to eliminate the microshorts by increasing barrier thickness failed. Thicker barriers produced only resistive junctions. In some cases, however, junctions with very thick Au layers did show indications of Josephson currents. Figure 3 shows a junction which exhibits switching and hysteretic behavior suggesting that at least part of the supercurrent is a Josephson current.

At this time we lean toward the explanation that the large sub-gap conductances are due to material problems such as surface roughness and non-stoichiometry. The hint toward more ideal junction behavior in junction with Au layers leads us to believe that further progress will be obtained by additional improvement of the surface quality of the YBCO.

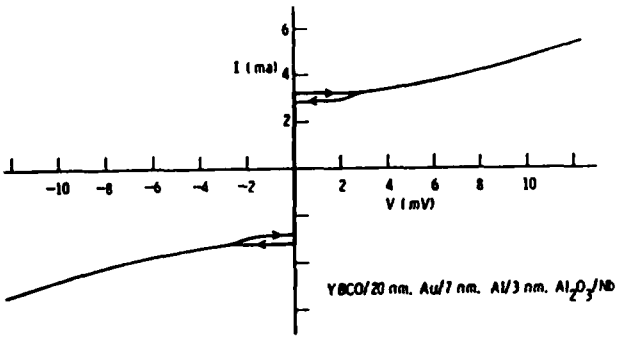

Figure 3
A junction with a thick proximity layer at 4.2K.

REFERENCES

1. J. Talvacchio, J.R. Gavaler, J. Greggi, M.G. Forrester, and A.I. Braginski, IEEE Trans. Magn. 25(2), 2538, (1989)

2. J.R. Gavaler, A.I. Braginski, J. Talvacchio, M.A. Janocko, M.G. Forrester, and J. Greggi, MRS Vol. EA-14: High Temperature Superconductors II, eds. D.W. Capone II, W.H. Butler, B. Batlogg, and C.W. Chu (Mater. Res. Soc., Pittsburgh, 1988) pp. 193-196.

3. J. Geerk, X.X. Xi, and G. Linker, Z. Phys. B - Condensed Matter 73, (1988) 329.

4. Mark Lee, A. Kapitulnik, and M.R. Beasley, Proc. of the NEC Symposium on Mechanisms of High Temperature Superconductivity, Oct. 24, 1988, Tokyo, Japan.

5. G.R. Wagner, R.M. Silver, J. Talvacchio, J.R. Gavaler, and A.J. Panson, Extended Abstracts, 2nd FED Conference, Halcodate, Japan, 1989, (unpublished).

Physica B 165&166 (1990) 1513-1514
North-Holland

OPTIMIZATION OF T_c AND J_c IN SPUTTERED YBCO FILMS*

J. R. GAVALER and J. TALVACCHIO

Westinghouse Science and Technology Center, Pittsburgh, PA U.S.A.

We have sputtered, from single targets, $\leq$100 nm thick epitaxial as-deposited YBCO films which have T_c's of >90K (R=0) and J_c's as high as 10^5 Amps/cm^2 at 91K and 10^7 Amps/cm^2 at 65K. The critical variables for achieving these values are identified.

1. INTRODUCTION

Since the discovery of $YBa_2Cu_3O_7$ (YBCO), many techniques have been investigated for preparing thin films of this compound. One of the most successful has been sputtering. The first sputtered films which had close to bulk T_c's required annealing at $\geq$850°C. It was found that these high annealing temperatures tended to degrade the near-surface and substrate regions. Although ways were found to minimize this degradation (1,2), it became clear that, ultimately, higher quality films would be obtained by finding means to sputter films that were crystalline as-deposited thereby eliminating the high temperature post-annealing step. That other workers reached a similar conclusion is indicated by the many recent papers on sputtered crystalline as-deposited films (see for example refs. 3 and 4). At this time, however, there are significant differences in the data reported on such films and also there is no consensus on optimum experimental procedures. In this paper we report critical temperature, T_c, and current, J_c, data on our sputtered films and discuss what we believe are the crucial variables for optimizing these properties.

2. EXPERIMENTAL PROCEDURE

All of our experiments were done in a non-baked vacuum chamber which has a base pressure in the low 10^{-6} Torr range. Two sputter guns each containing a 5 cm diameter target are mounted horizontally in the chamber. The substrate holder is a 5.7 cm diameter nickel block mounted on a manipulator which can be be oriented toward either of the two targets. In one of the configurations the substrates are positioned parallel to the target with a 5 cm separation between the substrates and the target. In the other, the substrates are positioned perpendicular to the target surface. In this configuration if one drew a line normal to the center of the target and another line normal to the center of nickel block, the intersection of these lines would be 5.8 cm from the substrate holder and 5.3 cm from the target surface.

Both rf and dc magnetron sputtering were employed. The substrates were 1 x 1 x .05 cm single crystal $SrTiO_3$(100), $LaAlO_3$(100), MgO(100), yttrium stabilized ZrO_2(100) (YSZ), and R-plane sapphire. The nickel block temperature was determined by a thermocouple located in the block. Using these temperatures, the substrate temperatures were estimated to an accuracy of $\pm$ 20°C. Either pure oxygen or various mixtures of oxygen and argon were employed as the sputtering gases. Following deposition, films were annealed at 400°C for 20 minutes in 25 Torr oxygen. Two types of sputtering targets were used. Both had the stoichiometric 1:2:3 composition. However they were processed differently so that in one case the target consisted predominantly of the superconducting orthorhombic phase. In the other the tetragonal non-superconducting phase was dominant. All of the films to be discussed were between 50 and 100 nm thick unless otherwise noted.

T_c's (defined as R=0) were measured by the standard 4-point Van der Pauw method. J_c's were determined by passing current through a 25 micron x 1 mm bridge and observing the onset of resistance. A 5 microvolt criterion was used to define J_c which wwas equivalent to $<10^{-10}$ ohm-cm over most of the temperature range employed

3. RESULTS AND DISCUSSION

We have optimized T_c and J_c in our sputtered YBCO films to a level where they are now similar to or higher than those found in films made by any growth method. To illustrate: In films $\leq$100 nm thick, T_c's of over 90K have been reproducibly obtained. In the best cases, J_c's as high as 10^5 Amps/cm^2 at 91K and 10^6 Amps/cm^2 at 85K were measured. In thinner films T_c's and J_c's were also very high. In a 30 nm film with a T_c of 87K, J_c at 80K was 2 x 10^6 Amps/cm^2 and at 65K, 10^7 Amps/cm^2.

We have found that there is no one narrow set of experimental conditions required to sputter films of this quality. In fact, certain variables could be and were changed over a wide range without significantly affecting film properties. On the other hand, what were thought to be minor variations in experimental procedure sometimes produced dramatic changes in

*Supported in part by AFOSR Contract F49620-88-C-0039

T_c and J_c. In the remainder of this paper we will discuss the important variables in the sputtering process and comment on their importance toward optimizing T_c and J_c.

Of the five substrate materials used only films deposited on sapphire failed to achieve T_c's >90K. In some films the susceptibility was measured. In the best cases the transition was only 0.5K wide and complete ~0.5K below the "R=0" point. On all of the substrates with the exception of sapphire epitaxial YBCO(001) films were grown which, from x-ray diffraction analysis, had single phase c-axis orientations and lattices parameters in the range 11.69 to 11.72 angstroms. Our highest J_c's were obtained on $LaAlO_3$ substrates. The values reported in the first paragraph of this section were for films deposited on this material. To provide a comparison of J_c's obtained on the different substrates the following values were obtained at 65K: $LaAlO_3$ - 10^7Amps/cm^2; $SrTiO_3$ - $2x10^6$ Amps/cm^2; MgO - $8x10^5$ Amps/cm^2; and YSZ - $2x10^5$ Amps/cm^2.

We have observed no significant difference between rf and dc magnetron sputtering with respect to maximizing T_c and J_c. The same is true regarding the two substrate-target geometries studied. However, certain variables had to be optimized separately to obtain similar results with the two geometries. In the perpendicular case, one (non-unique) set of conditions which produced films with optimum properties used 150 mTorr of argon and 20 mTorr of oxygen as the sputtering gas. The substrate temperature was 670°C, and power was 40 watts. The deposition rate was 10 nm/hour. In the parallel geometry T_c's >90K were obtained using 450 mTorr of oxygen, a substrate temperature of 730K, and 70 watts sputtering power. Deposition rate was 30 nm/hour. These films, initially, had J_c's about an order of magnitude lower than the perpendicular films. This was true despite the fact that the two types of films had similar 1:2:3 stoichiometry (from EDS analysis) and the same c-axis structure (from x-ray analysis). Ultimately this difference was related to the influence of the residual gas impurities in the system on the sputtering process. In a non-baked vacuum chamber the main residual gas is water vapor. When ~10 mtorr of water was added to the sputtering gas in the parallel configuration, T_c's of 90K (~5K higher than without water) were obtained at a 670°C substrate temperature. These films now had J_c's similar to those from the perpendicular geometry. The addition of water vapor when using the perpendicular geometry produced no improvement in the properties of these films. A negative aspect from the addition of water was the appearance of Cu-O particles in the films when an excess was present. Unfortunately it was found that exactly controlling the water pressure while sputtering was difficult. In an extreme case, films with composition $Y_4Ba_7Cu_{89}O_x$ were obtained. We refrain at this time from speculating on the positive role of adding water vapor in the parallel sputtering process. We d point out, however, that this role is sufficiently subtle that it can not readily be correlated with changes in cation stoichiometry or in lattice parameters.

Finally, we have found that sputtering from superconducting YBCO target produces films with better properties compared to those deposited from a non-superconducting target. When using the perpendicular geometry the difference in T_c's is only slight viz., ~90K to ~85K. Howeve in the parallel geometry differences could be very large. For example, two films deposited from these two types of targets on MgO had T_c's of 85K and 44K. Analyses of the films showed the same cation stoichiometry in both and very similar lattice parameters--11.718 and 11.726 angstroms. The film with the larger parameter had the higher T_c. This result was studied in more detail by further degrading the surface region of the lower-T_c target. This was done b sputtering several hours at high power in pure argon. Following this treatment, a series of films were sputtered in pure O_2 using the parallel geometry. Initial films were not orthorhombic and very non-stoichiometric. Afte several hours, 1:2:3 stoichiometry and c-axis growth returned. However, the films were still non-superconducting and the lattice parameter was unusually small, 11.624 angstroms. As sputtering was continued, superconductivity reappeared and T_c gradually rose reaching a maximum value of 84K. Lattice parameters also gradually rose to 11.682 angstroms. This resul indicates that under the conditions used, the oxygen in the system could not totally regenerate the target surface to the condition present in a newly fabricated superconducting target. It is worth noting that the addition o water vapor in any of the experiments using a non-superconducting target produced no effect other than an undesirable one of producing Cu-O particles in some of the films.

In conclusion, our data suggest that under the conditions studied, oxygen from the sputtering target plays a key role in optimizin T_c and J_c in our films. Also in some cases the addition of water vapor to the sputtering gas improves superconducting properties.

ACKNOWLEDGEMENTS

We gratefully acknowledge the valuable technical contributions of T. Mullen (EDS) A. Stewart (x-ray) and H. Pohl (film preparation).

REFERENCES

(1) J.R. Gavaler and A.I. Braginski, Physica C 153-155 (1988) 1435.
(2) J. Talvacchio, J.R. Gavaler, J. Greggi, M.G. Forrester, and A.I. Braginski, IEEE Trans. Magn. 25(2), (1989) 2538
(3) A. Hohler, H. Neeb and C. Heiden, Physica C 162-164 (1989) 607
(4) D.C. Bullock et al, ibid. 643

in *Superconductivity Applications for Infrared and Microwave Devices* SPIE Proc. Vol. 1292 (1990)

High-T_c film development for electronic applications*

J. Talvacchio and G. R. Wagner
Westinghouse Science and Technology Center
Pittsburgh, Pennsylvania 15235

ABSTRACT

We describe the requirements and status of high-T_c superconductor (HTS) films for the development of electronic applications with an emphasis on passive microwave devices. One of the most general requirements, a low rf surface resistance relative to Cu, has been achieved in films of several different HTS compounds. However the best films, made of $YBa_2Cu_3O_7$ (YBCO) by any one of several techniques, have in common a residual surface resistance that is much greater than predicted by conventional superconductivity theory. Improvement in films is also limited by the current size and selection of single-crystal substrate materials. Other issues that must be resolved to develop a full integrated circuit technology for HTS are substrate heating during film deposition, deposited epitaxial insulators, and determination of which interfaces in a multilevel circuit must be formed *in situ*.

1. INTRODUCTION

The emphasis of this paper is on the materials requirements for HTS passive microwave devices for three reasons. First, the development of HTS Josephson junctions is sufficiently difficult that a wide range of fabrication alternatives are being explored. To describe all of them would require a separate paper. Secondly, passive microwave devices are particularly important since they are expected to be the first practical application of HTS. Finally, many of the HTS materials issues considered here have broader implications. The general requirements of high-speed and/or low-noise operation in circuits with some level of integration apply to all of superconducting electronics. Only films on single-crystal epitaxial substrates are considered here. Both bulk fabrication and deposition of films on curved surfaces are desirable for some device configurations but microwave properties are inferior in these cases.

2. REQUIREMENTS FOR SPECIFIC MICROWAVE DEVICES

Figures of merit for several passive devices are listed in Table 1. The most important requirement is an rf surface resistance, R_s, which is low compared to normal metals (Cu, Au). For operation at $\lesssim$ 80K, all three of the highest T_c superconductor families can be considered: YBCO, Bi-Sr-Ca-Cu-O (BSCCO), and Tl-Ba-Ca-Cu-O (TBCCO). However, a search of the literature,[1] indicates that only three measurements of R_s of BSCCO films have been published,[2-4] and no results were obtained in the range 2-19 GHz that were better than the R_s of Cu. BSCCO films should be considered to have largely-unknown rf properties. Including Westinghouse, only three laboratories have explored the properties of TBCCO films at microwave frequencies. References 5 and 6 are the most recent of six publications on R_s of TBCCO.

* Supported in part by AFOSR Contract No. F49620-88-C-0039 and WRDC Contract No. F33615-88-C-1841

Table 1 - Materials issues in the fabrication of HTS microwave devices.

DEVICE	FIGURES OF MERIT	IMPLICATIONS FOR FABRICATION
Bandpass Filter	Insertion Loss, Bandwidth Volume	Low R_s → c-axis films. Integration of a filter-bank on a single wafer.
Resonator (oscillator)	Q	Low-loss dielectric, preferably sapphire.
	Phase noise	Single-crystal film.
Delay Line	Delay length Volume	Large film area. Thin dielectric.
Antenna Array	Efficiency Gain	Very large areas (UHF). Very low R_s (mm wave).
Additional Requirements for many devices:	Operation at $\leq$ 80K	YBCO, BSCCO, and TBCCO are all feasible.
	Mechanical, packaging	Films on both sides of substrate.
	Crossovers	Deposited, epitaxial, dielectrics.
	Interface with normal metal	Low-resistance contacts.

In contrast, more than 100 papers have been published on the surface resistance of YBCO films. The lowest R_s is obtained for films grown epitaxially on single-crystal insulating substrates with the film's c-axis parallel to the growth direction. All of the components in Table 1 require such films. For high-Q resonators, the requirement of low phase noise may also demand that essentially single-crystal films are used. Since YBCO is the most highly developed materials system, the fabrication issues listed in Table 1 will be evaluated in this paper with reference to YBCO.

3. SUBSTRATES FOR HTS FILMS

Several of the requirements in Table 1 relate to substrate properties. Table 2 contains a list of the important single-crystal substrates for HTS films and their dielectric properties. Epitaxial c-axis YBCO films can be grown on the (100) face of any of these substrates. The best dc YBCO film properties are generally obtained for films grown on substrates with a perovskite or perovskite-related structure. The values of the loss tangent, tan δ, summarized in Fig. 1, are too high for $SrTiO_3$ or yttria-stabilized zirconia (YSZ) to be used in rf applications. MgO, $LaAlO_3$, and $LaGaO_3$ have a tan δ for T $\leq$ 77K which is acceptable for all but the highest-Q applications. For those applications, only sapphire has acceptably low dielectric losses.

Table 2 - Dielectric properties of substrates for high-T_c films.

Substrate	ϵ_r	tan δ	f (GHz)	Temp. (K)	Ref. #
$SrTiO_3$	~230	3×10^{-2}	9.5	300	7,8
	215	1.4×10^{-1}	10 kHz	300	9
	310	3×10^{-2}	10-1000	300	10
	1900	6×10^{-2}	10-1000	80	10
	strongly T-depen.	$1\text{-}2\times10^{-3}$	22	77-500	11
	strongly T-depen.	$2\text{-}24\times10^{-3}$	22	37-600	12
ZrO_2(YSZ)	38	4×10^{-3}	33	300	13
	27	5.4×10^{-3}	1 MHz	300	14
	28	4×10^{-3}	10	300	15
	26	1.6×10^{-2}	10-1000	300	10
	25.4	7.5×10^{-3}	10-1000	80	10
	25	$2\text{-}6\times10^{4}$	2-20	4.2	16
MgO	~8	3×10^{-4}	--	300	7,17
	9.6	2×10^{-3}	1 kHz	300	18
	--	9.1×10^{-3}	1 MHz	300	14
	9.87	9×10^{-4}	10-1000	300	10
	9.6	4×10^{-5}	10-1000	80	10
	--	1×10^{-6}	0.5	4.2	19
Al_2O_3	8.6-10.5	1×10^{-3}	--	300	7
	9.5-11.5	2×10^{-4}	--	300	8
	8.5-10.5	0.1	0.1	750	7
	--	1.5×10^{-8}	9	77	20
	--	4.3×10^{-7}	72	77	20
	--	2×10^{-9}	3	4.2	21
	10.65	6×10^{-5}	10	?	17
$LaGaO_3$	25	1.8×10^{-3}	1 MHz	300	14
	25	1.5×10^{-6}	0.5-15	4.2	22
$LaAlO_3$	23	--	9	300	23
	16	5.8×10^{-4}	10	300	24
	16	8.3×10^{-5}	10	77	24
	16	5.0×10^{-6}	10	4.2	24
	26	$<5\times10^{-4}$	500	4.2-90	25
	24.5	2×10^{-6}	0.5-15	4.2	22
$KTaO_3$	4000	--	?	300	26

The real part of the dielectric constant can also limit application. In microstrip configurations where two YBCO films are separated by the substrate thickness, the width of conducting lines and spacing between them are determined by the range of substrate thickness that can be used conveniently, ~ 0.3 to 0.6 mm. For UHF circuits, substrate area can be reduced by using a substrate with ϵ_r = 20-25. For mm-wave circuits, fabrication tolerances become unreasonably small unless a low dielectric constant substrate is used.

Due to its combination of favorable rf properties, mechanical properties, and availability, sapphire appears *a priori* to be the preferred substrate. Epitaxial growth of c-axis YBCO occurs on the $(1\bar{1}02)$ surface which has a two-dimensional rectangular lattice. However, sapphire reacts more readily with YBCO than the other substrates of Table 1 and has a poor lattice match. From x-ray diffraction studies, we have found, in agreement with reference 27, that the YBCO[100] direction in the plane of the film lies parallel to the diagonal of the rectangular surface grid of sapphire. Figure 2 shows how the lattice mismatch between various substrates and YBCO correlates with the x-ray rocking-curve width (full width at half maximum) for the (005) peak. For both sapphire and YSZ, the length of a diagonal in the two-dimensional surface grid is the appropriate lattice spacing. For all others, a <100> direction in the film is parallel to a <100> direction in the substrate. The rocking curve widths also correlate with dc critical current density[28] and R_s, with the best results obtained for films grown on $LaAlO_3$ and $SrTiO_3$.

Another advantage of the perovskite-structure substrates is a close thermal expansion match to YBCO. One disadvantage is the occurrence of a structural transformation at a temperature between the deposition and operating temperatures. After cycling through the transformation, strain in the crystal is relieved by twinning and through surface

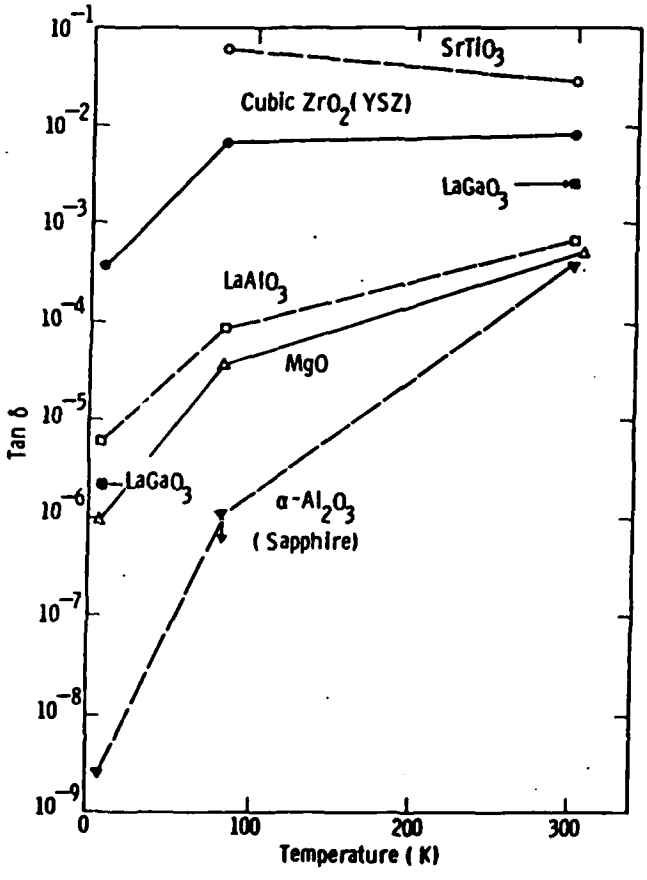

Fig. 1. The dielectric loss tangent, tan δ, plotted as a function of temperature for the important single-crystal substrates. The data points represent a synthesis of the data in Table 1. The lines drawn between data points are included simply to distinguish data on different substrates.

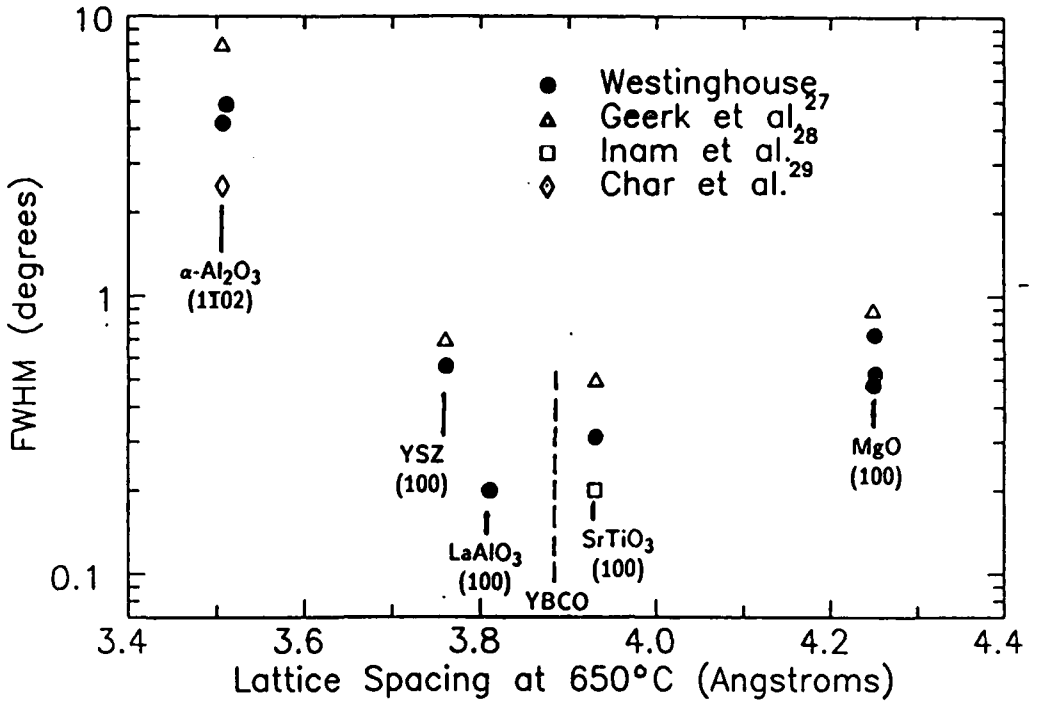

Fig. 2. X-ray rocking curve widths (full width at half maximum) for the (005) peak of epitaxial YBCO films grown on various substrates. The data is seen to correlate with the difference between the lattice constant of YBCO and the substrate at the deposition temperature of ~650°C. For sapphire and YSZ, the lattice spacing is the length of a diagonal in the two-dimensional surface lattice that lies parallel to a <100> direction in the YBCO film. The data of Geerk, Inam, and Char et al, are from references 27, 28, and 29, respectively.

oughness. For $LaGaO_3$, a cubic-to-tetragonal transformation at 150°C results in a ough surface with, at times, discontinuities in the YBCO film. In the case of $LaAlO_3$, a cubic-to-rhombohedral (90.1°) transformation at ~450°C does not disrupt the film although surface roughness is on the order of 50 nm (by profilometer measurement) with a period of 50 μm. Both perovskites can be produced by Czochralski growth and are available in sizes up to 2-inch diameter. Substantially larger sizes would be useful for UHF antenna arrays. It is hoped that $NdGaO_3$ will have all the advantages of $LaAlO_3$ without rough surfaces. Its' structural transformation at 1350°C is at a temperature much greater than growth temperatures. The $NdGaO_3$ that is starting to be made available commercially has a lower purity than the available $LaAlO_3$.

In summary, $LaAlO_3$ is the preferred substrate at present for its lattice match to YBCO, chemical stability in contact with YBCO, availability in sizes up to 2 inches in diameter, reasonably low tan δ, and manageable dielectric constant. Nevertheless, there is a substantial effort underway to make use of sapphire by growing YBCO on a buffer layer of epitaxial MgO(100),[30,31] $LaAlO_3$(100), or $SrTiO_3$(100)[32] on sapphire.

4. R_s AND YBCO FILM GROWTH

The best YBCO films grown by sputtering, co-evaporation, and laser ablation have comparable critical temperatures, transition widths, critical current densities, and dependence on thickness for ultrathin films $\leq$ 10 nm thick. In this section, we will show that they also have comparable R_s values. The films have in common a

deposition temperature of 650-750°C, growth in the presence of molecular or activated oxygen, and a cooldown from the deposition temperature in > 10 torr O_2 to transform to the orthorhombic YBCO structure.

Our measurements of R_s were made with X-band resonators in either a stripline or microstrip configuration. In the stripline configuration, shown in Fig. 3, a Nb film was patterned in a half-wavelength long line on one side of a 0.700 x 0.250 x 0.020 inch substrate and a Nb ground plane was deposited on the other side. Following Ref. 33, an HTS film was used as the second ground plane and R_s was calculated from the Q measured in transmission. The substrate of the HTS film was inside the resonator so current flowed in the film layer adjacent to the substrate. Measurements of R_s were made only at 4.2K. In the microstrip configuration, two nominally identical HTS films were mounted with both of their substrates in the cavity. One film was patterned in a half-wavelength line and the other was used as a ground plane. Again, R_s was calculated[34] from Q measured in transmission. In both cases, the resonators were weakly coupled to the rest of the circuit so the unloaded Q could be assumed to be equal to the loaded Q.

Figure 4 shows the result of a microstrip measurement as a function of temperature. Measurements were made in liquid helium, liquid nitrogen, and with a cryorefrigerator. The YBCO films were deposited by off-axis sputtering from a stoichiometric $YBa_2Cu_3O_7$ target at a substrate temperature of 670°C by dc magnetron sputtering. The substrates were 0.500 x 0.250 x 0.017 inch $LaAlO_3$ held to the substrate block by silver paste. The sputtering gas consisted of 20 mtorr O_2 and 130 mtorr Ar. Additional deposition details are found in Ref. 35. Figure 4 shows two general features of R_s measurements. The first is a nearly temperature independent residual resistance for $T << T_c$. The second feature is a strongly temperature-dependent R_s in the vicinity of T_c which is sensitive to T and T_c.

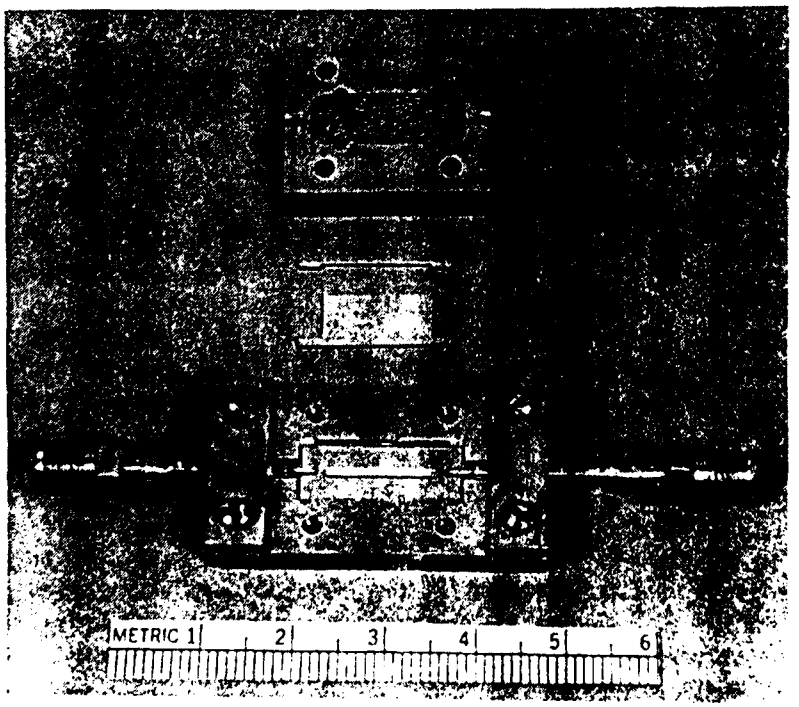

Fig. 3. Nb and YBCO end-coupled stripline resonator. The patterned conductor and bottom ground plane are epitaxial Nb films grown on sapphire. The top ground plane is a YBCO film to be evaluated. Capacitive coupling to the resonator is accomplished by adjustable pins.

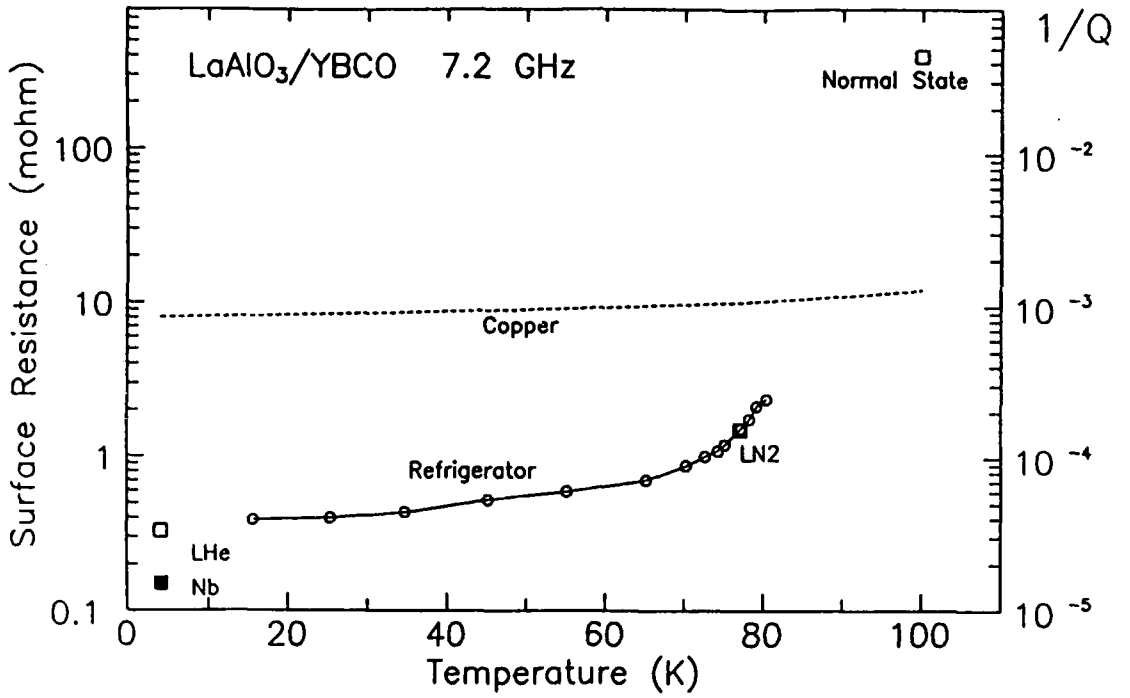

Fig. 4. R_s and 1/Q plotted as a function of temperature for a microstrip resonator. The assumption must be made that two YBCO films deposited on $LaAlO_3$ have the same surface resistance for a value of R_s to be calculated.

Two ways of comparing the surface resistance of YBCO made by different techniques and at different laboratories are shown in Table 3. The better comparison is made in the last column of Table 3 which states that the best YBCO films obtained from several sources have the same R_s at $T << T_c$ if they are measured at one laboratory. The second comparison shows that the residual resistance of YBCO at 4.2K is approximately two times greater than the R_s of Nb at 4.2K, although the specific value of R_s for both YBCO and Nb vary by more than an order magnitude in measurements made in different laboratories. To permit this comparison to be made, it was assumed that R_s scales with frequency as f^2. The discrepancy in R_s of Nb may be simply an issue of calibration or it might reflect the poorer quality of Nb films compared with bulk Nb. For bulk Nb at 10 GHz, R_s = 20 to 60 $\mu\Omega$. It is also possible that films have a higher effective R_s when they are patterned. For any technique used to measure R_s, a verification of sensitivity and of Nb quality can be made by cooling Nb below 4.2K and observing a higher Q than obtained at 4.2K.

Figure 4 and Table 3 lead to several important conclusions. The mechanism responsible for the residual resistance appears to be common to films made by all techniques and is independent of which film surface is being measured (free surface or interface with the substrate). Therefore, the loss mechanism must be related to a property of the entire film and not just to a surface problem. The magnitude of the surface resistance at 10 GHz and $T << T_c$ is at least an order of magnitude lower than that of Cu. Since R_s for a normal metal increases with frequency as the square root of f and for a superconductor as f^2, the state of the art represents a tremendous improvement over Cu for $f << 10$ GHz and little improvement for $f >> 10$ GHz. Whether or not the current YBCO film technology is sufficient to satisfy the requirements of a particular application depends not only on how high Q must be, but also on the operating frequency of a particular application. With regard to the previous

Table 3 - Comparison of the lowest R_s measured for YBCO and Nb at 4.2K normalized to 10 GHz by assuming $R_s \propto f^2$.

Reference	Side of Film Measured	Film Patterned	R_s(Nb)	R_s(YBCO)	R_s(YBCO)/R_s(Nb)	Deposition Technique[a]
Westinghouse	substrate	yes	0.3 mΩ	0.6 mΩ	2	S
Belohoubek, DSRC	substrate	yes	0.15[36]	0.3[37]	2	L,L[b]
Hammond, STI	both	no	--	0.6[37]	--	L,S
Padamsee, Cornell	both	no	--	0.6[37]	--	L,S
Drabeck, UCLA	surface	no	--	0.05[38]-0.6[37]	--	L,L,S
Piel, Wuppertal	surface	no	~0.06[38c]	0.1[39]	$\lesssim$ 2	L,S,E
Taber, H-P	surface	no	0.02[40]	0.02-0.04[40]	1-2	S,S
Cooke, LANL	surface	no	--	0.04[41]	--	L,E
Oates, Lincoln Lab	both	yes	0.05-0.2[38]	$\gtrsim$ 0.4[38]	$\gtrsim$ 2	S,E

[a] L – Laser-ablated, S – Sputtered, E – Co-Evaporated
[b] Laser-ablated films obtained from two different sources
[c] Nb R_s (4.2K, 87 GHz) = 10-25 mΩ; scaled to 10 GHz using Mattis-Bardeen Theory instead of f^2.

discussion of substrates, note that all of the results in Table 3 were obtained for films grown on perovskite substrates with a close lattice match to YBCO.

5. REMAINING MATERIALS ISSUES

Since several film deposition techniques give comparable dc and rf YBCO film properties, an additional set of materials requirements can be used to ultimately determine a preferred technique. The requirements include surface smoothness, integration with other deposited layers, and scaling to large areas. These issues have been partially addressed for the techniques of sputtering, co-evaporation, and laser ablation. The problem of surface smoothness is most serious for laser ablation since YBCO particles can be ejected from the target and deposited on the substrate. Sputtering has produced uniform YBCO films over substrate areas as large as 2 inches in diameter.[35,42] In principle, laser ablation will also produce films over a 2-inch diameter by sufficiently separating the target and substrates but, high-quality laser-ablation on this scale has yet to be demonstrated.

Integration of HTS films with epitaxial deposited dielectrics is crucial for crossovers and compact microstrip transmission and delay lines. The same insulators that have been used successfully as substrates and buffer layers on sapphire are the best candidates for dielectrics deposited between YBCO film layers. Epitaxial trilayers

consisting of YBCO films separated by deposited $SrTiO_3$,[43] MgO,[31] and $LaAlO_3$,[44] have been demonstrated, although $SrTiO_3$ is useful only for low-frequency applications.

There are several materials requirements listed in Table 1 which have not yet been addressed experimentally. One example is growth of as-deposited crystalline films on both sides of a substrate. In the case of YBCO growth on sapphire, the optimum growth temperature falls in a range of approximately 15°C. Temperature profiles that are uniform to this extent will have to be obtained on a thermally-floating substrate which is maintained at 650-700°C by radiation rather than conduction. Another unresolved issue is whether epitaxial multilayers must be formed *in situ*. Even if epitaxial dielectric films will grow on YBCO underlayers that have been patterned, it is unknown whether the rf properties of the insulating film are degraded relative to *in-situ* fabrication.

6. CONCLUSIONS

Many of the requirements for rf applications using HTS films are attained by state-of-the-art YBCO films. At all frequencies up to mm-waves, and temperatures extending to within a few degrees of T_c, the surface resistance is much less than that of normal metals. $LaAlO_3$ is a suitable substrate for all but the highest-Q applications and those requiring areas greater than 2-inch diameter wafers.

We want to acknowledge the assistance of S. H. Talisa, B. R. McAvoy, D. H. Watt, and G. B. Draper with the measurements of surface resistance, T. T. Braggins, M. G. Forrester, and J. R. Gavaler with YBCO film development, N. J. Doyle and A. M. Stewart with x-ray measurements, and colleagues outside of Westinghouse who made their data available to us prior to publication through preprints and presentations.

7. REFERENCES

1. "Bibliography of High-T_c Superconductivity," *J. Superconductivity* 2(1), pp. 1-210 (1989) and 3(1), pp. 1-153 (1990).

2. C. L. Bohn, J. R. Delayen, U. Balachandran, and M. T. Lanagan, "Radio Frequency Surface Resistance of Large-Area Bi-Sr-Ca-Cu-O Thick Films on Ag Plates," *Appl. Phys. Lett.* 55(3), pp. 304-306 (1989).

3. C. L. Lichtenberg, J. Wosik, M. Davis, and J. C. Wolfe, "Microwave Microstrip Resonator Measurements of $YBa_2Cu_3O_{7-x}$ and $Bi_2Sr_2Ca_1Cu_2O_{8-y}$ Thin Films," submitted to *Appl. Phys. Lett.* (1989).

4. J. H. Takemoto, F. K. Oshita, H. R. Fetterman, P. Kobrin, and E. Sovero, "Microstrip Ring Resonator Technique for Measuring Microwave Attenuation in High-T_c Superconducting Thin Films," *IEEE Trans. Microwave Theory and Techniques* 37(10), pp. 1650-1652 (1989).

5. R. B. Hammond, G. V. Negrete, M. S. Schmidt, M. J. Moskowitz, M. M. Eddy, D. D. Strother, and D. L. Skoglund, "Superconducting Tl-Ca-Ba-Cu-O Thin Films Microstrip Resonator and Its Power Handling Performance at 77K," IEEE Microwave Symp. (1990).

6. D. W. Cooke, et al., "Microwave Characterization of High-Temperature Superconductors," submitted to SPIE's Symp. Microelectronic Integrated Processing: Growth, Monitoring & Control, Santa Clara, CA (1989).

7. *Landolt-Bornstein Numerical Data and Functional Relationships*, Vol. II(6), Springer-Verlag, Heidelberg, 1959, pp. 462-558.

8. A. F. Harvey, *Microwave Engineering*, Academic Press, New York, 1963, pp. 253-254.

9. K. Araki, I. Iwasa, Y. Kobayashi, S. Nagata, and M. Morisue, "Ultra Broad Band Measurements on High-T_c Ceramic Superconducting Transmission Lines," *IEEE Trans. Magn.* 25, 980-983 (1989).

10. B. P. Gorshunov, G. V. Kozlov, S. I. Krasnosvobodtsev, E. V. Pechen, A. M. Prokhorov, A. S. Prokhorov, O. I. Syrotynsky, and A. A. Volkov, "Submillimetre Properties of High-T_c Superconductors," *Physica C* 153-155, 667-670 (1988).

11. G. Rupprecht and R. O. Bell, "Microwave Losses in Cubic Strontium Titanate above the Phase Transition," *Phys. Rev.* 123(1), 97-98 (1961).

12. G. Rupprecht, R. O. Bell, and B. D. Silverman, "Nonlinearity and Microwave Losses in Cubic Strontium Titanate," *Phys. Rev.* 125(6), 1915-1920 (1962).

13. J. S. Thorp and H. P. Buckley, "The Dielectric Constants of Current-Blackened Single Crystal Yttria-Stabilized Zirconia," *J. Mater. Sci.* 8, pp. 1401-1408 (1973).

14. R. L. Sandstrom, E. A. Giess, W. J. Gallagher, A. Segmuller, E. I. Cooper, M. F. Chisholm, A. Gupta, S. Shinde, and R. B. Laibowitz, "Lanthanum Gallate Substrates for Epitaxial High-T_c Superconducting Thin Films," *Appl. Phys. Lett.* 53(19), 1874-1876 (1988).

15. M. T. Lanagan, J. K. Yamamoto, A. Bhalla, and S. G. Sankar, "The Dielectric Properties of Yttria-Stabilized Zirconia," *Mater. Lett.* 7, 437 (1989).

16. A. C. Anderson, B.-Y. Tsaur, J. W. Steinbeck, and M. S. DiIorio, "RF Surface Resistance of $YBa_2Cu_3O_{7-x}$ Thin Films," *MIT Lincoln Laboratory Quarterly Tech. Rep.,* March 11 (1988).

17. J. Musil and F. Zacek, "Microwave Measurements of Complex Permittivity by Free Space Methods and Their Applications," in *Studies in Electrical and Electronic Engineering Vol. 22*, Elsevier, New York, 1986, pp. 254-262.

18. J. S. Thorp and N. Enayati-Rad, "The Dielectric Behavior of Single-Crystal MgO, Fe/MgO and Cr/MgO," *J. Mater. Sci.* 16, pp. 255-260 (1981).

19. D. Oates (Lincoln Laboratory), unpublished.

20. V. B. Braginsky, V. S. Ilchenko, and Kh. S. Bagdassarov, "Experimental Observation of Fundamental Microwave Absorption in High-Quality Dielectric Crystals," *Phys. Lett. A* 120, 300-303 (1987), and references therein.

21. V. B. Braginsky and V. I. Panov, "Superconducting Resonators on Sapphire," *IEEE Trans. Magn.* MAG-15(1), 3-33 (1979).

22. W. G. Lyons, "Low-Loss Substrates for High-Temperature Superconductors," *MIT Lincoln Laboratory Quarterly Tech. Rep.,* October (1989).

23. J. D. Adam (Westinghouse), unpublished.

24. R. W. Simon, C. E. Platt, K. P. Daly, A. E. Lee, and M. K. Wagner, "Improvement of Average Film Quality in $RBa_2Cu_3O_{7-x}$ Sputtered Films," *IEEE Trans. Magn.* MAG-25, 2433-2436 (1989), and *Appl Phys. Lett.* 53, 2677-2679 (1988).

25. M. C. Nuss, P. M. Mankiewich, R. E. Howard, B. L. Straughn, T. E. Harvey, C. D. Brandle, G. W. Berkstrasser, K. W. Goossen, and P. R. Smith, "Propagation of Terahertz Bandwidth Electrical Pulses on $YBa_2Cu_3O_7$ Transmission Lines on $LaAlO_3$ Substrates," Appl. Phys. Lett. 54, 2265-2267 (1989).

26. R. W. Simon, A. E. Lee, C. E. Platt, K. P. Daly, J. A. Luine, C. B. Eom, P. A. Rosenthal, X. D. Wu, and T. Venkatesan, "Growth of High-Temperature Superconductor Thin Films on Lanthanum Aluminate Substrates," in *Science and Technology of Thin-Film Superconductors,* edited by R. McConnell and S. A. Wolf (Plenum, New York, 1989), pp. 337-346.

27. J. Geerk, G. Linker, and O. Meyer, "Epitaxial Growth and Properties of YBaCuO Thin Films," *Mater. Sci. Reports* 4, 193-260 (1989).

28. A. Inam, M. S. Hegde, X. D. Wu, T. Venkatesan, P. England, P. F. Miceli, E. W. Chase, C. C. Chang, J. M. Tarascon, and J. B. Wachtman, "As-Deposited High T_c and J_c Superconducting Thin Films Made at Low Temperatures," *Appl. Phys. Lett.* 53(10), 908-910 (1988).

29. K. Char, D. K. Fork, T. H. Geballe, S. S. Laderman, R. C. Taber, R. D. Jacoqitz, F. Bridges, G.A.N. Connell, and J. B. Boyce, "Properties of Epitaxial $YBa_2Cu_3O_7$ Thin Films on Al_2O_3 {1012}." *Appl. Phys. Lett.* 56(8), 183-185 (1990).

30. J. Talvacchio, G. R. Wagner, and H. C. Pohl, "$YBa_2Cu_3O_7$ Films Grown on Epitaxial MgO Buffer Layers on Sapphire," *Physica C* 162-164, 659-660 (1989).

31. A. B. Berezin, C. W. Yuan, and A. L. de Lozanne, "$Y_1Ba_2Cu_3O_{7-x}$ Thin Films Grown on Sapphire with Epitaxial MgO Buffer Layers," submitted to *Appl. Phys. Lett.* (1990).

32. K. Char, N. Newman, S. M. Garrison, R. W. Barton, R. C. Taber, S. S. Laderman, and R. D. Jacowitz, "Microwave Surface Resistance of YBCO Thin Films on Sapphire," submitted to *Appl. Phys. Lett.* (1990).

33. A. C. Anderson, B.-Y. Tsaur, J. W. Steinbeck, and M. S. DiIorio, "RF Surface Resistance of $YBa_2Cu_3O_{7-x}$ Thin Films," *MIT Lincoln Laboratory Quarterly Tech. Rep.*, March 11 (1988).

34. M. V. Schneider, "Microstrip Lines for Microwave Integrated Circuits," *Bell System Technical Journal*, 1421-1444, May-June 1969.

35. J. Talvacchio, J. R. Gavaler, M. G. Forrester, and T. T. Braggins, to appear in *Science and Technology of Thin Film Superconductors II*, edited by R. D. McConnell and S. A. Wolf (Plenum, New York, 1990).

36. R. Brown, V. Pendrick, and D. Kalokitis, "A Low Loss Substrate for Microwave Application of High Temperature Superconductor Films," submitted to Appl. Phys. Lett. (1990).

37. A. Inam, L. Nazar, M. S. Hegde, C. T. Rogers, T. Venkatesan, R. W. Simon, K. Daly, H. Padamsee, J. Kirchgessner, D. Moffat, D. Rubin, Q. S. Shu, D. Kalokitis, A. Fathy, V. Pendrick, R. Brown, B. Brycki, E. Belohoubek, L. Drabeck, G. Gruner, R. Hammond, F. Gamble, B. M. Lairson, and J. C. Bravman, "Microwave Properties of Highly Oriented $Y_1Ba_2Cu_3O_{7-x}$ Thin Films," *Appl. Phys. Lett.* 56(12), 1178-1180 (1990). Based on the temperature dependence of R_s for the best Westinghouse films and the data presented by Inam in the range, 50K-90K, a ratio, $R_s(77K)/R_s(4.2K) = 2.5$ was assumed.

38. Data presented at the *Symposium on High Temperature Superconductors in High Frequency Fields*, Williamsburg, Virginia, March 1990.

39. N. Klein, G. Muller, H. Piel, B. Roas, L. Schultz, U. Klein, and M. Peiniger, "Millimeter Wave Surface Resistance of Epitaxially Grown $YBa_2Cu_3O_{7-x}$ Thin Films," *Appl. Phys. Lett.* 54(8), 757-759 (1989).

40. R. C. Taber, "A Parallel Plate Resonator Technique for Microwave Loss Measurements on Superconductors," submitted to *Rev. Sci. Instr.* (1990).

41. D. W. Cooke, E. R. Gray, R. J. Houlton, B. Rusnak, E. A. Meyer, J. G. Beery, D. R. Brown, F. H. Garzon, I. D. Raistrick, A. D. Rollet, and R. Bolmaro, "Surface Resistance of $YBa_2Cu_3O_7$ Films on $SrTiO_3$ and $LaGaO_3$ Substrates," *Appl. Phys. Lett.* 55(9), 914-916 (1989).

42. N. Newman, K. Char, S. M. Garrison, R. W. Barton, R. C. Taber, C. B. Eom, T. H. Geballe, and B. Wilkens, "YBCO Superconducting Films with Low Microwave Surface Resistance over Large Areas," submitted to *Appl. Phys. Lett.* (1990).

43. J. J. Kingston, F. C. Wellstood, P. Lerch, A. H. Miklich, and J. Clarke, "Multilayer $YBa_2Cu_3O_x$-$SrTiO_3$-$YBa_2Cu_3O_x$ Films for Insulating Crossovers," *Appl. Phys. Lett.* 56(2), 189-191 (1990).

44. R. W. Simon, J. F. Burch, K. P. Daly, W. D. Dozier, R. Hu, A. E. Lee, J. A. Luine, H. M. Manasevit, C. E. Platt, S. M. Schwarzbek, D. St. John, M. S. Wire, and M. J. Zani, "Progress toward a YBCO Circuit Process," to appear in *Science and Technology of Thin Film Superconductors II*, edited by R. D. McConnell and S. A. Wolf (Plenum, New York, 1990).

PHYSICAL REVIEW B VOLUME 41, NUMBER 16 1 JUNE 1990

Anomalous Hall effect in superconductors near their critical temperatures

S. J. Hagen, C. J. Lobb, and R. L. Greene*
Center for Superconductivity Research, Department of Physics and Astronomy, University of Maryland, College Park, Maryland 20742

M. G. Forrester and J. H. Kang
Westinghouse Science and Technology Center, 1310 Beulah Road, Pittsburgh, Pennsylvania 15235

(Received 5 March 1990)

Measurements on epitaxial $YBa_2Cu_3O_7$ thin films show that the Hall voltage just below the superconducting transition temperature has sign opposite to the Hall voltage in the normal state. This can result either from quasiparticle effects, or from unusual vortex motion. Because we observe a similar effect in Nb thin films, we argue that vortex motion is responsible. A simple interpretation of the Hall effect then requires that the vortex velocity have a component *antiparallel* to the transport current. This motion, while contrary to existing flux flow models, could result from vortex motion damping similar to that expected in superfluid ^{4}He.

Transport measurements[1,2] on the high-temperature superconductors $RBa_2Cu_3O_7$ (R=Y,Er) and $Bi_2Sr_2CaCu_2O_8$ have shown an unexpected reversal of the sign of the Hall voltage V_H at temperatures below the superconducting transition. Although the Hall voltage in the normal state is positive (i.e., holelike) and linear in magnetic field, V_H in the mixed state is negative for small field and positive for larger field, in contradiction of microscopic[3] and flux flow[4,5] theories for the Hall effect in superconductors. Our measurements on $YBa_2Cu_3O_7$ and Nb thin films provide evidence that this sign reversal below T_c results from vortex motion with a velocity component *opposite* to the direction of the superfluid transport current.

We measured the Hall resistivity ρ_{xy} and magnetoresistivity ρ_{xx} of thin films of epitaxial c-axis-oriented $YBa_2Cu_3O_7$ (thickness = 1500 Å) in magnetic fields up to 70 kG oriented perpendicular to the film. The films were dc magnetron sputtered from a stoichiometric target onto rotating substrates of (100) $SrTiO_3$, MgO, $LaAlO_3$, or cubic zirconia. A layer of Au sputtered onto the leads *in situ* provided low-resistance (~1 Ω) contacts; the films were then etched into an eight-lead Hall bar pattern (bar area 50 μm×3.9 mm). The films had T_c ~88–90 K (midpoint) and ρ_{xx}(300 K) = 450–750 μΩ cm. We measured Hall resistance and magnetoresistance both dc (with current reversal) and ac (phase sensitive at 100 Hz) at current densities $J \sim 10^2$–10^4 A/cm^2, obtaining the Hall resistance from the transverse resistance by subtracting the positive and negative magnetic-field data.

Figure 1 shows typical ρ_{xx} and ρ_{xy} data as a function of field at $T < T_c$. Although ρ_{xy} is nearly temperature independent just above T_c, it decreases to negative values in the superconducting state, eventually becoming zero as temperature or field decreases (Fig. 2). Note that ρ_{xy} changes sign while ρ_{xx} is still close to its normal-state value. Higher fields drive the region of negative ρ_{xy} to lower temperatures (inset of Fig. 1).

Figure 2 shows ρ_{xy} in the immediate neighborhood of T_c(=90 K). At low field, ρ_{xy} becomes negative at tem-

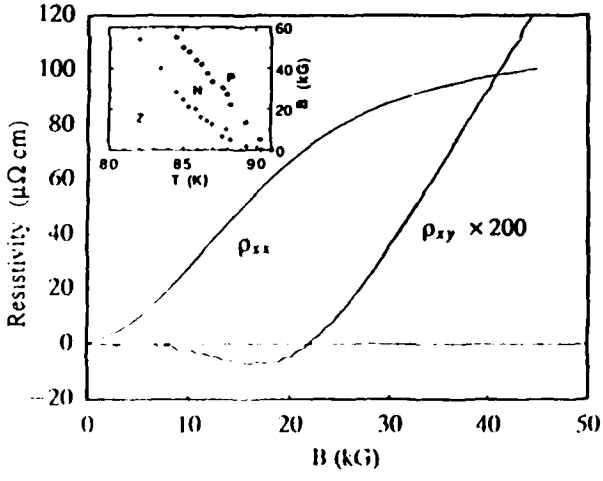

FIG. 1. Hall resistivity ρ_{xy} and longitudinal resistivity ρ_{xx} vs magnetic field in $YBa_2Cu_3O_7$ film at T = 86.0 K. Inset: Field and temperature regimes where ρ_{xy} is positive (P), negative (N), and zero (Z) for a film with T_c(midpoint) ≃ 89 K.

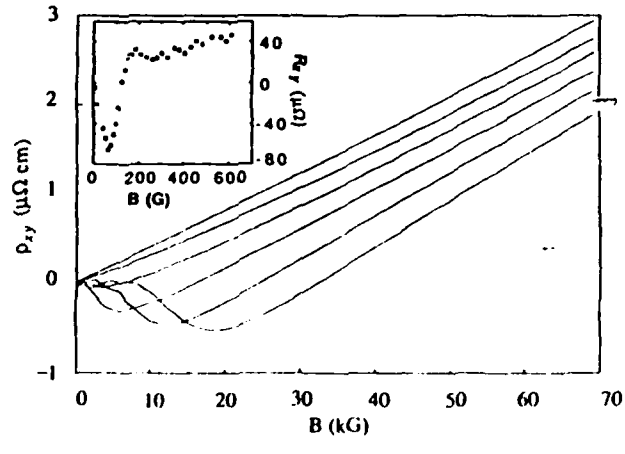

FIG. 2. Hall resistivity ρ_{xy} vs magnetic field in $YBa_2Cu_3O_7$ near T_c (≃90 K) showing linearity at high field. Temperatures from top to bottom are 93.0, 91.5, 90.5, 89.8, 89.1, and 88.4 K. Inset: Hall resistance of Nb film vs field at T = 9.16 K.

atures close to T_c; positive ρ_{xy} is then recovered at high field. However, for fields exceeding $H_{c2}(T)$ the full normal state ρ_{xy} is not observed. From the upper critical field slope of -19 kG/K obtained by Welp *et al.*,[6] it is clear that the sample should no longer be in the superconducting state at $B \sim 70$ kG and $(T_c - T) \sim 2$ K. However, $\rho_{xy}(T < T_c)$ remains less than $\rho_{xy}(T > T_c)$ at high fields $H \gg H_{c2}$, even though the slope $d\rho_{xy}/dH$ approaches its normal-state value.

Sign reversal of ρ_{xy} in the mixed state was observed by previous authors[1,2] and attributed to grain effects, possible two-carrier quasiparticle effects, or conventional flux motion. In low-T_c superconductors, many different behaviors were observed in the Hall effect below T_c. Sign reversal, although not always observed, was found in some V foils[7] and In-Pb alloys.[8] Existing flux flow[4,5] and microscopic[3] theories for the Hall effect in the mixed state predict no sign change and therefore do not account for this data.

In order to study the Hall effect in well-characterized samples of the low-T_c superconductor, we prepared Nb thin films. The films (1300 Å thick) were prepared by dc sputtering onto sapphire substrates and etched into the Hall bar pattern. Their resistivity at $T = 273$ K was 13 $\mu\Omega$ cm (cf. bulk value ~ 12.5 $\mu\Omega$ cm), with $\rho_{xx}(300\text{ K})/\rho_{xx}(9.5\text{ K}) = 45$ and $T_c = 9.25$ K. The Hall resistivity for $T > T_c$ and $H > H_{c2}$ is positive and linear in field, but for $T < T_c$ and $H < H_{c2}$ we find ρ_{xy} reverses to negative values just as in $YBa_2Cu_3O_7$ (inset of Fig. 2). Thus the reversal occurs in both low-temperature elemental superconductors and high-temperature oxide superconductors, whose electronic properties are very different, which strongly suggests that the phenomenon is a general property of the vortex state.

Josephson[9] demonstrated that the motion of flux vortices at a velocity $\mathbf{v}_L$ through a superconductor produces an electric field given by Faraday's law,

$$\mathbf{E} = -\frac{n}{c}\mathbf{v}_L \times \bar{\phi}_0 = -\frac{\mathbf{v}_L \times \mathbf{H}}{c}, \tag{1}$$

where n is the areal density of vortices and $\bar{\phi}_0 = \phi_0 \mathbf{H}/H$, so that flux flow in the direction of $\mathbf{J} \times \bar{\phi}_0$ [Fig. 3(a)] generates a field E parallel to the transport current J and therefore dissipates energy. Similarly, a component of flux motion along J produces a transverse field parallel to $-\mathbf{J} \times \bar{\phi}_0$; if the charge carriers are of the same sign in the normal and superconducting states (as expected for a BCS superconductor), this field is observed as a Hall voltage of the *same* sign as in the normal metal [Fig. 3(b)]. Thus a reversal of the sign of the Hall voltage upon entering the mixed state indicates either that the sign of the charge carriers has changed or that the flux-line velocity $\mathbf{v}_L$ has a component *opposite* to the direction of the transport current. Because it is difficult to see why the charge carriers should change sign in the superconducting state not only in copper-oxide superconductors but also in elemental superconductors like Nb and V, we argue that this unexpected flux motion is in fact a more likely explanation of the negative Hall effect near T_c.

In standard models of flux motion,[4,5] the transport current J produces a force F that drives the flux motion.

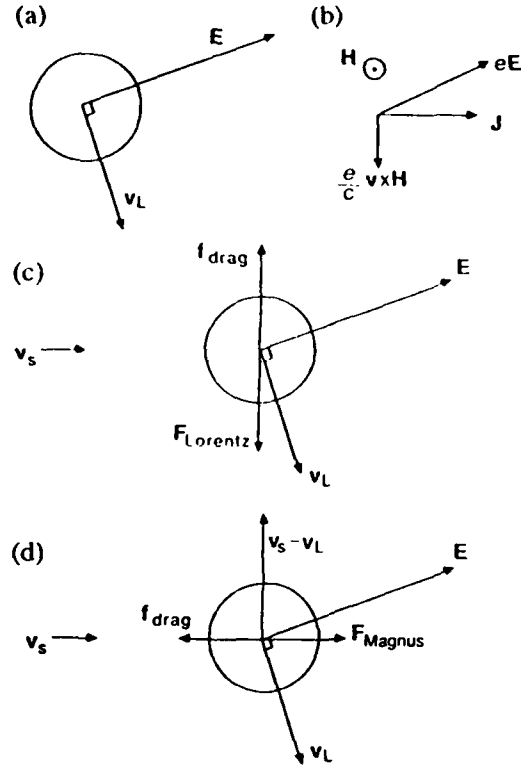

FIG. 3. (a) Electric field generated by vortex motion [Eq. (1)]. (b) Lorentz force $(e/c)\mathbf{v} \times \mathbf{H}$ on free charge carrier $(q = +e)$ balanced by electric field E to give the normal-state Hall effect. Field H is directed out of the page. (c) Forces on vortex core in Bardeen-Stephen model for flux flow. The Lorentz force $\mathbf{J} \times \bar{\phi}_0/c$ is balanced by an opposing viscous force. (d) Forces on vortex core in Nozieres-Vinen model. The Magnus force $n_s e(\mathbf{v}_s - \mathbf{v}_L) \times \bar{\phi}_0/c$ is balanced by a drag force antiparallel to the superfluid velocity $\mathbf{v}_s$.

This force can be balanced by a frictional force f so that the net force $\mathbf{F} + \mathbf{f} = 0$. In the Bardeen-Stephen model,[5] the driving force per unit length is the Lorentz force $\mathbf{F} = \mathbf{J} \times \bar{\phi}_0/c$; the frictional force is assumed to act in the opposite direction [Fig. 3(c)]. Normal electrons passing through the vortex cores experience the usual magnetic force and a Hall voltage results just as in the normal state. Thus the vortex velocity has a small component parallel to J and the Hall effect in flux flow is of the same sign as in the normal state.

In the Nozieres-Vinen model,[4] the force on a vortex is the Magnus force

$$\mathbf{F} = \frac{n_s e}{c}(\mathbf{v}_s - \mathbf{v}_L) \times \bar{\phi}_0, \tag{2}$$

where n_s is the superfluid electron density and $\mathbf{v}_s = \mathbf{J}/n_s e$ is the superfluid velocity. If $\mathbf{f} = 0$, the vortices move with $\mathbf{v}_L = \mathbf{v}_s$ and produce a transverse field $\mathbf{E} = -\mathbf{v}_L \times \mathbf{H}/c = -\mathbf{J} \times \mathbf{H}/n_s ec$ in the same direction as for the normal-state Hall effect. A frictional drag introduced through $\mathbf{f} \propto -\mathbf{v}_s$ does not affect the sign of the Hall effect [Fig. 3(d)].

Because neither of these models can produce a sign change in the Hall effect near T_c, we suggest an analogy

to the case of vortex motion in superfluid ^{4}He. In superfluid ^{4}He, relative motion between the vortices and the superfluid produces a Magnus force

$$\mathbf{F}=\frac{\rho_s h}{m}(\mathbf{v}_s-\mathbf{v}_L)\times\mathbf{z}, \tag{3}$$

where ρ_s is the superfluid density and $\mathbf{z}$ is a unit vector indicating the vortex circulation. Hall and Vinen, and Ambegaokar, Halperin, Nelson, and Siggia (AHNS) discuss a general drag force of the form[10]

$$\mathbf{f}=-\eta\mathbf{v}_L-\eta'\mathbf{z}\times\mathbf{v}_L. \tag{4}$$

The condition $\mathbf{F}+\mathbf{f}=0$ then produces an equation of motion

$$\mathbf{v}_L=\frac{h\rho_s}{m}D\mathbf{v}_s\times\mathbf{z}+C\mathbf{v}_s. \tag{5}$$

Here

$$D=\frac{\eta}{(h\rho_s/m-\eta')^2+\eta^2}, \tag{6a}$$

$$C=\frac{h\rho_s}{m}\frac{h\rho_s/m-\eta'}{(h\rho_s/m-\eta')^2+\eta^2}. \tag{6b}$$

AHNS note that in the limit of no drag forces $\eta=\eta'=0$ and the coefficients $D=0$ and $C=1$. The vortices then flow with the superfluid and at the same velocity, as in the Nozieres-Vinen superconductor with $\mathbf{f}=0$. However, we observe that for large damping, if $\eta'>h\rho_s/m$, we have $C<0$ and $\mathbf{v}_L$ has a component *opposite* to the direction of the superfluid flow. Such motion is consistent with energy conservation, as the force in η' does no work. Therefore a similar damping force

$$\mathbf{f}=-\eta\mathbf{v}_L-\eta'\bar{\phi}_0\times\mathbf{v}_L \tag{7}$$

acting against the Magnus force in a superconductor would cause "upstream" vortex motion for $\eta'>n_s e/c$ and reverse the sign of the Hall voltage.

Therefore we propose that under weak pinning the vortices in the mixed state of a superconductor move under the influence of the Magnus force (2) described by Nozieres and Vinen and a frictional force (7). Near the superconducting transition the number of superconducting electrons is small and the drag term in η' may be large enough to produce a flux velocity component opposite to the direction of the transport current: thus the Hall effect has sign opposite to that of the normal state. [We note that a Lorentz force $\mathbf{F}=\mathbf{J}\times\bar{\phi}_0/c$ combined with a frictional force (7) will produce a sign change in ρ_{xy} for any $\eta'>0$.] If the flux lines become pinned to the crystal lattice the vortex motion slows and the Hall voltage vanishes. This picture is consistent with Fig. 1, where ρ_{xx} is close to zero at the field where ρ_{xy} vanishes. We note that the temperatures and fields at which ρ_{xy} disappears in $YBa_2Cu_3O_7$ are comparable[11] to those of the "irreversibility" or "melting" lines[12] observed in other measurements on this material. Thus the appearance of nonzero Hall voltage may mark an increase in flux motion in $YBa_2Cu_3O_7$. By contrast, at high field or temperature, large numbers of quasiparticles will be excited and contribute a positive Hall effect, driving the Hall voltage positive towards its normal-state value. In the case of copper-oxide superconductors, fluctuations[2] persisting to high fields and temperatures may prevent the Hall voltage from fully recovering its normal-state (linear in H) behavior. Thus the fact that $\rho_{xy}(T\le T_c)$ in $YBa_2Cu_3O_7$ becomes positive and linear at high fields but remains offset from its normal-state value (Fig. 2) can be attributed to the presence of strong fluctuations.

In summary, we suggest that the sign reversal of the Hall effect observed near the superconducting transition in both the high-temperature copper-oxide superconductors and some low-temperature superconducting metals indicates a component of flux-flow velocity *opposite* to the direction of the superfluid transport current.[13] Such a velocity component could result from vortex-motion damping resembling that in superfluid ^{4}He.

We acknowledge useful discussions with D. R. Nelson, who suggested the analogy between vortex motion in thin ^{4}He films and superconductors, and with S. Yip. We also received assistance with high-T_c film growth from J. Talvacchio and J. R. Gavaler, and programming assistance from W. Jiang. Sample fabrication at Westinghouse was supported by U.S. Air Force Office of Scientific Research Contract No. F49620-88-C-0039.

---

*Also at IBM Research Division, Yorktown Heights, NY 10598.

[1]M. Gallffy and E. Zirngiebl, Solid State Commun. **68**, 929 (1988); S. N. Artemenko, I. G. Gorlova, and Y. I. Latyshev, Pis'ma Zh. Eksp. Teor. Fiz. **49**, 352 (1989) [JETP Lett. **49**, 403 (1989)]; Phys. Lett. A **138**, 428 (1989); L. Forro and A. Hamzic, Solid State Commun. **71**, 1099 (1989).

[2]Y. Iye, S. Nakamura, and T. Tamegai, Physica C **159**, 616 (1989).

[3]K. Maki, Phys. Rev. Lett. **21**, 1223 (1969).

[4]P. Nozieres and W. F. Vinen, Philos. Mag. **14**, 667 (1966).

[5]J. Bardeen and M. J. Stephen, Phys. Rev. **140**, A1197 (1965).

[6]U. Welp, W. K. Kwok, G. W. Crabtree, K. G. Vandevoort, and J. Z. Liu, Phys. Rev. Lett. **62**, 1908 (1989).

[7]N. Usui, I. Ogasawara, K. Yasukochi, and S. Tomoda, J. Phys. Soc. Jpn. **27**, 574 (1969).

[8]C. H. Weijsenfeld, Phys. Lett. **28A**, 362 (1968).

[9]B. Josephson, Phys. Lett. **16**, 242 (1965).

[10]H. E. Hall and W. F. Vinen, Proc. R. Soc. London **238**, 215 (1956); see also V. Ambegaokar, B. I. Halperin, D. R. Nelson, and E. D. Siggia, Phys. Rev. B **21**, 1806 (1980).

[11]The similarity was previously noted by Iye, Nakamura, and Tamegai, Ref. 2.

[12]See, for example, *Strong Correlation and Superconductivity: The Proceedings of the IBM Japan International Symposium*, edited by H. Fukuyama, S. Maekawa, and A. P. Malozemoff (Springer-Verlag, Berlin, Heidelberg, 1989), and references therein.

[13]While this manuscript was being completed, we received a

preprint on the Hall effect in the mixed state of $YBa_2Cu_3O_7$ by T. R. Chien, N. P. Ong, and Z. Z. Wang. These authors emphasize the regime of positive Hall voltage, which they attribute to flux flow, but assert that negative Hall voltages are due to a transition either to flux creep or else to exotic processes such as the nucleation of vortex loop excitations. While we agree that a positive Hall voltage can result within the conventional flux flow model of Nozieres and Vinen, resistivity and magnetization measurements have shown that the fields and temperatures at which the negative Hall effect appears are more likely characterized by flux flow than flux creep. Also, while a transition from flux flow to flux creep must affect the rate of vortex motion, it should not appreciably change the forces acting on a moving vortex or (consequently) the *direction* of the resulting motion. Thus one should not expect a sign change in the Hall voltage to accompany such a transition.

in *Science and Technology of Thin Film Superconductors II*
edited by R. McConnell and S. A. Wolf
(Plenum, New York, 1990)

YBCO AND LSCO FILMS GROWN BY OFF-AXIS SPUTTERING*

J. Talvacchio, M. G. Forrester, J. R. Gavaler, and T. T. Braggins

Westinghouse Science and Technology Center
Pittsburgh, Pennsylvania 15235

ABSTRACT

Using off-axis, dc magnetron sputtering we have produced $YBa_2Cu_3O_7$ (YBCO) and $La_{1.85}Sr_{0.15}CuO_4$ (LSCO) films at temperatures of 650-700°C which have a critical temperature, normal-state conductivity, critical current density, rf surface resistance, c-axis growth orientation, and surface structure comparable to the best films produced by laser ablation, co-evaporation in activated oxygen, or other sputtering techniques. In contrast to the other techniques, off-axis sputtering has simultaneously produced uniform film properties across a 2-inch diameter substrate holder *and* used stoichiometric oxide targets. The use of stoichiometric targets permitted YBCO films to be easily integrated with other epitaxial oxide films over this relatively large area. Low-energy electron diffraction showed that the 1:2:3 structure was maintained within the length of one unit cell from the film surface for YBCO and $PrBa_2Cu_3O_7$ (PrBCO) films and multilayers.

1. INTRODUCTION

We have previously published a table which summarized the growth of as-deposited crystalline YBCO films by sputtering.[1] In several of the references cited in the table, an off-axis geometry was used to minimize bombardment of the substrates by charged or neutralized negative oxygen ions.[2-4] A conceptually similar geometry was employed by Li *et al.*[5] in which the inside wall of a hollow cylindrical target was sputtered.

One reason for minimizing resputtering from substrates is to permit the use of a stoichiometric target and avoid a lengthy composition calibration each time a new superconductor, buffer layer, or tunnel barrier material is introduced. When resputtering effects are present during YBCO deposition, Cu is preferentially removed from the films so Cu-rich targets must be used.[1] The composition of YBCO films deposited in a relatively low sputter-gas pressure was measured as a function of substrate position by Kageyama and Taga.[6] Their conclusion is that the best substrate position for reproducing the target composition at their pressure was off-axis at 90° – the position used in this work. The penalty for off-axis sputtering was a reduction in deposition rate by a factor of three.

This paper reports the properties of YBCO films deposited by dc sputtering from a stoichiometric target positioned at an angle 90° from substrates heated to 650°C. The specific geometrical arrangement is closest

* Supported in part by AFOSR Contract No. F49620-88-C-0039

to that of Eom *et al.*, who presented some similar results using rf sputtering.[7] We have also obtained results similar to those reported here by using a stoichiometric YBCO target placed parallel to a substrate holder when we used a very high sputter-gas pressure, $\gtrsim$ 0.5 torr,[8] in conditions similar to those of Poppe *et al.*,[9] among others.

2. FILM GROWTH

Figure 1 shows details of the deposition geometry. The target was an approximately 2-inch diameter pressed and sintered pellet of $YBa_2Cu_3O_7$, $La_{1.85}Sr_{0.15}CuO_4$, or for deposition of an epitaxial non-superconducting layer, $PrBa_2Cu_3O_7$. The sputter gas was ~200 mtorr Ar and 20 mtorr O_2. The dc magnetron sputtering source was operated between 40 and 80 W resulting in deposition rates between 0.2 and 1.0 nm/min. As indicated in Fig. 1(a), the 5.7 cm diameter substrate holder was rotated on its symmetry axis. Stationary heater filaments made of Kanthal or Pt-10% Rh were used. The typical deposition temperature estimated from thermocouple and pyrometer measurements was 650-700°C for YBCO and PrBCO. The highest T_c LSCO films were deposited between 600 and 650°C. After deposition, the chamber was filled to 20 torr O_2 and the samples were subsequently cooled to 400°C for a 15-30 min soak and then to room temperature.

3. TRANSPORT PROPERTIES

Figures 2(a) and 2(b) show typical data for resistivity as a function of temperature for a YBCO and LSCO film, respectively. The transition temperatures defined by resistance, R = 0, were 88K for YBCO and 30K for LSCO for these particular films. For YBCO, single-crystal $LaAlO_3$(100), $SrTiO_3$(100), $SrTiO_3$(110), and yttria-stabilized ZrO_2(100) (YSZ) substrates were used with no difference in T_c within the range of 87-92K. The T_c's of YBCO grown on MgO(100) were always in the lower half of this range. Ultrathin YBCO films grown on $LaAlO_3$ and MgO had T_c = 85K for 10 nm thickness and 75K for 5 nm thickness.

The variation of T_c across a two-inch diameter area is shown in Fig. 3 to be ±1%. The inductive transition in Fig. 3 was defined as the midpoint of an ac susceptibility curve as shown in the inset of Fig. 2(a). Part of the

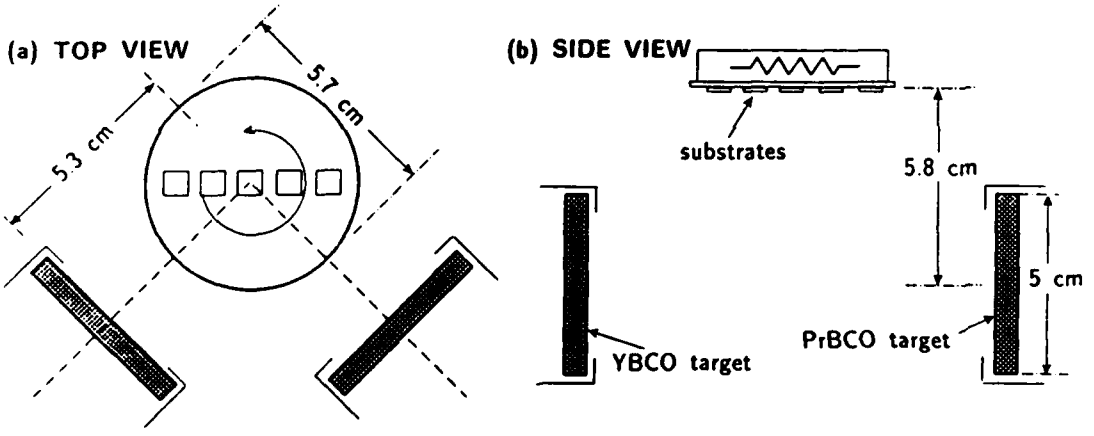

Fig. 1. The configuration used for off-axis sputtering shown in (a) top view and (b) side view. The positions of two sputtering targets are shown although only one is needed for each film layer. Several small substrates are usually mounted on the heated substrate holder with silver paint.

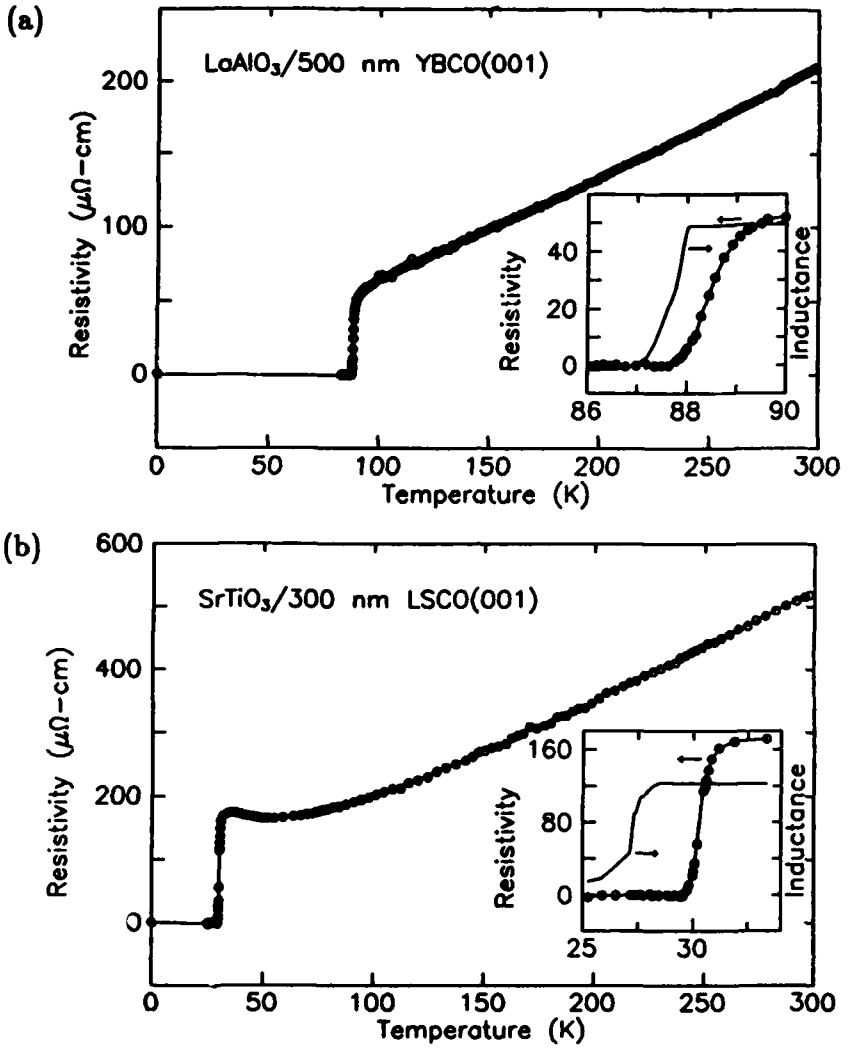

Fig. 2. Resistivity for (a) a YBCO(001) film and (b) a LSCO(001) film. The inset figures compare the resistive transition to the transition measured by the change of inductance of a coil placed against the film.

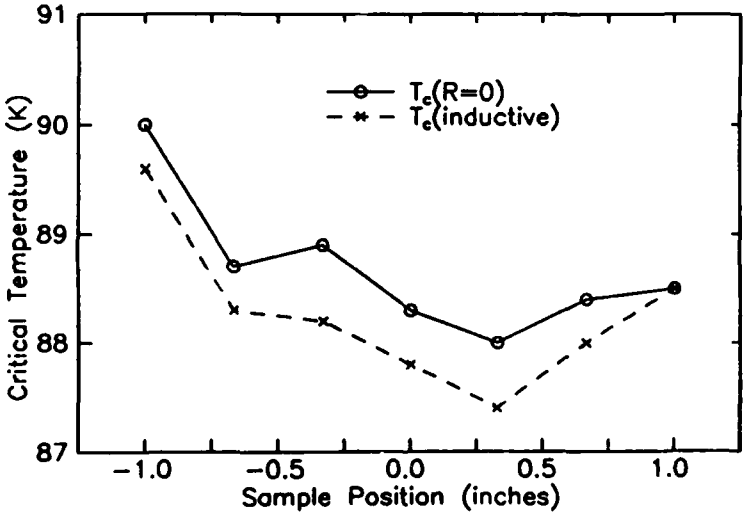

Fig. 3. T_c plotted as a function of sample position for 400 nm thick YBCO deposited on seven 6 mm x 6 mm $LaAlO_3$ chips placed in a row across the sample holder to test film uniformity.

difference in T_c between films in the center and on the edges of the substrate holder might be explained by a 20°C temperature gradient from center to edge measured by optical pyrometer. However, since the substrate holder rotated above a stationary heater during deposition, the asymmetry across the holder was more surprising. We speculate that minor differences in the way samples were fastened to the substrate holder with silver paint were responsible for the asymmetry.

The transition temperatures of LSCO films grown on $LaAlO_3$ or $SrTiO_3$ [Fig. 2(b)] were $\lesssim$ 30K, much lower than for bulk LSCO, but as high as that of the best LSCO films previously reported.[10] The overall processing temperature was kept much lower than in the earlier work, where either deposition or post-annealing at $\gtrsim$ 800°C was necessary. Specifically, such a post-annealing step did not increase the T_c of off-axis sputtered films over the as-deposited value. As shown by Suzuki in Ref. 10, the normal state resistivity in the a-b plane of $La_{2-x}Sr_xCuO_4$ is a sensitive function of x. Our LSCO sputtering target had $x = 0.15$ and EDS analysis indicated that the films had $x = 0.17 \pm 0.01$. Both the room-temperature resistivity and

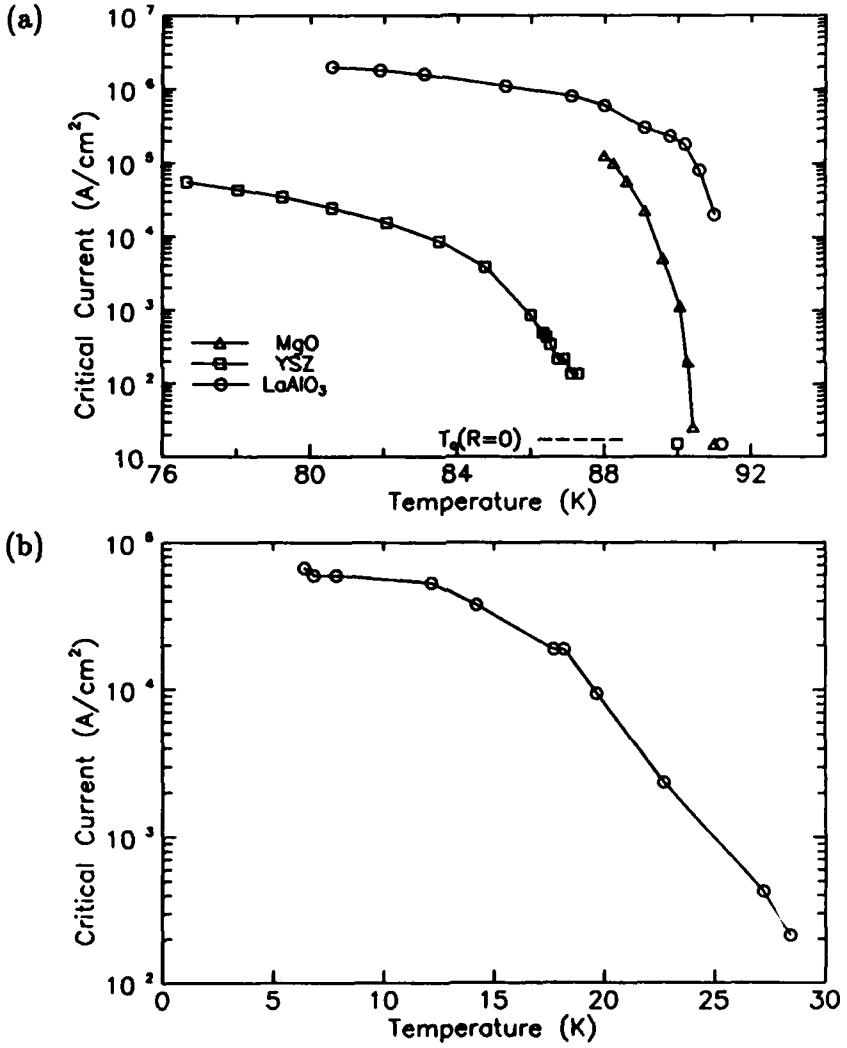

Fig. 4. Transport critical current density measured in self-field plotted as a function of temperature for (a) YBCO films on various substrates, and (b) an LSCO film deposited on $LaAlO_3$. In all cases, the film was patterned into a 25 μm wide bridge with voltage taps spaced 1 mm apart and a 5 μV criterion ($\rho < 10^{-8}$ Ω-cm for $J_c > 10^4$ A/cm^2). The particular data for a YBCO film on MgO in (a) was measured on a parallel-sputtered film.

temperature dependence of the resistivity are in reasonable agreement with Suzuki for these values of x for T > 50K. However, for x = 0.15, Suzuki observed a nearly temperature-independent resistivity between 30K and 50K. Some of our samples exhibited a negative temperature coefficient of resistance in this region that Suzuki only obtained for x = 0.10.

The dc critical current density was measured for both the YBCO and LSCO films. Several examples are shown in Fig. 4. In the case of YBCO grown on $LaAlO_3$, J_c was greater than 10^5 A/cm^2 for all T ≤ 91K, and $J_c > 10^6$ A/cm^2 for T ≤ 85K. These temperatures, the highest reported for exceeding 10^5 and 10^6 A/cm^2 in YBCO, were probably an indication of good film homogeneity rather than an intrinsic difference in flux pinning compared with films made by other techniques since the J_c for T ≤ 77K is no better than that of other high-quality YBCO films. The measurement of lower J_c's for YBCO grown on MgO and YSZ, especially in the temperature range just below T_c, has been reported by Geerk[11] and others, and correlates with the lattice mismatch between YBCO and these different substrates.

The transport critical current in the a-b plane of an as-deposited LSCO(001) film shown in Fig. 4(b) is the first such measurement reported. Although J_c was nearly two orders of magnitude higher than the best transport-J_c data in bulk samples,[12] it was nearly two nearly two orders of magnitude lower than YBCO at comparable reduced temperatures. A limitation of our measurements was that they were performed on films with a fixed Sr content, x ≃ 0.17, and J_c is likely to be sensitive to Sr content.

The rf surface resistance, R_s, of the off-axis sputtered YBCO films was measured at X-band in both stripline and microstrip configurations. In the stripline configuration, a Nb film was patterned in a half-wavelength long line on one side of a 0.700 x 0.250 x 0.020 inch substrate and a Nb ground plane was deposited on the other side. Following Ref. 13, an HTS film was used as the second ground plane and R_s was calculated from the Q measured in transmission. The substrate of the HTS film was inside the resonator so current flowed in the film layer adjacent to the substrate. Measurements of R_s were made only at 4.2K. In the microstrip configuration, two nominally identical HTS films were mounted with both of their substrates in the cavity. One film was patterned in a half-wavelength line and the other was used as a ground plane. Again, R_s was calculated[14] from Q measured in transmission. In both cases, the resonators were weakly coupled to the rest of the circuit so the unloaded Q could be assumed to equal the loaded Q.

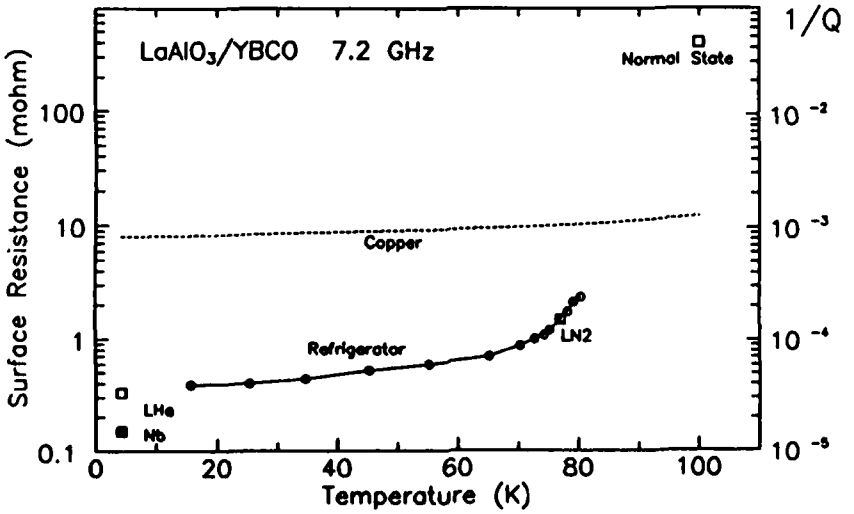

Fig. 5. R_s and 1/Q plotted as a function of temperature for a microstrip resonator.

Figure 5 shows the result of a microstrip measurement as a function of temperature. Measurements were made in liquid helium, liquid nitrogen, and with a cryorefrigerator. The R_s data had a nearly temperature independent residual resistance for $T << T_c$ that was comparable to that measured for other high-quality YBCO films when both the measurement technique and calibration to the R_s of Nb at 4.2K are used for normalization.[15]

4. STRUCTURAL PROPERTIES

All of the YBCO and LSCO films used for transport measurements had a c-axis orientation. Two examples of the x-ray diffraction evidence for the growth orientation are shown in Fig. 6. For YBCO, the c-axis lattice constant was 1.169 ± 0.001 nm. Rocking curve measurements on the (005) peak of 100 nm thick YBCO showed that the width depended on the substrate material. The full width at half of maximum (FWHM) was 0.2° for YBCO on $LaAlO_3$(100), 0.3° for $SrTiO_3$(100), 0.48-0.72 for MgO(100), and 0.55 for YSZ(100). A comparison made in Ref. 15 showed that the lattice mismatch between YBCO and various substrates was more important than the deposition technique in determining the rocking curve width.

In the case of YBCO, the structure of film surfaces was studied by two *in-situ* electron diffraction techniques, LEED and RHEED. Figure 7(a) shows a LEED pattern obtained from the surface of a YBCO film grown on $LaALO_3$(100) which was cooled to $\lesssim$ 400°C in 20 torr O_2 immediately after deposition. The most important information from such LEED patterns is that the 1:2:3 structure was present to within 1-2 monolayers of the surface. In earlier experiments with amorphous YBCO deposits that were

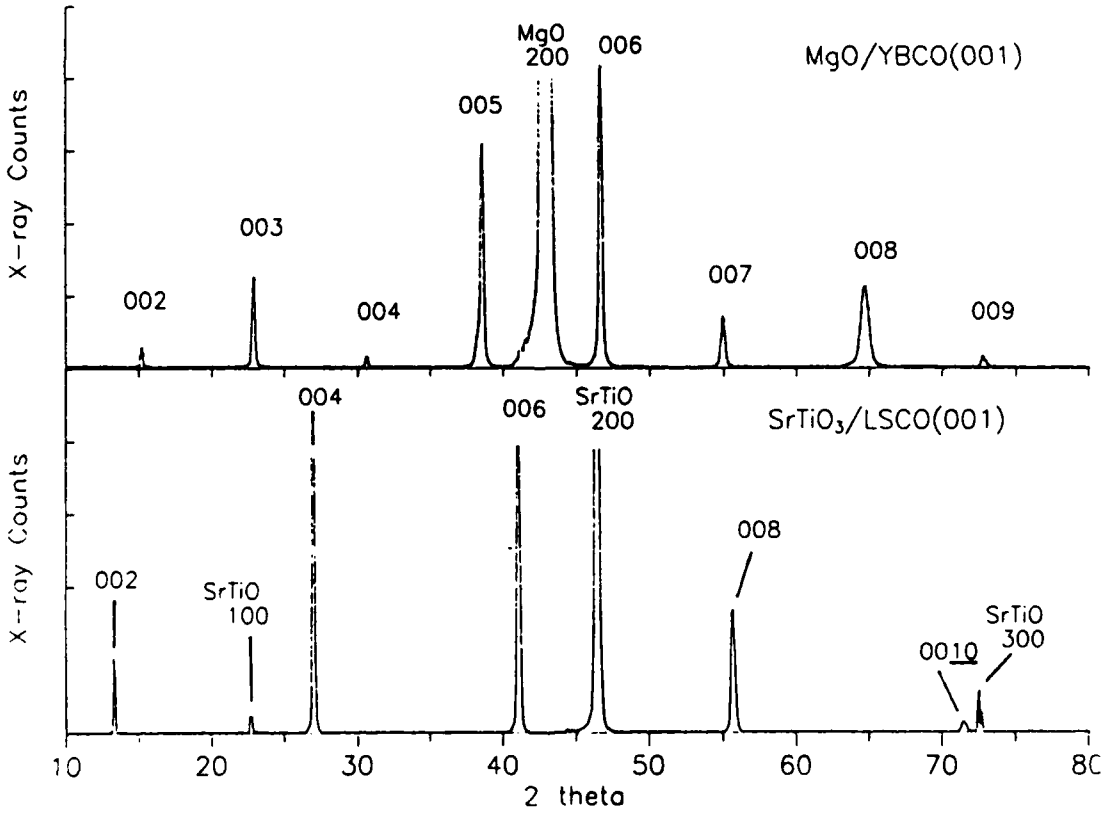

Fig 6. X-ray diffraction data for (a) a YBCO(001) film grown on MgO(100) and (b) a LSCO(001) film grown on $SrTiO_3$(100). Both films have a c-axis orientation typical of YBCO and LSCO films grown by off-axis sputtering for all substrate materials that were used.

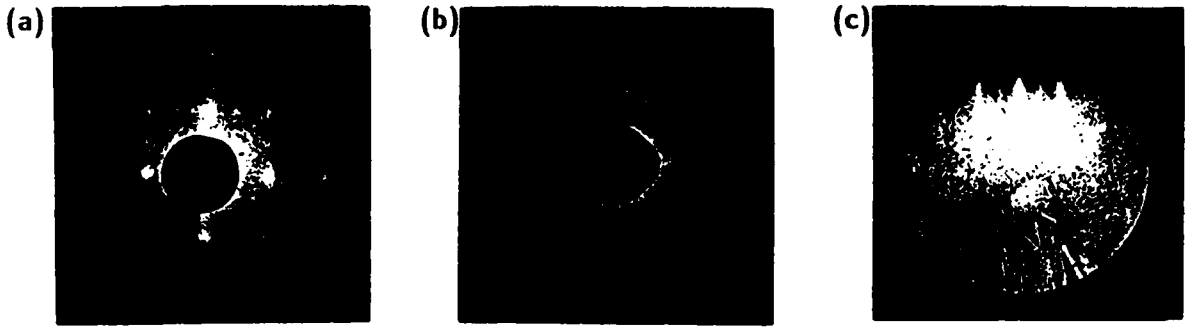

Fig. 7. *In-situ* LEED patterns of (a) a YBCO(001) film surface and (b) the surface of a PrBCO(001) layer grown on top of YBCO. (c) RHEED pattern of a YBCO(001) film grown on MgO that shows the smoothness of the surface and the same extra diffracted beams seen by LEED.

crystallized into an epitaxial film during an *in-situ* post-anneal (that is, with exposure only to vacuum and high-purity O_2),[16] no LEED pattern was ever observable. The 2×1 LEED pattern shows that the surface unit cell size doubled in one direction in some domains on the film surface and doubled in an orthogonal direction in other domains. The period doubling did not occur when a film was cooled from the deposition temperature in vacuum. Two possible explanations for the pattern are that the YBCO surface "reconstructed" when it had an orthorhombic structure or that oxygen adsorbed on the the surface of the orthorhombic structure had a distorted lattice that doubled the unit cell in one direction. In either case, it is likely that the domains corresponded to the two possible orientations of the a and b axes in the plane of the surface and that a new anisotropy within the a-b plane has been observed.

Our LEED data cannot be correlated with any work in the literature. To obtain the only previously published LEED pattern of a YBCO film, Sakisaka *et al.* needed to clean a surface that had been exposed to the atmosphere.[17] LEED patterns obtained from YBCO single crystals cleaved in vacuum also do not show the 2×1 surface structure.[18] In both of these cases, the termination layer at the surface might be different from the one we obtained.

The LEED pattern in Fig. 7(a) also contains information about the orientation of the film. Domains with an a-axis orientation (a-axis in the growth direction) would have exhibited a 3×1 pattern that was never observed. By comparing the LEED patterns of a sample before and after YBCO deposition, we were able to identify the in-plane substrate/film orientation relationship. For all of the substrates used in this work, these comparisons showed that YBCO(001) grew epitaxially and not simply with a well-defined texture in the growth direction.

Figure 7(c) is a RHEED pattern from a YBCO(001) film deposited on MgO. The presence of streaks instead of diffraction spots indicates that the surface is relatively smooth. RHEED patterns of films on $LaAlO_3$ consisted of diffraction spots due to the roughness of the $LaAlO_3$ after cycling through its cubic-to-rhombohedral structural transformation. The lower-intensity streaks were due to the 2×1 surface structure that was observed less ambiguously with LEED.

The LEED pattern in Fig. 7(b) was obtained from the surface of a PrBCO(001) film grown epitaxially on a YBCO underlayer. No evidence of either a 3×1 pattern due to a-axis growth or a 2×1 "reconstructed" pattern was found. The x-ray diffraction pattern of a YBCO/PrBCO bilayer is shown in Fig. 8(b). It confirms the c-axis orientation of both layers found

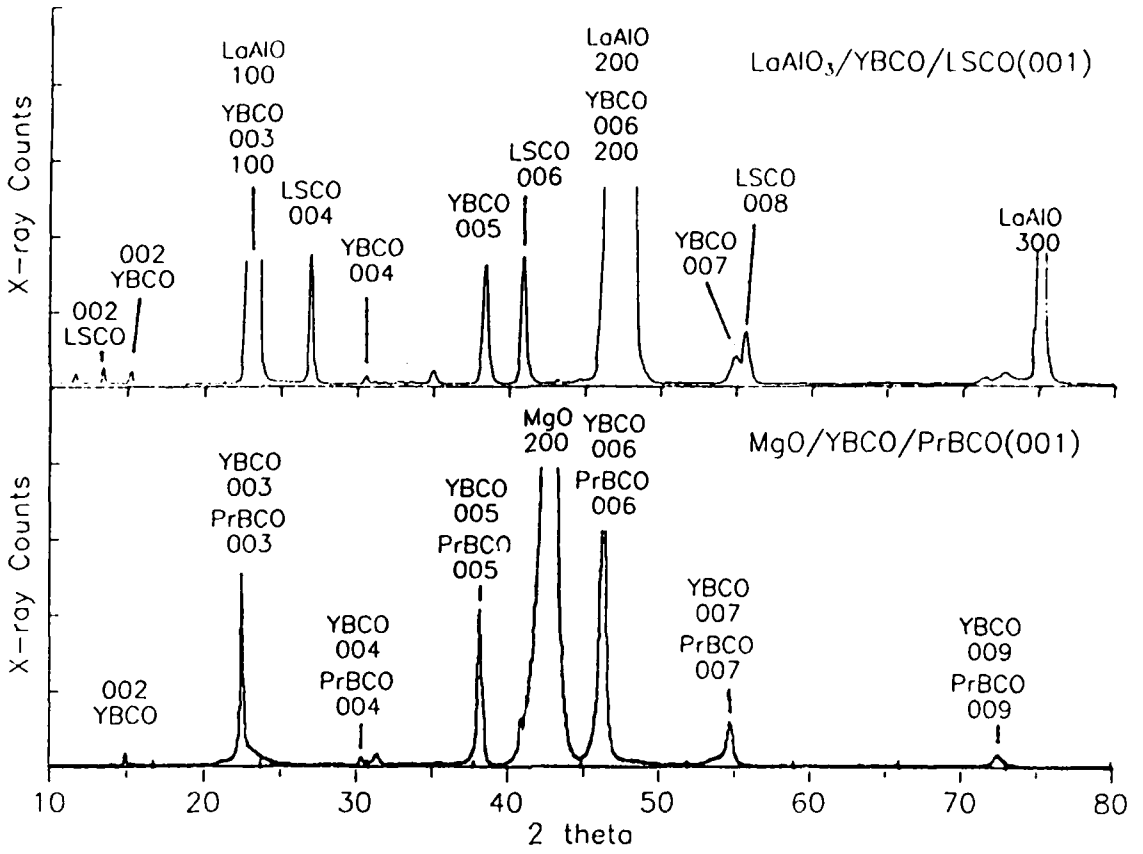

Fig. 8. X-ray diffractometer data for (a) a YBCO/LSCO(001) bilayer grown on $LaAlO_3$ and (b) a YBCO/PrBCO(001) bilayer grown on MgO.

from LEED. Following Rogers *et al.*,[19] we have made epitaxial multilayers of YBCO and PrBCO and studied vertical transport in these structures.[20] Multilayers have also been made in the YBCO/LSCO system. Figure 8(a) contains diffractometer data from a YBCO/LSCO bilayer showing the c-axis orientation of each layer in agreement with Eom *et al.*[21]

For most applications of epitaxial HTS multilayer structures, such as Josephson junctions or microstrip transmission lines, film surfaces must be sufficiently smooth to prevent shorts from occurring between layers. Figures 9(a) and 9(b) show two SEM micrographs of YBCO films grown under nominally identical conditions except for substrate temperature. The

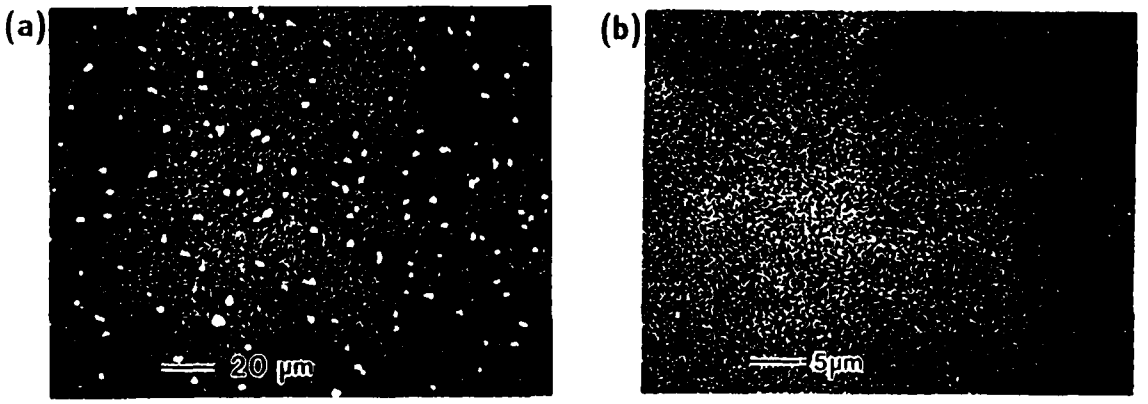

Fig. 9. Scanning electron micrographs of YBCO films deposited at (a) ~700°C and (b) ~650°C. The white spots in (a) are CuO precipitates. Completely particle-free films have T_c = 70-80K.

particles on the surface of the film in Fig. 9(a) were CuO precipitates which appear white due to charging. The particles could be identified as precipitates rather than debris from the target since they often decorated subsurface scratches on poorly polished substrates. Particle density could be controlled to some extent by substrate temperature, but other deposition parameters, such as substrate preparation, also affected the particle density. To date, the best properties have been obtained for films with at least some CuO particles.

CONCLUSIONS

The most important conclusion from this work is that off-axis dc magnetron sputtering is an effective way to sputter multi-component oxide films from a stoichiometric target with a minimal adjustment of deposition parameters for each new material. The properties measured by transport: normal-state resistivity, transition temperature, critical current density, and rf surface resistance are at least as good as those of films made by other techniques. Most of the structural properties can also be obtained by other techniques. Two new demonstrations that have been made with this technique are uniformity over a 2-inch diameter area and a 1:2:3 structure within the first 1-2 monolayers of the surface of YBCO(001) and PrBCO(001).

ACKNOWLEDGMENTS

The authors acknowledge the assistance of J. H. Uphoff, J. C. Brown, and C. L. Jones with film patterning and dc measurements; S. H. Talisa, B. R. McAvoy, D. H. Watt, and G. B. Draper with the measurements of surface resistance under WRDC Contract No. F33615-88-C-1841; N. J. Doyle and A. M. Stewart with x-ray measurements; and T. J. Mullen with EDS measurements.

REFERENCES

1. J. Talvacchio, J. R. Gavaler, J. Greggi, M. G. Forrester, and A. I. Braginski, Comparison of $YBa_2Cu_3O_7$ Films Grown by Solid-State and Vapor-Phase Epitaxy, *IEEE Trans. Magn.* 25(2):2538 (1989).
2. R. L. Sandstrom, W. J. Gallagher, T. R. Dinger, R. H. Koch, R. B. Laibowitz, A. W. Kleinsasser, R. J. Gambino, B. Bumble, and M. F. Chisholm, Reliable Single-Target Sputtering Process for High Temperature Superconducting Films and Devices, *Appl. Phys. Lett.* 53(5):444 (1988).
3. N. Terada, H. Ihara, M. Jo, M. Hirabayashi, Y. Kimura, K. Matsutani, K. Hirata, E. Ohno, R. Sugise, and F. Kawashima, Sputter Synthesis of $Ba_2YCu_3O_y$ As-Deposited Superconducting Thin Films from Stoichiometric Target--A Mechanism of Compositional Deviation and Its Control, *Jpn. J. Appl. Phys.* 27(4):L639 (1988).
4. M. Kawasaki, S. Nagata, Y. Sato, M. Funabashi, T. Hasegawa, K. Kishio, K. Kitazawa, K. Fueki, and H. Koinuma, High T_c Yb-Ba-Cu-O Thin Films Deposited on Sintered YSZ Substrates by Sputtering, *Jpn. J. Appl. Phys.* 26(5):L738 (1987).
5. H. C. Li, G. Linker, F. Ratzel, R. Smithey, and J. Geerk, In Situ Preparation of Y-Ba-Cu-O Superconducting Thin Films by Magnetron Sputtering, *Appl. Phys. Lett.* 52(13):1098 (1988).
6. Y. Kageyama, and Y. Taga, Effect of a Declination Angle of Substrate Position on Magnetron Sputter Deposition from a $YBa_2Cu_3O_{7-x}$ Target, *Appl. Phys. Lett.* 55(10):1035 (1989).

7. C. B. Eom, J. Z. Sun, K. Yamamoto, A. F. Marshall, K. E. Luther, T. H. Geballe, and S. S. Laderman, In Situ Grown $YBa_2Cu_3O_{7-d}$ Thin Films from Single-Target Magnetron Sputtering, *Appl. Phys. Lett.* 55(6).595 (1989).
8. J. R. Gavaler, and J. Talvacchio, Optimization of T_c and J_c in Sputtered YBCO Films, accepted for publication in Proc. LT-19 (1990).
9. U. Poppe, J. Schubert, R. R. Arons, W. Evers, C. H. Freiburg, W. Reichert, K. Schmidt, W. Sybertz, and K. Urban, Direct Production of Crystalline Superconducting Thin Films of $YBa_2Cu_3O_7$ by High-Pressure Oxygen Sputtering, *Solid State Commun.* 66(6):661 (1988).
10. M. Suzuki, Hall Coefficients and Optical Properties of $La_{2-x}Sr_xCuO_4$ Single-Crystal Thin Films, *Phys. Rev. B* 39(4):2312 (1989).
11. J. Geerk, G. Linker, and O. Meyer, Epitaxial Growth and Properties of YBaCuO Thin Films, *Mater. Sci. Reports* 4:193 (1989).
12. S. Yomo, C. Murayama, H. Takahashi, N. Mori, K. Kishio, K. Kitazawa, and K. Fueki, High Pressure Study and the Critical Current of High T_c Superconductor $(La_{0.9}Sr_{0.1})_2CuO_{4-y}$, *Jpn. J. Appl. Phys.* 26(5):L603 (1987).
13. A. C. Anderson, B.-Y. Tsaur, J. W. Steinbeck, and M. S. DiIorio, RF Surface Resistance of $YBa_2Cu_3O_{7-x}$ Thin Films, *MIT Lincoln Laboratory Quarterly Tech. Rep.*, March 11 (1988).
14. M. V. Schneider, Microstrip Lines for Microwave Integrated Circuits, *Bell System Technical Journal*, 1421 (May-June 1969).
15. J. Talvacchio and G. R. Wagner, High-T_c Film Development for Electronic Applications, to be published in "Superconductivity Applications for Infrared and Microwave Devices," SPIE Proc. Vol. 1292 (1990)
16. J. R. Gavaler, A. I. Braginski, J. Talvacchio, M. A. Janocko, M. G. Forrester, and J. Greggi, Fabrication of High-T_c Superconducting $YBa_2Cu_3O_7$ Films, in: "MRS Vol. EA-14: High-Temperature Superconductors II," D. W. Capone II, W. H. Butler, B. Batlogg, and C. W. Chu, ed., Mater. Res. Soc., Pittsburgh, (1988).
17. Y. Sakisaka, T. Komeda, T. Maruyama, M. Onchi, H. Kato, Y. Aiura, H. Yanashima, T. Terashima, Y. Bando, K. Iijima, K. Yamamoto, and K. Hirata, Angle-Resolved Photoemission Investigation of the Electronic Band Properties of $YBa_2Cu_3O_{7-x}(001)$, *Phys. Rev. B* 39(13):9080 (1989).
18. N. G. Stoffel, P. A. Morris, Y. Chang, M. Tang, R. Zanoni, L. Dottl, Q. B. Chen, R. Joynt, D. L. Huber, M. Onellion, and G. Margaritondo, Cleaved Single Crystals of High-T_c Superconductors: Electron Spectroscopy and Electron Diffraction Studies, *Surface Sci.* 211/212:1123 (1989).
19. C. T. Rogers, A. Inam, M. S. Hegde, B. Dutta, X. D. Wu, and T. Venkatesan, Fabrication of Heteroepitaxial $YBa_2Cu_3O_{7-x}$-$PrBa_2Cu_3O_{7-x}$-$YBa_2Cu_3O_{7-x}$ Josephson Devices Grown by Laser Deposition, *Appl. Phys. Lett.* 55(19):2032 (1989).
20. M. G. Forrester, J. Talvacchio, J. H. Kang, J. R. Gavaler, and T. T. Braggins, Fabrication and Characterization of YBCO-Based S-N-S-type Josephson Junctions, submitted to *IEEE Trans. Magn.* (1990).
21. C. B. Eom, J. Z. Sun, S. K. Streiffer, K. Yamamoto, J. C. Bravman, and T. H. Geballe, Synthesis and Properties of $YBa_2Cu_3O_7$/ $La_{2-x}Sr_xCuO_4$ Multilayered Superconducting Thin Films Grown in-situ by Off-Axis Sputtering, (Abstract) *Bull. Am. Phys. Soc.* 35(3):383 (1990).

Flux-flow Nernst effect in epitaxial $YBa_2Cu_3O_7$

S. J. Hagen, C. J. Lobb, and R. L. Greene*
Center for Superconductivity Research, Department of Physics and Astronomy, University of Maryland, College Park, Maryland 20742-4111

M. G. Forrester and J. Talvacchio
Westinghouse Science and Technology Center, 1310 Beulah Road, Pittsburgh, Pennsylvania 15235

(Received 23 July 1990)

From measurements of thermally driven flux-vortex motion (flux-flow Nernst effect) in an epitaxial $YBa_2Cu_3O_7$ film we determine the entropy S_ϕ transported by a moving vortex and demonstrate agreement with recent Ettingshausen-effect results. Because a Nernst effect is a distinctive signature of vortex motion in a superconductor, this experiment also reveals the field and temperature regions of the mixed state in which vortices move freely. We can therefore correlate these measurements with other transport studies of the mixed state.

A substantial effort has been directed toward the study of flux-vortex motion in high-temperature superconductors. Magnetization, magnetoresistance, decoration, and mechanical-oscillator studies have all been used to probe the motion and pinning of vortices in $YBa_2Cu_3O_7$, $Bi_2Sr_2CaCu_2O_y$, and other copper oxide superconductors.[1] Recently, some authors have observed thermoelectric effects of vortex motion.[2,3] Palstra *et al.*[2] measured the flux-flow Ettingshausen effect (temperature-gradient induced transverse to a transport current) in a crystal of $YBa_2Cu_3O_7$, and Zeh *et al.*[3] observed the Nernst effect (electric-field induced transverse to a temperature gradient) in a $YBa_2Cu_3O_7$ film.

Measurement of these and other thermoelectric effects in the low-temperature superconductors[4] not only provided evidence for the model of flux flow but gave information about thermodynamic properties of flux vortices. The flux-flow Ettingshausen and Nernst effects, for example, are related to the entropy S_ϕ transported by a moving flux line. However, the recent studies[2,3] of these two effects in $YBa_2Cu_3O_7$ disagree by a factor $\sim 10^3$ in the magnitude of S_ϕ, even though thermodynamics requires agreement between the two experiments. We report here a more complete study of the flux-flow Nernst effect and S_ϕ in an epitaxial $YBa_2Cu_3O_7$ film, which extends the work of Zeh *et al.*[3] to higher fields and lower temperatures and demonstrates that S_ϕ obtained from the Nernst effect does agree with the Ettingshausen result,[2] as required thermodynamically. We also show that the Nernst effect, as a distinctive signature of vortex motion, indicates the field and temperature ranges in which vortices move freely in $YBa_2Cu_3O_7$, and therefore supplements other transport evidence for unusual flux motion properties in this material. In particular, we show how the Nernst effect correlates with the flux-flow resistivity and Hall effect.

The Nernst effect is the transverse electric field E_y generated in a conductor subjected to a temperature gradient dT/dx and perpendicular magnetic field B_z (Fig. 1, inset). The Nernst coefficient ν, given by

$$\nu = E_y/(B_z dT/dx) , \tag{1}$$

is small in the normal state, but was observed[4,5] to be orders of magnitude larger in conventional type-II superconductors. This is because flux vortices flowing down a temperature gradient produce a transverse electric field according to Josephson's relation[6]

$$\mathbf{E} = -\mathbf{v}\times\mathbf{H} , \tag{2}$$

where $\mathbf{v}$ is the velocity of motion. Since quasiparticles do not contribute significantly to this effect, the presence of a Nernst voltage in a superconductor is *direct* evidence of vortex motion.

The core of a flux vortex can be described as containing bound quasiparticles with higher entropy than the superconducting background. Motion of a vortex thus causes a flow of entropy. One thermodynamic consequence[7] of this is a force per unit length on a vortex $\mathbf{F} = -S_\phi \nabla T$ in a temperature gradient ∇T, where S_ϕ is the transport entropy per unit vortex length. If this force is opposed by a viscous force $\mathbf{f} = -\eta\mathbf{v}$ (and if we neglect pinning) then the steady-state condition $\mathbf{F}+\mathbf{f}=0$ and Eqs. (1) and (2) give the Nernst coefficient

$$\nu = S_\phi/\eta . \tag{3}$$

The viscosity η can be determined from the flux-flow resistance through the Lorentz-force relation[7] $\rho_{xx} = E_x/j = \phi_0 H/\eta$. Thus S_ϕ can be obtained by measuring the Nernst voltage and magnetoresistance.

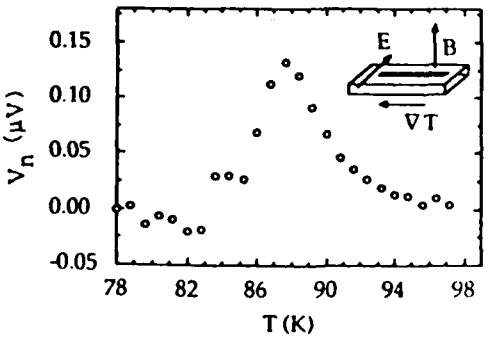

FIG. 1. Nernst voltage at $dT/dx \approx 1.3$ K/cm and $B = 3$ T. Inset shows sample configuration.

We measured the Nernst effect in a thin (~1500 Å) epitaxial c-axis oriented film of $YBa_2Cu_3O_7$ prepared by off-axis dc magnetron sputtering onto a substrate of yttria-stabilized (100) ZrO_2. The preparation and characterization of such films is described elsewhere.[8] A layer of Au was deposited *in situ* for electrical contacts and the film was etched into a 50-μm × 3.9-mm bar pattern. The patterned film had T_c(midpoint) ≈ 90.3 K and $\Delta T_c \sim 1$ K.

One end of the substrate is cemented to a copper base, and two miniature ceramic chip heaters attached to the other end produce the temperature gradient along the film. Two 25-μm chromel-constantan thermocouples measure this temperature gradient, and six 50-μm Au wires provide electrical connections to the film. Stray thermal voltages are minimized by heat sinking these wires to the copper base before connecting them to Dewar wiring. We measure the film resistivity ρ_{xx} and Hall resistivity ρ_{xy} in addition to thermoelectric properties.

Slow (~15 mHz) square-wave pulses of heater power produce a small oscillating temperature gradient (≤ 2 K/cm) and transverse voltage (~10–500 nV) across the film; these are measured by signal averaging. We take the Nernst voltage $V_n = E_y d$ as the part of the transverse voltage that changes sign under field reversal; the remaining symmetric part is much smaller (typically < 20 nV). The magnitude of V_n is linear in the applied temperature gradient, as expected.

Figure 1 shows a measurement at $B = 3.0$ T. V_n is zero for $T \geq 96$ K, grows as T approaches T_c from above, peaks at a temperature just below T_c, then decreases to zero again by about 82 K. At this field, a temperature gradient $dT/dx \approx 1.3$ K/cm ($\Delta T \approx 0.5$ K) along the film generates up to 150 nV across the film, corresponding to an average flux-line velocity ≤ 0.1 cm/sec. Through Eq. (2), the sign of V_n verifies that magnetic flux diffuses from the warmer to the cooler region of the sample.

Figure 2(a) shows $E_y/(dT/dx) \propto V_n$ versus temperature near T_c for $B = 2$, 3, 4, and 6 T. Clearly V_n does not increase linearly with applied field (i.e., the Nernst coefficient ν is field dependent); instead the broad maximum below T_c is shifted to lower temperature as field increases. To calculate the vortex transport entropy S_ϕ we first obtain the flux-flow viscosity η from the magnetoresistance, shown in Fig. 2(b) for $B = 2$, 3, 4, and 6 T, and then use Eq. (3). The resulting S_ϕ (Fig. 3) begins to increase in the normal state as the temperature decreases towards T_c, then increases almost linearly with decreasing temperature below T_c, with $\partial S_\phi/\partial T (T \leq T_c) \approx -9.5 \times 10^{-15}$ J/m K^2. S_ϕ shows a weak field dependence as the slope $|\partial S_\phi/\partial T|$ decreases slightly for high field. The appearance of finite S_ϕ in the normal state (noted also in Ref. 2) is not understood, but may be a fluctuation effect.

Because the Nernst and Ettingshausen effects are related thermodynamically, values of S_ϕ obtained from the two measurements should agree. We find our Nernst data agree closely with the Ettingshausen results of Palstra *et al.* (Our curves are shifted upward in temperature by ~3 K relative to theirs, apparently because of a higher T_c.) Thus we obtain similar results for S_ϕ by an independent technique, using a $YBa_2Cu_3O_7$ film instead of a crystal sample. However, the Nernst result for S_ϕ in Ref. 3, given

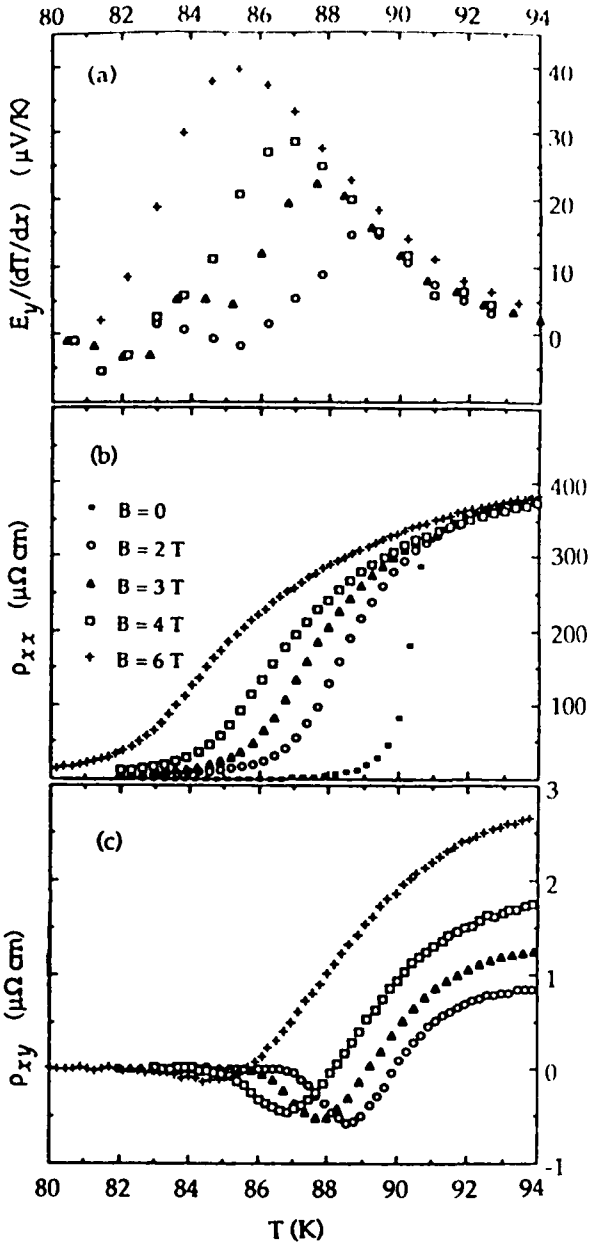

FIG. 2. (a) Nernst effect $E_y/(dT/dx)$, (b) resistivity ρ_{xx}, and (c) Hall resistivity ρ_{xy} vs temperature for $B = 2$, 3, 4, and 6 T.

for $T = 87$ K, is roughly 10^3 smaller than found here and in Ref. 2; the sample configuration in Ref. 3 may be more sensitive to vortex pinning at the film edges, which would tend to reduce V_n.

However, it is difficult to compare S_ϕ with a theoretical prediction for its value. Although measurements of S_ϕ in low-T_c alloys[9] showed good agreement with expressions[10] developed for superconductors in the dirty limit $l \ll \xi$, these expressions cannot apply to copper oxide superconductors like $YBa_2Cu_3O_7$ [where[11] the coherence length $\xi_{ab}(0) \sim 16$ Å and the electronic mean free path $l_{ab}(100\ \text{K}) \sim 70$ Å] except perhaps very near T_c. The theoretical understanding of S_ϕ in clean superconductors is uncertain. Maki[10] has calculated the entropy carried by a single vor-

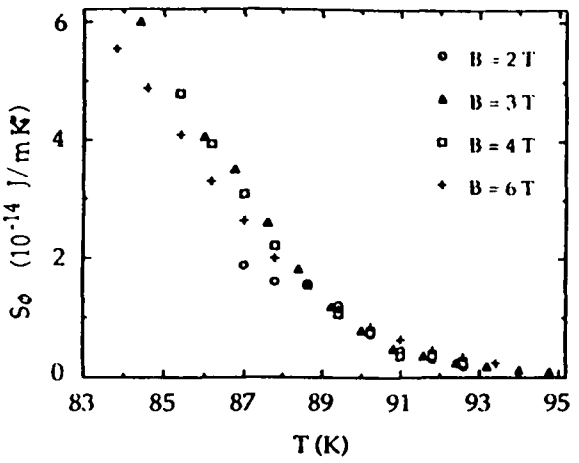

FIG. 3. Vortex entropy per unit length S_ϕ vs temperature for $B=2$, 3, 4, and 6 T.

tex using time-dependent Ginzburg-Landau theory:

$$S_\phi = -\phi_0 M L(T)/T , \tag{4}$$

where M is the (spatially averaged) magnetization and $L(T)$ in the clean limit is a function of order l/ξ that increases linearly with l. Using Maki's expression[10] for M to evaluate (4) (with $L \approx 4$, $T=88$ K, and $B=2$ T), we obtain $S_\phi \sim 1.8\times10^{-14}$ J/m K, in good agreement with experiment. However, (4) predicts a field dependence in S_ϕ that is not seen in our data. Also, Ettingshausen-effect studies[12] on clean Nb samples ($l/\xi \sim 13$ and ~ 660) demonstrated a strong increase of S_ϕ with l/ξ, but still did not confirm Eq. (4). If, as suggested by those authors,[12] the samples were still not clean enough for clean limit expressions to apply, then S_ϕ data for $YBa_2Cu_3O_7$ certainly should not be compared to existing theory.

The entropy S_ϕ in Fig. 3 increases with decreasing temperature below T_c (as in low-T_c superconductors[4,9]), but must eventually decrease again and approach zero at low T. This decrease is not observed in Fig. 3 since V_n disappears by $T \sim 80$–85 K. The quantity $S_\phi = E_y\phi_0/(\rho_{xx}dT/dx)$ cannot accurately be determined once V_n and the resistivity ρ_{xx} both become small.

Since V_n is directly proportional to the flux-line velocity, Fig. 2(a) shows that this velocity reaches a maximum a few K below T_c and then approaches zero at low temperatures, even as the thermal force ($\propto S_\phi$) is increasing. The temperature at this maximum decreases with increasing field. It is interesting to compare this behavior with that of the flux-flow Hall resistivity ρ_{xy}, shown in Fig. 2(c). At high fields and temperatures ρ_{xy} is positive as in the normal state. At an intermediate range of fields and temperatures, however, ρ_{xy} changes sign[13] and displays a negative minimum, then approaches zero again for lower temperature, even while the resistivity ρ_{xx} remains finite. We find that the field and temperature values at the minima in ρ_{xy} correspond closely to those at the maxima in V_n.

We have previously[13] argued that, if dissipation in this temperature and field range is due to flux-vortex motion, the sign reversal of ρ_{xy} indicates vortex motion with a velocity component opposite to the transport current. The eventual vanishing of ρ_{xy} at lower temperatures would then indicate a qualitative change in vortex motion. Because the Nernst measurement detects vortex motion directly, the results in Fig. 2 support this interpretation of the Hall data: The large Nernst voltage indicates free flux motion at the temperatures and fields where ρ_{xy} is negative. The disappearance of V_n at lower temperatures coincides with the disappearance of the Hall effect and a crossover in the temperature dependence[14] of ρ_{xx}, and therefore indicates an abrupt change in flux-flow properties, such as a transition to flux creep or other dissipative mechanisms. Similarly the Nernst data strongly support magnetization, I-V, susceptibility, and other evidence[1] that flux motion is reversible at high fields and temperatures but pinned or irreversible at lower fields and temperatures.

In summary, we have measured the Nernst voltage in the superconducting state of epitaxial $YBa_2Cu_3O_7$ and obtained the vortex transport entropy S_ϕ. These systematic measurements resolve an earlier disagreement with Ettingshausen-effect results on single-crystal samples. However, we believe current theory cannot generate a prediction for S_ϕ. We find that the Nernst effect, as a probe of flux motion independent of possible quasiparticle effects, clearly identifies the field and temperature regimes in which vortices move freely in this superconductor, and therefore can clarify the results of other transport studies in the mixed state.

We acknowledge useful discussions with S. Yip. Sample fabrication at Westinghouse was supported by U.S. Air Force Office of Scientific Research Contract No. F49620-88-C-0039.

*Also at IBM Research Division, Yorktown Heights, NY 10598.

[1] For a review see *Strong Correlation and Superconductivity: the Proceedings of the IBM Japan International Symposium*, edited by H. Fukuyama, S. Maekawa, and A. P. Malozemoff (Springer-Verlag, Berlin, 1989), and references therein.

[2] T. T. M. Palstra, B. Batlogg, L. F. Schneemeyer, and J. V. Waszczak, Phys. Rev. Lett. **64**, 3090 (1990).

[3] M. Zeh, H.-C. Ri, F. Kober, R. P. Huebener, A. V. Ustinov, J. Mannhart, R. Gross, and A. Gupta, Phys. Rev. Lett. **64**, 3195 (1990).

[4] R. P. Huebener, *Magnetic Flux Structures in Superconductors* (Springer-Verlag, Berlin, 1979).

[5] F. A. Otter and P. R. Solomon, Phys. Rev. Lett. **16**, 681 (1966).

[6] B. D. Josephson, Phys. Lett. **16**, 242 (1965).

[7] Y. B. Kim and M. J. Stephen, in *Superconductivity*, edited by R. D. Parks (Marcel Dekker, New York, 1969), Vol. 2.

[8] J. Talvacchio, M. G. Forrester, J. R. Gavaler, and T. T. Braggins, in *Science and Technology of Thin Film Superconductors, Vol. II*, edited by R. McConnell and S. Wolf (Plenum, New York, in press).

[9] J. Lowell, J. S. Munoz, and J. B. Sousa, Phys. Rev. **183**, 497 (1969); Y. Muto, K. Mori, and K. Noto, Physica (Amsterdam) **55**, 362 (1971); F. Vidal, Phys. Rev. B **8**, 1982 (1973).

[10]C. Caroli and K. Maki, Phys. Rev. 164, 591 (1967); K. Maki, J. Low Temp. Phys. 1, 45 (1969); Physica (Amsterdam) 55, 124 (1971).

[11]U. Welp, W. K. Kwok, G. W. Crabtree, K. G. Vandervoort, and J. Z. Liu, Phys. Rev. Lett. 62, 1908 (1989); M. Gurvitch and A. T. Fiory, Phys. Rev. Lett. 59, 1337 (1987).

[12]A. T. Fiory and B. Serin, Physica (Amsterdam) 55, 73 (1971).

[13]S. J. Hagen, C. J. Lobb, R. L. Greene, M. G. Forrester, and J H. Kang, Phys. Rev. B 41, 11630 (1990), and references therein.

[14]T. T. M. Palstra, B. Batlogg, R. B. van Dover, L. I Schneemeyer, and J. V. Waszczak, Phys. Rev. B 41, 6621 (1990).

IEEE Trans. Magn.
Vol. 27, No. 2 (1991

FABRICATION AND CHARACTERIZATION OF $YBa_2Cu_3O_7$/Au/$YBa_2Cu_3O_7$ JOSEPHSON JUNCTIONS

M. G. Forrester, J. Talvacchio,* and J. R. Gavaler*
Westinghouse Science & Technology Center
1310 Beulah Road
Pittsburgh, PA 15235

M. Rooks
National Nanofabrication Facility
Cornell University
Ithaca, NY

J. Lindquist
FEI Company
Beaverton, OR

Abstract

We have fabricated all-high-T_c Josephson junctions in a planar S-N-S geometry, by bridging narrow gaps ($\approx$ 0.1 - 0.2 μm) in epitaxial $YBa_2Cu_3O_7$ (YBCO) films with Au. The resulting devices exhibit a variety of non-hysteretic I-V characteristics, with I_cR_N of order 0.1 to 10 mV, and exhibit Shapiro steps under microwave irradiation, and weak periodic modulation of the critical current with applied magnetic field. The transport properties of the junctions appear to be dominated by the Au/YBCO interfaces rather than by the Au itself.

Introduction

The development of an integrated circuit technology based on high temperature superconductors (HTS) requires the controlled fabrication of Josephson junctions. Current low temperature superconducting (LTS) circuit technology is based on S-I-S tunnel junctions, typically of the type $Nb/AlO_x/Nb$, whose reproducibility and controllability has made possible the fabrication of complex circuits, and whose hysteretic I-V characteristics suggest various logic schemes relying on the zero-voltage and gap-voltage states to define logical "0" and "1".[1]

At present there is no HTS tunnel junction technology, due to the materials problems associated with the growth of a homogenous barrier compatible with the high-temperature deposition conditions for *in-situ* HTS films. This has led to an interest in the fabrication of non-hysteretic S-N-S junctions, as an interim basis for electronic circuits, using logic schemes which do not require hysteretic junctions. Such junctions may additionally replace grain-boundary weak links currently used in many HTS SQUID's. The first such junction reported was a planar YBCO/Au/YBCO bridge fabricated from a post-annealed YBCO film using electron-beam lithography to define the 1 μm junction length, and which exhibited a critical current up to 16 K.[2] Subsequent developments have emphasized an *in-situ* trilayer approach, using, for example, $PrBa_2Cu_3O_7$ as the normal barrier.[3] While the latter approach, which more closely parallels LTS Nb technology, is ultimately preferable, further materials development is needed to reduce the density of defects, such as micro-shorts, which currently dominate the electrical characteristics of such devices.

Here we report preliminary results on the fabrication of planar junctions, with lengths, d, as short as 0.1 μm, which exhibit Josephson effects up to 70 K.

Sample Fabrication

Our YBCO films were deposited by off-axis dc magnetron sputtering from a stoichiometric target, onto substrates of (100) and (110) $SrTiO_3$. The deposited films were epitaxial, with (001) orientation on (100) substrates and (103)/(013) orientation on (110) substrates. Thicknesses used varied from $\approx$ 50 to 200 nm. Films typically exhibited transition temperatures in the 88-92 K range, room-temperature resistivity of 300 μΩ-cm, and critical currents in excess of 10^6 A/cm^2 at 77 K. Further details of the film properties and deposition conditions have been reported elsewhere.[4]

After the post-deposition cool-down the YBCO films were coated, *in-situ*, with 50 to 100 nm sputtered Au, to

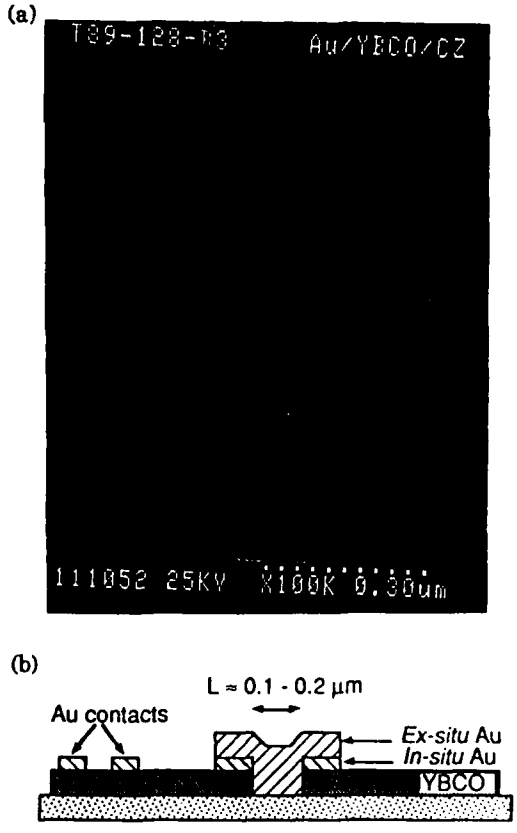

Figure 1. (a) Micrograph of a $\approx$ 0.1 μm-wide slot in a Au/YBCO bilayer, formed by electron-beam lithography and broad-beam ion milling. (b) Schematic diagram of completed planar junction.

* Supported in part by AFOSR contract no. F49620-88-C-0039.
Manuscript received September 24, 1990.

protect the top surface of the YBCO during subsequent processing.

Fabrication by Electron-Beam Lithography

A film of a slow-milling material, such as Si_3N_4 or Ti, was deposited on the Au/YBCO bilayers to serve as an ion-milling mask for patterning of the YBCO. The resulting trilayer was coated with a layer of PMMA resist. After exposure of the narrow slots by 50 keV electrons the resist pattern was transferred into the masking layer by reactive ion etching (RIE), and then into the Au/YBCO by 500 eV Ar ion milling. Although the actual devices were not isolated at this point, various test patterns included on each chip enabled us to check that the milled slots were electrically open (> 10^4 Ω). Figure 1a shows an example of a 0.1 μm slot defined in this manner.

After removal of the remaining mask layer, photolithographic processing and ion milling were used to isolate the junctions and their individual four-point current and voltage leads, and to define the junction width, w, of 10 μm. The sample was then coated with ≈ 200 nm of sputtered Au (ρ ~ 1 μΩ-cm at room temperature), and the Au selectively patterned by RIE to define the junctions and their contact pads. Some samples were annealed at 600 °C in flowing O_2 to improve the Au/YBCO contact. Figure 1b shows a schematic diagram of a completed junction.

Samples were wire-bonded into a 32-lead sapphire chip carrier for electrical measurements.

Fabrication by FIB etching

A more direct approach to junction fabrication is to use a focussed ion beam (FIB) to etch the submicron slots directly, without the use of masking layers and resists. We have used a 30 keV Ga ion beam, with a nominal FWHM of 60 nm, which produced slots of approximately 0.2 μm at the film's top surface. Test samples were again checked for electrical open circuit to ensure complete etching, and etch time and current were chosen so as to over-etch somewhat, to avoid shorts due to defects such as surface particles on the YBCO.[4] The side walls of the etched slots appeared less steep than those produced by e-beam lithography and broad-beam ion milling, possible because of the approximately gaussian shape of the beam resulting in partial etching of the film by the beam "tails." Further reductions in linewidth are expected by use of a slightly smaller aperture, and shorter etching times.

Subsequent processing of the FIB samples was identical to the e-beam approach.

Measured characteristics

Figure 2 shows a set of I-V characteristics as a function of temperature for an e-beam-fabricated junction with a length of approximately 0.1 μm, on $SrTiO_3$ (100). At low temperatures the measured behavior is not unlike the RSJ model prediction (in the absence of thermal fluctuations) of $V = R(I^2 - I_c^2)^{1/2}$. However, for increasing temperatures the characteristic broadens much more than predicted by the thermal fluctuation model of Ambegaokar and Halperin.[5]

Figure 3 shows a set of dV/dI vs. I curves, at 42 K,

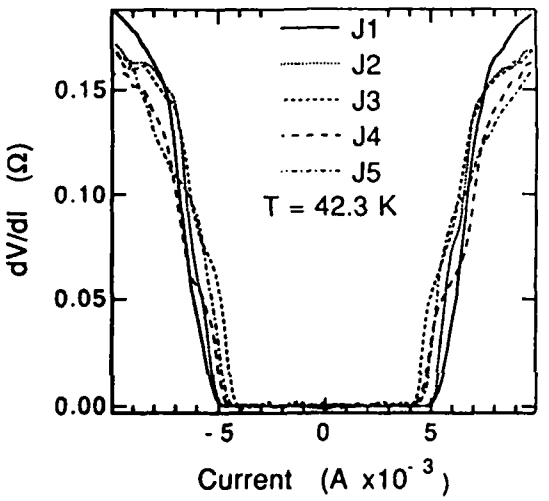

Figure 3. Differential resistance vs. current for five FIB-fabricated junctions on one chip.

for five junctions on a FIB-fabricated sample, on $SrTiO_3$ (100), which was annealed according to the procedure discussed above. The nominal junction length was 0.2 μm. The similarity of the characteristics is encouraging, suggesting that the junctions are reasonably homogeneous and reproducible within a chip.

Figure 4 shows the measured critical current I_c, determined by an arbitrary voltage criterion of 5 μV, for

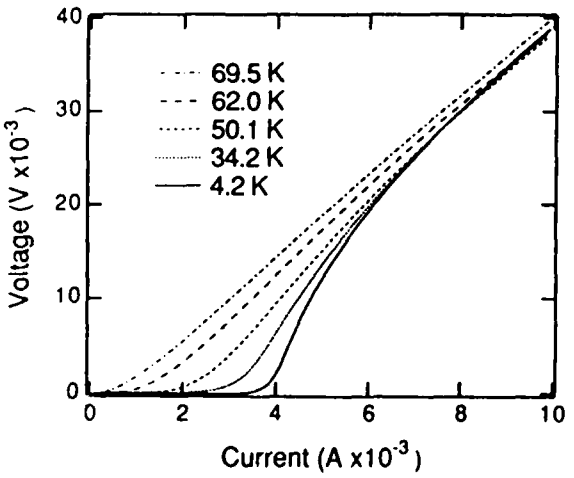

Figure 2. Current -voltage characteristics for a ≈ 0.1 μm long e-beam-fabricated YBCO/Au/YBCO junction.

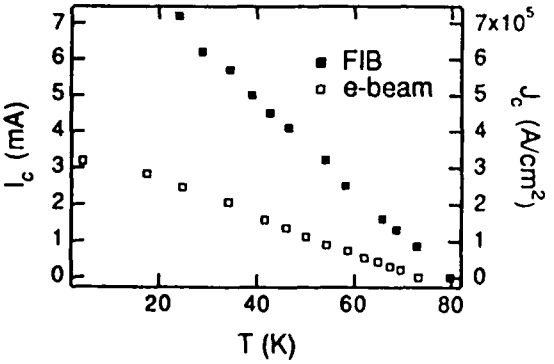

Figure 4. Critical currents for the e-beam junction of Fig. 2, and junction J5 of Fig. 3.

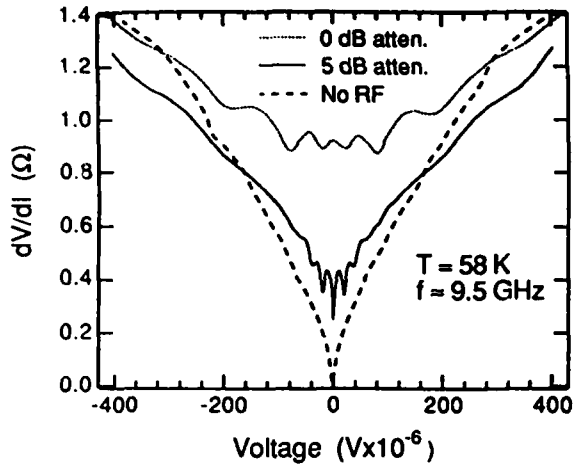

Figure 5. Differential resistance vs. voltage for the e-beam junction of Fig. 2, showing rounded Shapiro steps induced by 9.5 GHz radiation. The "0 dB" and "5 dB" curves are displaced vertically by 0.5 Ω and 0.25 Ω, respectively, for clarity.

the sample of Figs. 2 and 3. The annealed FIB-fabricated sample, despite its greater length, exhibited a larger critical current than the unannealed e-beam junction of Fig. 2, as well as a lower resistance (≈ 0.1 Ω, compared to 4 Ω), consistent with an improvement in the quality of the Au/YBCO interfaces upon annealing.

The response of the sample of Fig. 2 to f = 9.5 GHz radiation is shown in Fig. 5, at a temperature of 58.5 K. Radiation was weakly coupled in through a half-wave antenna approximately 5 mm above the sample. The characteristics exhibit weak Shapiro steps at voltages V=nhf/2e. Above approximately 67 K the steps washed out completely due to thermal fluctuations, while below about 38 K there was apparently insufficient microwave power to produce steps.

Measurements of dV/dI vs. applied magnetic field, at a fixed bias current above I_c, for a 0.1 × 10 μm junction are shown in Figure 6, for a temperature of 56 K. The data show an extremely weak periodic modulation, with maxima in dV/dI (corresponding to minima in I_c) occurring with a period of approximately 7 gauss. The expected period, ΔB, is given by the relation

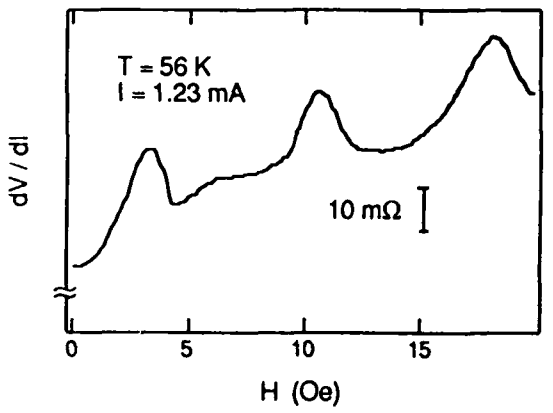

Figure 6. Weak periodic modulation of the sample differential resistance, at a fixed bias current above I_c, as a function of magnetic field, reflecting periodic modulation of the junction critical current.

$$\Delta B = \frac{\Phi_0}{w\,(d + 2\lambda)}, \qquad (1)$$

where λ is the penetration depth of the YBCO and Φ_0 is the flux quantum. Using w = 10 μm, d = 10 μm, and λ = 0.15 μm yields ΔB = 5 gauss, in reasonable agreement with the measured value. The weak modulation depth may be partially due to the sample being in a self-field-limited regime, $w > 2\lambda_J$, where the current flows within a characteristic width λ_J of each edge of the junction, and partially to inhomogeneous coupling across the width of the junction. The Josephson penetration depth, in SI units, is given by

$$\lambda_J^2 = \frac{\hbar}{2eJ_c\,\mu_0(2\lambda + d)}, \qquad (2)$$

where J_c is the critical current density. Applying this expression straightforwardly to the junction of Fig. 6, which had $J_c \approx 7.5 \times 10^4$ A/cm^2 at 56 K, yields $\lambda_J \approx 0.9$ μm, so that w (10 μm) >> 2 λ_J.

Discussion

The results presented above give unambiguous evidence of Josephson behavior in these planar junctions. However, the nature of the junctions is far from clear, and almost certainly does not represent true S-N-S behavior. For example, the resistance of the junctions, ~ 0.1 - 1 Ω, is much greater than the ~ mΩ expected for the resistance of the Au alone, and must be dominated by the Au/YBCO interfaces, suggesting that the actual devices have an S-I-N-I-S character. In fact, the measured resistances are consistent with a specific contact resistance of the order 10^{-8} to 10^{-9} Ω-cm^2, which is quite typical of measured Au/YBCO contact resistances.

The approximately linear temperature dependence of the measured critical current also disagrees with the $I_c \propto \exp(-d/\xi_N(T))$ form expected for an S-N-S junction, and is also, at least close to T_c, consistent with S-I-N-I-S behavior.

It is also unclear which surface of the YBCO provides the strongest superconducting proximity effect coupling through the Au — the milled side walls, or the top surface which is protected by *in-situ* Au. In principle this will depend on the growth orientation of the film, with c-axis films potentially having stronger coupling through the side walls, and a-axis through the top surface. The effective length, d, for a junction fabricated from an a-axis film would then be somewhat larger than the slot width, by some geometrical factor. The results here were obtained with c-axis films.

The use of a-axis films may ultimately be preferable, because it will likely be easier to reproducibly control the YBCO/*in-situ* Au interface than that formed with the *ex-situ* Au at the side walls.

Summary and Conclusions

We have fabricated Josephson junctions with a planar S-N-S geometry, with lengths as short as 0.1 μm, which exhibit Josephson effects to 70 K. The measured characteristics are consistent with a S-I-N-I-S device geometry, with the junction resistance being dominated by the Au/YBCO interfaces.

The intra-chip consistency of some of the measured junctions is encouraging, indicating that the characteristics are not dominated by small numbers of isolated defects such as shorts. However the chip-to-chip reproducibility needs improvement.

Because of their relatively high I_cR_N products, the junctions show promise for use in circuits based on flux quantum logic schemes, which do not require hysteretic junctions,[6] as well as for SQUID applications.

Acknowledgments

We are pleased to acknowledge A. Foley and J. Uphoff for building the measurement apparatus, and the staff of the National Nanofabrication Facility and FEI Company for assistance with sample fabrication.

References

1. See, for example, Y. Tarutani, M. Hirano, and U. Kawabe, "Niobium-Based Integrated Circuit Technologies," *Proc. of the IEEE*, Vol. 77, 1164, 1989.

2. P. M. Mankiewich, D. B. Schwartz, R. E. Howard, L. D. Jackel, B. L. Straughn, E. G. Burkhardt, and A. H. Dayem, "Fabrication and Characterization of an YBa2Cu3O7/Au/YBa2Cu3O7 S-N-S Microbridge," in *Proceedings of the 5th International Workshop on Future Electron Devices*, Miyagi-Zao, 1988, p. 157.

3. C. T. Rogers, A. Inam, M. S. Hegde, B. Dutta, X. D. Wu, and T. Venkatessan, "Fabrication of Heteroepitaxial $YBa_2Cu_3O_{7-x}$–$PrBa_2Cu_3O_{7-x}$–$YBa_2Cu_3O_{7-x}$ Josephson Devices Grown by Laser Deposition," *Appl. Phys. Lett.* 55, 2032, 1989.

4. J. R. Gavaler and J. Talvacchio, "Optimization of T_c and J_c in Sputtered YBCO Films," *Physica B* 165, 1513, 1990, and J. Talvacchio, M. G. Forrester, J. R. Gavaler, and T. T. Braggins, "YBCO and LSCO Films Grown by Off-Axis Sputtering," to appear in *Science and Technology of Thin-Film Superconductors II*, edited by R. McConnell and S. A. Wolf, Plenum, New York, 1990.

5. V. Ambegaokar and B. I. Halperin, "Voltage Due to Thermal Noise in the dc Josephson Effect," *Phys. Rev. Letters*, 22, 1364, 1969.

6. V. K. Kaplunenko, M. I. Khabipov, V. P. Koshelets, K. K. Likharev, O. A. Mukhanov, V. K. Semenov, I. L. Serpuchenko, and A. N. Vystavkin, "Experimental Study of the RSFQ Logic Elements," IEEE Trans. on Magnetics, Vol. 25, no. 2, 861-864, 1989.

Proc. ASC '90
IEEE Trans. Magn.
Vol. 27, No. 2 (1991

LARGE-AREA YBCO FILMS FOR MICROWAVE APPLICATIONS*

J. Talvacchio, M. G. Forrester, J. R. Gavaler, and T. T. Braggins
Westinghouse Science & Technology Center
Pittsburgh, PA 15235

Abstract

We have developed techniques for the in-situ deposition of epitaxial YBCO films on two-inch diameter wafers of $LaAlO_3$(001) or α-Al_2O_3(1$\bar{1}$02) with a Sr-doped La_2CuO_4(001) (LSCO) buffer layer. The inductively-measured transition temperature varied within the values of 91.1 ± 0.5K across the surface of the $LaAlO_3$ wafer, and 90.7 ± 0.4K across the buffered sapphire wafer. The epitaxial LSCO buffer layer acted not only as a barrier to diffusion of Al into the YBCO films, but improved the YBCO(005) x-ray rocking curve widths from 4° for films grown on bare sapphire to 1.2° for films on the LSCO-buffered sapphire. The typical buffer-layer thickness was 40 nm although layers as thin as 4 nm appeared to be equally effective. The transport critical current density was greater than 10^6 A/cm^2 at 77 K for films on buffered sapphire. At 8.8 GHz and 4.2K, the rf surface resistance was lower than that of gold, indicating that the films on sapphire will be useful in large-area UHF applications.

Introduction

In a recent review of materials issues in the fabrication of microwave devices from high temperature superconductors (HTS),[1] the requirement that was common to all applications was a low rf surface resistance, R_s. Each microwave component considered individually also required either a larger area, lower dielectric constant, or lower dielectric loss than is available from $LaAlO_3$ substrates, the best substrate alternative at present. In a practical subsystem, integration of components places an additional demand on the size and uniformity of high-quality HTS films.

Sapphire substrates for YBCO films have received a great deal of attention since they fulfill the requirements of large size, low dielectric constant, and low dielectric loss, with good mechanical properties. However, since sapphire has a poor lattice match to YBCO and Al diffuses into YBCO readily at high (≥750°C) temperature, epitaxial buffer layers have been used as a diffusion barrier and to grade the lattice parameter. Buffer layers of MgO(100),[2-4] $SrTiO_3$(100),[5] and $LaAlO_3$(100)[6] have been investigated to date – all deposited on the (1$\bar{1}$02) face of sapphire (R-plane). These buffer layer materials share the fact that – in bulk, single-crystal form – they are the popular substrates for HTS film growth.

In this paper, we describe the properties of epitaxial YBCO films grown on sapphire with a new buffer layer material, Sr-doped La_2CuO_4 (LSCO). The YBCO film properties are compared with those of films grown on $LaAlO_3$. The uniformity of film properties is presented for YBCO grown on two-inch diameter substrates of each type.

The use of bulk La_2CuO_4 as a substrate material for YBCO films has been reported just once where YBCO was screen-printed on a polycrystalline La_2CuO_4 ceramic to produce a poor-quality film.[7] In our work, the $La_{2-x}Sr_xCuO_4$ buffer layers had $x \simeq 0.2$, a c-axis growth orientation, and the a and b axes were aligned with the sapphire substrate in the plane of the film.

* Supported in part by AFOSR
Contract No. F49620-88-C-0043.
Manuscript received September 24, 1990.

In the a-b plane, there is a close lattice match between LSCO and YBCO. The lattice constant of LSCO is nearly independent of x. LSCO is tetragonal with a_o = b_o = 0.3797 nm at the YBCO deposition temperature of ~700°C. At this temperature, YBCO is also tetragonal with an a-b lattice constant +2.4% larger than LSCO. There is a similar mismatch of +2.0% between YBCO and $LaAlO_3$.

Film Deposition

Both LSCO and YBCO films were deposited by 90° off-axis dc magnetron sputtering from single, stoichiometric targets. The sputter gas was typically 150 mtorr Ar and 50 mtorr O_2. Our results with this technique and the effects of varying the sputter-gas composition were published previously.[8] The optimum deposition temperature for LSCO was 620-680°C. The YBCO was deposited at 680-720°C. The details of the deposition-chamber configuration were also published.[9] The functions of the deposition system which were specifically used in this work were the capabilities of mounting a two-inch wafer on the 5.7 cm diameter circular substrate holder and rotating the holder about its symmetry axis. Silver paint was used for both mechanical and thermal anchoring of the substrates whether a series of small chips or a single large wafer was used. After deposition, the chamber was filled to 20 torr O_2 and the samples were first cooled to 400°C for a 15-20 min soak and then to room temperature.

Electrical Properties

Data on the critical temperature, T_c, critical current density, J_c, and rf surface resistance for our YBCO films deposited on $LaAlO_3$ substrates by off-axis sputtering were published in Ref. 9. Examples of T_c and J_c for YBCO grown on LSCO-buffered sapphire substrates are shown in Fig. 1 and Fig. 2. The normal-state resistivity of the sample in Fig. 1 was characteristic of samples placed at the outer 5 mm edge of the substrate holder during growth. These samples had resistivity values at room temperature approximately 25% higher than the ρ(300K) ≃ 250 $\mu\Omega$-cm obtained over the rest of the sample holder, presumably due to a lower substrate

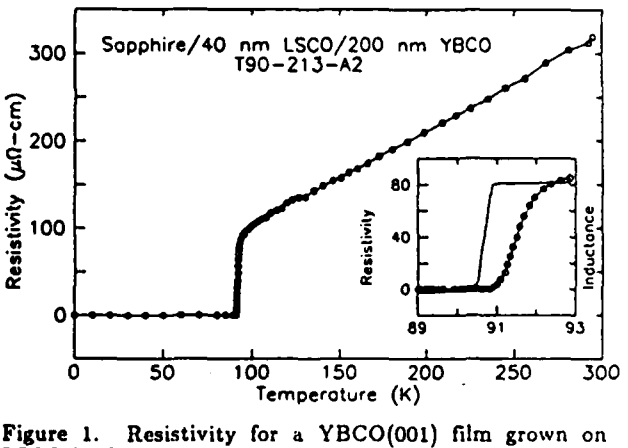

Figure 1. Resistivity for a YBCO(001) film grown on LSCO-buffered sapphire. The inset figure compares the resistive transition (open circles) to the transition measured by the change of inductance of a coil placed against the film (solid line).

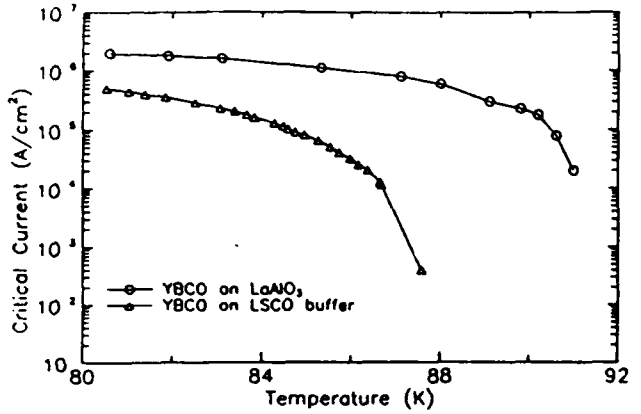

Figure 2. Transport critical current density measured in self-field plotted as a function of temperature for YBCO films deposited on $LaAlO_3$ and LSCO-buffered sapphire. The T_c's (R=0) for these films were 91.2K and 88K, respectively. In both cases, the film was patterned into a 25 μm wide bridge with voltage taps spaced 1 mm apart. There was no change in T_c from patterning the films in a phosphoric acid etch. A 5 μV criterion ($\rho < 10^{-8}$ Ω-cm for $J_c > 10^4$ A/cm^2) was used to define J_c. The film on sapphire had $J_c > 10^6$ A/cm^2 for temperatures less than 78K.

temperature. The temperature dependence of the resistivity was independent of sample position with ρ(T>100K) extrapolating to zero resistivity at zero kelvin and superconducting transition widths of ~1K. The ac susceptibility transition (inset in Fig. 1) was typically 1K wide and occurred at 0.5 to 1K lower temperature than the resistive transition.

The critical current density data in Fig. 2 represents the highest such data obtained for our YBCO films grown on $LaAlO_3$ and sapphire. Few such measurements have been made since the dc current-carrying capacity is not directly related to the suitability of films for microwave applications. However, the dc critical current at T > 77K was an indicator of film homogeneity that generally correlated with the widths of the resistive and inductive superconducting transitions. Fig. 2 shows that YBCO films on both types of substrates had $J_c = 10^5$ A/cm^2 within a few kelvin of the superconducting transition, and $J_c > 10^6$ A/cm^2 at 77K.

The rf surface resistance of YBCO on buffered sapphire (LSCO 30 nm thick) was measured at 4.2K by two different techniques, an 8.8 GHz all-YBCO microstrip resonator and a 4 GHz stripline resonator with a Nb resonator bar.[1] In both cases, the film served as a ground plane with the substrate turned so it was inside the resonator. In both cases, R_s was lower than that of Au. The calculation of R_s from the measured Q was more straightforward for the stripline resonator (although the unloaded Q was always assumed to equal the loaded Q). The measured Q was 5.7k for YBCO on sapphire corresponding to R_s = 6 mΩ, and Q was 3.8k for Au corresponding to R_s = 8 mΩ. In contrast, R_s for our YBCO on $LaAlO_3$ was < 1 mΩ at 77K and 10 GHz. Since R_s scales with frequency as f^2 for (most) YBCO, and is proportional to $f^{1/2}$ for a normal metal, the R_s of YBCO on sapphire represents a substantial improvement over Au at UHF despite its marginal improvement at X-band.

Substantially better R_s results at 4.2K have been reported for YBCO grown on $SrTiO_3$-buffered sapphire.[5] In those measurements, rf currents were concentrated at the free surface of the film rather than the substrate interface. Both LSCO and $SrTiO_3$ are lossy materials in the vicinity of 77K which can lower the effective surface resistance of YBCO in the types of rf measurements we performed. However, by keeping the buffer layer thin, rf losses can be made negligible. Although the typical LSCO buffer layer thickness used in this study was 40 nm, YBCO films grown on buffer layers as thin as 4 nm appeared to be equivalent to YBCO on the thicker buffer layers.

The LSCO buffer layers grown by off-axis sputtering were significant by themselves.[9] They were grown epitaxially on $SrTiO_3$ and $LaAlO_3$ substrates in addition to sapphire. Typical T_c's (R=0) for LSCO films on these substrates were 30K, 27K, and 21K, respectively. The highest T_c's obtained, 31K, were the highest reported for films in this materials system.[10] A transport critical current density of 7×10^4 A/cm^2 at 4.2K was the highest reported for this material.

Structural Properties

X-ray diffractometer data for an LSCO film on sapphire and a YBCO film on buffered sapphire are shown in Fig. 3. In both cases, the c-axis orientation exhibited in the figure was representative of all of the films. LSCO deposited on the A-plane of sapphire [α-$Al_2O_3(11\bar{2}0)$] was also highly oriented with roughly equal fractions of a-axis and c-axis orientation and no (103) x-ray peak, the largest peak observed in powder patterns.

The diffraction data in Fig. 3 proved only that the films were highly oriented in the growth direction. Fig. 4 contains RHEED patterns obtained from the surfaces of a LSCO film on sapphire and a YBCO film grown on buffered sapphire. The RHEED patterns showed that the films were also highly oriented in the

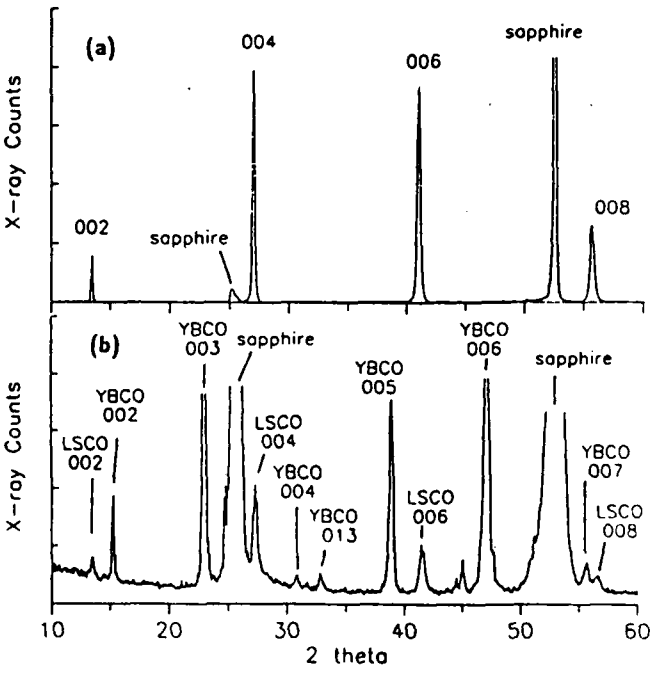

Figure 3. X-ray diffraction data for (a) a 300 nm thick LSCO(001) film grown on α-$Al_2O_3(1\bar{1}02)$, and (b) a 100 nm thick YBCO(001) film grown on a 30 nm LSCO buffer layer on sapphire. The LSCO film in each case had an exclusively c-axis orientation. The YBCO film in (b) had a predominantly c-axis orientation. Small YBCO(013) and YBCO(200) diffraction peaks indicated the presence of some misaligned grains.

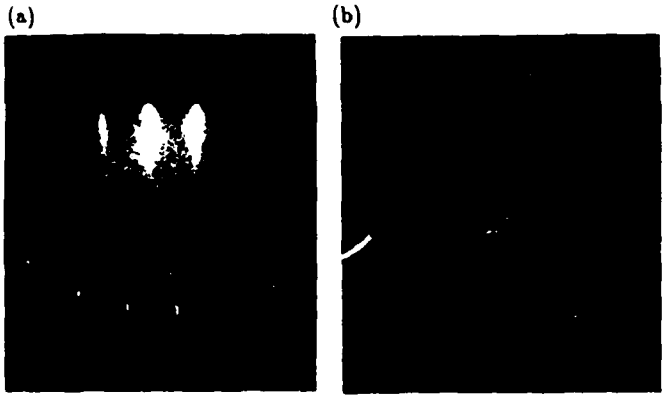

Figure 4. Ex-situ 9 kV RHEED patterns from the surfaces of (a) a LSCO(001) film on sapphire, and (b) a YBCO(001) film grown on LSCO-buffered sapphire, showing that the films grew epitaxially. In both cases the electron beam was parallel to [010] directions in the films.

a-b plane, that is, that they grew epitaxially. Both RHEED patterns in Fig. 4 were obtained after the films were briefly exposed to the atmosphere during a transfer from one vacuum system to another. The LSCO RHEED pattern was recorded after cleaning the surface by heating the sample to 500°C in 20 torr O_2 in the RHEED vacuum chamber. The YBCO pattern was recorded without surface cleaning.

Although the RHEED patterns in Fig. 4 were readily obtained, LEED patterns could not be obtained for either LSCO grown on sapphire or YBCO grown on buffered sapphire. LEED patterns were obtained for both LSCO and YBCO grown on $LaAlO_3$ or $SrTiO_3$ substrates indicating greater crystalline order in these films than in the ones grown on sapphire.

A quantitative comparison of the crystalline order of epitaxial YBCO deposited on various substrates is

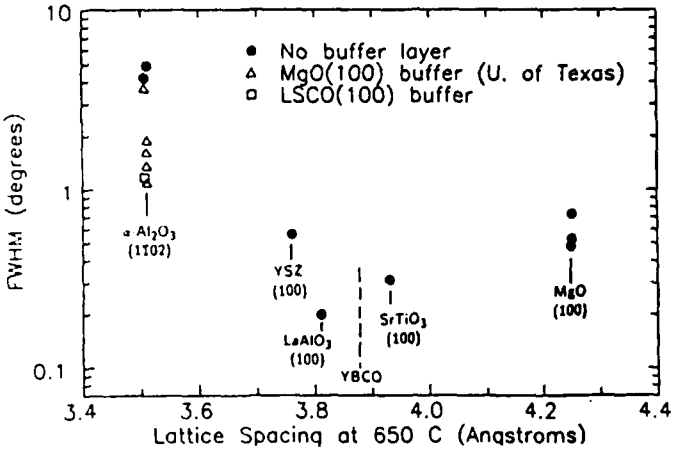

Figure 5. X-ray rocking curve widths for the (005) peak of epitaxial YBCO films grown on various substrates. The data is seen to correlate with the difference between the lattice constant of YBCO and that of the substrate at the deposition temperature of 700°C. For sapphire and yttria-stabilized zirconia (YSZ), the lattice spacing is the length of a diagonal in the two-dimensional surface lattice that lies parallel to a <100> direction in the YBCO film. The data on MgO-buffered sapphire is from Ref. 11.

presented in Fig. 5 where the YBCO(005) x-ray rocking curve width (full width at half maximum) is plotted as a function of the substrate lattice constant at 700°C. The lattice constant of YBCO is shown as a dashed line. The narrowest rocking curves were measured for films grown on substrates with the smallest lattice mismatch with YBCO.

The rocking curve width was also dependent on the film thickness. Most of the YBCO films in Fig. 5 were 100 nm thick. The exceptions were the films on bare sapphire (400-500 nm) and MgO-buffered sapphire (120-300 nm) from Ref. 11. The rocking curve width of the 100 nm thick YBCO film on LSCO-buffered sapphire was just 1.17° – substantially smaller than for YBCO on bare sapphire – but still large compared with YBCO on $LaAlO_3$ or $SrTiO_3$.

We speculate that R_s for YBCO on sapphire will not be reduced unless the rocking curve width is reduced. One possible route is to increase the buffer layer thickness. The rocking curve widths of the (006) peak of 800 nm thick LSCO films were 0.68°, 0.18°, and 0.28° for sapphire, $LaAlO_3$, and $SrTiO_3$ substrates, respectively. For such thick buffer layers to be practical, the Sr content should be reduced or eliminated to have an insulator instead of a normal conductor at 77K. Surface roughness is not a limitation on buffer layer thickness. Even the 800 nm thick LSCO films were very smooth. The appearance of multiple Laue zones in the RHEED pattern in Fig. 4(a) gives a clear indication of this smoothness.

Film Uniformity

Fig. 6 shows the transition temperature and indicates the location on the substrate holder of five YBCO films grown on $LaALO_3$ chips without rotating the holder. The resistive transition was defined by R=0. The inductive transition was defined as the temperature where 50% of the change in susceptibility had occurred. The transitions were all qualitatively like the one shown in Fig. 1. The variation in T_c across the substrate holder was less than 1K. The excellent uniformity displayed in Fig. 6 is similar to results obtained in Refs. 9 and 12 with individual chips placed on a stationary two-inch diameter holder.

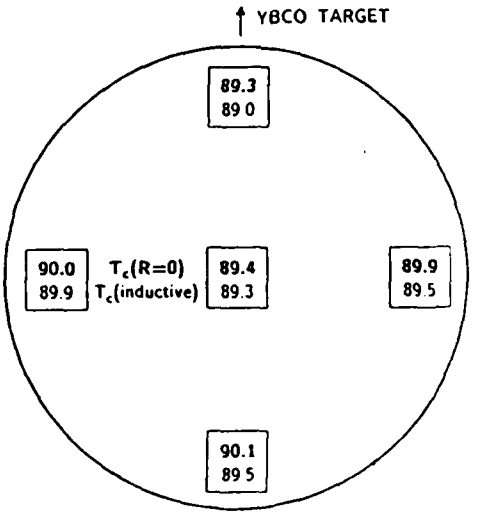

Figure 6. The resistive and inductive transition temperatures of YBCO films on five $LaAlO_3$ chips spaced across a two-inch diameter area and coated without rotating the substrate holder. The variation in T_c was less than 1K.

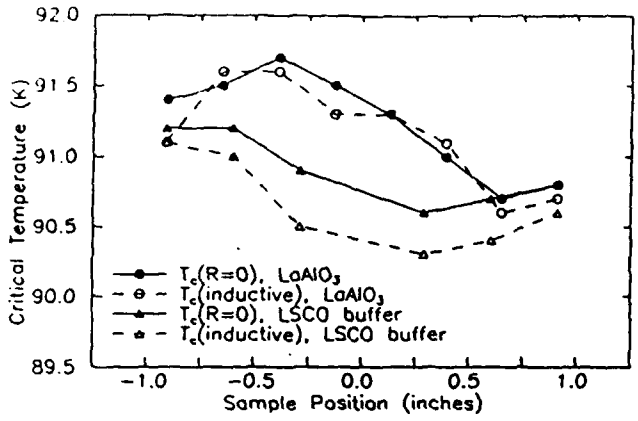

Figure 7. Resistive and inductive transition temperatures measured on a series of chips cut from two-inch diameter, YBCO-coated $LaAlO_3$ and buffered sapphire wafers and plotted as a function of distance from the center of the wafer.

In Fig. 7, the resistive and indcutive transition temperatures are plotted as a function of distance from the center of a two-inch diameter wafer of $LaAlO_3$ or LSCO-buffered sapphire. The YBCO films were deposited before dicing the wafer and the substrate holder was rotated during deposition. The film on $LaAlO_3$ was 150 nm ±10% thick everywhere on the wafer. The variation of ±10% was due to the difficulty in measuring accurate film thicknesses on heavily-twinned $LaAlO_3$. The inductively-measured transition temperature varied within the values of 91.1 ± 0.5K across the surface of the $LaAlO_3$ wafer, and 90.7 ± 0.4K across the buffered sapphire wafer. Assuming a constant film thickness across the wafer, the room-temperature resistivity was in the range of 260 ± 20 μΩ-cm over all but the outer 5 mm of the wafer for both types of wafers. The outer 5 mm ring had a resistivity approximately 25% higher at all temperatures.

Conclusions

- LSCO(001) films as thin as 40 angstroms grown epitaxially on R-plane sapphire are effective buffer layers for growth of YBCO. It is not clear at this point whether LSCO is superior to $SrTiO_3$ or MgO buffer layers. It has an *a priori* advantage over MgO in having a closer lattice match to YBCO.

- Although T_c and J_c are high for YBCO on buffered sapphire, R_s is only low enough for practical applications at UHF. However, the need for large substrates is particularly acute in UHF applications since device size is often determined by wavelength.

- Rocking curve widths show that YBCO is not as well aligned on buffered sapphire as on single-crystal perovskite substrates. The mosaic spread in the growth direction and in the plane of YBCO films is perhaps the most important parameter in determining rf surface resistance. The YBCO(005) x-ray rocking curve width improved from 4° for films grown on bare sapphire to 1.2° for films on the LSCO-buffered sapphire.

- Excellent uniformity has been obtained for growth of YBCO on 2-inch diameter $LaAlO_3$ and sapphire wafers. The capability of producing films on this scale not only increases the possible size of microwave components but permits them to be integrated on a single wafer.

Acknowledgments

The authors acknowledge the assistance of J. H. Uphoff, J. C. Brown, S. J. Pieseski, and C. L. Jones with film patterning and dc measurements; G. R. Wagner, S. H. Talisa, B. R. McAvoy, D. H. Watt, and G. B. Draper with the measurements of surface resistance; N. J. Doyle and A. M. Stewart with x-ray measurements; and T. J. Mullen with EDS measurements. We also acknowledge the collaboration with A. B. Berezin and A. L. de Lozanne of the University of Texas which helped us to compare LSCO with MgO buffer layers.

References

1. J. Talvacchio and G. R. Wagner, "High-T_c Film Development for Electronic Applications," in Superconductivity Applications for Infrared and Microwave Devices, SPIE Proc. Vol. 1292, Bellingham, Washington, 1990.

2. E. J. Tomlinson, Z. H. Barber, G. W.Morris, R. E. Somekh, and J. E. Evetts, "Optimization of Thin-Film $YBa_2Cu_3O_7$ Deposition by DC Sputtering onto Sapphire Substrates," *IEEE Trans. Magn.* 25, 2530-2533, 1989.

3. J. Talvacchio, G. R. Wagner, and H. C. Pohl, "$YBa_2Cu_3O_7$ Films Grown on Epitaxial MgO Buffer Layers on Sapphire," *Physica C* 162-164, 659-660, 1989.

4. A. B. Berezin, C. W. Yuan, and A. L. de Lozanne, "$Y_1Ba_2Cu_3O_{7-x}$ Thin Films Grown on Sapphire with Epitaxial MgO Buffer Layers," *Appl. Phys. Lett.* 57, 90-92, 1990.

5. K. Char, N. Newman, S. M. Garrison, R. W. Barton, R. C. Taber, S. S. Laderman, and R. D. Jacowitz, "Microwave Surface Resistance of Epitaxial YBCO Thin Films on Sapphire," *Appl. Phys. Lett.* 57, 409-411, 1990.

6. A. E. Lee, C. E. Platt, J. R. Burch, R. W. Simon, J. P. Goral, and M. M. Al-Jassim, "Epitaxially-Grown Sputtered $LaAlO_3$ Films," submitted to *Appl. Phys. Lett.*, 1990.

7. U. V. Varadaraju, G. V. Subba Rao, K. D. Chandrasekaran, and A. Baradarajan, "Superconductivity Behaviour in Screen-Printed $YBa_2Cu_3O_7$ Films," *Thin Solid Films* 164, 119-121, 1988.

8. J. R. Gavaler and J. Talvacchio, "Optimization of T_c and J_c in Sputtered YBCO Films," *Physica B* 165-166, 1513-1514, 1990.

9. J. Talvacchio, M. G. Forrester, J. R. Gavaler, and T. T. Braggins, "YBCO and LSCO Films Grown by Off-Axis Sputtering," in Science and Technology of Thin Film Superconductors II, edited by R. McConnell and S. A. Wolf, Plenum, New York, 1990.

10. M. Suzuki, "Hall Coefficients and Optical Properties of $La_{2-x}Sr_xCuO_4$ Single-Crystal Thin Films," *Phys. Rev. B* 39, 2312-2317 1989.

11. A. B. Berezin, C. W. Yuan, and A. L. de Lozanne, "YYBCO Thin Films on Sapphire with an Epitaxial MgO Buffer," submitted to *IEEE Trans. Magn.*, 1990.

12. N. Newman, K. Char, S. M. Garrison, R. W. Barton, R. C. Taber, C. B. Eom, T. H. Geballe, and B. Wilkens, "YBCO Superconducting Films with Low Microwave Surface Resistance over Large Areas," *Appl. Phys. Lett.* 57, 520-522, 1990.